UNCLASSIFIED

Technical Report No. 178-4

DEVELOPMENT OF A CONTROLLER ELEMENT FOR COMPATIBLE OPERATOR CONTROL OF EARTHMOVING MACHINES

Final Technical Report

D. E. Johnson
H. R. Warr
A. F. Kingsford
L. G. Johnson

Systems Technology, Inc.
Hawthorne, California 90250

March 1970

Contract No. DAAG02-69-C-0186
for
U. S. Army Mobility Equipment
Research and Development Center
Fort Belvoir, Virginia 22060

UNCLASSIFIED

AD

Technical Report No. 178-4

DEVELOPMENT OF A CONTROLLER ELEMENT FOR COMPATIBLE OPERATOR CONTROL OF EARTHMOVING MACHINES

Final Technical Report

D. E. Johnston
D. H. Weir
R. F. Ringland
L. G. Hofmann

Systems Technology, Inc.
Hawthorne, California 90250

March 1970

Contract No. DAAK02-68-C-0186
for
U. S. Army Mobility Equipment
Research and Development Center
Fort Belvoir, Virginia 22060

FOREWORD

This program was sponsored by the Construction and Maintenance Equipment Branch, U. S. Army Mobility Equipment Research and Development Center, Fort Belvoir, Virginia, under Contract DAAK02-68-C-0186. The Technical Monitors were Mr. T. W. Smith and Mr. Hamilton Reese.

The research was performed during the period from January 1968 through January 1969. The STI Technical Director was I. L. Ashkenas, and Mr. D. E. Johnston served as Project Engineer. The mathematical model for the vehicle and soil load dynamics was accomplished by Mr. L. G. Hofmann. The tractor simulation and experiments were conducted by Mr. R. F. Ringland. Mr. D. H. Weir accomplished the closed-loop analyses and contributed to all aspects of the program.

The authors are indebted to the Technical Monitors and to Mr. N. F. Oglesby, Branch Head, for their assistance in providing design information and photographic services. The efforts of other STI staff members; including J. Nagy in constructing the mockup, A. Campbell in design aspects, and W. R. Atkinson during the experimental phase; contributed substantially to the accomplishment of the program. Finally, the care and diligence of the STI production staff in preparing the report draft is gratefully acknowledged.

ABSTRACT

Manual control of dozing with an earthmoving tractor is studied to determine ways to modify the manipulator and control system properties to improve performance and reduce operator workload. The Universal Engineer Tractor is used as a numerical example. Linearized equations are derived for longitudinal and lateral motions which include manipulator and suspension properties, vehicle hull and blade dynamics, and terrain loads on the blade. The resultant detailed dynamic model is reduced to a simplified equivalent for analysis and simulation. Transfer functions are computed and used to study the operator's blade control in response to various visual and motion cues. This indicates which feedbacks the operator should use, and how the controlled element dynamics can be improved through design modifications. A fixed-base mock-up and dynamic simulation are used to evaluate competing manipulator/controller configurations. As a result, a prototype manipulator is defined which has the potential of improving dozing performance, reducing training time, and easing the operator workload.

CONTENTS

FIGURES

TABLES

SECTION I

INTRODUCTION

This report is the fourth and final report on the development of a controller element for compatible operator control of earthmoving machines (Ref. 1).

The objectives of this program were to:

- Demonstrate the application of a systems design approach to the definition of such controllers.
- Design, fabricate, and demonstrate an example control system that fully integrates the human operator into the control of the machine process action with safety and yet enables the operator to identify himself with the machine dynamics to minimize the error in the expected or desired earthmoving process state variable.

The operation of earthmoving and terrain manipulation machines is a complex and demanding task for even a skilled operator under good conditions. Confound this with low levels of training, the presence of a battle field environment, and a proliferation of available tools to increase machine versatility, and the operator's control problems appear very formidable indeed. Integration of manipulators and the enhancement of the operator's sensation of the state of his machine and task provide a very promising route towards simplification and improved performance.

Mathematical models of the human operator now exist which permit estimation of the dynamic response, stability, and average performance of manually controlled systems. These models permit identification of those controlled system parameters having the greatest effect on these three properties; further, they permit one to indicate ways in which these properties can be improved by appropriate modifications to elements within the controlled system — the manipulator, controlled element dynamics, and the display.

The dynamics of the effective controlled element and their quantitative definition play a central role in the understanding and integration of the

manual control function. Their most useful form is the set of transfer functions relating manipulator motions to "selected machine" motions — motions of the tool due to the combined motion of vehicle and tool relative to vehicle. The dynamic response of the combined machine to external forces and operator control action is then directly computable from the derived controlled element transfer functions and the human operator model. These response properties may be evaluated for their "good" and "bad" features to identify those parameters having the greatest influence on the response; in effect providing a design review of the control aspects of the machine. This is the fundamental approach taken in this study.

The technical approach is applicable to any of several earthmoving and terrain manipulation machines. In the present program only one example, the Universal Engineer Tractor (UET-E4), is subjected to detailed analysis, simulation, and modification. The UET is a crawler type vehicle having a hydraulic transmission and hydraulically operated tools. Its more important capabilities include both earthmoving (dozing and scraping) and transport (hauling and towing). Of these, dozing and tilt dozing were selected as the processes to be studied. The UET is somewhat unique because in this task the dozing blade is a rigid part of, and forms the front of, the vehicle. The blade height is controlled by raising and lowering the front of the vehicle. This is accomplished by positioning rotary hydraulic actuators on each front corner which in turn raise or lower the front of the vehicle relative to its track assembly. The operator station is located toward the rear of the vehicle and the sides of the body extend over the track. Thus the operator cannot directly observe the position of the body relative to the track and has considerable difficulty seeing the dozing load being cut or pushed by the blade.

The system approach demonstrated herein integrates human operator, controller, vehicle, and control task dynamic and operational considerations in the definition of three potential controller modifications, each offering substantial improvement in man/machine performance over the existing controller. The organization of the material is as follows.

Section II describes the overall dozing task and identifies the various subtasks, operator cues, controls used, and potential performance

measures or criteria. The controlled element dynamics (manipulator, vehicle, hydraulic system, and load contributions) are summarized in Section III for the various motion quantities of potential concern in the more demanding dozing subtasks. The controlled element dynamics are presented in the form of transfer functions for the complete eight-wheeled mathematical model and for a simpler equivalent three-wheeled model. Section IV presents the mathematical model of the human operator and explains the adjustment rules and criteria for its application. The results of the closed-loop analysis, synthesis, and simulation are presented in Section V. The summary findings of a series of single-loop closures for operator control of the vehicle using each of the potential motion cues is presented. The operator equalization required for each, measures of system stability, and judgments of resulting performance are postulated. A multiloop control strategy is developed which the operator could be expected to adopt in order to minimize his workload. The dynamic simulation is described along with the experimental program to verify the analytical predictions and to obtain quantitative and qualitative evaluation of improved controller configurations. Finally, the results of the simulation evaluation program are presented. Considerations of mechanizational feasibility are approached in Section VI where the configuration for the prototype controller is selected and various preliminary design and installation details are worked out. Section VII presents the conclusions of the study and recommendations for future work.

The various appendices present detailed information and analyses to support the material and discussion of the main text.

SECTION II

CLASSIFICATION OF MACHINE TASKS

Based on discussions with MERDC personnel during the initial program coordination meeting at Ft. Belvoir, it was decided that a representative earthmoving machine task for demonstrating feasibility is that of dozing. This task selection was made on the basis that, to make the evolved prototype most effective, the candidate operations and maneuvers should involve "continuous-type" control (e.g., grading, dozing, steering) rather than "on/off" type control (ejector ram, bilge pump, etc.). Furthermore, the continuous-type control task should meet the following criteria to the extent practicable:

- Be significant to the mission of the selected vehicle
- Involve a significant problem area; i.e., requiring a high degree of skill or training
- Lend itself to integration of the control devices and possible controlled element modification
- Provide a good basis for demonstrating the fruitfulness of the proposed approach to man-machine integration problems
- Be representative of tasks required with similar existing and planned vehicles and equipment

A task scenario was then prepared for the general operations and maneuvers involved in dozing (see Fig. 1). This scenario encompasses one cycle of the dozing operation whereas an actual dozing job would be expected to require several cycles (Fig. 2). The cutting and pushing phases identified in Fig. 1 are the major phases in terms of simultaneous, "continuous" control activity of several blade or vehicle motions (depth, roll, yaw). These are also the major phases in terms of time consumed in the overall work cycle. It is during these phases that the operator is performing a closed-loop tracking task; that is, he is manipulating the front suspension levers so as to minimize deviations in blade height and tilt from that desired. The subtasks of these phases then provide the fundamental operations upon which to focus attention in this program, i.e.,

CYCLE PHASE	SUBTASK	OPERATOR CUES	CONTROLS USED	POTENTIAL PERFORMANCE MEASURES/CRITERIA*
Setting up	Select transmission ratio	Soil composition and depth of cut	Transmission lever	Time
	Align dozer for cut	Position and heading	Steering wheel, throttle	Time
	Position blade for cut	Blade height, hull attitude, and terrain preview	Front suspension levers	Lever activity; time
Cutting	Increase power and blade depth to desired level	Blade and hull attitude, terrain preview, exhaust sound, load spillage	Front suspension levers, throttle	"Smoothness" of entry contour (Δh or h_e); speed change (Δu); lever activity (δ_s)
	Maintain desired cut plane and speed	Same as preceding	Same as preceding	Same as preceding
	Maintain direction	Heading angle	Steering wheel and/or front suspension levers	Heading error
	Reduce cut depth to zero	Blade and hull attitude, terrain preview, exhaust sound, load spillage	Front suspension levers, throttle	"Smoothness" of exit contour Lever activity Load spillage (blade height error)
Pushing	Track terrain contour	Same as preceding	Same as preceding	Load spillage (blade height error) Lever activity
	Maintain direction	Heading angle	Steering wheel	Heading error
Dumping	Raise blade	Blade and hull attitude, terrain preview, exhaust sound	Front suspension levers, throttle	?
Return	Halt forward motion	Forward velocity, exhaust note	Throttle	Time
	Select transmission ratio (reverse)	Transmission lever position	Transmission lever	Time
	Accelerate to constant velocity	Reverse velocity, exhaust note	Throttle	Time
	Maintain direction	Heading angle	Steering wheel	Path (heading error)
	Halt reverse motion	Reverse velocity, dozer position	Throttle	Position error Time

*Performance criteria vary somewhat depending upon which cycle in a job is referred to, e.g.,:

1. Early cycles (first one or two) — the objective may be to smooth the terrain to make the command bandwidth for subsequent cycles small, thus easing the task.
2. Intermediate cycles (most of the remaining) — the objective is to maximize the earth moved per unit time while maintaining smooth terrain contour
3. Final cycles (last two or three) — objective is to smooth terrain so that it approximates that desired; dozer is essentially functioning as a crude grader.

Figure 1. Dozing Task Scenario (One Cycle)

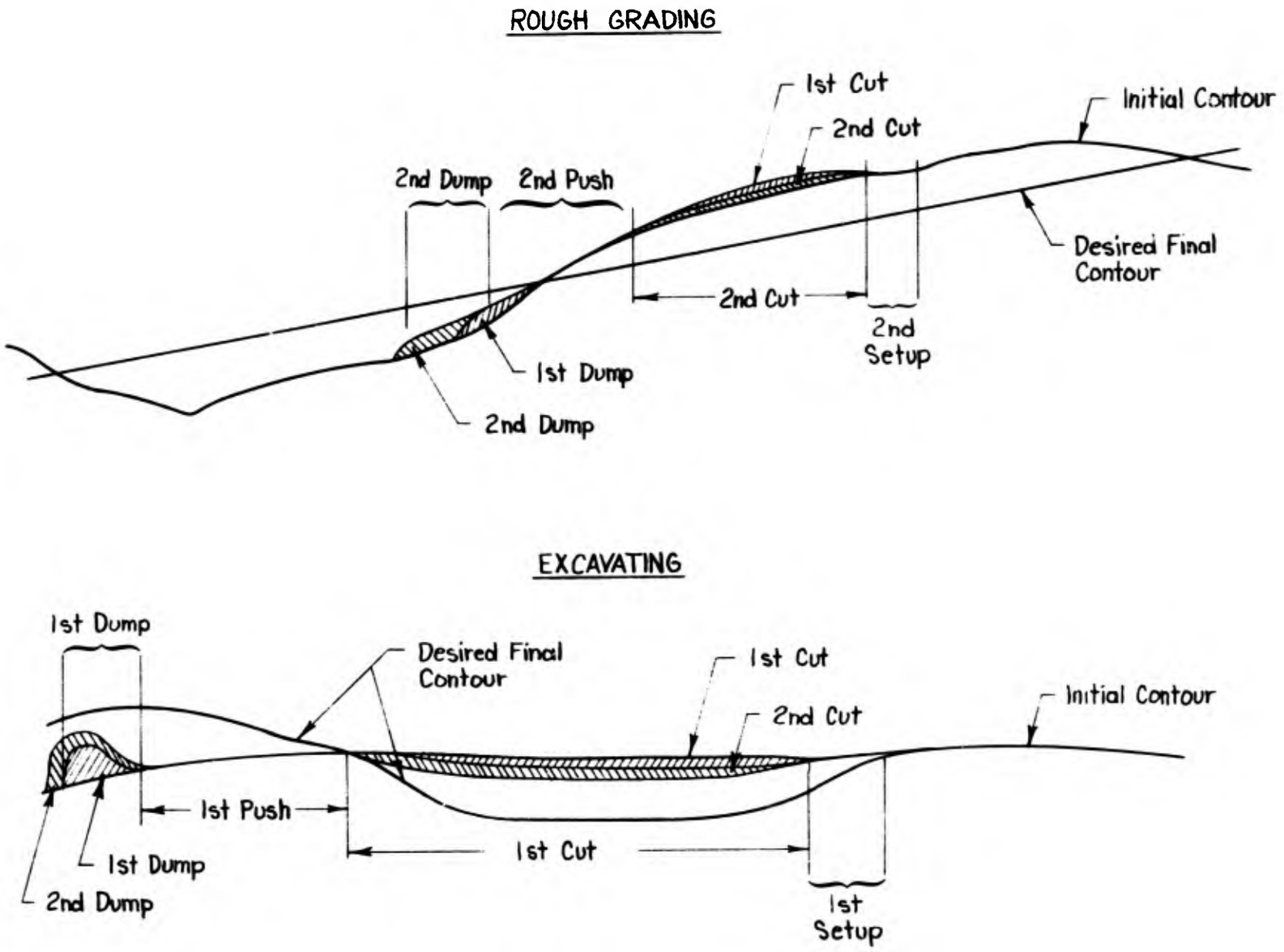

Figure 2. Assumed Dozing Operations

to maintain a desired cut plane and velocity in the presence of terrain contour and soil composition variations, and to follow or track nominal terrain undulations with blade height in order to push a load with minimum spillage.

As a double check on the foregoing, a visit was made to the Naval Heavy Equipment Operator Training School at Port Hueneme, California. Instructor personnel were questioned in detail regarding problems encountered in training inexperienced operators on conventional dozing equipment, the most difficult tasks to master, the cues the trainees are taught to use, the measures used to evaluate operator performance, etc. The instructors indicated that the two major problems with new personnel involve "overcontrolling" the blade and trying to take too deep a cut. The latter, of course, is a matter of judgment and the recruit soon learns to take shallow cuts (e.g., 2 to 3 inches, depending upon the soil composition). The former, overcontrolling, is a closed-loop control and coordination problem which leads to "washboarding," stalling the vehicle, loss of load, loss of time, etc. Here it is a matter of time (and training) until the operator obtains a "feel" for the machine, learns to make small continuous adjustments in blade height (tight, closed-loop tracking), and learns to think ahead of or "lead" the blade (terrain preview, tractor attitude, blade side-spillage, exhaust tone, etc.). For the type of construction accomplished by the Sea Bees, a student completing dozing training is expected to smooth any given terrain to within ±0.2 ft (i.e., the lowest or highest points within the area worked should not deviate more than ±0.2 ft from the desired height).

Thus the comments by NHEOTS personnel support the selection of the cutting and pushing tasks (Fig. 1) as representative of the more crucial closed-loop type dozing operation and verify that these closed-loop "tracking" tasks are indeed difficult to master.

SECTION III

DEFINITION OF THE CONTROLLED ELEMENT DYNAMICS

In any manual control analysis it is necessary to write equations for the overall controlled element dynamics for the process or task(s) under investigation. For the UET dozing operation the controlled element consists of the manipulator, the road wheel actuation system, and the tractor/blade combination. The equations should take into account important soil characteristics and forces on the tracks and blade. The major technical effort here involves establishing realistic but simple equations for the hydraulic system, track system, vehicle, and blade load.

The controlled element dynamics are described at three levels of completeness and complexity:

- An eight-wheeled model* which includes soil forces and moments on the blade and the effects of actuator leakage.
- A three-wheeled model which includes soil loads on the blade and actuator leakage, but employs a simplified equivalent road wheel geometry.
- A simplified model which is like the three-wheeled model, except that soil loads and actuator leakage are not included.

The first is most complete while the last provides most insight due to its simplicity. The middle one is a reasonable compromise of accuracy and utility and it is the primary model of the tractor dynamics used in this study. Physical data for the UET are given in Appendix A.

A. MANIPULATOR CHARACTERISTICS

The suspension lever force-to-displacement characteristic and the displacement-to-valve flow relationship are given in Figs. B-2 and B-3 of

*The term "model" is used to refer to the set of differential equations, transfer functions, describing functions, etc.; which describe the dynamics of the operator/tractor system or its components.

Appendix B. These properties may be combined to yield the lever force-to-valve flow characteristic shown in Fig. 3. This nonlinear characteristic is such that the operator has an extremely difficult time with fine control over the flow rate. To start the flow, he must exert better than 9 lb force, yet 10 lb corresponds to full valve opening. As a result the operator will have a tendency to "pulse" the stick, the number of pulses used depending on the desired blade motion. This will cause the blade to move in a stepwise fashion. If the operator produces primarily a stick force (rather than displacement), the nonlinearity of Fig. 3 will result in a lag. This means that the operator must produce lead equalization and this is consistent with "pulse-like" control movements (Ref. 2).

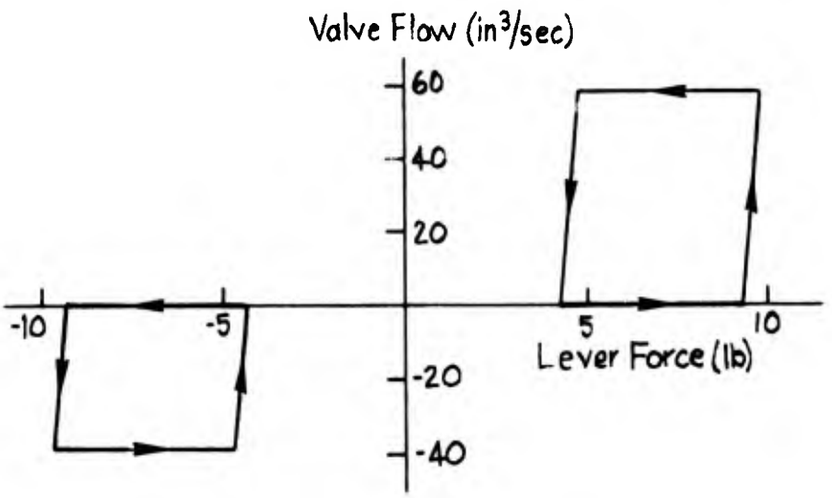

Figure 3. Suspension Lever Force to Valve Flow Characteristic

B. DESCRIPTION OF EIGHT- AND THREE-WHEELED MODELS

Equations and transfer functions are given in Appendix B for the three-wheeled and eight-wheeled models. These include soil forces and moments and actuator leakage. Appendix B starts by developing the eight-wheeled model which has the full wheel complement, hydraulic system details, propulsive forces and moments, and soil forces and moments. The number of wheels are then reduced to a basic three: two in front driven by the suspension levers and a fixed one in the rear. The tractor motions considered in each case are:

- Forward speed, u
- Height of blade and center of mass, Δ_Z and Z_{cm}
- Pitch angle, θ
- Road arm angle, a
- Roll angle, φ
- Heading angle, ψ

The tractor dynamics involve a pure time delay between the time successive road wheels encounter a terrain point. This pure delay is represented by a second-order Padé approximation to simplify the analyses and simulation. The size of the delay (at 2 fps) is such that the approximation is good for frequencies up to about 1 rad/sec. Beyond this, the error tends to be conservative since the approximation gives less phase lead in the effective controlled element than really exists. On the other hand, soil deformation tends to smooth or "filter" the sharp edges of the terrain, thereby suppressing the high frequency effects of a pure delay. The operator time delay and neuromuscular lags ultimately limit the operator/tractor system bandwidth, despite phase lead from the tractor. In view of these considerations, closed-loop analyses can be made beyond the limits of the Pade approximation with confidence that the results will be conservative estimates. Finally, since all the loop closures are done under the same approximating assumptions, the relative comparison of the results will be both valid and useful.

The operator controls the tractor motions by using the suspension levers together or separately. Throttle and steering wheel are assumed to be fixed because only dozing and tilt dozing are the tasks. The same stick force and valve characteristics are used in each case, also.

Longidudinal transfer functions are given in Table I for the eight-wheeled vehicle at 2 ft/sec, and the three-wheeled vehicle at both 2 ft/sec and 6 ft/sec. The 2 ft/sec results show the good agreement between the eight- and three-wheeled models. The two different entries in Table I for the three-wheeled vehicle show the speed effect. The frequencies of most numerator and denominator factors are functions of speed; in particular, those factors associated with the Padé approximations to pure time delays. These include the quadratic factors having damping ratios in the vicinity

TABLE I

LONGITUDINAL TRANSFER FUNCTIONS*

POLYNOMIAL [SYMBOL]	EIGHT-WHEELED MODEL AT 2 fps	THREE-WHEELED MODEL AT 2 fps	THREE-WHEELED MODEL AT 6 fps
Longitudinal Denominator $[\Delta_{long}(s)]$	10.7[-.77 , .043][.79 , .073][.79 , .45][.81 , .71](.14)(.33)(2.4)(2236)	8.57[-.77 , .040][.80 , .072](.14)(.32)(2.19)(2139)	8.57[-.75 , .088][.86 , .17](.42)(.96)(6.59)(2137)
Forward Velocity Numerator $[N_q^u(s)]$	-1120[.86 , .33][.79 , .45][.82 , .61][.82 , .88](.21)	-453[.82 , .68][.86 , .33](.205)	-560[.86 , .98][.82 , 2.04](.57)
Vertical Velocity Numerator $[N_q^w(s)]$	182[.79 , .45][.82 , .61][.82 , .88](0)(.0043)(.057)(.14)(-.48)	73.9[.82 , .68](0)(.0043)(.057)(.14)(-.48)	73.9[.82 , 2.04](0)(.013)(.17)(.42)(-1.43)
Height at Center of Mass Numerator $[N_q^{zcm}]$	182[.79 , .45][.82 , .61][.82 , .88][-.030 , .60](.057)(.14)	73.9[.82 , .68][-.030 , .60](.057)(.14)	73.9[.82 , 2.04][-.03 , 1.81](.17)(.42)
Surload Height Numerator $[N_q^h]$	102[.82 , .34][.79 , .45][.82 , .61][.82 , .88](.057)	41.2[.82 , .68][.82 , .34](.057)	123[.82 , 1.02][.82 , 2.04](.17)
Pitch Angle Numerator $[N_q^\xi]$	-39.8[.79 , .45][.82 , .61][.82 , .88](0)(.057)(.14)(.84)	-16.1[.82 , .68](0)(.057)(.14)(.84)	-16.1[.82 , 2.04](0)(.17)(.42)(2.51)
First Road Arm Angle Numerator $[N_q^{\theta_1}]$	-93.8[.82 , .61][.82 , .88](-.0044)(.057)(.14)(.28)(1.61)	92.4(0)(.00021)(.057)(.14)(.32)(2.19)	92.4(0)(.00059)(.17)(.42)(.96)(6.6)
Blade Height Numerator $[N_q^z]$	571[.82 , .34][.79 , .45][.82 , .61][.82 , .88](.057)(.14)	231[.82 , .68][.82 , .34](.057)(.14)	231[.82 , 1.02][.82 , 2.04](.17)(.42)

*A shorthand notation is used to simplify table entries, i.e.,

$$A[s^2 + as + b] = A[s^2 + 2\zeta\omega s + \omega^2] \rightarrow A[\zeta , \omega]$$

$$A(s + 1/T) = A(s + \alpha) \rightarrow A(\alpha)$$

of .82, as well as certain first-order factors. In addition, first-order factors associated with load are also direct functions of speed. Some of the additional poles and zeros in the eight-wheeled version cancel identically while the others nearly cancel, leaving only a small residual effect. Two additional quadratic factors in both the denominator and the various numerators for the eight-wheeled version are a direct result of including all eight wheels in the equations. Additional differences in the numerical values are due to the assumptions made concerning the location of the first set of equivalent road wheels in the simpler model — they are located midway between blade edge and the rearmost road wheels. The effect of the additional factors is to add closely speced pole/zero pairs in the transfer functions which do little more than modify the gains associated with each. Frequency response plots would show only minor differences. Thus the three-wheeled model is a very good approximation to the eight-wheeled model.

C. EFFECT OF ACTUATOR LEAKAGE

The effect of actuator leakage may be observed by comparison of the three-wheeled model of Table I and the simplified model of Table II. The major difference between the transfer functions is due to actuator leakage as influenced by blade load dynamics. Leakage is not included in the simplified model.

The detailed effect of leakage is illustrated in Appendix B by breaking the three-wheeled transfer function for blade height to flow into parts due to leakage and those due to kinematics and soil load. The graphical results in Figs. 9 and 10 of that appendix show the benefits of reduced leakage, and the penalty for increased leakage, in a relatively simple way. The effect is to destabilize the low frequency poles. The major result is that any leakage is detrimental, but tolerable as long as it is not excessive.

TABLE II

TRANSFER FUNCTIONS FOR SIMPLIFIED MODEL

Road arm angle

$$\frac{a_1 + a_2}{q_1 + q_2} = \frac{N_q^a}{\Delta_{long}}(s) = \frac{.0101}{s} \quad ; \quad \frac{a_1 - a_2}{q_1 - q_2} = \frac{N_{\Delta q}^{\Delta a}}{\Delta_{lat}}(s) = \frac{.0101}{s}$$

Blade height

$$\frac{z}{q_1 + q_2} = \frac{N_q^z}{\Delta_{long}}(s)$$

$$= \frac{.0126[s^2 + 2(.816)(.342U_o)s + (.342U_o)^2][s^2 + 2(.816)(.171U_o)s + (.171U_o)^2]}{s^2(s + .159U_o)(s + 1.096U_o)}$$

Pitch angle

$$\frac{\theta}{q_1 + q_2} = \frac{N_q^\theta}{\Delta_{long}}(s) = \frac{.00879[s^2 + 2(.816)(.342U_o)s + (.342U_o)^2](s + .418U_o)}{s^2(s + .159U_o)(s + 1.096U_o)}$$

Roll angle

$$\frac{\phi}{q_1 - q_2} = \frac{N_{\Delta q}^{\Delta \phi}}{\Delta_{lat}}(s) = \frac{.00163[s^2 + 2(.816)(.342U_o)s + (.342U_o)^2]}{s^2(s + .836U_o)}$$

SECTION IV

OPERATOR DYNAMIC RESPONSE CHARACTERISTICS

All phases of dozing require some form of operator control operation. As the task becomes more demanding, the operator may change his dynamic characteristics or may alter the system structure (close other loops) to obtain the required increase in control fidelity. The operator's closure of feedback loops modifies the effective dynamics of the tractor or controlled element and in turn determines maneuver times, stability margins, and transient response characteristics. The possible feedback loops he can introduce are determined by the sensory information available.

The quasi-linear describing function model describes the dynamic response of a skilled, attentive human operator in a closed-loop control task. It has resulted from a series of response measurement programs accomplished over a period of about two decades (Refs. 3-6), and it is well suited to the analysis of dozing and other earthmoving control tasks. It consists of a describing function component with parameters which depend on the system and situation, an additive remnant, and a set of rules which tell how to adjust the describing function parameters. This quasi-linear model is shown in the single-loop block diagram of Fig. 4. In its most complete form the describing function contains gain, indifference threshold, time delay, equalizer, and neuromuscular dynamics. The indifference threshold is a higher order effect that can often be ignored when the inputs are large and under other conditions it can be accounted for by using decreased driver gain. The neuromuscular system dynamics are based on very low and very high frequency data, and can be approximated (in some cases) at the mid-frequencies of interest in dozing as a first-order lag or even as an added increment to the time delay. With these simplifications, the general operator describing function reduces to:

$$Y_p \doteq K_p \left(\frac{T_L j\omega + 1}{T_I j\omega + 1} \right) e^{-j\omega(\tau + T_N)} \qquad (1)$$

where K_p is the gain

$\left(\frac{T_L j\omega + 1}{T_I j\omega + 1}\right)$ is a simplified equalization characteristic

τ is the time delay

T_N is the neuromuscular system time constant

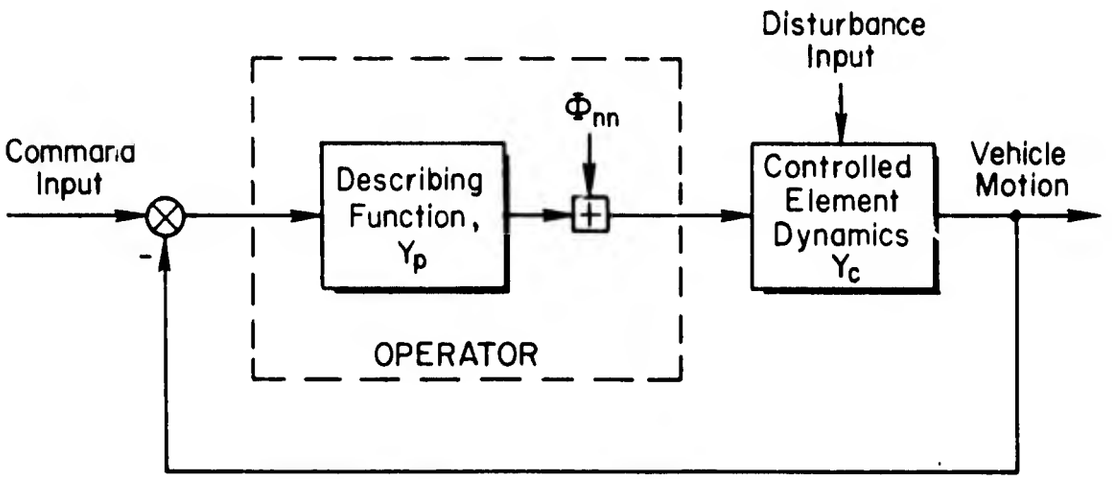

Figure 4. Operator Model for Single-Loop Control

The form of Eq. 1 is adequate for a variety of operators, inputs, vehicle dynamics, control system characteristics, and loop structures. Most of the parameters are adjustable as needed, and typical values are illustrated by the subsequent system analyses.

The equalizing characteristic and the gain, K_p, are the major adaptive elements of the human which allow him to control many differing dynamic devices. The major "adjustment rules" are that a particular equalization is selected from the general form $K_p(T_L j\omega + 1)/(T_I j\omega + 1)$ such that:

- The driver/vehicle system can be stabilized
- The amplitude ratio of the product of driver and vehicle, $|Y_p Y_c|$, has approximately −20 dB/decade slope in the crossover region
- $|Y_p Y_c| >> 1$ at low frequencies

The major "cost" of equalization is an increase in effective time delay incurred when low frequency lead is needed as part of the compensation.

The model of Eq. 1 is best suited to stable controlled elements, for tasks with low frequency inputs, and where the remnant is relatively small. The dynamics of the UET-type dozer are such that the operator is faced with a conditionally stable control task, regardless of which loop structure he adopts. This leads to low frequency phase droop due to neuromuscular effects, and small phase margins which limit the extent of the stable crossover region. These mid-frequency influence of these low frequency neuromuscular effects can be accounted for by including an additional term, α/ω, in the exponential kernel of Eq. 1; i.e.,

$$Y_p \doteq K_p \left(\frac{T_L j\omega + 1}{T_I j\omega + 1}\right) e^{-j(\tau_e \omega + \alpha/\omega)} \qquad (2)$$

In addition to adding the "α-effect," τ and T_N have been added together to give an effective time delay, τ_e. Values of τ_e for various equivalent vehicle dynamics and forcing function bandwidths are given in Fig. 5. Values of α and τ_e for representative unstable vehicle dynamics are given in Fig. 6, i.e., $Y_c = K/s(s - 1/T)$. In this case, the product $\alpha\tau_e$ remained nearly constant at 0.11, but values from 0.04 to 0.2 have been observed. Constancy of $\alpha\tau_e$ implies that a favorable decrease in τ_e is accompanied by an adverse increase in α, such that the net phase angle curve has a constant concave-downward shape which moves back and forth in frequency on a Bode plot with variation in τ_e. The experimental results in Figs. 5 and 6 are maximum values for skilled subjects in fixed-base simulators without motion feedbacks, and will ordinarily be somewhat reduced during field operations. This leads, in practice, to larger phase and gain margin criteria, typical examples of which are used in the subsequent operator/vehicle loop closures.

The rationale of operator equalization can be adequately and simply expressed by using an approximate "extended crossover model" (Ref. 3). Both experimental data and consideration of the requirements of good

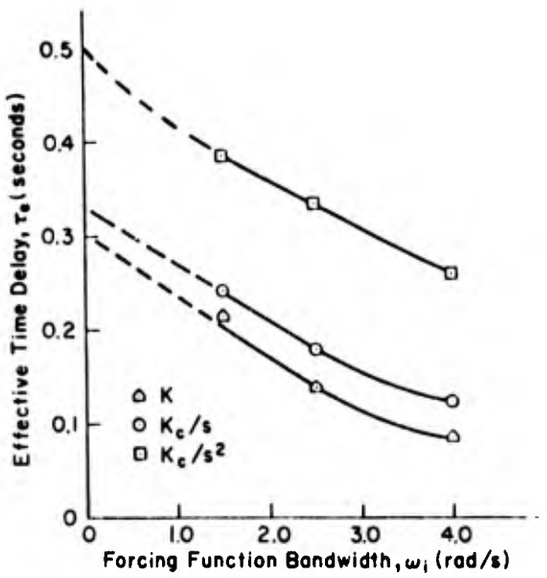

Figure 5. Variation of Effective Time Delay

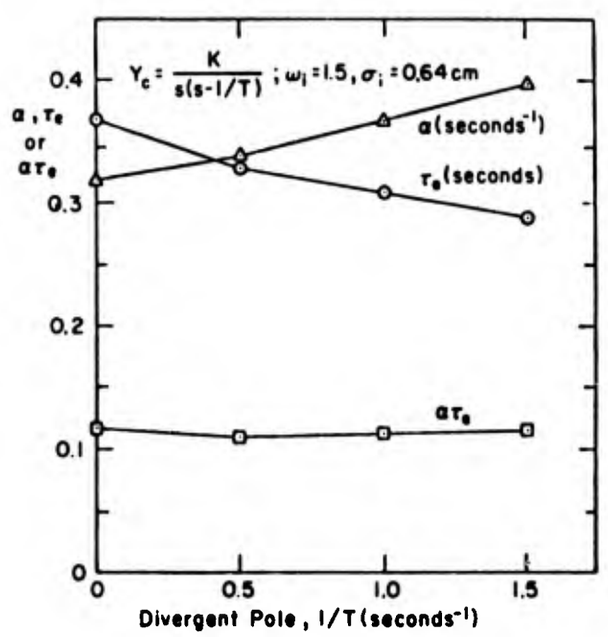

Figure 6. Variation of α, τ_e, and $\alpha\tau_e$ with 1/T

feedback system performance lead to the conclusion that the operator adjusts his describing function, Y_p, such that the open-loop function, Y_pY_c, in the vicinity of the gain crossover frequency, ω_c, has the approximate form

$$Y_pY_c \doteq \frac{\omega_c e^{-j(\tau_e\omega + \alpha/\omega)}}{j\omega} \qquad (3)$$

where τ_e is an effective pure time delay which includes the neuromuscular time constant, T_N, as well as τ and any net high frequency controlled element lag. The gain term, ω_c, is the crossover frequency. The operator adopts either proportional control, or lead or lag equalization such that the product of the equalization and the vehicle has the form shown, with which it operates on the perceived motion error. The numbers (ω_c, τ_e, and α) in the crossover model depend on the operator equalization. The crossover frequency is greatest and the effective time delay is least when the driver's equalization is a low frequency lag. Alternatively, ω_c is least and τ_e the greatest for low frequency lead. Thus the closed-loop bandwidth and performance will be reduced for low frequency lead and greatest when only lag is needed.

Driver Remnant. The remnant is that portion of the driver's output which is not linearly correlated with the input. It is considered to be an additional random process, often denoted by a power spectrum. Its major source appears to be nonstationarity in the operator's behavior (Ref. 3). For nominally good vehicle dynamics the remnant power is about 30 dB down relative to the input, and it can be neglected in predicting operator/vehicle closed-loop response characteristics.

Driver Response in Multiple-Loop Situations. Single-loop control as depicted in Fig. 4 is usually insufficient to satisfy the guidance and control requirements of the operator/vehicle system. In this case the operator will adopt a multiloop structure where he responds to more than one cue or a combination of cues. Experimental measurements (Ref. 6) of operator response in such a multiloop situation show that his describing function in the outer loop can be obtained by application of the single-loop model, above. The inner loops supplied by the driver act as equalization

for the outer loop, or provide feedbacks or crossfeeds which suppress subsidiary, undesirable controlled element degrees of freedom (vehicle motions). Because their role is so dependent on outer-loop requirements, the single-loop model rules are not generally applicable to the inner loops. Data indicates that the types of inner loops closed and their equalization are compatible with:

- Making outer-loop adjustments per the single-loop adjustment rules more feasible
- Reducing the sensitivity of the closed-loop system to changes in either inner- or outer-loop driver response
- Selecting a loop structure and equalization which gives best subjective opinion rating (Ref. 4)

It frequently happens that the driver describing function synthesized for the inner loop alone via the single-loop model is also the one which best enhances the outer-loop closures; particularly with a good stable basic vehicle, and a control task which is merely following command inputs or suppressing disturbances.

SECTION V

SYSTEM ANALYSIS AND SIMULATION

A. SINGLE-LOOP ANALYSES

A basic problem in describing, analyzing, and improving manual control of a vehicle is to determine what sensory feedback loops or cues the operator is using. There are two approaches to determining this operator/vehicle control structure:

- Experimentally, from perceptual studies which observe operator sensing and response
- Analytically, from a consideration of vehicle motions which must be sensed and commands which must be inserted to satisfy the guidance and control needs.

The first relies on experimental observation of dozing operations with extensive instrumentation, eye-movement camera, carefully defined input, etc.; and is relatively difficult. The analytical or control theory approach uses models of the operator and dozer to evolve good, "sufficient" systems and provide a basis for rejecting feedbacks or cues which do not satisfy the manual control needs. This does not lead to a unique solution, so the initial results are a number of "sufficient systems." Consideration must then be given to the operator's ability to perceive (sense) the vehicle motion and input quantities (e.g., blade height), and to the nature of the operations required on the sensed quantities in closing the loops. Those potential systems which involve readily sensed quantities and good system performance are then accepted as suitable candidates. These analytical results can be correlated with observations of dozing operations, comments of expert operators, etc. The analytical approach is relatively straightforward, given the current state of knowledge of typical operator/vehicle control laws and closed-loop analysis techniques.

It should be emphasized that representative manual control structures are being sought, not "the" structure. Any of several good alternatives will suffice. Within that structure, then, the effect of varying manipulator characteristics, adding artificial augmentation to the actuator

control system, improving the display (enhancing cue detection), etc., can be studied both analytically and experimentally with a simulation. Of course, one measure of a "good" improvement is one which is helpful with (insensitive to selection of) any of the several good perceptual structures. In fact, the operator probably employs some perceptual redundancy, and varies his attention to the several cues as the control task and situation (input, criteria, vehicle dynamics, etc.) change.

The task being analyzed is dozing with the operator controlling the suspension levers. Primary attention is given to motions such as blade height which should relate in some way to dozing. The throttle and steering wheel positions are assumed to be fixed. The operator is assumed to be controlling the roll or tilt angle of the dozer, also to keep it horizontal.

A study of the single-loop system possibilities has been accomplished, using the longitudinal and lateral dynamics of the tractor and the operator describing function of Sections III and IV. The quality of the resultant single-loop systems was judged by:

- The required operator equalization
- The attainable operator/tractor closed-loop performance in dozing
- The predicted subjective opinion of the operator as determined by the amount of lead equalization required, the sensitivity of the system characteristics to changes in his adaptation, the minimum gain for stable operation, etc.

A relatively low frequenc · forcing function was assumed, based on the data in Refs. 7 and 8 which show a terrain spectrum bandwidth of about 0.5 rad/sec. The results are given in Table III, and the individual analyses are given in Appendix C. The predicted system characteristics correspond most closely to a skilled, alert operator who is fully attentive and attempting to minimize the error in whatever motion he is controlling. Less skilled operators will have larger effective time delays, lower crossover frequencies, and lower possible stability margins. The increase in phase lag may make stable operation unattainable below a certain skill level — a common observation in practice. The phase lag

TABLE III

SUMMARY OF SINGLE-LOOP SYSTEM POSSIBILITIES

	FEEDBACK CUE	OPERATOR EQUALIZATION	τ_e (sec)	α (sec^{-1})	ω_c (rad/sec)	φ_m (deg)	K_m (dB)	K_{min} (dB)	$\tau_{e_{max}}$ (sec)	RELATIVE PREDICTED SUBJECTIVE OPINION	ABILITY TO SENSE	REMARKS
LONGITUDINAL DOZING CONTROL	c.g. height z_{cm}	Second-order lead	0.67	—	0.5	—	—	—	—	Uncontrollable	Poor	Combination of vehicle instability and α-effects make stable operation unlikely, despite lead
	Blade height Δz	$\frac{K(s+2.19)}{(s+0.68)}$	0.36	0.33	1.8	18	4.5	-6	0.53	Good	Good	
	Pitch angle θ	$\frac{K(s+2.19)}{(s+0.84)}$	0.36	0.33	1.7	22	8	-10	0.59	Fair, lacks reference	Fair	Poor for z_a disturbance input, operator can't "see" equivalent θ input
	Forward speed u	$K(s+2.19)$	0.36	0.33	2.0	0	2	0	0.36	Fair to poor	Good	Threshold may make it difficult to lead equalize
	Acceleration $\dot{u}$	$\frac{K(s+2.19)}{(s+1.5)}$	0.3	0.4	1.9	42	7	-6	0.69	Fair	Fair, vestibular	Vestibular cue; large threshold and may be more difficult to lead equalize
	Surload height h	$K(s+2.19)$	0.36	0.33	2.0	6	3	-3	0.42	Fair, (if sensed)	Fair	Sensed intermittently with present design
	Road arm a	K	0.3	0.4	2.0	45	9	-19	0.69	Fair, lacks reference	Poor	Operator can't "see" equivalent a, input due to z_a disturbance
	Acceleration $\dot{u} + g\theta$	$\frac{K(s+2.19)}{(s+1.5)}$	0.3	0.4	1.8	30	6	-7	0.59	Fair, lacks reference	Fair, vestibular	Operator can't "see" equivalent reference input. Vestibular cue; large threshold and maybe more difficult to lead equalize
LATERAL TILT-DOZING CONTROL	Tilt angle φ	K	0.36	0.33	1.6	46	7	-9	0.86	Good	Good	

ω_c is crossover frequency

φ_m is phase margin

K_m is gain margin

K_{min} is the allowable gain reduction for stable operation (at constant τ_e)

$\tau_{e_{max}}$ is the maximum allowable effective time delay for stable operation (at constant gain)

contributed by the tractor also increases (high frequency lead decreases) with speed, so that a less skilled operator can or must drive more slowly to retain stable operation. This is also observed during operator learning, and it is significant to have it verified from theoretical considerations. The relationship of dozing speed and skill suggests that the time required to perform a given dozing task should be a good performance measure in the field.

The results in Table III suggest possible single-loop systems for manual control as well as candidate inner loops for multiloop control by the operator. The table also identifies possible augmentation loops for automatic control. These would employ feedbacks which are difficult for the operator to sense, e.g., $\dot{u}$, a, or $\dot{u} + g\theta$.

B. MULTILOOP SYSTEM STRUCTURES

The best single-loop candidate for longitudinal control in Table III is blade height, Δz, because:

- It requires lag equalization which correlates with good subjective opinion
- It is easy to sense visually
- The reference input provided by desired terrain height is readily compared with blade height to determine blade height errors.

Other possible single-loop candidates include forward velocity, u, forward acceleration, and surload height, h, each of which appears inferior to blade height for one or more reasons.

The analyses, combined with preliminary simulation experiments indicate that a necessary outer loop is forward velocity (speed). If this loop is not closed, imperfections in the operator's control of other single loops, actuator leakage, etc., will cause speed to drift off in practice, usually resulting in the tractor stalling. Since forward velocity alone is only a fair loop, it is appropriate to consider the addition of an inner loop selected from among the single-loop possibilities already examined. The resultant multiloop system has the general structure shown in Fig. 7. Blade height is the likely inner-loop candidate since it was the best single-loop

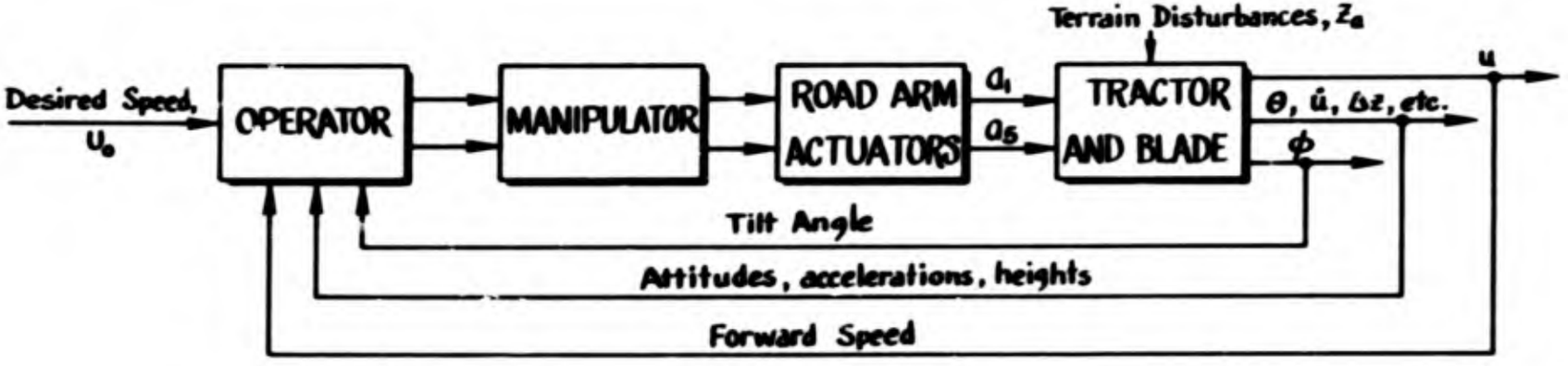

Figure 7. Multiloop Control Structure

system. Analyses (not included here) show that it does provide the needed lead equalization, permitting the outer velocity loop to be closed by the operator with simple gain equalization. Put another way, blade height is assumed to be the primary control loop based on the Table III results, and an outer forward velocity loop provides the needed trim to prevent low frequency speed drifts.

Note that other possible inner loops such as forward acceleration and surload height are not necessarily ruled out as ways of driving a tractor. Rather, blade height is a sufficient inner loop, and satisfies the present need for a good system structure within which to study the effect on operator control of modifying the manipulator. This then is one of the key results needed to prepare the simulation program.

The specific manner in which the operator can be expected to close the various loops is indicated in Fig. 8. It again contains the dynamics of the operator, the manipulator, and the controlled element. Lateral and longitudinal motions are assumed to be independent except for the common manipulators. Longitudinal control has a multiloop structure, involving a describing function for forward speed control, Y_{p_u}, which provides a reference for blade height control by the inner loop operator describing function, $Y_{p_{\Delta z}}$. This is a series operator structure. Control of roll in the lateral axis is accomplished by the operator describing function, Y_{p_ρ}. This multiloop control structure derived from control engineering principles is consistent with information obtained from motion pictures and discussions with equipment operators.

An alternate inner loop might be forward acceleration, $\dot{u}$, rather than blade height. This implies use of vestibular (otoliths) information by the operator and it cannot be simulated by motion cues in a fixed-base simulation such as the one used in this study. It was simulated using the visual modality, however. The analyses in Section III show that the dynamics of forward acceleration are quite similar to those of blade height. Thus, the blade height simulation also provides an approximate equivalent to forward acceleration if that is the dominant cue.

The way in which the operator might sense blade height is shown in Fig. 9. Blade height error, Δz, is the distance between the lip of the

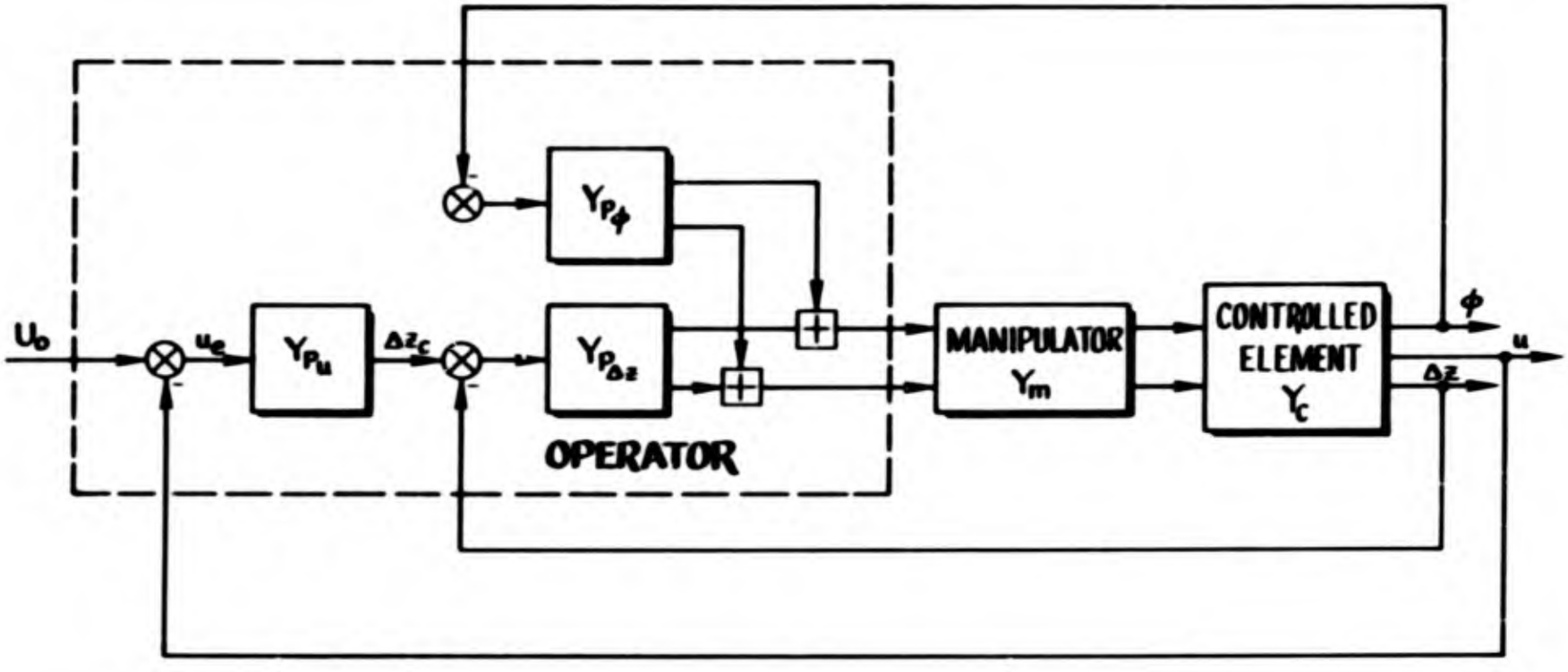

Figure 8. Estimated Operator Control Structure for the Study of Competing Manipulators

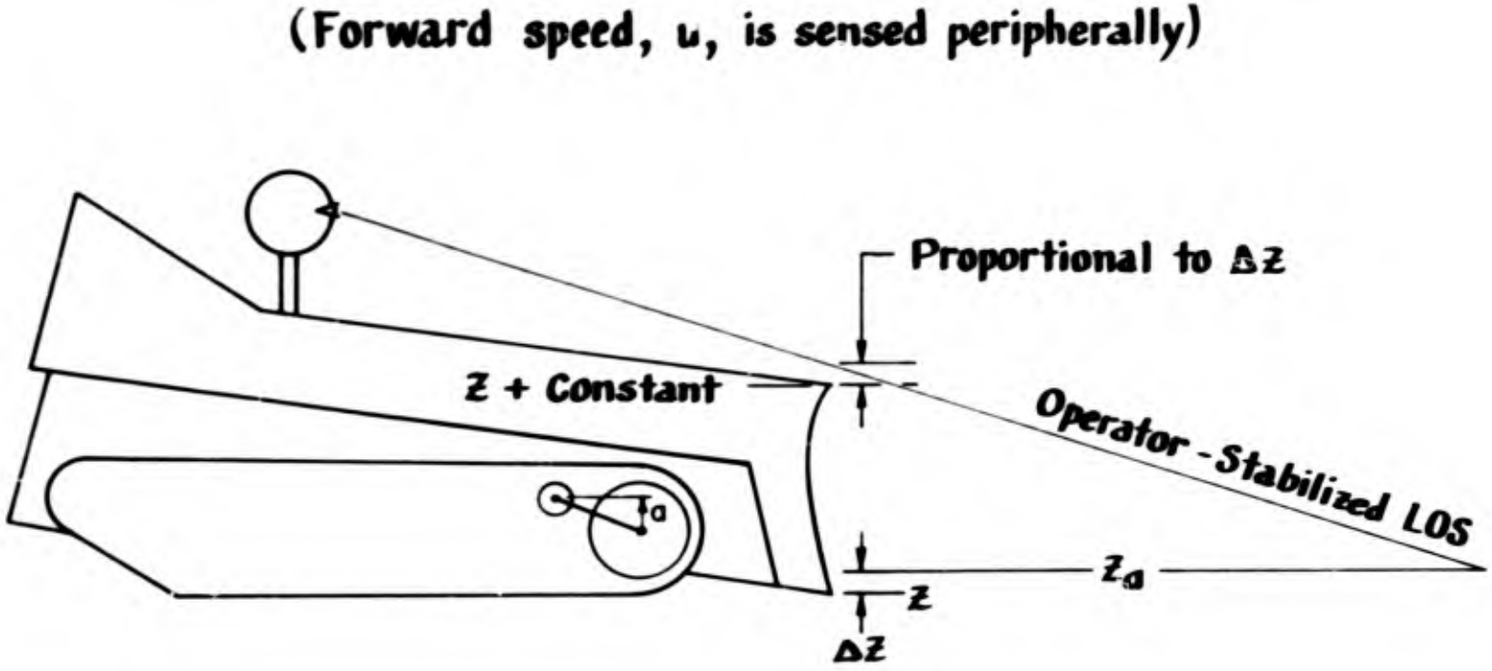

Figure 9. Possible Visual Sensing of Blade Height (Error)

blade and the desired height of the blade, corresponding to the desired terrain profile. The operator cannot see the lip of the blade in front of the tractor, but he can see the top of the blade which is proportional to the height of the lip. He might compare the top with an operator-stabilized line-of-sight (a relatively fixed line in space). As the blade top moves up and down he sees an error proportional to the blade height error at the bottom of the blade. Another possibility for blade height sensing would be to look at the edge of the blade on the left side and observe its motion relative to the terrain input.

The analyses and simulation use a nominal forward speed for the tractor of 2 ft/sec. The speed does have a significant effect on the closed-loop dynamics. As the tractor goes faster, the lags in the tractor and tool move to higher frequency and the limiting factor in the closed-loop system bandwidth becomes the operator's lags rather than those of the tractor. Thus, the faster the tractor goes the more difficult it is to control the dozing task, and one measure of operator skill level might be the speed that he can sustain. This is probably an obvious result in field practice, but it is interesting to have it confirmed from theoretical considerations.

One way of improving the "effective" controlled element is to add augmentation loops around the vehicle to change its effective dynamic response. In Fig. 8 this means adding additional feedback loops around the block labeled controlled element dynamics. The closed-loop system surveys of Appendix C indicate that forward acceleration would be a good augmentation feedback. This would modify the transfer function of the vehicle to reduce the need for operator equalization and ease the operator's control task. Stability augmentation systems are common in the aerospace field and have become increasingly evident in the more sophisticated land vehicles where the requirement for high performance compromises vehicle stability and handling.

C. SIMULATION AND MOCK-UP

The tractor mock-up and simulation consisted of three major portions: a wooden mock-up of the operator's control station in which different

electromechanical control lever mechanizations could be installed, the display, and an analog computer simulation of the tractor and hydraulic valve dynamic characteristics.

The display for longitudinal control contained blade height error and forward speed error (Fig. 10). The blade height error was presented as a horizontal line on a CRT about three feet in front of the seated subject. The line also tilted corresponding to the tilt or roll angle of the blade. The forward speed was displayed on a meter to the left of the subject in that region of the visual field corresponding to the left edge of the blade. A low level of ambient illumination was used to highlight the display presentation. Subjects who had also driven conventional dozers or the UET felt that a good level of realism was attained.

Subject familiarization and training were accomplished initially with a mock-up of the existing tractor manipulators. This consists of two suspension levers with the valve flow and force nonlinearities shown in Fig. 11. Once the subject had reached an asymptotic level of skill with the existing manipulator characteristics the first change was made. This involved linearizing the valve flow and force characteristics, but retaining the two levers of the standard configuration (Fig. 12). The next change was to use a single manipulator lever with two axes of motion. The first of these was an isometric stick (Fig. 13), which operated largely on force input and displaced very slightly. The second single manipulator was more isotonic, having a lower force gradient and displacing a couple of inches with the full operator input (Fig. 14).

The simulation also included augmentation mechanizations. The first augmentation scheme involved closing a road-arm-poisition to valve flow loop. This tended to maintain the angular position of the arm the same as the commanded position. It had the primary effect of eliminating the actuator leakage. A second augmentation scheme was to feedback the output of a pendulous accelerometer, $\dot{u} + g\theta$, to valve flow.

Simulation equations and details of the analog computer wiring are presented in Appendix D. The equations of Appendix D have been rearranged slightly to suit the analog simulation. The basic difference between the

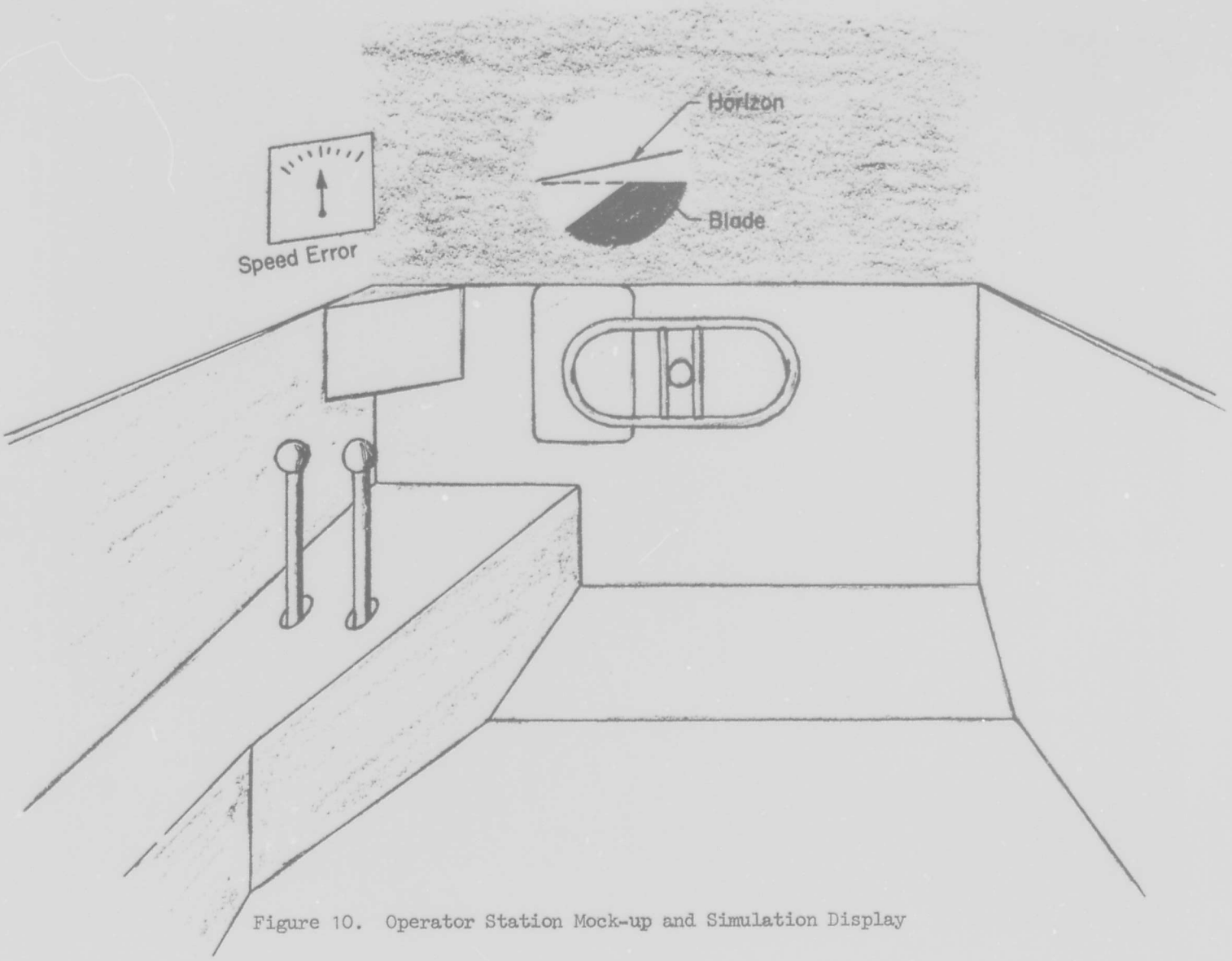

Figure 10. Operator Station Mock-up and Simulation Display

EXISTING TWO LEVER (EACH LEVER)

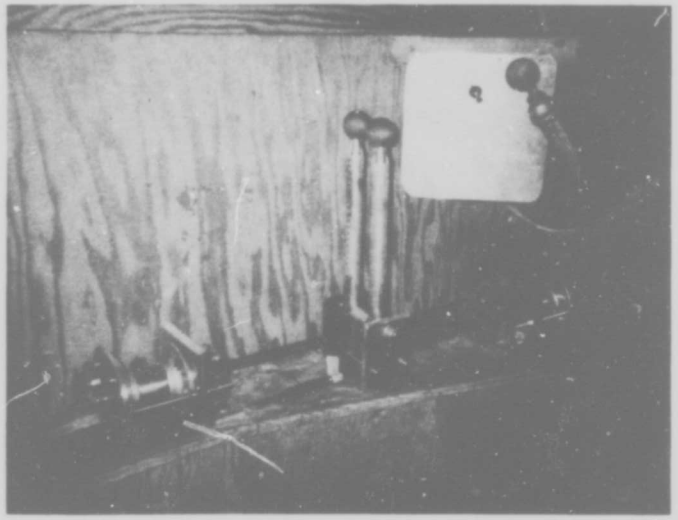

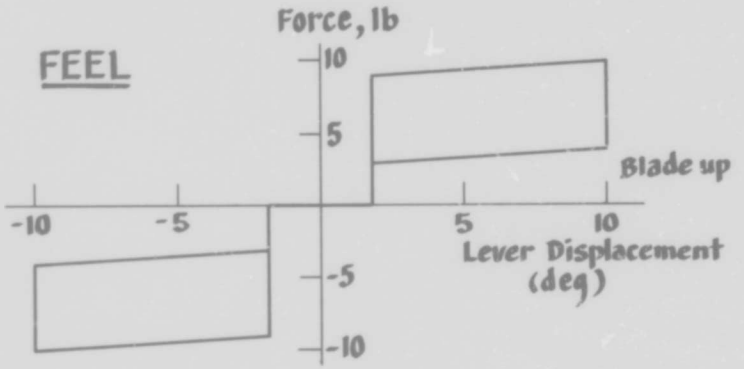

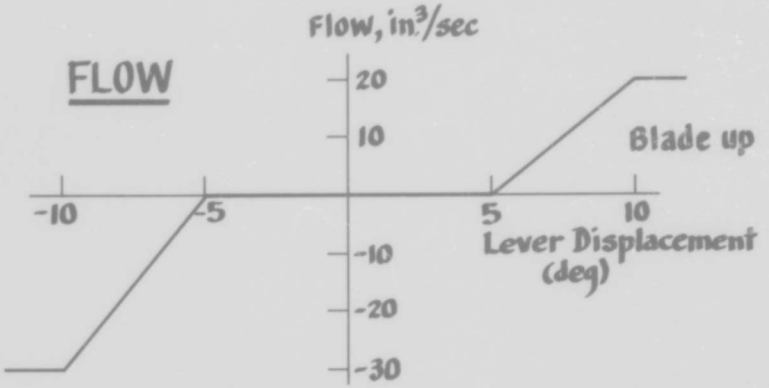

Figure 11. Existing Two Lever (Each Lever)

LINEAR TWO LEVER (EACH LEVER)

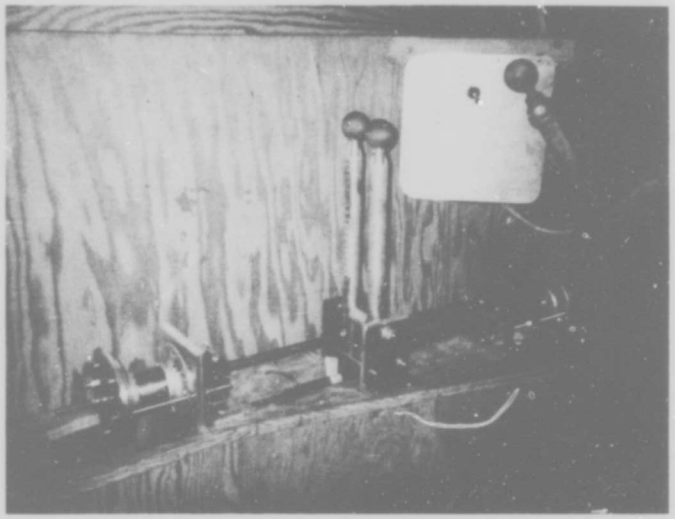

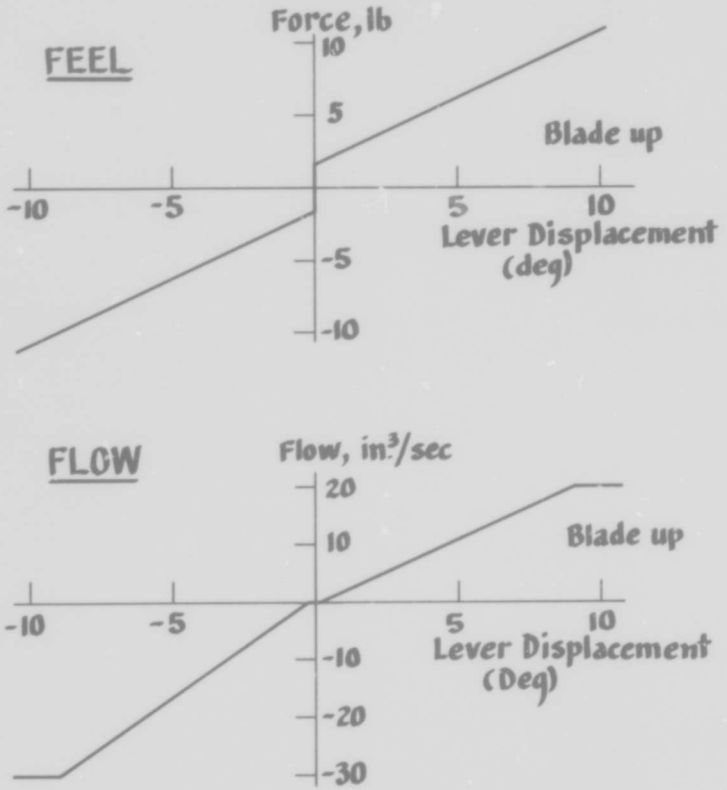

Figure 12. Linear Two Lever (Each Lever)

COMBINED, ISOMETRIC (BOTH VALVES)

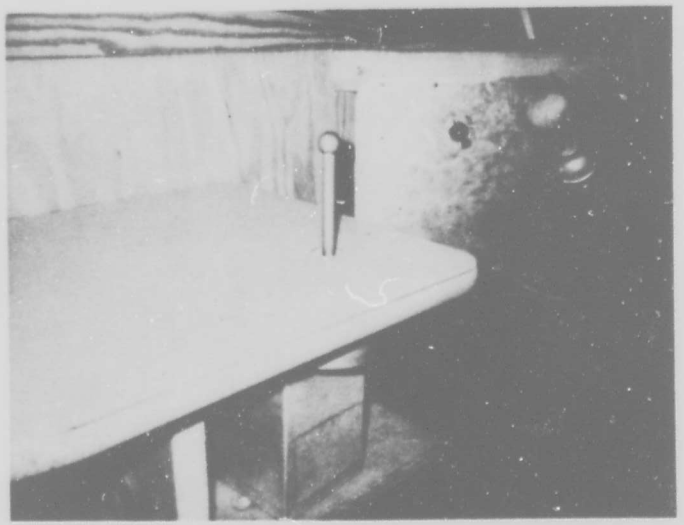

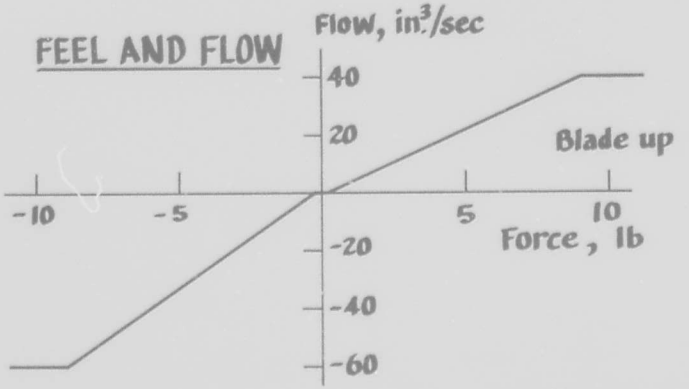

Figure 13. Combined, Isometric (Both Valves)

COMBINED, ISOTONIC (BOTH VALVES)

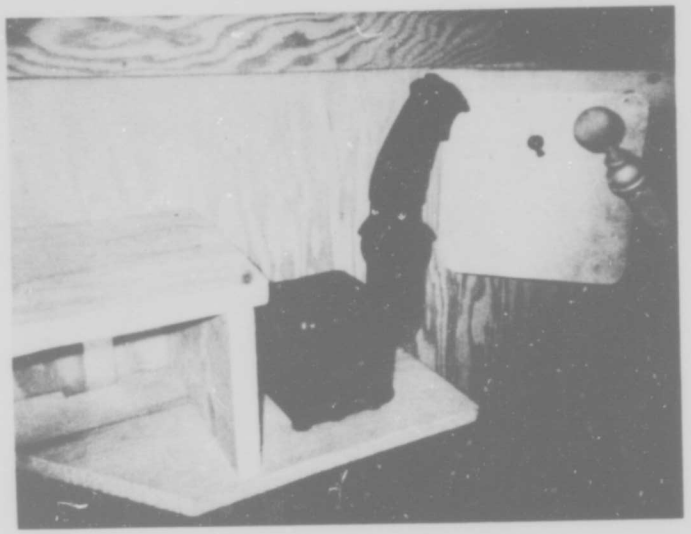

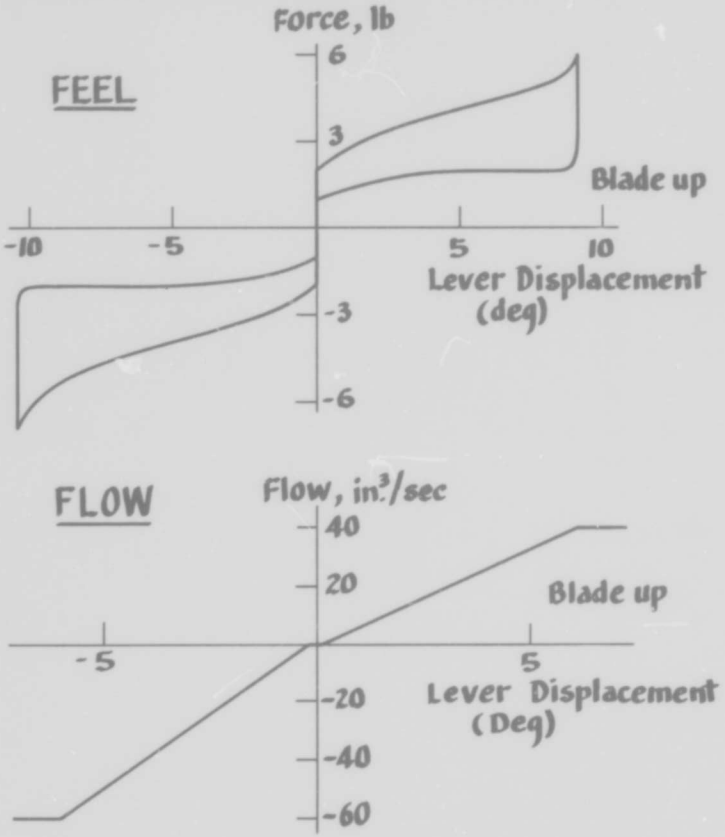

Figure 14. Combined, Isotonic (Both Valves)

equations in Appendix B and D is in the simulation of the kinematic pure time delays. A slightly different approximation to the time delay is used in Appendix D, to provide better response characteristics to discrete inputs such as steps. The differences are slight, however, for steady-state dozing control in the presence of random-appearing terrain inputs. For practical purposes, the dynamics used in the closed-loop analyses of Appendix C are the same as those used in the simulation.

D. EXPERIMENTAL PLAN AND RESULTS

The overall objective of the experimental program was to obtain measures of the relative merits of various manipulators and augmentation schemes in the simulated tractor dozing task. This section outlines the procedures followed and discusses the results obtained at each point in the experimental program.

One subject was used throughout the experimental program. He is a medium built, 27 year old male junior engineer with no prior experience as a dozer operator. He has driven automobiles regularly for about 10 years and has a good mechanical aptitude. He is probably typical of the good Army equipment operator trainee, and his early training runs in this simulation program showed learning characteristics similar to those evidenced at training schools such as the Navy's Port Hueneme. The staff engineers on the project also served as subjects for purposes of subjective evaluation. Table IV gives the general outline of the experimental plan.

The subject was asked to maintain forward speed and blade depth constant, and blade tilt at zero in the presence of a random longitudinal terrain disturbance, z_a. The disturbance had an rms level of 1.18 in. and consisted of the sum of 4 equal-amplitude sine waves with random phase:

$$\omega_1 = 0.1887 \text{ rad/sec}$$
$$\omega_2 = 0.3141 \text{ rad/sec}$$
$$\omega_3 = 0.5025 \text{ rad/sec}$$
$$\omega_4 = 0.8165 \text{ rad/sec}$$

The subject's instructions are reproduced in Fig. 15.

TABLE IV

EXPERIMENTAL PLAN OUTLINE

EXPERIMENTAL CONDITION	TITLE	AUGMENTATION
I	Familiarization, Standard Manipulator	None
II	Training, Standard Manipulator	None
III	Display Experimentation, Standard Manipulator	None
IV	Effect of Linearized Manipulator	None
V	Effect of Augmentation, Linearized Manipulator	Various
VI	Gain Experimentation, Isometric Manipulator	None
VII	Effect of Isometric Manipulator	Various
VIII	Effect of Isotonic Manipulator	Various

You are the operator of an Army engineer tractor, and the task is "dozing." The horizontal green bar shows the terrain height and tilt relative to the dozer blade. The vertical needle on the left indicates forward speed of the tractor. Both forward speed and blade height are controlled by the front suspension levers on the left. Pulling back a lever raises that side of the blade, and pushing forward lowers the blade. Pulling back a lever makes it go faster, and vice versa.

The purpose of dozing is to move the most soil in a given time. This is accomplished by keeping the speed constant at 2 ft/sec, and by keeping the blade height and tilt angle as close to the reference level as possible, i.e., following the terrain contour at a constant depth.

Figure 15. Instruction to Subjects

At the end of a run time of 100 sec the scores were noted, the computer reset, and a new run started. Generally speaking, 5 runs were made in quick succession, followed by a break during which the experimeter usually changed the task in some fashion (e.g., removed augmentation). At least 1 run out of every 5 was recorded in its entirety for subsequent analysis of operator control technique, etc.

During the first few runs the subject was unable to control (i.e., to maintain the simulation signals within the saturation levels of the computer amplifiers) the dynamics for more than a few seconds. As he became more proficient (after about 15 tries), the time durations during which he was able to maintain control were recorded; and finally, many runs later when control could be maintained for 100 sec, the scores were recorded. A running plot of these scores was kept so that the subject's proficiency, learning speed, etc., could be assessed. Performance scores were recorded for each experimental run. The integral of the absolute motion error was measured for each of the following:

- Combined lever motion, $\delta_R + \delta_L$
- Differential lever motion, $\delta_R - \delta_L$
- Blade height, $z - z_a = \Delta z$
- Forward speed, u
- Roll angle, ϕ

In addition to the performance scores, time histories of the operator control action in the tractor and blade motions were made for many of the runs to permit detailed analysis. These and the run-by-run performance scores are too voluminous to present here but are available in Ref. 12.

Comparisons of the performance with the various manipulator configurations are presented in Table V. No controlled element augmentation was included for any of these runs. The numbers in the table are the integral absolute errors as a percentage of some standard level of that motion, such as a full valve opening in the case of valve flow. Comparing the existing two lever performance with the linearized two lever performance reveals a significant improvement in performance and a reduction in the operator

TABLE V

EFFECT OF CHANGING MANIPULATOR

	PERFORMANCE MEASURE	MANIPULATOR CONFIGURATION			
		Existing	Two Lever, Linear	Combined, Isometric	Combined, Isotonic
LONGITUDINAL CONTROL	Combined Lever Activity (% of full valve opening)	83	21	14	23
	Blade Height Error (% RMS terrain variation)	58	34	29	45
	Forward Speed Error (% nominal, 2 ft/sec)	10	4.5	5	8
TILT CONTROL	Differential Lever Activity (% of full valve opening)	14	5	5	2
	Tilt Angle Error (% existing system value)	100	90	117	114

control activity or effort. Roll control results show a reduction in differential level activity but little change in the roll angle error performance. Proceeding to the combined isometric manipulator we see a further reduction in the lever activity and some improvement in blade height error. The forward speed error is about the same. In the last column, for the combined manipulator with isotonic characteristics, we see a slight increase in lever activity over the isometric case, and a considerable increase in the blade height error. The forward speed error also goes up. Examples of the run-by-run scores are shown in Fig. 16. These scores represent the integrated error voltages at the end of the runs. Because of different excitation voltages for the combined manipulators, the displacement scores shown in Fig. 16 cannot be compared directly and the results of Table V must be used.

The isotonic manipulator is worse than the isometric manipulator in these results primarily because of deficiencies in the former rather than any inherent advantage of isometric over isotonic. The isotonic manipulator was somewhat banged-up, and had considerable friction and free motion (see Fig. 14). It was perhaps more representative of well used Army field equipment than was the isometric manipulator which was a high quality laboratory device of more recent manufacture.

The roll or tilt control results show little difference between any of the manipulators, except that the differential lever activity with the existing two lever configuration is higher than that with any of the others. The tilt angle error performance scores are essentially the same. The isometric result is somewhat poorer, because of cross talk between axes in the manipulator. This cross talk could be eliminated in a prototype by an electrical deadband. The tilt angle performance is more a reflection of the operator's threshold of indifference rather than any manipulator effects. The important point in tilt angle control is that the basic controlled element dynamics are pretty good so that a degraded manipulator does not change the performance particularly.

The overall experimental results are summarized in Table VI. It has columns for the various manipulator configurations and rows for the various feedbacks, including none. The configurations are rated on the basis of

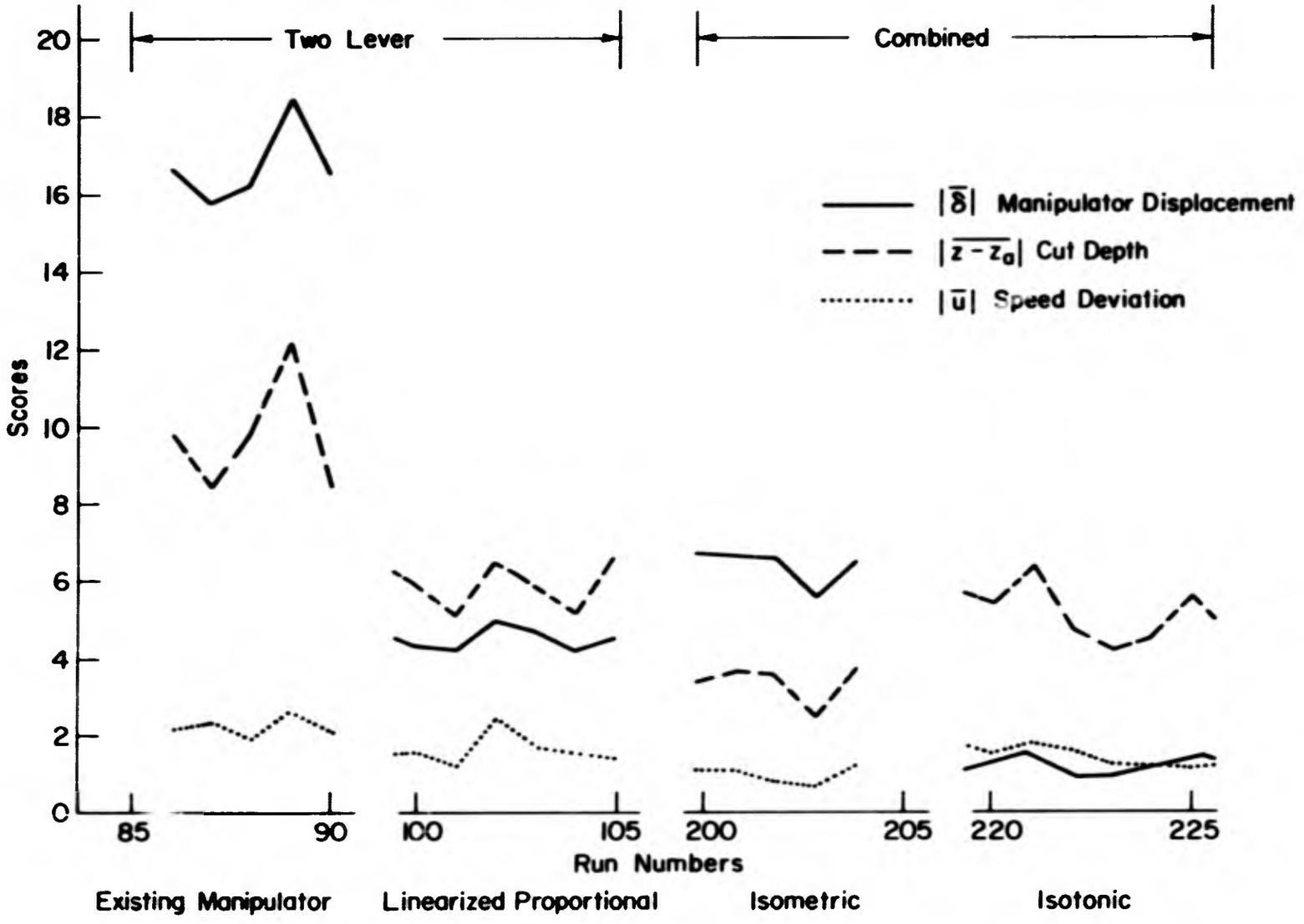

Figure 16. Effect of Manipulator Characteristics

TABLE VI

OVERALL EXPERIMENTAL RESULTS

FEEDBACK		MANIPULATOR			
		Existing	Two Lever, Linear	Combined, Isometric	Combined, Isotonic
None	P	Poor	Average	Average	Estimated Average*
	Op	Difficult	Easy	Easiest	Easy
	M	Mech valve	Mech or EH valve	EH valve	Mech or EH valve
Roadarm Angle ($a \rightarrow Q$)	P	—	Average	Average	Average
	Op		Moderate	Moderate	Moderate
	M		EH valve + arm sensor	EH valve + arm sensor	EH valve + arm sensor
Acceleration ($\ddot{u} + g\theta \rightarrow Q$)	P	—	Good	Best	Good
	Op		Easy	Easy	Easy
	M		EH valve + accelerometer	EH valve + accelerometer	EH valve + accelerometer

Legend: P — Performance
Op — Operational difficulty, workload
M — Mechanizational complexity

performance, operational difficulty (or workload), and mechanizational complexity. The performance ratings for the no feedback case are a condensation of the numerical results presented in Table V. The operational difficulty, or workload, was assessed on the basis of the lever activity and concentration required by the trained operator and the ability of untrained subjects to control the vehicle in the same task (100 seconds or more simulated dozing). These untrained subjects were allowed approximately five attempts at controlling each configuration. For the untrained operators, difficult indicates they could not maintain control, moderate indicates they could maintain control but had appreciable error score, and easy indicates they could maintain control with small error score. Thus this might be a measure of relative training time that would be required for new tractor recruits.

As before, with no feedback, the isometric manipulator was the easiest to operate, but its performance was about the same as the linearized two lever version. The combined isometric manipulator requires an electrohydraulic valve, whereas the two lever linear version and the combined isotonic version could be mechanized with either a mechanical or electrohydraulic valve. The first augmentation shown is road arm angle. It shows no improvement in performance over the no-feedback case. More significantly, the operational difficulty actually goes up — it is only "average" compared to the "easy" results for the no-feedback case. Road arm angle feedback requires at least a sensor for arm position plus an electrohydraulic valve. The next table entry involves feedback of a pendulous accelerometer output to flow rate. As an inner loop, this results in good performance and is easy to operate. The best results were achieved with the isometric manipulator. This mechanization involves an electrohydraulic valve and an accelerometer. Again, simple run results are shown in Fig. 17. As in Fig. 16, the deflection scores cannot be directly compared between the two lever and combined manipulators because of voltage level differences.

The acceleration feedback tended to be good for the simulated dozing task, which was to hold speed constant and cut at a constant depth. For other tasks, e.g., making a horizontal cut with varying depth of soil, this feedback could be less desirable and it may tend to oppose operator

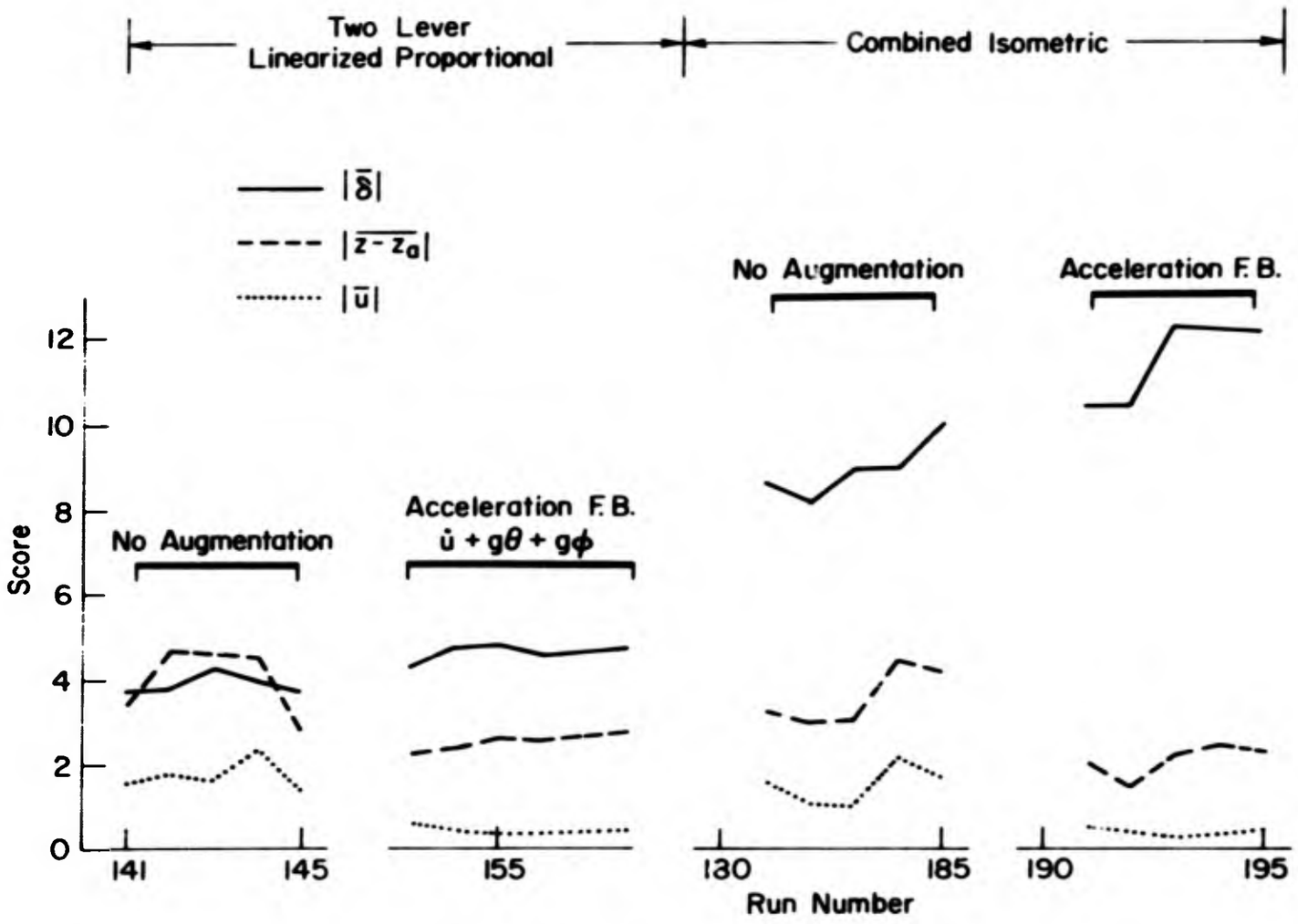

Figure 17. Effect of Stability Augmentation

control actions. Such opposition could be overcome, of course, by appropriate washout of the electrical signals.

E. LOAD FEEDBACK

Load feedback from the blade (tool) to the manipulator was not simulated specifically, but it was considered. The distinguishing property of load feedback is that it is nonvisual. It is closely related to feeding back acceleration, which was studied, because load and acceleration are proportional. It is commonly called "force feedback," but it can involve other tactile inputs through the hand, or some other nonvisual mode, e.g., auditory. Load feedback has some potential for dozing tasks, particularly under adverse conditions of weather, combat, visibility, etc. However, a feedback which involves kinesthetic, tactile, or auditory sensing by the operator introduces additional problems of design and operation, i.e.,

- A force, displacement, or sound level must be maintained proportional to the load; can be tiring to operator.
- The washout characteristics (time decay in sensitivity to a constant stimulus) of the human sensory system would result in imprecise control.
- The mechanization would be considerably more complicated particularly in view of the operational environment of the UET (open to elements, arctic clothing, noise, etc.).
- Vibration may adversely affect tactile or kinesthetic force feedback.
- It may be poor when pulsing control activity is required due to higher order lags in the controlled element.

It is clear from the experimental results presented above that properly tailoring the manipulator with good visual cues can provide substantial improvement in tractor control. The additional gain provided by load feedback is not expected to be significant for common dozing tasks under normal visibility conditions.

SECTION VI

PROTOTYPE DESIGN CONSIDERATIONS

A. SYSTEM CONFIGURATION

The preceding analysis and simulation indicated several desirable controller mechanization properties and changes. The simulation also provided laboratory verification of improvements that could result. The mechanizational changes in order of improved performance are:

1. Linearization of the present two-lever/valve control characteristics such that rate of change of road arm height is proportional to lever deflection.

2. Integration of the two levers into a single two-axis side-arm controller with the above linear (proportional) control properties in each axis.

3. Incorporation of a stability augmentation system utilizing forward acceleration feedback.

The major improvement stems from elimination of nonlinearities in the control device, including the elimination of bang-bang operation and substitution of proportional control. The last change decreases the order of the task dynamics as seen by the operator and further simplifies the control task.

Leakage causes biases which increase operator workload. Nevertheless, these improvements are pertinent whether or not leakage is present. This study was not concerned with reducing leakage, but that would lead to additional improvements.

Redesign of the existing valves and linkages to obtain proportional flow control and minimize nonlinearities is not considered practical. It is difficult to design valves so that the various forces (Bernoulli, spring, etc.) approach the ideal characteristics. In addition, the maintenance of minimum nonlinearities in linkages in the presence of accumulated dirt, grit, rust, wear, etc., from normal and extended field operations would involve unrealistic maintenance and adjustment requirements. From this standpoint, it is desirable to minimize or eliminate mechanical linkages between the manipulator and the valves. An electromechanical manipulator feeding electrical signals to an electrohydraulic transfer valve is ideal

under such circumstances. Mechanical linkages are eliminated and the valve provides linear flow versus electrical input. The force-producing system can then be built directly into the manipulator and the desired forces or force gradients easily controlled and/or modified. Furthermore, this type of manipulator-valve system is fundamental to a stability augmentation system such as acceleration feedback.

The two-lever manipulator, while acceptable in control of pitch attitude of the vehicle with no actuator leakage, proved awkward to operate differentially in control of roll attitude. This was especially noticeable with different leakages in the two-front actuation systems. The two-axis side stick allowed faster and more natural response in correcting for roll disturbances, uneven leakage, etc. All things considered, there was little difference between the isometric and isotonic manipulators in this study and simulation, even though other simulations (e.g., Ref. 13) have shown the isometric manipulator best for simple tracking tasks in a laboratory environment. However, the prototype control system is not intended for use in a lab and the actual vibration and jostling environment of this vehicle in its intended usage could result in control difficulty unless special precautions are employed. Inadvertent inputs can be reduced by incorporation of electrical breakout characteristics and appropriate arm support, but even so it is difficult to eliminate all jostling effects. It would appear easier to support the operator's arm and hand to minimize movement of the hand in the presence of jostling, than to minimize or eliminate force (i.e., force or pressure just due to mass inertia of the operator's hand in the jolting environment). An evaluation, Ref. 14, of side-stick characteristics in actual flight (vibration, turbulence, etc.) indicates that pilots preferred the isotonic with moderately stiff breakout and force gradient to avoid inadvertent inputs since low breakout and force gradients allowed actual hand movements (hence inadvertent inputs). Therefore, the isotonic stick with appropriate breakout force and force gradient is the first choice for this application.

Although the forward acceleration augmentation system afforded improved speed and blade height control for the dozing task analyzed here, its effect on other tractor tasks and roles should be thoroughly investigated before it is seriously considered for incorporation in the vehicle. For example,

this feedback might prove detrimental in such tasks as clearing large stumps, rocks, etc., since any contact with a large object which tends to decelerate the tractor will result in the blade being raised automatically by the acceleration (deceleration) feedback. The operator would then have to maintain a displacement of the manipulator (electrical command) to offset this feedback, which only occurs while the tractor is accelerating or decelerating. This also could give problems with throttle-induced speed changes because the blade would automatically lower or raise unless the operator coordinated displacement of the manipulator handle with the throttle. Conversely, such automatic operation might relieve the operator of some control actions on initiating and stopping constant throttle cuts, might provide smoother operation, and hence be beneficial. Thus it is felt that further study is necessary before such augmentation is actually tried. Finally, the incorporation of any automatic feedback will require a detailed dynamic analysis and test of the vehicle hydraulic system itself, in particular the actuators, to assure achievement of closed-loop system stability. Such analysis and testing is beyond the scope of the present contract effort. However, it is felt that the augmentation schemes investigated here hold sufficient promise for the future that this prototype system should contain provisions for later incorporation of augmentation.

In summary, the major features of the prototype control system should include a single manipulator lever (integrated two-axis) with arm support for the operator, an artificial feel system consisting of a breakout force followed by linear force gradient proportional to manipulator displacement, hydraulic fluid flow directly proportional to lever displacement, and provision for future augmentation feedbacks. The block diagram for a single axis would thus be of the form shown below.

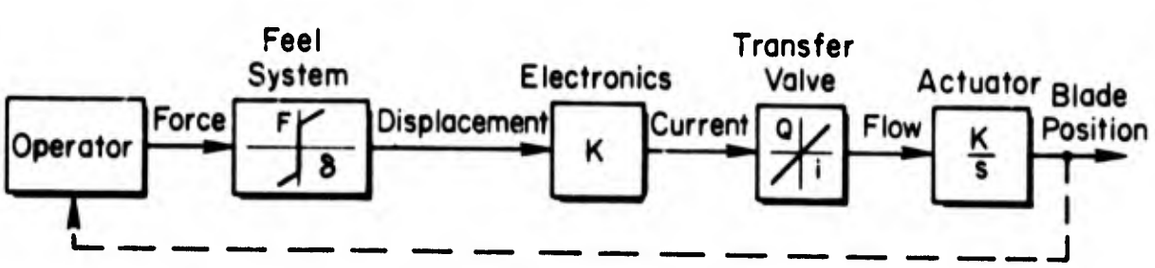

Another feature which could ease the operator's task is a trim capability to automatically offset leakage within the hydraulic actuators. Leakage is a function of the vehicle load (ballast) and actuator condition (wear). The heavier the load and the greater the wear — the greater the leakage. This results in the actuators not holding the commanded road arm position, i.e., the front of the vehicle settles and the blade digs in. Leakage generally will not be equal on both sides of the vehicle, so it also will roll. An adjustable trim input to each of the electro-hydraulic transfer valves would allow the operator to bias a steady flow of hydraulic fluid from the transfer valves to the actuators to exactly match or cancel the leakage within the actuators. Thus the operator would not have to continuously "pump" the side stick to counteract the settling and rolling tendency due to leakage.

The prototype controller unit which incorporates all of these features is shown in Figs. 18 and 19. Figure 18 is the integrated manipulator, arm rest, and electronic assembly. Figure 19 presents the complete system in functional schematic form. These are discussed in more detail in the following sections, and preliminary specifications are presented in Appendix E.

B. HUMAN FACTOR CONSIDERATIONS

1. Manipulator/Arm Rest Location

Results of the analysis and simulation indicated the prototype manipulator should have the two-axis control integrated into a single manipulator, that is, one lever or grip which has 2 degrees of freedom to allow control of collective or differential front road arm angles. The simulation also indicated that an arm rest would be required. However, these requirements are only the beginning. To be fully effective in improving man-machine performance, the manipulator configuration and location must be designed with the physical characteristics of the operator in mind. General operational considerations dictate the lever position should be tailored for operation from either the sitting or standing position, for operation in extreme environments, should not be tiring to the operator, etc. Accordingly, the prototype manipulator is configured on the human factors data and recommendations contained in Refs. 15, 16, and 17, for example.

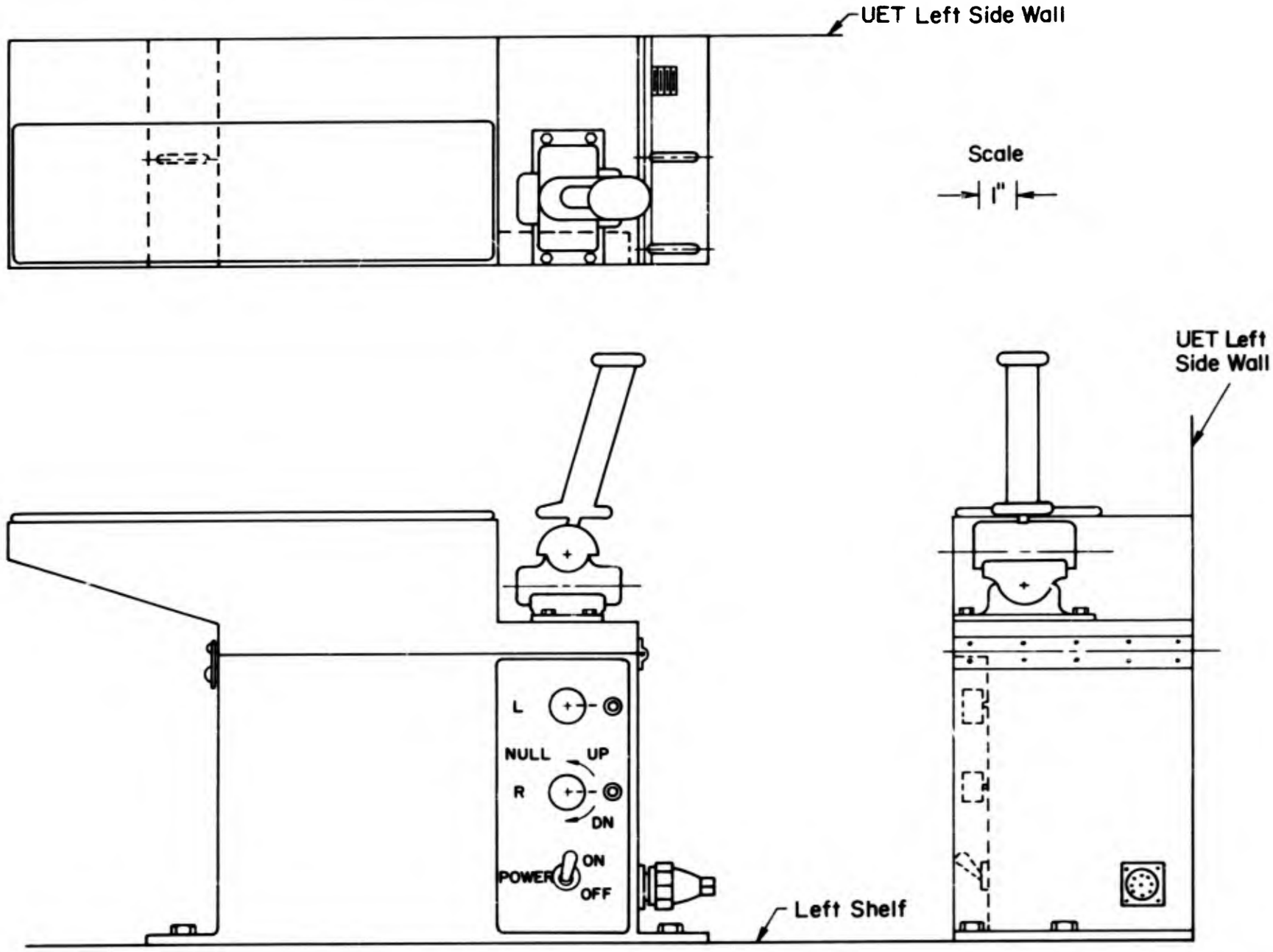

Figure 18. Prototype Controller Unit

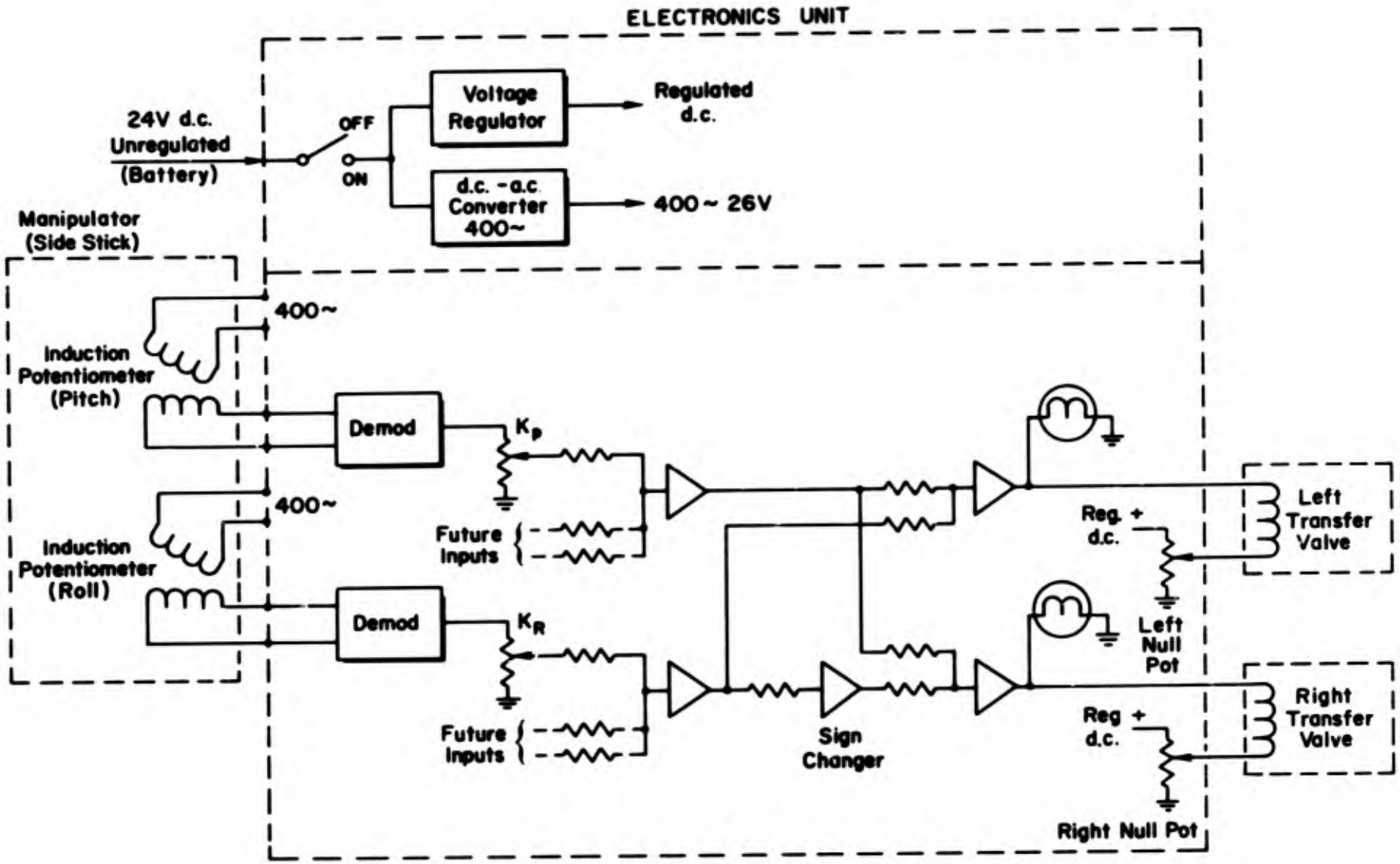

Nominal Gain : 1.5 ma output/deg induction pot input (Pitch and Roll)
Gain Adjustment : K_p, K_R variable 0 → 3.0 ma/deg
Induction Pots : Input: 26V , 400~, 39 ma , 0.25 watt
Output Transformation Ratio: 2.308
Transfer Valves : ± 15 ma , 200 Ω

Figure 19. Functional Schematic, Prototype Control System

Figure 20 is a layout of the present operator station of the UET-E4 based on information provided by MERDC. The seat height and seated operator size represents the 95th percentile (large) human dimensions given in Ref. 15. The seat fore-aft position represents the midposition of seat travel for the UET-E4 and is approximately the most forward position that can be achieved without the 95th percentile operator's knee hitting the steering wheel. To manipulate the control levers, the operator must reach forward approximately 3 in. and rest his left hand on the top of the levers so that his arm makes about a 130 deg angle at the elbow. This position is considered acceptable by Ref. 18. There is no arm support in the present vehicle.

A 5th percentile (small) operator would have to move the seat to the full forward position (approximately 2 in.) and would still have to reach forward 3 in. to grasp the top of the levers.

Figure 21 indicates the proposed layout for the integrated manipulator and arm rest configuration for the same 95th percentile operator. The present lever position is shown for comparison. For this prototype manipulator location, the operator's arm would be in a more natural or relaxed position at his side, with the arm making a 90 deg angle at the elbow — the optimum position per Ref. 16. In order for this operator to make use of the arm rest, he would have to lower the seat approximately 2 in. The 5th percentile man, however, would leave the seat at the height shown for his forearm to contact the arm rest. He again would move the seat forward 2 in. so his hand would contact the manipulator handle and with the arm at the same natural position at his side.

Figure 22 indicates the integrated manipulator for the 95th percentile operator in a standing position. Again the seat, present levers, etc., are shown in the same position as Figs. 20 and 21 for comparison. In the standing position the operator's arm hangs straight down or slightly back to grasp the manipulator handle.

2. Manipulator Design

To assist in properly configuring the manipulator handle, Fig. 23 indicates the dimensions of the 95th percentile hand (again from Ref. 15) with

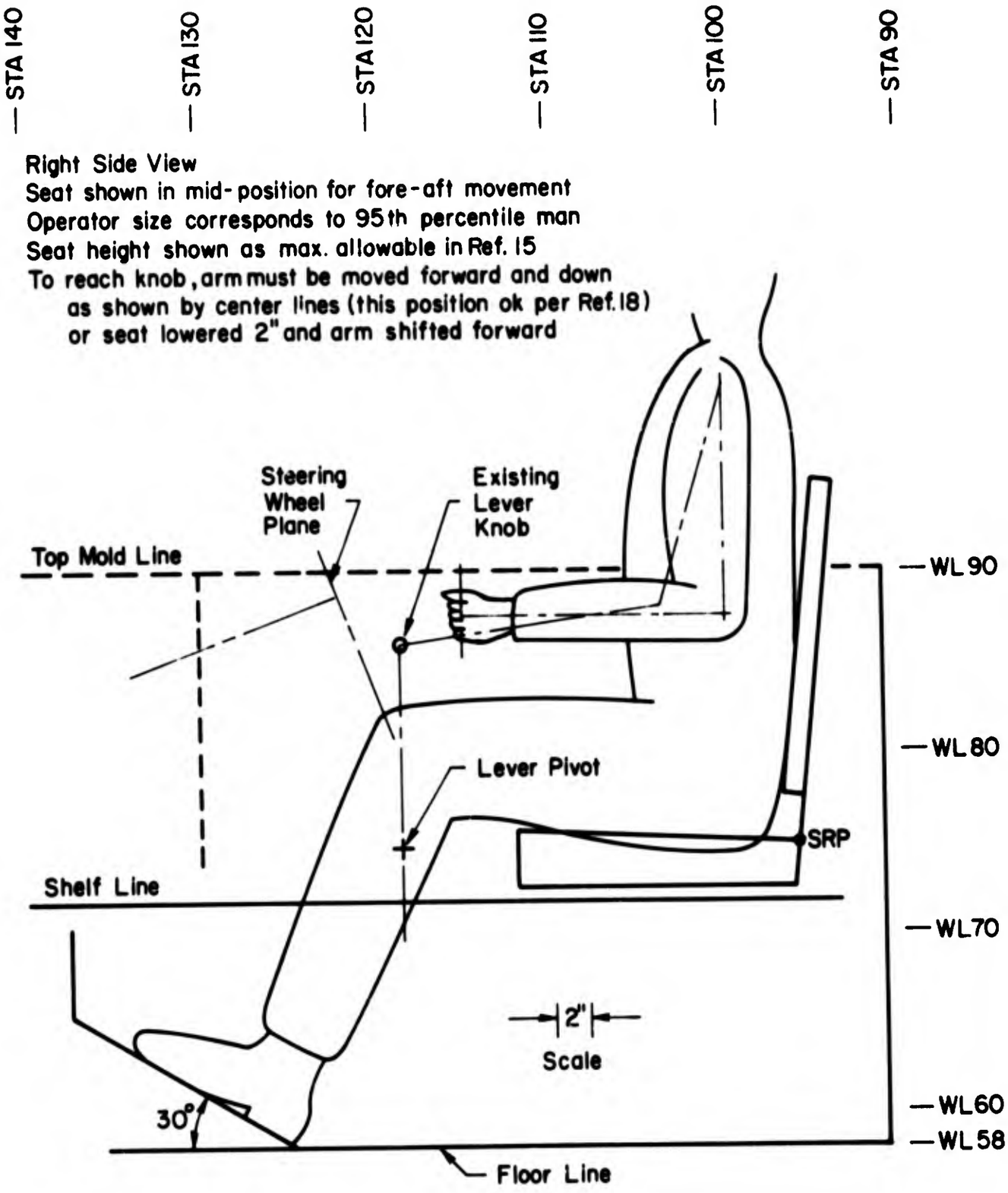

Figure 20. Present Operator Station

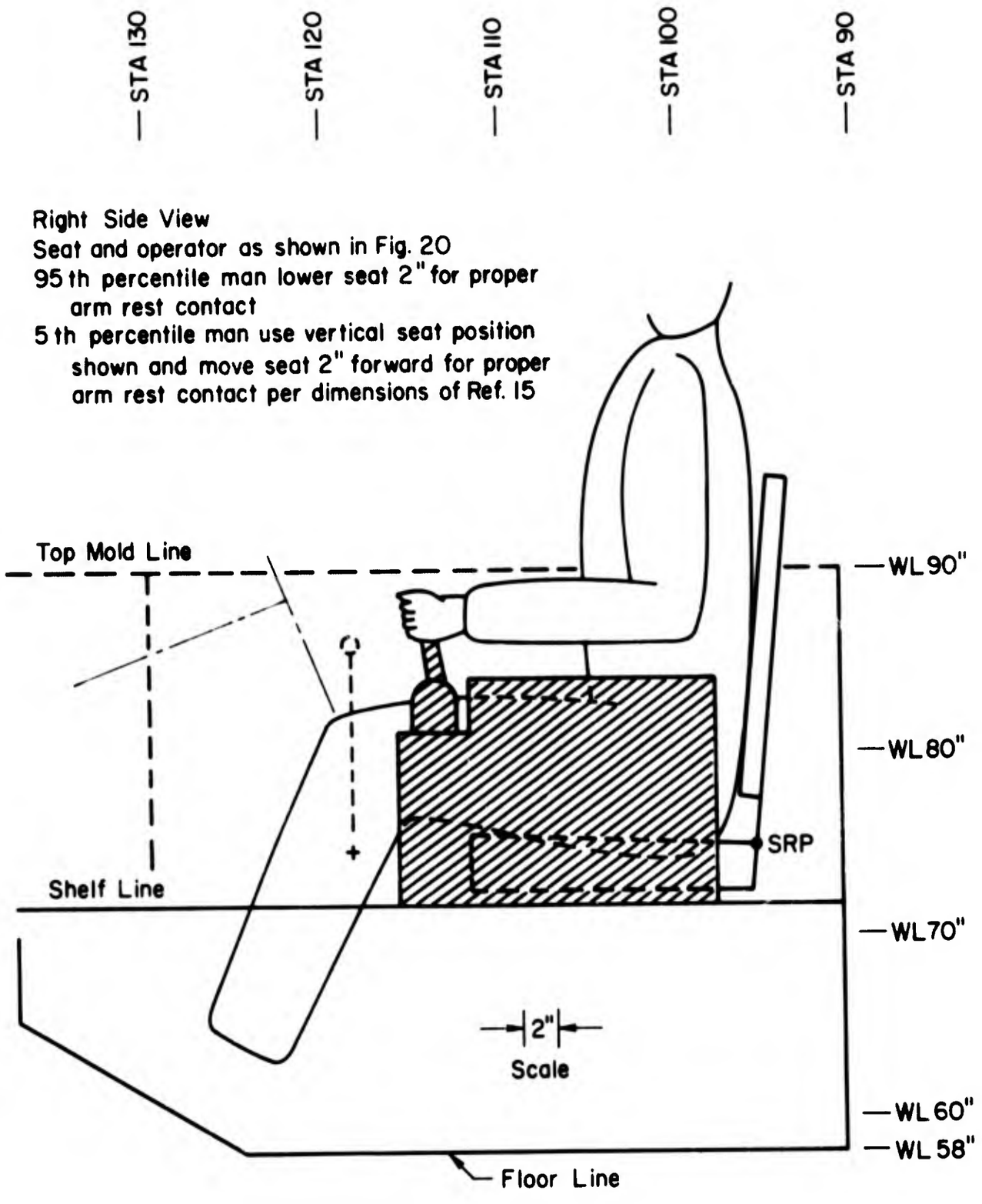

Figure 21. Proposed Operator Station — Seated

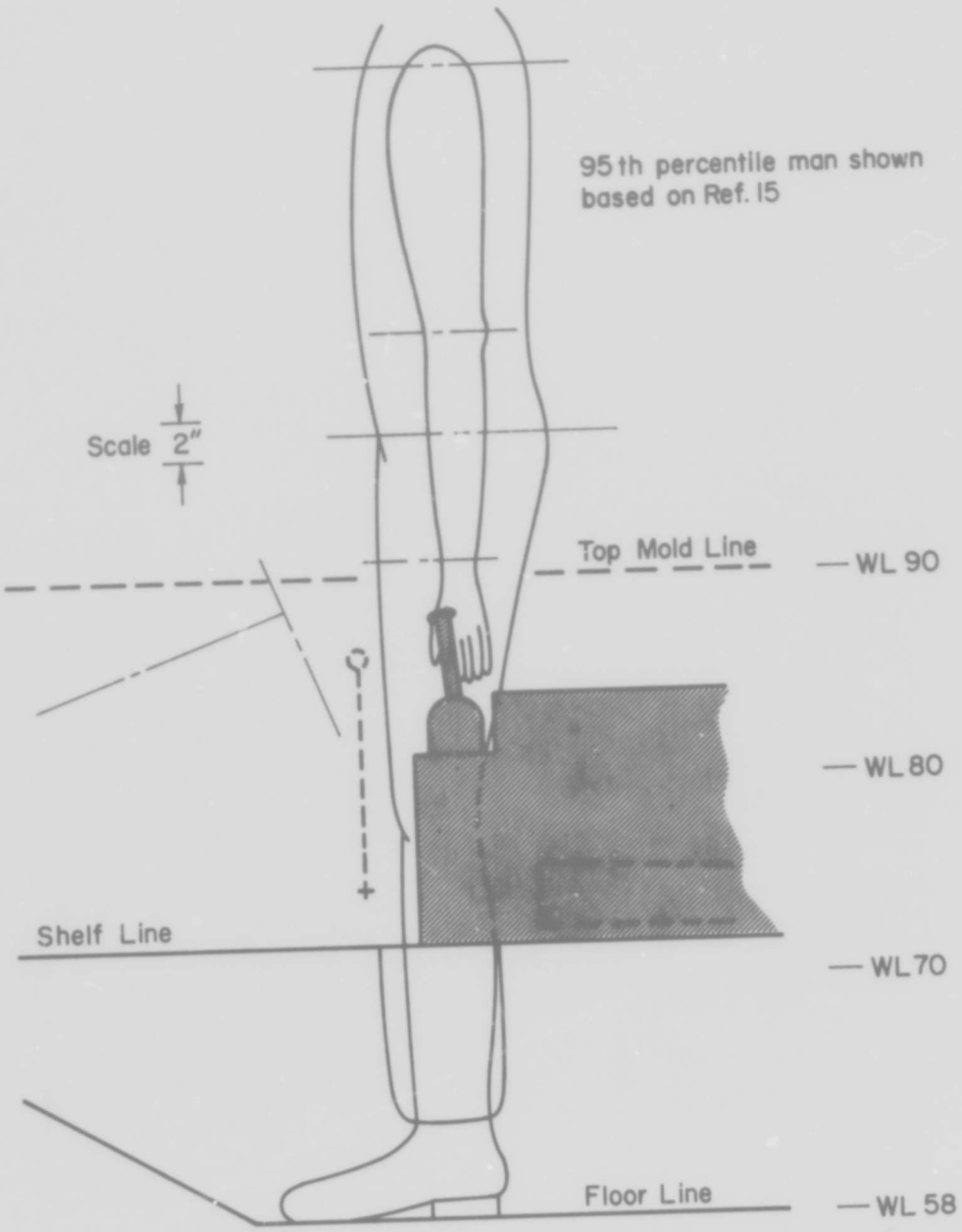

Figure 22. Proposed Operator Station — Standing

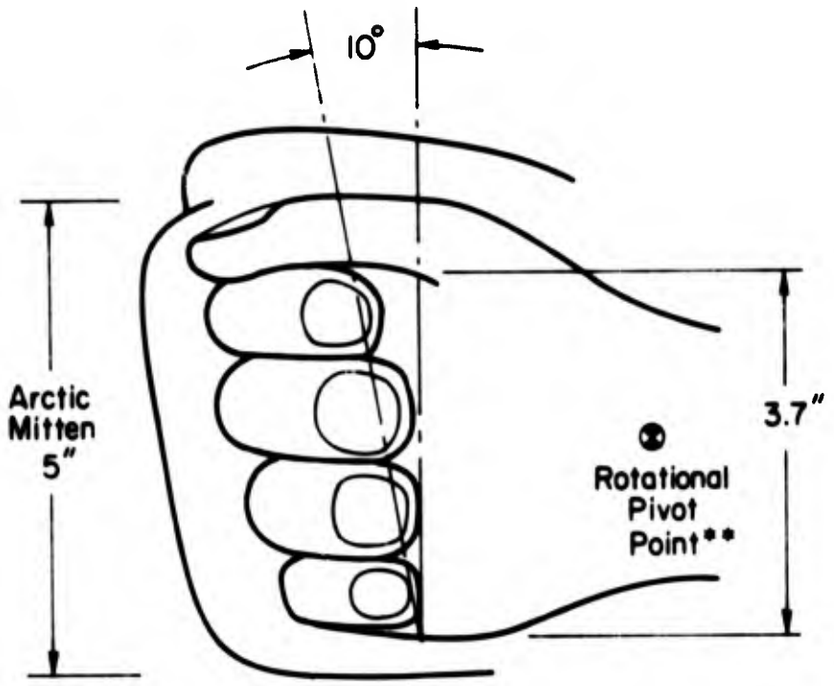

Figure 23. Dimension of 95th Percentile Hand Width With and Without Arctic Mitten*

*Ref. 17.

**Ref. 14.

an arctic mitten (dimensions from Ref. 17). This figure shows the manipulator handle must have a length of at least 5 in. in order that the operator may comfortably grasp it when wearing arctic clothing. Figure 23 also indicates the effective pivot point for wrist rotational movement obtained from the study of side arm manipulator requirements reported in Ref. 14. The latter study also showed that the manipulator should be tilted approximately 10 deg forward of the vertical for natural fit into the palm of the hand. This not only results in a comfortable grasp of the manipulator, but affords a more comfortable combination of wrist and arm motion to rotate the manipulator about an axis slightly below the hand or arm. The results of Ref. 14 also indicated the operator's preferred manipulator rotational freedom of ±5 deg in pitch and ±10 deg in roll. However, in controlling the UET simulator, the operators preferred equal throw (±10 deg) in pitch and roll.

A layout of a grip type manipulator incorporating all of these considerations is shown in Fig. 24. This grip also provides a wide flare at the base to support the bottom of the hand. While the grip design of Fig. 24 should be a great improvement over the present lever system for the seated operator, it is not optimum for the standing operator because he must grasp the top of the manipulator (as with the present lever). Although somewhat awkward, this is not considered serious since the operator rarely stands during dozing tasks (it is difficult to maintain one's balance in the jostling environment, it is also more tiring, and of course it is impossible if the cabin hatch is closed).

For the prototype installation an alternate manipulator configuration might also be fabricated and evaluated which may offer some advantage to the standing operator without seriously compromising the seated operator. Figure 25 presents a T-bar manipulator configuration that would be easier for the standing operator to grasp. In this configuration the manipulator's axes of rotation are reoriented so that the roll axis is coincident with the seated operator's wrist rotational pivot point (Fig. 23). Thus the seated operator controls differential road arm position (roll) by lateral wrist motion and controls collective (pitch) by fore-and-aft arm movement. In the standing position roll control is accomplished by forearm rotation. This type of manipulator was not evaluated in the UET simulator

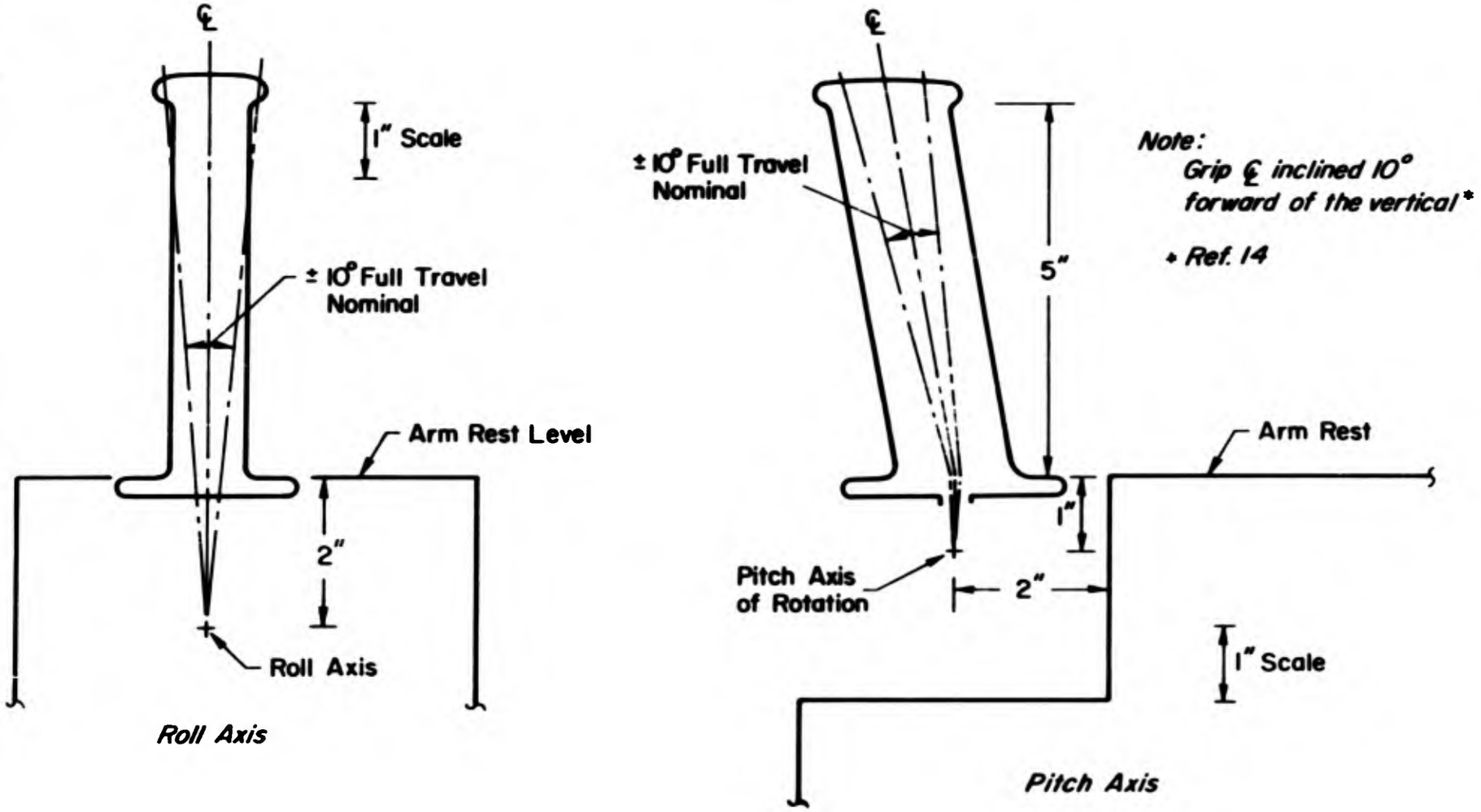

Figure 24. Grip Type Manipulator Configuration

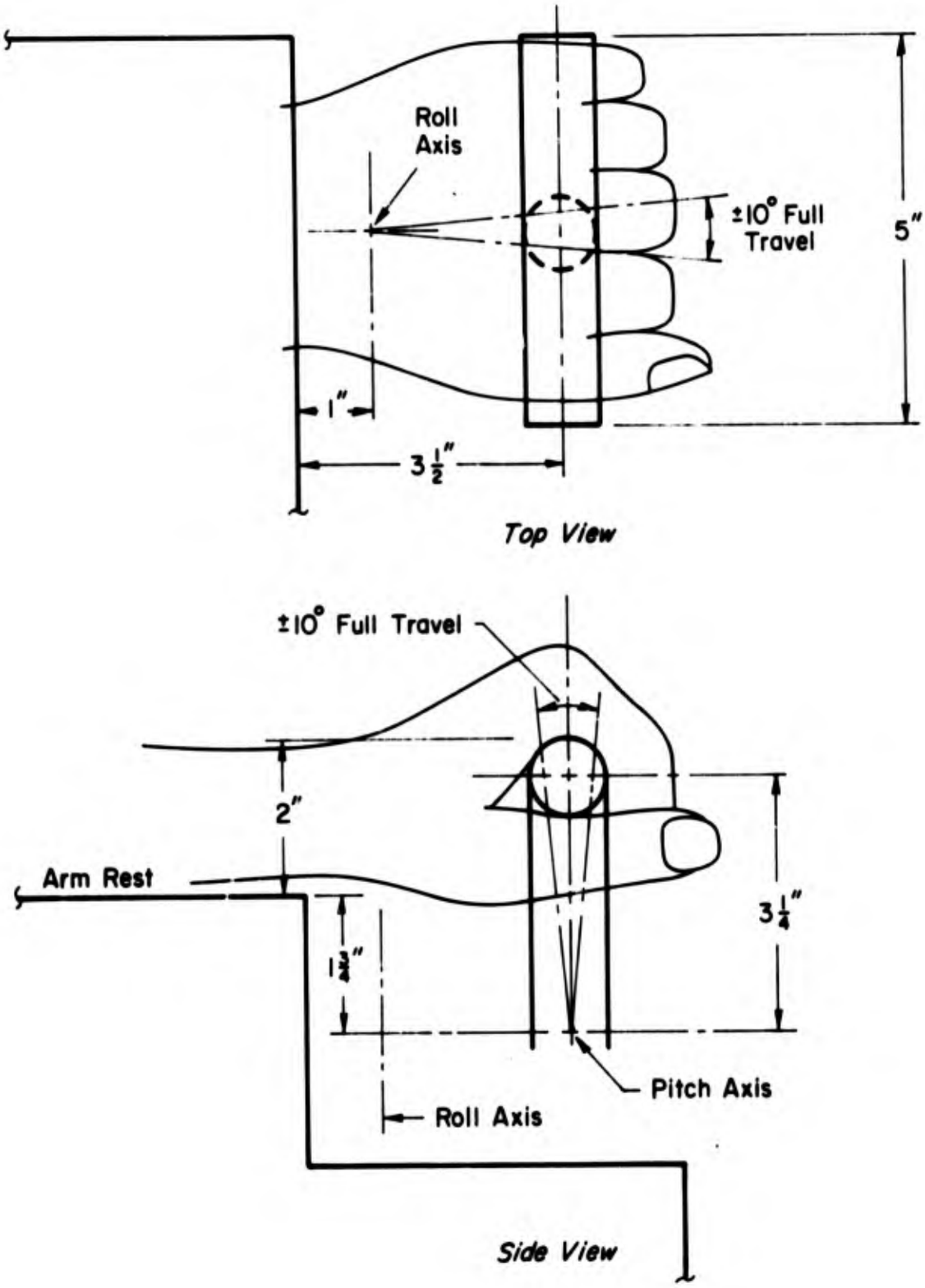

Figure 25. T-Bar Manipulator Configuration

and might degrade precision of pitch control somewhat because the arm muscular system is employed instead of the wrist muscular system as in the grip type of Fig. 24. However, this T-bar manipulator does offer an advantage in that it is more compact (does not stick up so far) and hence might be less of an obstruction to the operator when not being used and less subject to damage. Thus a tradeoff might be performed as a part of the prototype installation evaluation.

3. Force Feel Characteristics

From the human factors standpoint, per se, there is little to go on regarding feel forces for side stick manipulators in land vehicles. In the simulation of the dozing task little difference in performance was obtained with the two integrated side stick configurations evaluated. The operator did have a slight preference for the isometric (force) stick gradient (4.45 $in.^3/sec/lb$), but also objected to the low breakout force (0.5 lb). The characteristics of the isotonic stick were 2.0 lb breakout with 0.45 lb/deg thereafter and 6.67 $in.^3/sec/deg$. The operator did not object to the breakout force of the isotonic stick, but this high breakout followed by a relatively low spring gradient did give a tendency to overcontrol (i.e., use of higher flow rates on the average). Converting the isometric stick flow/force gradient to an equivalent force/displacement gradient for a ±10 deg travel isotonic stick with equivalent flow command gives a force gradient of 0.9 lb/deg. Thus, on the basis of simulator performance, the force gradient should lie between 0.45 and 0.9 lb/deg, and the breakout force should be between 0.5 and 2.0 lb. These characteristics form an acceptable feel boundary as shown in Fig. 26.

It is interesting to note that the study reported in Ref. 14 resulted in a pilot selection of 1 lb breakout followed by a gradient of 0.66 lb/deg in pitch and 0.2 lb/deg in roll as optimum. The breakout and gradient were highly dependent on desire to minimize inadvertent inputs in the particular task and environment (flight). This pitch feel characteristic is shown in Fig. 26 as the dashed line and obviously is in good agreement with the results of the UET simulation. However, the UET simulator operator preferred much closer harmony between pitch and roll control forces (identical feel characteristics were used in both axes).

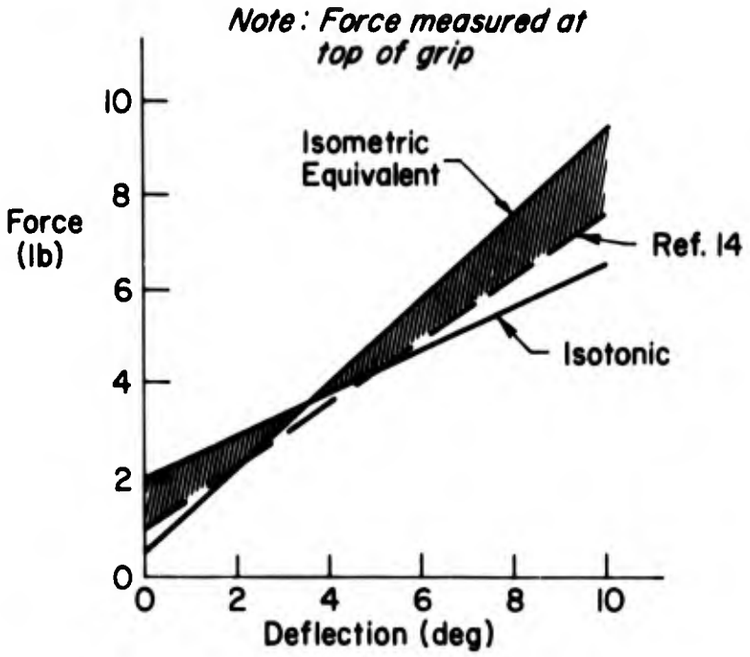

Figure 26. Desired Manipulator Feel Characteristics

Considering now the operational environment to be expected in dozing operations (jostling, jolting, etc.) as compared with an aircraft (gusts, moderate vibration, etc.), it would appear that a 1 lb breakout might not be sufficient to avoid frequent inadvertent inputs. It therefore will be specified (somewhat arbitrarily) that the breakout and gradient for the prototype system should fall within the shaded area of Fig. 26. Friction and stiction are to be eliminated within practical constraints and in no case should they cause the force characteristics to fall outside the shaded area of Fig. 26.

4. Switches and Other Controls

Since operator control of the front lever arms is only required for dozing type work, means must be provided to activate and deactivate the side arm manipulator. This is accomplished by a switch (see Fig. 18) controlling electrical power to the system. Null adjustments should be provided to correct for long-term change in each electro-hydraulic valve driver amplifier characteristics. This same null adjustment can be used to bias the electro-hydraulic valve so its output hydraulic flow exactly cancels the actuator leakage flow. As indicated previously, the change in leakage will be a function of load plus a gradual increase as actuator wear increases. Thus the null adjustments are accessible (Fig. 18) to the operator so that he may compensate for load and wear whenever he sets up for a dozing operation, i.e., at the beginning of the day.

The power switch and null adjustments are readily accessible by either hand and visible to the operator by glancing at the controller console. They also are protected from inadvertent change due to accidental bumping.

References 15 and 17 provide specific guidelines as to directions of operation, size of switch and knob, minimum distances between controls, etc. The detailed design layout of Appendix E reflects these guidelines as well as protective means to prevent inadvertent operation.

5. Indicator Lights

Failure indication lights (Fig. 19) are provided for each valve driver amplifier output. These lamps will light whenever full amplifier output

exists. They thus serve as hardover monitors to warn of any unsafe condition prior to engaging the system.

C. ENVIRONMENTAL CONSIDERATIONS

The environment imposed on the controller by the UET concept is exceptionally severe (see, for example, Refs. 19 and 20). The UET is required to operate in all climatic, weather, and ground conditions (tropics, desert, and arctic). Under noncombat operating conditions the operator's cockpit area is completely exposed to the elements. Furthermore, the location of the controller box on the left shelf of the cockpit will provide a tempting step for crawling over the side of the vehicle. Thus ruggedness and self-protection from the sand, dust, and water are essential.

With the exception of the electrohydraulic valves, all exposed surfaces will be of appropriately treated aluminum in keeping with the overall UET construction materials. The case/arm rest will be welded plate and will enclose the electronics. A moisture- and dust-proof seal will be employed between the case and its cover. All holes through the case (i.e., for wires, potshafts, etc.) will be appropriately sealed against moisture and dust. A soft synthetic rubber boot will encase the universal of the two-axis side stick. This will be securely fastened to the case at the bottom and will fit snugly at the top around the shaft which supports the manipulator grip. The manipulator grip will be of machined aluminum.

An arm rest pad will be provided to protect the operator's arm from direct contact with metal. This serves two functions. It provides insulation from direct contact with extremely hot or cold metal surfaces in severe climatic situations and also provides some padding against vibration and shock in rough going. The pad covering shall be of the same type material as the seat covering.

The electronics will be completely solid state with all vibration and shock sensitive elements potted.

D. MAINTENANCE CONSIDERATIONS

The improved controller unit consists of three major assemblies or packages: one combination case and manipulator assembly, and two

valve-manifold packages. Each is independently bolted to the hull. The two valve-manifold packages are line replaceable units (LRU) and will be located as close as possible to their respective actuators, but in a readily accessible position which will depend upon the specific test vehicle employed.

The case-manipulator assembly is accessible on the left shelf of the operator's station and may be removed by unfastening three bolts and one cannon connector. Thus the complete assembly may be removed for maintenance and calibration at a remote site (base shop) and may be treated as a LRU. In addition, quick access to the electronics is provided by unlatching the hinged arm rest cover for maintenance operations within the vehicle. The cover is secured by a single draw-hook latch. All electronic modules are plug-in type LRU's with friction or spring retainers. Electrical test points are provided on the electrical chassis which allows measurement of the inputs and outputs of each module for easy fault isolation. All electrical tests can be accomplished with a portable multimeter. Access to the electrical test points will be from the top with the cover open. All electronic balance and gain adjustments will be screwdriver-adjust type and also will be accessible from the top with the cover open.

Because of the complexity of the two-axis stick and feel subassembly, any maintenance on this device will be a shop repair action and will require removal of the complete case assembly from the vehicle.

E. INSTALLATION CONSIDERATIONS

1. Hydraulic

A simplified schematic of the hydraulic installation for the left wheel control is shown in Fig. 27. The right wheel control would be the same except for replacing L for R on the line codes. The sprung-unsprung valves (manual control and wheel) are shown in the unsprung mode. The existing hydraulic connections are shown by the solid lines and the new lines for the EHTV are shown dashed. The installation requires four tees to be attached at the connections to the existing Hydreco or Husco valve banks. New lines from these tees are then run to the EHTV manifold. The existing valve bank need not be disturbed further since the manually operated levers

that control the left and right front wheel valves will be disconnected and removed in the operator's cockpit.

Note that in the sprung mode the wheel valve moves so that line 3L is blocked while the sprung-unsprung valve opens 17L to return (line 7). Thus any inadvertent operation of the EHTV will not affect the rotary actuator and no additional valves, switches, etc., are necessary for protective means.

2. Electrical

A simplified schematic of the electrical installation is shown in Fig. 28. The 24V electrical supply from the instrument panel should be obtained from the ignition switch such that electrical power is not available to the electronics unit unless the ignition switch is on.

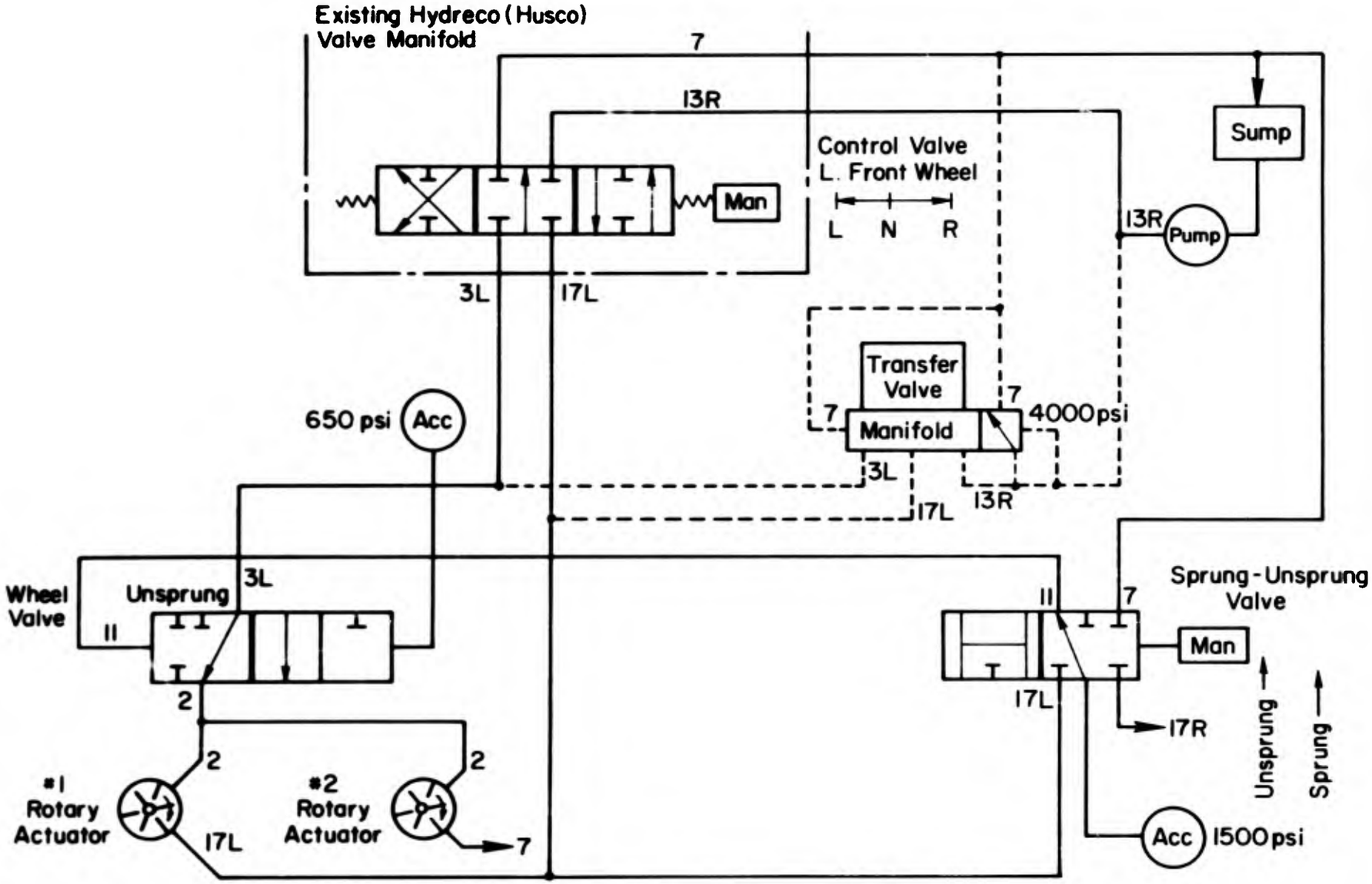

Figure 27. Simplified Hydraulic Schematic — Left Side Only
(All Valves in Unsprung Mode)

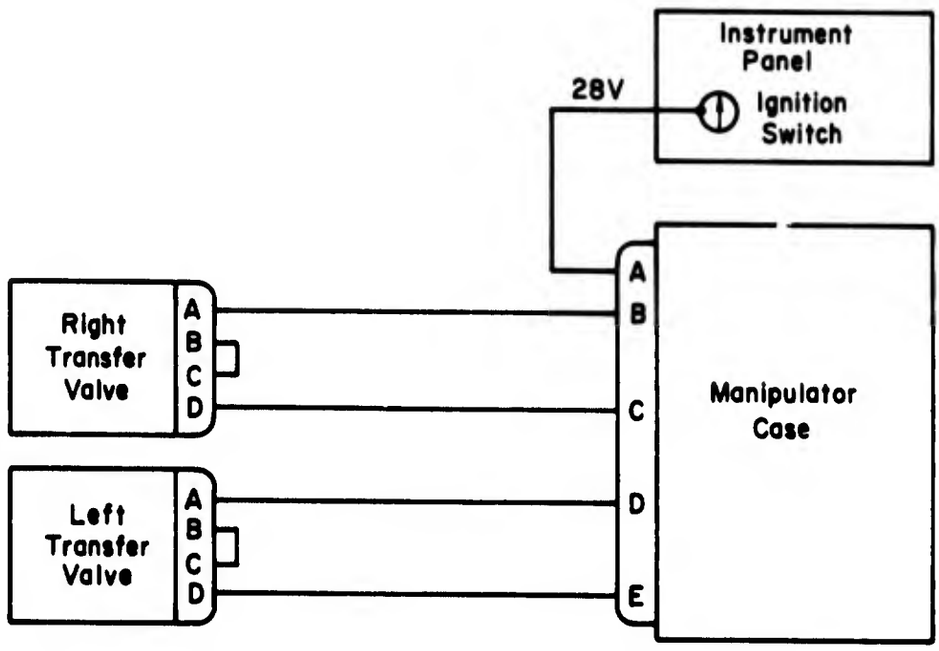

Figure 28. Electrical Installation

SECTION VII

CONCLUSIONS AND RECOMMENDATIONS

The objectives of this program were to:

- Demonstrate the application of a system design approach to the definition of a controller which fully integrates the operator into the control dynamics of large earth-moving machines so as to minimize error in expected or desired earthmoving process state variables.
- Design and demonstrate an example control system.

These objectives have been accomplished. The system approach demonstrated has integrated human operator, controller, vehicle, and control task dynamic and operational considerations for the UET-E4 tractor in dozing operations. The approach resulted in the definition of three potential controller modifications, each offering substantial improvement in man/machine performance over the existing controller. The performance improvement and decreased operator workload obtained with each configuration was demonstrated by means of an operational mockup in lieu of the actual vehicle. A preliminary design has been accomplished for the configuration offering the greatest improvement per unit of sophistication.

The first step in the design approach required mathematical modeling of the various dynamic elements (operator, vehicle, controller, and control task). The second step involved analysis and synthesis of the closed-loop system. This analytical process resulted in:

- A mathematical model which encompassed the complicated interaction between the tracked vehicle, its suspension system, the dozing load, and the disturbed terrain contour passing under the vehicle.
- Identification of the performance measures and motion cues the operator can best employ to control the vehicle in the dozing task.
- Prediction of the extreme difficulty of the control task, the control technique the operator would adopt, the low bandpass achievable, and the large control errors that would result.

The third step involved simulation of the complete system with an actual operator in the loop. This simulation included major nonlinear effects which are difficult to handle analytically. The simulation verified the analytical results, including:

- Predicted performance measures and motion cues most beneficial to (and hence used by) the operator in dozing.
- Predicted control task difficulty, operator control technique, and resulting task performance.
- Quantitative and qualitative assessment of performance improvement and decreased operator workload afforded by improved controller configurations.

The particular characteristics of the UET-E4 in the dozing task result in controlled element dynamics which have one unstable second-order mode, and output motion quantities approximately four integrations removed from the parameter directly controlled by the operator (hydraulic fluid flow) over the control frequency band normally selected by the human operator. These controlled element dynamics are speed sensitive and the controller is essentially bang-bang. Thus one could predict, on the basis of Ref. 21 alone, that control of the vehicle is a difficult and demanding task. Indeed, several hours of practice were required for the operator to achieve control over the simulator and become proficient in the control task with the existing UET-E4 control system.

The closed-loop analysis revealed the operator would close two loops in order to maintain reasonable control; blade height relative to the average terrain height as an inner loop, and vehicle velocity as the outer loop. The system analysis also indicated that the unstable second-order mode could be stabilized by an automatic stability augmentation scheme employing feedback of longitudinal acceleration. This simplifies the operator's task considerably by reducing the amount of lead the operator must generate and, hence, his concentration. It also relieves the operator of much of the lever activity necessary to maintain a constant cut.

Since the latter involves considerable complexity and sophistication, other, more simple, mechanizational improvements were also investigated. Three basic controller configurations resulted:

1. Linearization of the present two-lever/valve control characteristics such that rate of change of road arm height is proportional to lever deflection.

2. Integration of the two levers into a single-lever, two-axis, side-arm controller with the above linear proportional control characteristics in each axis.

3. Incorporation of the stability augmentation system utilizing forward acceleration feedback.

All of these configurations gave substantial improvement in tractor control, decreased operator workload, and decreased training time. As predicted, the acceleration feedback stability augmentation system provided the easiest control task and best performance. However, the major improvement stemmed from eliminating nonlinearities in the manipulators, and providing hydraulic fluid flow linearly proportional to manipulator displacement. This result, plus the fact that acceleration feedback poses several potential and unresolved problems regarding coordination of throttle control, applicability to other dozing tasks, etc., led to deferring consideration of the augmentation scheme for the prototype controller.

In comparing the two-lever versus the single-lever, two-axis manipulator, the latter proved less awkward in roll control and allowed faster, more precise control in pitch. Also, redesign of the existing valves and linkages to obtain linear proportional flow control with proper force breakout and gradient is not considered practical. On the other hand, the desired characteristics are readily achievable with an electromechanical manipulator feeding signals to an electrohydraulic transfer valve.

The configuration selected for the prototype controller therefore consists of the single-lever, two-axis electromechanical manipulator with an integrated force-feel system; an electronic amplifier and signal mixing unit, and two electrohydraulic transfer valves. This system is simple, relatively easy to mechanize, and forms the basic forward loop for future incorporation of acceleration feedback.

It is recommended that:

- This prototype system be fabricated, installed, and tested in the UET-E4.
- The investigation of acceleration feedback stability augmentation be continued.
- This analysis and simulation approach be applied in defining the control systems for future earthmoving vehicles.

REFERENCES

1. A Force Feedback Sensing and Multi-Axis Position Motion Correspondence Controller Element for Compatible Operator Control of Earthmoving and Materials Handling Machines, USAMERDC, Fort Belvoir, Va., Contract No. DAAK02-68-C-0186, Jan. 1968.

2. McRuer, D. T., L. G. Hofmann, H. R. Jex, G. P. Moore, A. V. Phatak, D. H. Weir, and J. Wolkovitch, New Approaches to Human-Pilot/Vehicle Dynamic Analysis, AFFDL-TR-67-150, June 1967.

3. McRuer, Duane, Dunstan Graham, Ezra Krendel, and William Reisener, Jr., Human Pilot Dynamics in Compensatory Systems — Theory, Models, and Experiments with Controlled Element and Forcing Function Variations, AFFDL-TR-65-15, July 1965.

4. McRuer, Duane T., Dunstan Graham, and Ezra S. Krendel, "Manual Control of Single-Loop Systems," J. Franklin Inst., Part I, Vol. 238, No. 1, Jan. 1967, pp. 1-29, Part II, Vol. 238, No. 2, Feb. 1967, pp. 145-168.

5. Magdaleno, R. E., G. P. Moore, and D. T. McRuer, Small Perturbation Dynamics of the Neuromuscular System in Tracking Tasks, Systems Technology, Inc., Tech. Rept. 154-1, Oct. 1967.

6. Stapleford, R. L., D. T. McRuer, and R. Magdaleno, Pilot Describing Function Measurements in a Multiloop Task, NASA CR-542, Aug. 1966.

7. Bogdanoff, J. L., and F. Kozin, On the Statistical Properties of the Ground Contour and Its Relation to the Study of Land Locomotion, Army Tank-Automotive Center Rept. 7823 LL 78, Mar. 1962.

8. Bogdanoff, John L., Frank Kozin, and Louis J. Cote, Atlas of Off-Road Ground Roughness P.S.D.'s and Report on Data Acquisition Technique, Army Tank-Automotive Center, Land Locomotion Lab., Rept., Sept. 1966.

9. McDonnell, J. D., and H. R. Jex, A "Critical" Tracking Task for Man-Machine Research Related to the Operator's Effective Delay Time, NASA CR-674, Jan. 1967.

10. Peters, Richard A., Dynamics of the Vestibular System and Their Relation to Motion Perception, Spatial Disorientation, and Illusions, Systems Technology, Inc., Tech. Rept. 168-1, Feb. 1968.

11. McAvoy, T. J., "Least Square Dead Time Approximations," IEEE Trans. on Computers, Vol. C-17, No. 2, Feb. 1968, pp. 174-178.

12. Weir, D. H., D. E. Johnston, and R. F. Ringland, Development of a Controller Element for Compatible Operator Control of Earthmoving Machines, Systems Technology, Inc., Tech. Rept. 178-3, Oct. 15, 1968.

13. McRuer, D. T., and R. E. Magdaleno, Human Pilot Dynamics with Various Manipulators, AFFDL-TR-66-138, Dec. 1966.

14. Graves, Harry C., A. James Bailey, and David L. Mellen, Study and Development of an Electric Side Stick Controller for Aerospace Vehicles, ASD-TR-61-603, May 1962.

15. Human Engineering Data and Factors, Military Vehicles, Ordnance Tank Automotive Command, R&D Div. Detroit Arsenal.

16. Male Physical Dimensions for Construction and Industrial Equipment Design, SAE Recommended Practice J833, 1962.

17. Chaillet, Robert F., and Alfreda R. Honigfeld, Human Factors Engineering, Design Standard for Wheeled Vehicles, Army Human Eng. Labs., Aberdeen Proving Ground, Md., HEL Standard 6-66, Sept. 1966.

18. Brissenden, Roy F., Some Ground Measurements of the Forces Applied by Pilots to a Side-Located Aircraft Controller, NACA TN 4171, Nov. 1957.

19. Anon., Development of Universal Engineer Tractor (Crawler), Univ. of Pittsburgh Army Materal Res. Staff, Tech. Info. Rept. 12-2-2A1, Jan. 1964.

20. Hardy, R. D., and R. P. White, The Universal Engineer Tractor: A High Speed Tracked Vehicle with Low Speed, High Drawbar Performance, SAE Paper No. 616C, Automotive Engineering Congress, Detroit, Mich., Jan. 1963.

21. Ziegler, P., and R. Chernikoff, "A Comparison of Three Types of Manual Controls on a Third-Order Tracking Task," Ergonomics, Vol. 11, No. 4, July 1968.

22. McRuer, D. T., I. L. Ashkenas, and D. Graham, Aircraft Dynamics and Automatic Control, Systems Technology, Inc., Tech. Rept. 129-1, Aug. 1968.

23. Dynamics of the Airframe, BuAer Report AE-61-4II, written and edited by Servomechanisms Section and Aerodynamics Section, Northrop Aircraft, Inc., Sept 1952, Chapter 2.

24. Servomechanisms, Section 3, Amplification, U. S. Army Materiel Command Engineering Design Handbook, AMCP 706-138, Apr. 1965.

25. Truxal, J. G., Editor-in-Chief, Control Engineers' Handbook, McGraw-Hill Book Co., Inc., New York, N. Y., 1958.

26. Marks, L., Mechanical Engineers' Handbook, 6th Ed., 1958, pp. 11-8 and 11-9.

27. Bekker, M. G., Theory of Land Locomotion, Univ. of Michigan Press, Ann Arbor, Mich., 1956.

APPENDIX A

BASIC DATA FOR UNIVERSAL ENGINEER TRACTOR

This appendix presents a set of "typical data" for a composite UET. Though minor differences may exist relative to the UET-E4, the values are sufficiently accurate for purposes of this study.

PRINCIPAL TRACTOR PARAMETERS

Net weight ≐ 30,500 lb (E3)
Center of gravity at station 132
Gross weight (ballasted) ≐ 53,000 lb (E3)
Length ≐ 230 in. (E2)
Width ≐ 110 in. (E2) with "wings;" 86 in. without "wings"
Height ≐ 87 in. (E2)
Dozer blade width = 110 in. (E2)
Ground clearance (blade full down) = -8 in. (E2)
Ground clearance (transport mode) ≐ 15.6 in. (E2)
Tread (track center to track center) ≐ 92 in. (E2)
Tread width = 18 in. (E2)
Road wheel diameter (including tires) ≐ 28 in. diameter (E2)
Ground pressure (ballasted) ≐ 13.9 psi
Engine: Cummins Diesel, V8-265
Horsepower ≐ 285 (net) at 2800 rpm (E2)
Transmission: Allison 4460 (E2)
Single-stage torque converter
Drive ranges: 6 forward, 2 reverse
Range selector: manual operated, mechanical
Maximum speed (transport mode) ≐ 30 mph
Maximum grade ≐ 60 percent (E2)
Maximum drawbar pull — a function of ballast and terrain characteristics, say between 20,000 lb and 45,000 lb (E2)
Steering: clutch-brake (unsprung mode) (E2)
Turning radius (unsprung): pivot about one track (E2)
Note: Longitudinal response (acceleration, deceleration) to throttle/brake application under various loading conditions was not available.

SUSPENSION PARAMETERS (E3)

Road arm length ≐ 15 in.

Nominal orientation ≐ 26 deg

Wheel center locations

- No. 1 Sta 199.99
- No. 2 Sta 169.15
- No. 3 Sta 128.69
- No. 4 Sta 95.90

Rotary actuator center locations

- No. 1 Sta 186.51
- No. 2 Sta 155.67
- No. 3 Sta 142.17
- No. 4 Sta 109.38

Rotary actuator parameters

- Displacement: 49.6 $in.^3$/rad
- Torque capability: 48,800 in.-lb 1000 psi
- Leakage:
  - Vane (at 3000 psi): 0.08 gal/min (0.308 $in.^3$/sec) assumed total for 3 vanes
  - Wheel valve: 5 cc/min (0.00508 $in.^3$/sec)
  - Check valve: 30 cc/min (0.0305 $in.^3$/sec)
  - Leveling valve: 40 cc/min (0.04065 $in.^3$/sec)
- Travel:
  - Internal: 77 deg range
  - External: 72 deg ± 1 deg range (unsprung)
  - External, No. 1 unit ≐ 33.2 deg (sprung jounce stop)
- Friction: equivalent to 50 psi (2440 in.-lb)
- Effective area × moment arm: 16.267 $in.^2$ × in. per each of 3 vanes

HYDRAULIC SYSTEM PARAMETERS

Pressure: 4000 psi (unsprung)

Pump flow: 13 gal/min (50.1 $in.^3$/sec) each side of two-sided pump at rated engine speed

Note: Oil column parameters (pipe lengths, diameters, etc.) were estimated from E4 drawings.

Technical Report No. 178-4

APPENDIX B

EQUATIONS OF MOTION FOR A TYPICAL UNIVERSAL ENGINEER TRACTOR IN THE UNSPRUNG MODE

APPENDIX B

TABLE OF CONTENTS

BLANK PAGE

I. INTRODUCTION

The purpose of this appendix is to assemble in one place a dynamic and kinematic description of the universal engineering tractor. This description is intended to be adequately detailed that the dynamic behavior of tractor subsystems involved in bulldozing may be examined in detail, and complete enough that the entire description, when augmented with a model of the operator plus manipulators, may be used for systems analysis of the bulldozing task.

While these equations describe the universal engineer tractor specifically, they can also be used for any tracked bulldozer once minor modifications to the suspension system equations are made.

Nine major sections cover the following areas.

- Axis systems, assumptions and operating point specification.
- Newton's second law in hull-fixed axis; operating point and perturbation components of these equations.
- Blade lip, roadarm and tractor center of mass trajectories.
- Hydraulic, actuator force-torque, steering and propulsion systems.
- Propulsion forces and moments.
- Dozing forces, moments and kinematics.
- Summary of derived trim and linearized perturbation equations.
- Simplified models
- Effect of actuator leakage and blade load on simplified models.

The approach taken is to develop the equations of motion using linearized perturbation techniques such as are conventionally employed in stability and control analysis for aircraft. (See, for example, Ref. 22 or 23.)

This technique can be applied to produce two sets of equations which together describe the vehicle motions. One set consists of the operating point equations. These are nondynamic, that is, they describe the average or steady behavior of the vehicle. These equations are not necessarily linear. The second set consists of the perturbation equations. These describe the dynamic behavior of various quantities about their average or operating point values. When the perturbation equations are simplified to be a linear constant coefficient set, a transfer function description of the vehicle dynamics can be obtained. Such a description is needed to perform a systems analysis of the bulldozing task.

Three different dynamic models for the tractor in the dozing task are considered:

- An eight-wheeled model which includes soil loads and actuator leakage
- A three-wheeled model which includes soil load and leakage but has simpler geometry
- A simplified model which is like the three-wheeled model, but without soil load and leakage

Nomenclature and data for the models developed here are presented in Tables B-I and B-II. Table B-I presents data for the eight-wheeled model. Table B-II presents data for the three-wheeled model when it differs from Table B-I. The chief difference is associated with the parameters of the two "equivalent" front wheels. In these data, the subscript (o) means that the data corresponds to the selected operating condition of a 1 ft depth of cut and a given forward speed, U_o. The road arm and road wheel numbering system is shown in Fig. B-1 for reference.

The force versus displacement (feel) characteristics of the front suspension levers, as measured on an E3 model with new Husco valves, are shown in Fig. B-2. The forces were measured at approximately 10 in. from the lever pivot point. It is probable that the linkage system was not fully adjusted at the time of these measurements so that the deadzone and friction may be indicative of a "worst case" situation. These characteristics are assumed to be the result of combined zone, preload, friction,

TABLE B-I

DATA FOR EIGHT-WHEELED MODEL

SYMBOL (UNITS)	VALUE	DEFINITION
a_{10} , a_{50} (deg) a_{20} , a_{60} (deg) a_{30} , a_{70} (deg) a_{40} , a_{80} (deg)	97 86 −81.5 −70	Operating road arm angles measured from the unperturbed (body axis) vertical, positive sense being forward and up.
b (ft)	1.5	Height of road wheel center above tracks
c (lb/ft^2)	216	Soil cohesion coefficient
D_M (in^3/rad)	49.6	Actuator displacement
g (ft/sec^2)	32.2	Gravitational acceleration
I_x (slug-ft^2)	8,540	Roll moment of inertia
I_y (slug-ft^2)	34,160	Pitch moment of inertia
I_z (slug-ft^2)	41,330	Yaw moment of inertia
I_{xy}, I_{xz} (slug-ft^2)	$\doteq 0$	Product of inertia
ℓ (ft)	1.25	Road arm length
ℓ_1 (ft) ℓ_2 (ft) ℓ_3 (ft) ℓ_4 (ft)	5.58 8.08 11.42 14.33	Distances from dozer blade edge to road wheel centers (see sketch)
ℓ_b (ft)	5.00	Distance of right or left blade edge from centerline (see sketch)
: (in.^{5}/lb-sec)	2×10^{-4}	Linearized actuator leakage coefficient
m (slugs)	1,366	UET mass (5 cubic yards of earth in bowl)
$N_{\dot{\psi}_r}$ (ft-lb-sec)	−4,134	Yaw moment per yaw rate
ℓ_3 (ft)	3.83	Distance from tractor centerline to road wheel centerline (see sketch)
U_o (ft/sec)	variable	Operating forward speed
x_B (ft) y_B (ft) z_B (ft)	9.75 0 3.33	Location of blade edge center with respect to center of mass
x_{op} (ft) y_{op} (ft) z_{op} (ft)	−3.08 −3.17 −5.75	Location of operator's head with respect to center of mass
$(z_{i_o} + \ell \cos a_{i_o})$(ft)	1.83	Operating location of road wheel centers with respect to center of mass in vertical direction

TABLE B-I (Concluded)

SYMBOL (UNITS)	VALUE	DEFINITION
z_{a_o} (ft)	-1.00	Operating ambient terrain level with respect to blade edge
α_o (deg)	65	Operating blade angle with respect to horizontal
γ (lb/ft^2)	96	Soil density
η_s ---	1.25	Loosened soil expansion factor
φ_r (deg)	30°	Angle of repose of loosened soil

TABLE B-II

DATA ADJUSTMENTS FOR THREE-WHEELED MODEL

SYMBOL (UNITS)	VALUE	DEFINITION
a_{10} , a_{50} (deg)	90	Operating equivalent front road arm angles
D_M (in.^{3}/rad)	99.2	Equivalent actuator displacement
ℓ_B (ft)	7.165	Distances from blade edge to equivalent road wheels 1(5) and 4(8)
$\ell_B + \ell_{wB}$ (ft)	14.33	
L (in.^{5}/lb-sec)	4×10^{-4}	Equivalent actuator leakage coefficient

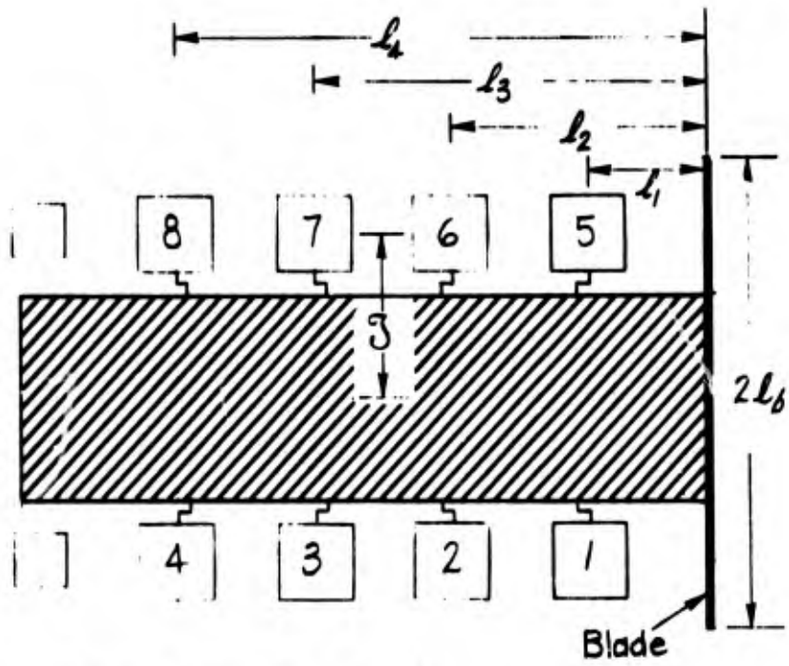

Figure B-1. Road Arm/Wheel Numbering Scheme

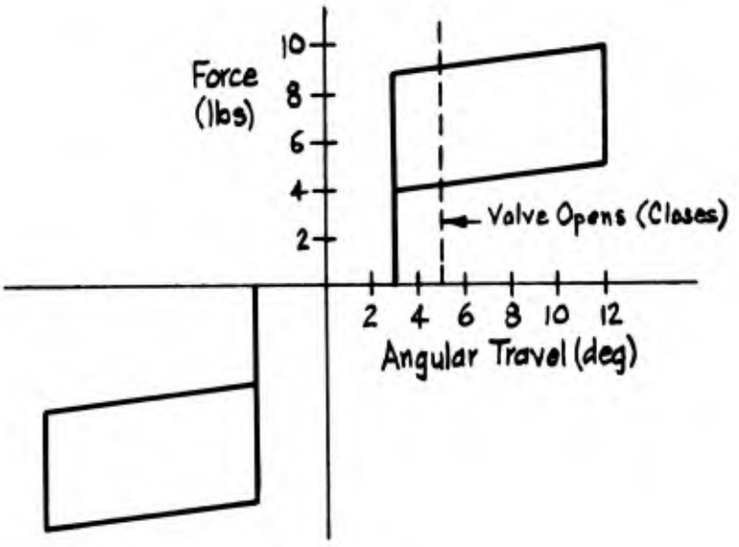

Figure B-2. Suspension Lever Feel Characteristics

and spring gradient. It is also assumed that reduction in deadzone will result in an equivalent reduction in total travel and point of initial opening of the control valve. The feel system in the mockup is currently adjusted to duplicate these characteristics.

The valve flow characteristics are given in Fig. B-3. The complete description of hydraulic system behavior involves consideration of numerous

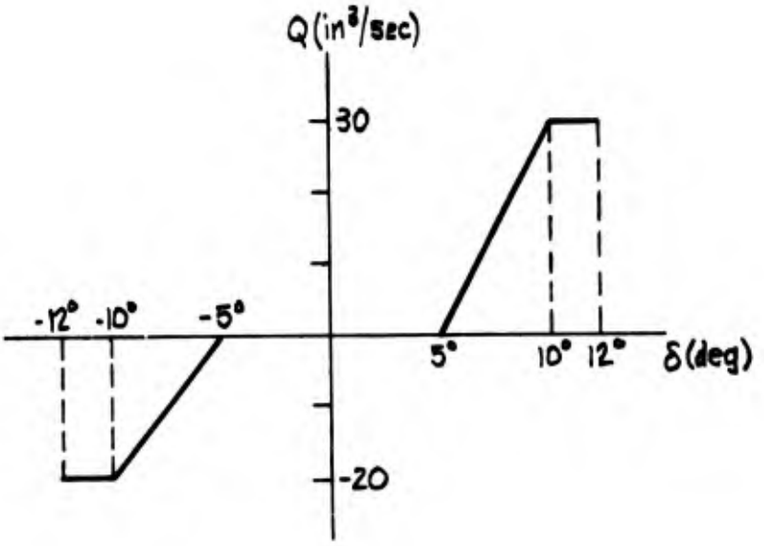

Figure B-3. Valve Flow Characteristics

nonlinearities having to do with flow and pressure drops through orifices, etc. These must be linearized for purposes of analysis. Examination of the known hydraulic system parameters reveals that the natural frequency of the system to be outside the frequency range of interest; consequently, fluid compressibility and line elasticity effects can be ignored. For analytical purposes, it is assumed that the operating load pressures within the actuators are the only factors (other than valve opening) affecting the flow of fluid. Thus, flow at full valve opening is less when the blade is being lifted than when it is being dropped. With these factors in mind the following relationship between lever deflection and fluid flow is assumed. The deadband includes both valve overlap and suspension lever "slop." The lever is limited to ±12 deg of travel.

II. DESCRIPTION OF AXIS SYSTEMS, ASSUMPTIONS, AND OPERATING POINT SPECIFICATION

Before starting with a detailed description of the problem some definitions of terminology are required.

Reference surface—a surface which represents the ideal grade desired after a single pass of the dozer.

Working surface—the actual grade achieved after a single pass of the dozer. Its elevation is measured with respect to reference surface and is positive in the downward direction.

Ambient surface—the actual grade existing prior to passage of the dozer on any given pass. Its elevation is measured with respect to the reference surface and is positive in the downward direction.

A. ASSUMPTIONS AND SIMPLIFICATIONS

1. Reference Surface and Operating Point

The reference surface will be assumed to be a horizontal plane. It might be argued that restriction of the reference surface to be a horizontal plane is quite limiting. While this is true, two considerations recommend this restriction. First, if dozer operational performance is to be satisfactory at all, it must be able to perform the restricted task of dozing with respect to a horizontal reference surface. Second, the grades of other reference surfaces will usually be small enough that these cases may be considered by other means within the framework of the equations to be developed.

The operating point for the dozer has the vehicle proceeding rectilinearly at constant forward speed, U_o, on this reference plane.

Furthermore, the hull will be oriented so the blade lip (a line) lies in the reference plane.

2. Dozing Kinematics

The surload is assumed to be semi-conical in shape. The base of the surload semi-cone has a diameter which is equal to or greater than the blade width. The surload cannot produce side forces on the blade. In addition, the working surface will be assumed undeformable. (This assumption will be made even when the working surface is the result of "fill" from the surload.) It is clear from these assumptions and definitions that the dozer tracks "walk" upon the working surface. Also, because of the above assumptions, the blade lip trajectory determines the working surface elevation.

3. Sprung and Unsprung Masses

The unsprung mass is taken to be zero. This is justifiable because the accelerations of each unsprung system (rondarm, roadwheel plus tread segment) will be small during dozing. For the purpose of computing the total dozer mass and inertia, the unsprung system will be counted at its actual value and as though it were rigidly attached to the hull in its operating point position.

4. Symmetry

The x-z plane is a plane of symmetry for the unperturbed tractor.

5. Gyroscopic Effects

Gyroscopic effects of the motor, drive train, roadwheels and sprockets are neglected.

6. Traction Properties

Longitudinal and side forces on the track are assumed to always be less than the breakaway level. This means no axial tread slip or net tread side slip effects are included in the model. The resistance of the tracks to tractor rotation about a vertical axis is assumed proportional to the rate of rotation. The case where the tracks are in a longitudinal slip condition can be treated by specialization of these results.

7. Steering System

The steering system is assumed to produce a torque decrement on the inside track. The torque decrement is related to the steering wheel displacement by a scale factor.

8. Propulsion System

Output torque of the engine is assumed to be proportional to the fuel flow and engine output speed. A governor with proportional and integral control paths adjusts the fuel flow to maintain the engine output speed at the set point speed determined by the "throttle" control. The torque output at the sprockets is assumed to be proportional to the difference between engine speed and sprocket speed.

9. Attitude Control System

The manipulator characteristics for the attitude control system are covered in another report. The inputs to the attitude control system of the dozer are here considered to be flows and pressures at the primary actuators in the front and at the interconnect between the primary actuators in the rear.

10. Linearization

The equations of motion are linearized. External forces are assumed to be linear functions of the dependent and independent variables. Product and squares of these variables are assumed to be negligible with respect to the variables themselves. Trigonometric functions of the variables are replaced by their small angle approximations.

B. AXIS SYSTEMS

1. X'Y'Z' System

X', Y', and Z' form an inertial coordinate system. The origin is at the operating point (unperturbed) center of mass location for the complete dozer. The orientation of the axes is such that Z' is positive in the downward direction and U_o is along X'.

2. XYZ System

The XYZ system is used to describe the elevation of the working surface at the unperturbed blade lip. The axes X, Y, and Z are parallel to X', Y', and Z' respectively, but the origin is at the center of the unperturbed blade lip.

3. xyz System

x, y, and z form a hull-fixed coordinate system. The origin is at the center of mass for the complete dozer. When the dozer is unperturbed; that is, at the operating point conditions; the x, y and z axes coincide with the X', Y', and Z' axes, respectively

The above verbal descriptions are presented pictorially in Figs. B-4 and B-5.

Transformations between the X'Y'Z' system and the XYZ system are governed by the following equations

$$\begin{aligned} X &= X' - x_B \\ Y &= Y' \\ Z &= Z' - z_B \end{aligned} \qquad (1)$$

where x_B, z_B, and $y_B = 0$ define the location of the blade lip center in the hull-fixed coordinate system. The origin of the xyz system is located in the X'Y'Z' system by X'_{cm} Y'_{cm} Z'_{cm}. X'_{cm} Y'_{cm} and Z'_{cm} are assumed to be small. The orientation of the xyz system with respect to the X'Y'Z' system is given by the Euler angle rotation set ψ, θ and φ. These angles are rotations about the z axis, y axis and x axis, respectively, and in that order. ψ, θ, and φ will be considered as small angles in the following so that the resolution of the unit vectors **ijk** in the xyz system into the X'Y'Z' system with unit vectors **I'J'K'** is given approximately by

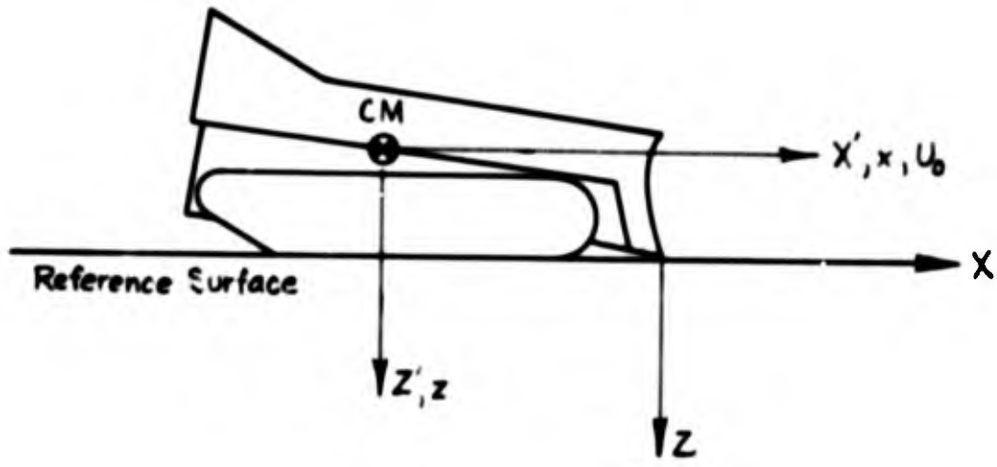

Y', Y, and y point outward from
the plane of the paper.

Figure B-4. Unperturbed Dozer and Coordinate Systems

$$\begin{vmatrix} \\ \\ \end{vmatrix}_{I'J'K'} = A \begin{vmatrix} \\ \\ \end{vmatrix}_{ijk} \tag{2}$$

$$A \doteq \begin{bmatrix} 1 & -\psi & \theta \\ \psi & 1 & -\varphi \\ -\theta & \varphi & 1 \end{bmatrix} \tag{3}$$

and is independent of the order of rotation. For the inverse transformation of the unit vectors

$$\begin{vmatrix} \\ \\ \end{vmatrix}_{ijk} = A^{-1} \begin{vmatrix} \\ \\ \end{vmatrix}_{I'J'K'} \tag{4}$$

$$A^{-1} \doteq \begin{bmatrix} 1 & \psi & -\theta \\ -\psi & 1 & \varphi \\ \theta & -\varphi & 1 \end{bmatrix} \tag{5}$$

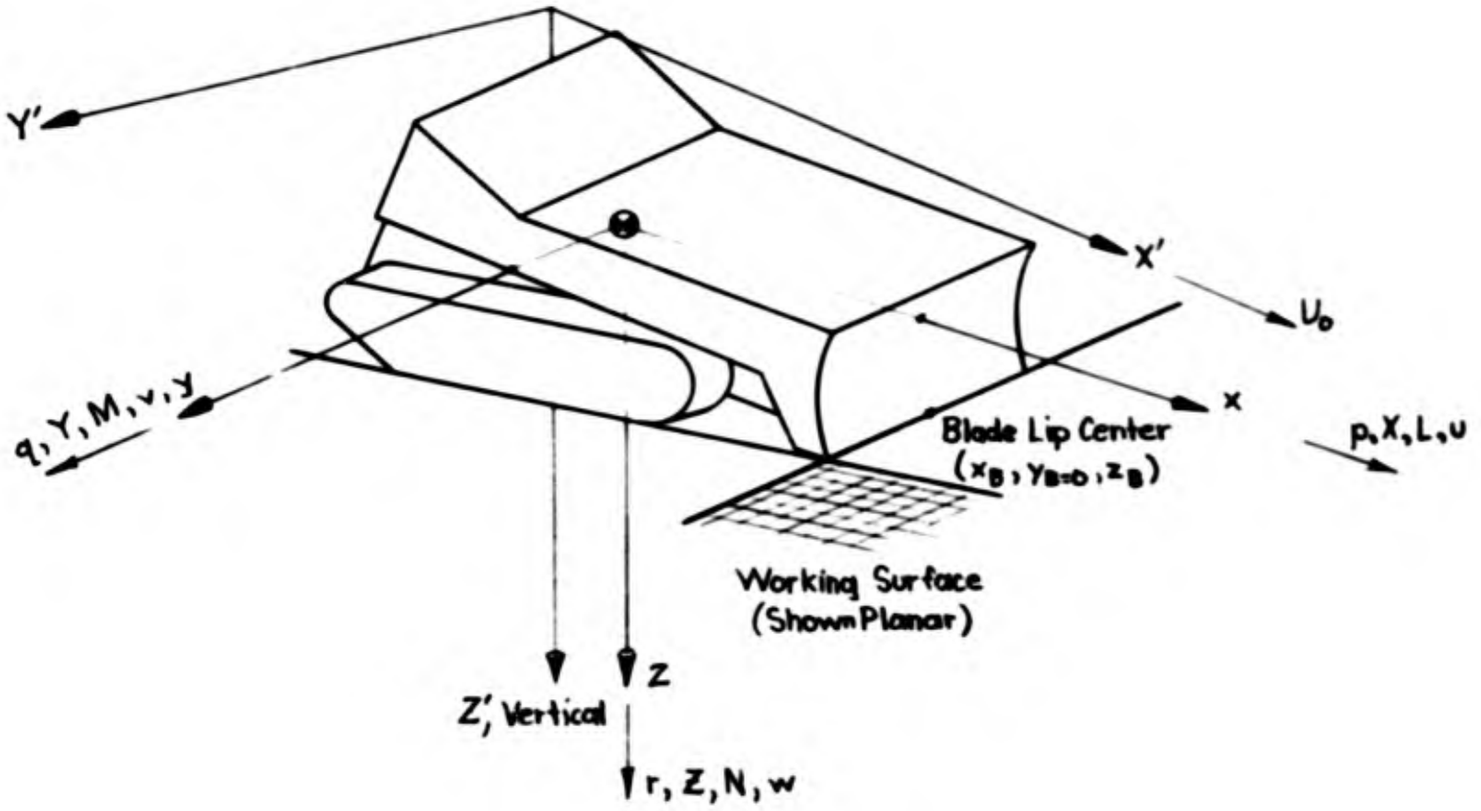

Figure B-5. Perturbed Dozer and Coordinate Systems

Notice that $AA^{-1} \doteq I$ to within the assumptions of 10, page B-9. The angular velocity of the xyz system with respect to the X'Y'Z' system has components p, q and r in the direction of the x, y, and z axes respectively. Forces along the x, y, and z axes are, respectively, X, Y, and Z. Moments about the x, y, and z axes are, respectively, L, M, and N. Velocities measured in the xyz system along the x, y, and z axes are, respectively; $U_o + u$, $v = 0$, and w. Refer to Fig. B-5.

Development of some kinematic equations will require differentiation with respect to time of a quantity measured in the rotating frame, xyz, but as seen from the inertial frame; X'Y'Z'. This can be accomplished routinely using Euler's equation:

$$\left[\frac{d}{dt}\left\{\cdot\right\}_{ijk}\right]_I = \frac{d}{dt}\left\{\cdot\right\}_{ijk} + \begin{vmatrix} i & p \\ j & q \\ k & r \end{vmatrix} \left\{\cdot\right\}_{ijk} \qquad (6)$$

The I subscript indicates the differential is total with respect to an inertial vector basis, e.g. **I'J'K'**.

III. OPERATING POINT AND PERTURBATION EQUATIONS

This section summarizes the steps which lead to operating point and perturbation equations. A summary of these equations specialized according to the assumptions in Section B-II for the dozer problem is given here. A complete exposition of this development is not included because there exist many good references on the subject, for example, Refs. 22 and 23.

The steps leading to these equations may be summarized as follows:

- Newton's second law, relating applied forces and moments to the rates of change of linear and angular momenta in inertial coordinates (X'Y'Z') is expressed in terms of the body-fixed coordinate system, xyz, which rotates and translates with respect to X'Y'Z'.
- Gravity force on the body is resolved into x, y, and z components.
- Kinematic relations between the Euler angles; ψ, θ and φ; describing the orientation of the xyz frame with respect to the X'Y'Z' frame (and the gravitational direction), and the angular rotation rates; p, q, and r are determined.
- Operating point equations* are obtained by recognizing that zero translational and rotational acceleration are implicit in the concept of a steady operating condition.
- Perturbation equations are obtained by subtracting the operating point motions from the total motion. The perturbation equations are then linearized by assuming that perturbations from the operating point are small. Then the products of perturbation quantities are negligible.

The operating point and perturbation equations of Ref. 22 are specialized for this specific application below.

---

*It is worthwhile to note that operating point equations are often called trim equations.

A. OPERATING POINT EQUATIONS*

1. Force Equations

$$\sum X_o = 0 = X_{Po} + X_{Bo} \tag{7}\dagger$$

$$\sum Y_o = 0 \tag{8}$$

$$\sum Z_o = -mg = Z_{So} + Z_{Bo} \tag{9}$$

2. Moment Equations

$$\sum L_o = 0 \tag{10}$$

$$\sum M_o = 0 = M_{So} + M_{Po} + M_{Bo} \tag{11}$$

$$\sum N_o = 0$$

B. LINEARIZED PERTURBATION EQUATIONS

1. Force Equations

$$m\left|\dot{u} + g\theta\right| = \sum X = X_S + X_P + X_B \tag{13}**$$

$$m\left|U_o r - g\varphi + \dot{v}\right| = \sum Y \tag{14}$$

$$m\left|\dot{w} - U_o q\right| = \sum Z = Z_S + Z_B \tag{15}$$

---

*Zero subscripts denote operating point values of variables.

†Subscripts B, P and S are used to indicate those force or moment components arising from soil forces on the blade, propulsion, and soil forces acting on the tracks, respectively.

**$\dot{(\cdot)}$ denotes $d(\cdot)/dt$ in the frame where $(\cdot)$ is defined.

2. **Moment Equations**

$$\dot{p}\, I_x - I_{xz}\, \dot{r} = \sum L = L_S + L_B \tag{16}$$

$$\dot{q}\, I_y = \sum M = M_S + M_P + M_B \tag{17}$$

$$\dot{r}\, I_z - \dot{p}\, I_{xz} = \sum N = N_S + N_P + N_B \tag{18}$$

3. **Kinematic Equations**

$$\dot{\psi} = r \tag{19}$$

$$\dot{\theta} = q \tag{20}$$

$$\dot{\Phi} = p \tag{21}$$

The constraint that the tracks have no <u>net</u> sideward movement relative to the soil results in the constraint that the side velocity of the tracks with respect to the soil equals zero, that is:

$$0 = v \cos \beta - w \sin \beta - z_B\, \dot{\Phi} \cos \beta \tag{22}$$

β is the small angle measured from a plane which approximates the working surface elevations at the roadwheel contact patches to the y axes. Linearization of the above equation gives

$$v = z_B\, \dot{\Phi} = z_B\, p \tag{23}$$

as the constraint. Since β drops out of the linearized constraint equation, the sense in which the plane approximates the working surface elevations at the roadwheel contact patches is of little consequence.

IV. DOZER CENTER OF MASS, BLADE LIP AND ROADWHEEL CONTACT PATCH TRAJECTORIES, AND HULL-ROADARM-ROADWHEEL KINEMATICS

A. DOZER CENTER OF MASS TRAJECTORY

Consider the alternate expressions for the inertial velocity of the dozer center of mass, V_{cm}.

$$V_{cm} = (U_o + \dot{X}'_{cm})\mathbf{I}' + \dot{Y}'_{cm}\,\mathbf{J}' + \dot{Z}'_{cm}\,\mathbf{K}' \tag{24}$$

and, using Eq 6

$$\begin{aligned} V_{cm} = {} & (U_o + u + q\,z_o - r\,y_o)\mathbf{i} \\ & + (z_B p + r x_o - p z_o)\mathbf{j} + (w - p y_o - q x_o)\mathbf{k} \end{aligned} \tag{25}$$

where (x_o, y_o, z_o) is location of the X'Y'Z' origin in xyz coordinates. Using Eq 2 to resolve the **i**, **j** and **k** components of Eq 25 into the I'J'K' basis, equating the coefficients of **I'**, **J'**, and **K'**, and linearizing gives the following three equations.

$$\dot{X}'_{cm} = u \tag{26}$$

$$\dot{Y}'_{cm} = U_o \psi + z_B p \tag{27}$$

$$\dot{Z}'_{cm} = w - U_o \theta \tag{28}$$

B. BLADE LIP TRAJECTORY

The blade lip trajectory can be developed by considering the following sketch illustrating the blade location in X'Y'Z' coordinates. Let R_{By} be the vector from the origin of X'Y'Z' to a point y on the blade lip. Then:

$$\begin{aligned} R_{By} = {} & (X'_{cm} + x_B + z_B\theta - y\psi)\mathbf{I}' + (Y'_{cm} + y + x_B\psi - z_B\varphi)\mathbf{J}' \\ & + Z'_{cm} + z_B - x_B\theta + y\varphi)\mathbf{K}' \end{aligned} \tag{29}$$

Notice that strictly speaking, $|y| \leq l_b$.

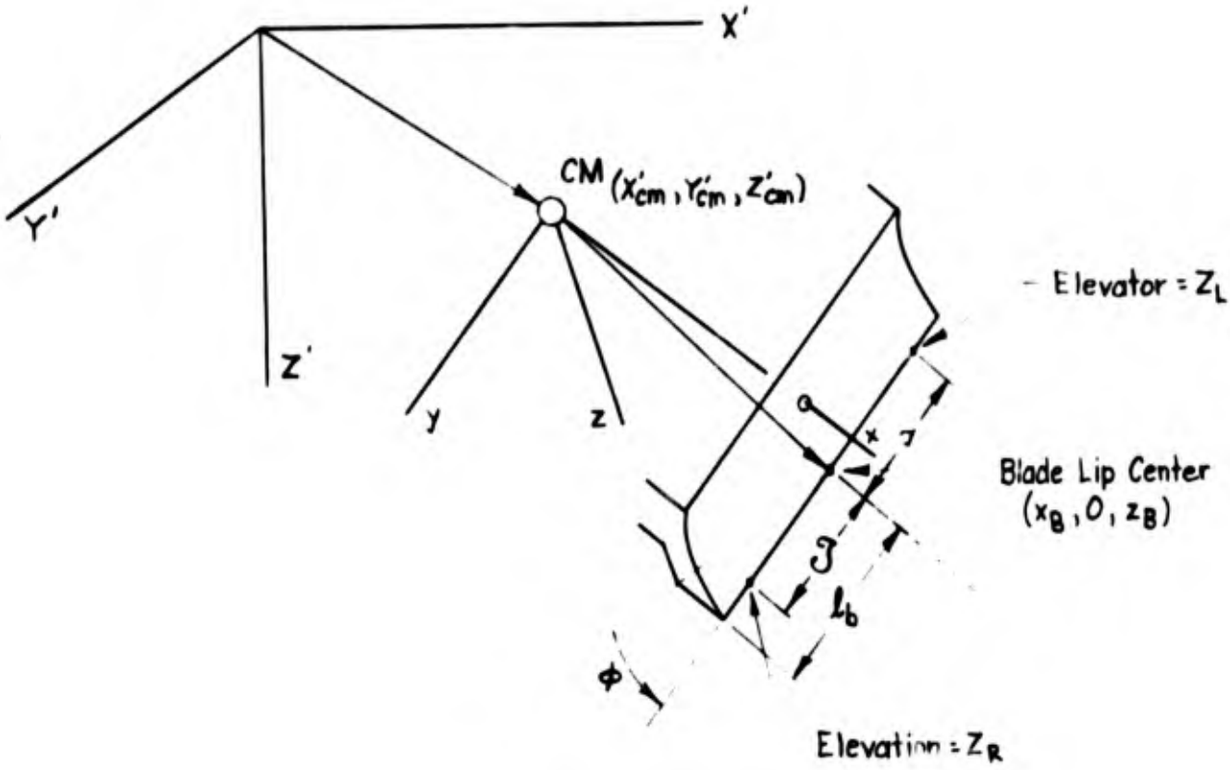

C. ROADWHEEL CONTACT PATCH TRAJECTORY

The elevation of the contact patches for the right and left hand roadwheels (treads are assumed to have zero thickness) will be assumed determined by the elevation with respect to the reference plane of points a distance, $|y| = \mathcal{J}$, to the right and left respectively of the center on the blade lip. See the preceding sketch. The elevation of these points on the blade lip are, respectively, Z_R and Z_L. The elevations for the right hand roadwheels are obtained by delaying the function Z_R by the times required for the dozer to advance the distance each roadwheel lies behind the blade lip. The sketch below defines the necessary notation. Notice that the l_i's are defined with the dozer in the unperturbed condition. The delay times are given by:

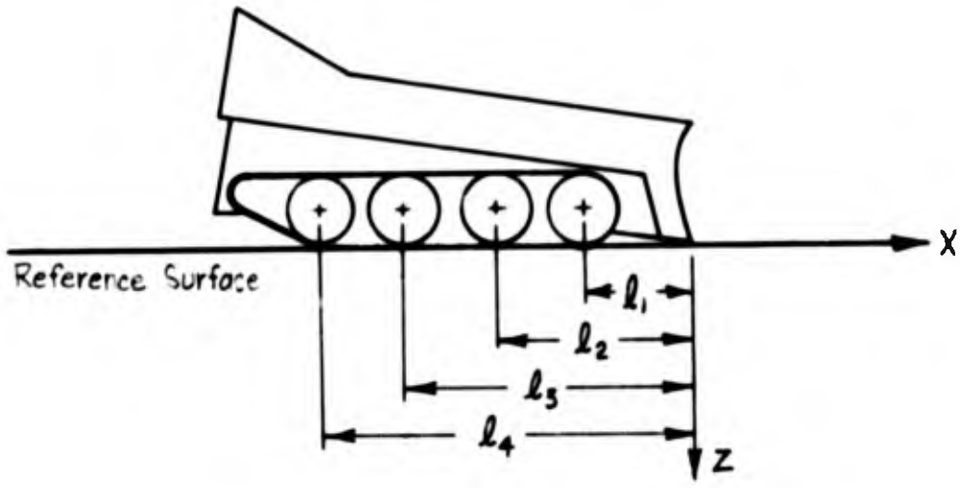

$$\tau_i = l_i/(U_o + u), \quad i = 1, 2, 3, 4$$

$$\tau_i \doteq l_i/U_o - (l_i/U_o^2)u = \tau_{i_o}(1 + u/U_o) \tag{30}$$

The elevation at the right hand roadwheel contact patches is given by:

$$\begin{aligned} Z_i(t) &= Z_R(t - \tau_i) \\ &\doteq Z_R(t - \tau_{i_o}) + \frac{\tau_{i_o}}{U_o}\dot{Z}_R(t - \tau_{i_o})u \qquad i = 1, 2, 3, 4 \end{aligned} \tag{31}$$

Similarly, for the left hand roadwheel contact patches the elevation is given by:

$$\begin{aligned} Z_{i+4}(t) &= Z_L(t - \tau_i) \\ &\doteq Z_L(t - \tau_{i_o}) + \frac{\tau_{i_o}}{U_o}\dot{Z}_L(t - \tau_{i_o})u \qquad i = 1, 2, 3, 4 \end{aligned} \tag{32}$$

Z_R and Z_L are obtained from Eq 29 and 1

$$Z_R = Z'_{cm} - x_B\theta + \mathfrak{J}\varphi \tag{33}$$

$$Z_L = Z'_{cm} - x_B\theta - \mathfrak{J}\varphi \tag{34}$$

If linear equations are desired, the terms involving u in Eq 31 and 32 must be deleted. These terms are shown here because $|u|$ may be an appreciable fraction of U_o since dozing speeds typically are very low. Under such circumstances, the effect on the delay time of speed perturbations from U_o may require simulation. When an FM tape loop is used to mechanize the delay, an alternate means to varying the tape speed is required in order to vary the delay unless the FM carrier and the tape drive are "geared" together. The terms involving u in Eq 31 and 32 provide an alternate means.

The linearized equations for the Z_i are:

$$Z_i(t) = Z_R(t - l_i/U_o); \quad i = 1, 2, 3, 4 \tag{35}$$

$$Z_{i+4}(t) = Z_L(t - l_i/U_o); \quad i = 1, 2, 3, 4 \tag{36}$$

D. HULL-ROADARM-ROADWHEEL KINEMATICS

The ith roadwheel contact patch location can also be specified in terms of the hull-roadarm-roadwheel kinematics. The longitudinal slope of the working surface is assumed to be zero at the contact patch. The following sketch illustrates the situation.

The location of the contact patch, R'_{cp_i}, is:

$$\begin{aligned} R'_{cp_i} = {} & (X'_{cm} + \left|X_{i_o} + l \sin \overline{a_i}\right| - Y_{i_o}\psi + \left|Z_{i_o} + l \cos \overline{a_i}\right|\theta)\mathbf{I}' \\ & + (Y'_{cm} + Y_{i_o} + \left|X_{i_o} + l \sin \overline{a_i}\right|\psi - \left|Z_{i_o} + l \cos \overline{a_i} + b\right|\varphi)\mathbf{J}' \\ & + (Z'_{cm} + \left|Z_{i_o} + l \cos \overline{a_i} + b\right| - \left|X_{i_o} + l \sin \overline{a_i}\right|\theta + Y_{i_o}\varphi)\mathbf{K}' \end{aligned} \tag{37}$$

The $\mathbf{K}'$ coefficient of Eq 37 and Eq 1 can be used to express the elevation of the contact patch in XYZ coordinates. Notice that $Z_{i_o} + l \cos a_{i_o} + b$ is equal to z_B. The resulting perturbation equation for the elevation of the contact patch, Z_i, is:

$$Z_i = Z'_{cm} - \left|X_{i_o} + l \sin a_{i_o}\right|\theta + Y_{i_o}\varphi - l \sin a_{i_o}\, a_i$$

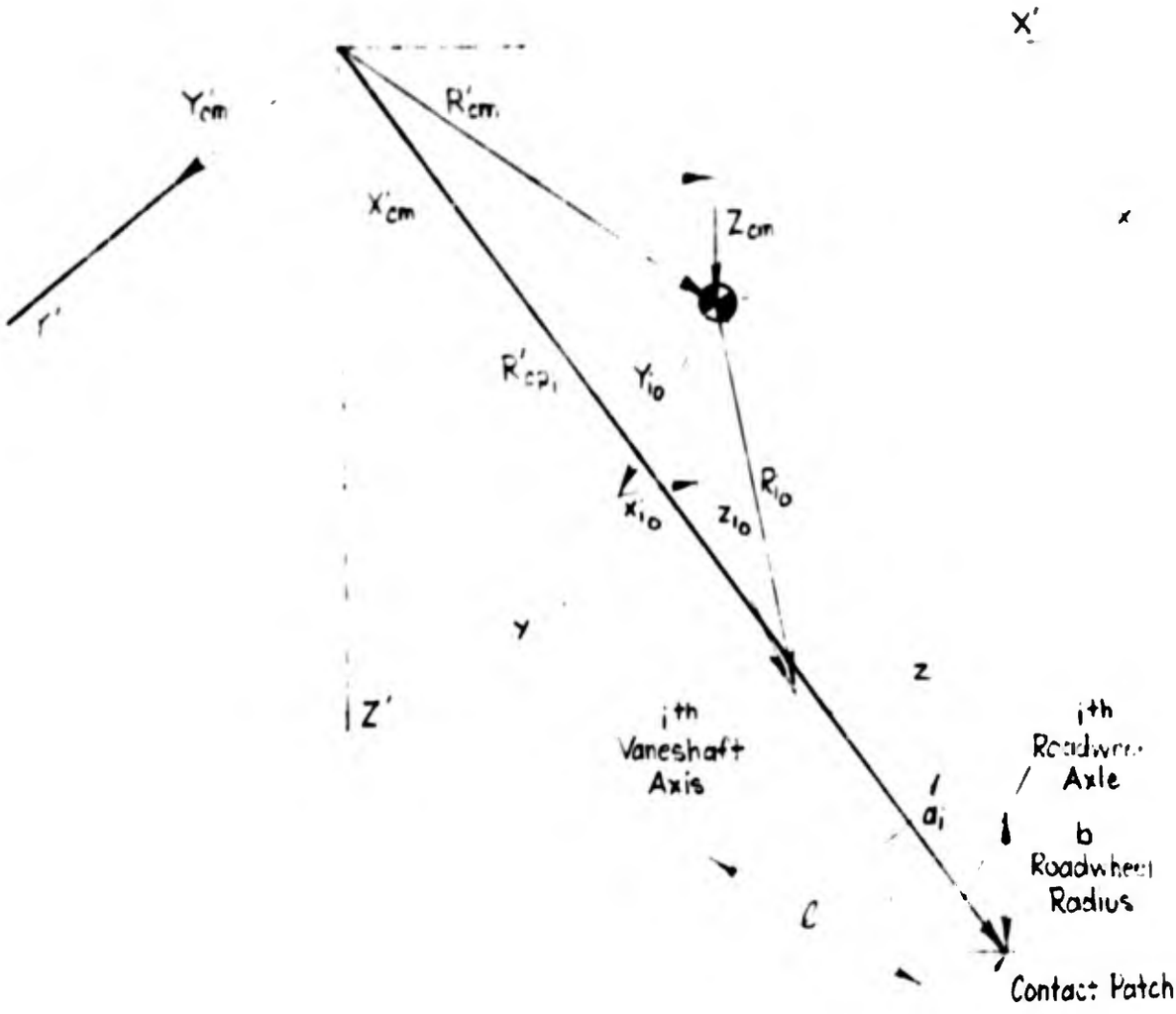

However, this equation will be used to solve for a_i so that

$$a_i = \frac{1}{l \sin a_{i_o}} \left\{ Z'_{cm} - Z_i - \left| X_{i_o} + l \sin a_{i_o} \right| \theta + Y_{i_o} \varphi \right\} \qquad (38)$$

$$\text{for } i = 1 - 8$$

V. HYDRAULIC SYSTEM, ACTUATOR FORCE-TORQUE, AND SUPPORT FORCE AND MOMENT EQUATIONS

A. HYDRAULIC SYSTEM

Actuator designations are shown in the sketch below. The directions for positive flows are also defined there. $\bar{Q}_i$ is the (operating point plus perturbation) flow which is positive for flow out of the ith actuator. $\bar{Q}_{T_i}$ is the transfer flow from the slave actuator; flow into the ith actuator is positive.

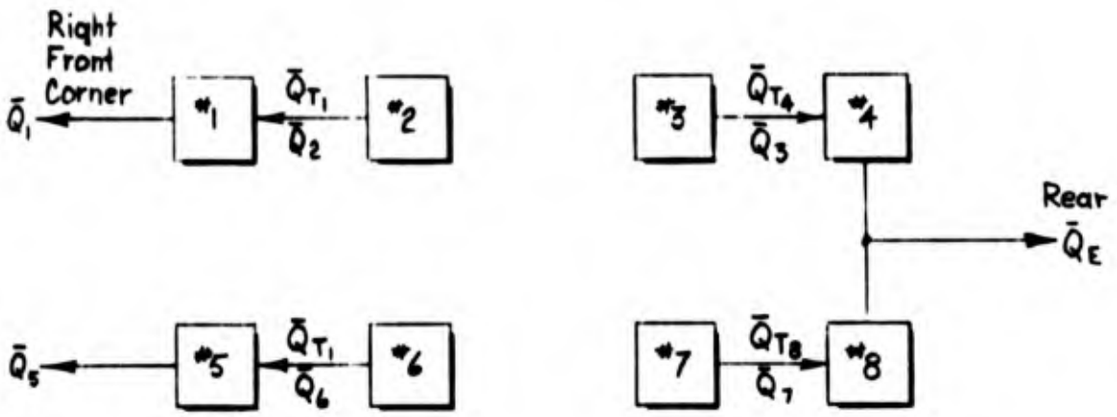

The equations for the hydraulic system will include the following effects:

Actuator - leakage, compressibility, displacement, load

Lines - leakage, inertance, compressibility, elastance (latter two are lumped into effective actuator compressibility)

The notation used to describe the primary and pressure slave rotary actuators is shown in the following two sketches. $\bar{T}_i$ denotes load torque on the ith vaneshaft.

Controlled or primary actuators (i = 1, 4, 5, 8)

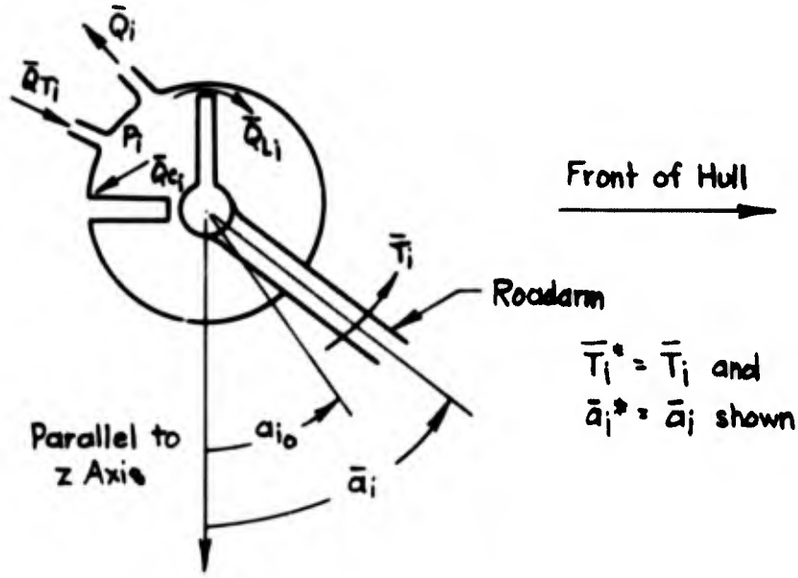

Pressure slave actuators (j = 2, 3, 6, 7)

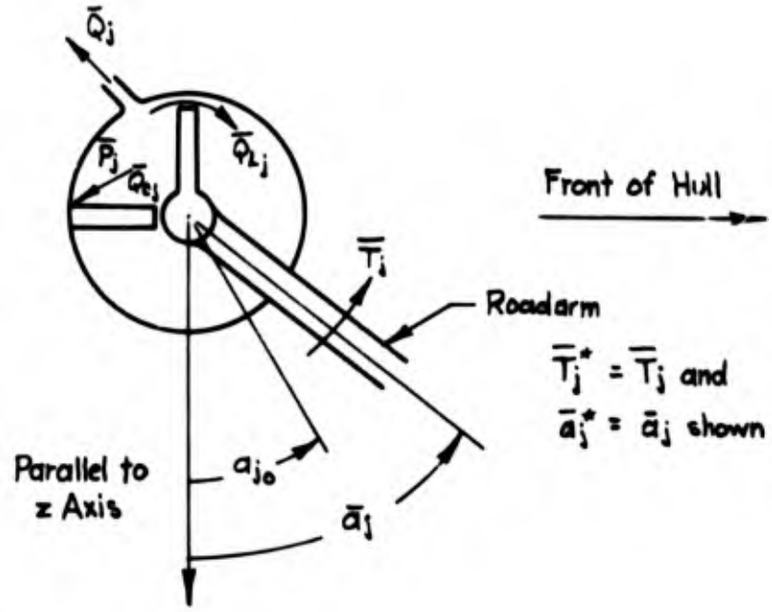

Leading roadarms are shown in the sketches. For leading roadarms, $\bar{T}^*_{(\cdot)} = \bar{T}_{(\cdot)}$ and $\bar{a}^*_{(\cdot)} = \bar{a}_{(\cdot)}$. The leading roadarms are on actuators $i = 1, 5$ and $j = 2, 6$. For trailing roadarms, $a_{(\ )}$ and $T_{(\ )}$ are negative numbers in the notational convention of the right handed coordinate system. However, these negative values still give rise to positive fluid displacements and pressures in the hydraulic system. Because of this, starred quantities which always give rise to positive fluid displacements and pressures when they themselves are positive, have been introduced to simplify thinking the problem through. Therefore, for actuators with trailing roadarms ($i = 4, 8$ and $j = 3, 7$), $\bar{T}^*_{(\cdot)} = -\bar{T}_{(\cdot)}$ and $\bar{a}^*_{(\cdot)} = -\bar{a}_{(\cdot)}$.

The basic hydraulic system equations are developed below.

The sum of the control, leakage, and compressibility flows must equal the sum of the actuator displacement and slave transfer flows

$$\bar{Q}_i + \bar{Q}_{L_i} + \bar{Q}_{c_i} = \bar{Q}_{a_i} + \bar{Q}_{T_i} \tag{39}$$

for the primary actuators. Where:

$$\bar{Q}_{L_i} = L\,\bar{P}_i \tag{40}$$

$$\bar{Q}_{c_i} = \frac{D_M}{B}(a^*_{i_o} - a^*_r)s\,P_i = C_i\,s\,P_i \tag{41}$$

$$P_i = \bar{T}_i^*/D_M \tag{42}$$

$$\bar{Q}_{a_i} = D_M\,s\,a^*_i \tag{43}$$

C_i is the compressibility coefficient for fluid in the ith actuator including a portion of the connecting line fluid compressibility and line elastance.

s is the Laplace variable—it may alternatively be regarded as the operator $d(\ )/dt$.

$P_{(\cdot)}$ is the pressure in the actuator, $(\cdot)$.

L is the actuator leakage coefficient.

D_M is the actuator volume displacement per unit rotation.

B is the fluid bulk modulus.

a_r^* is a reference actuator position determining the volume of fluid under compression.

$$\bar{Q}_{T_i} = \frac{L_j}{1 + L_j \kappa_j s} (\bar{P}_j - \bar{P}_i) \tag{44}$$

L_j is the line leakage coefficient between actuators i and j.

κ_j is the inertance of the fluid in that line.

For the pressure slave actuators, the sum of the transfer, leakage and compressibility flows must equal the actuator displacement flow.

$$\bar{Q}_{T_i} + \bar{Q}_{L_j} + \bar{Q}_{C_j} = \bar{Q}_{a_j} \tag{45}$$

Where:

$$\bar{Q}_{L_j} = L \bar{P}_j \tag{46}$$

$$\bar{Q}_{c_j} = \frac{D_M}{B} (a_{j_o}^* - a_r^*) s P_j = C_j s P_j \tag{47}$$

$$\bar{P}_j = \bar{T}_j^*/D_M \tag{48}$$

$$\bar{Q}_{a_j} = D_M s a_j^* \tag{49}$$

Theoretical methods for determining the constants required in Eq 39 through 49 are given on pp. 13-155 through 13-158 of Ref. 24.

The next step is to eliminate the hydraulic system variables which are of little interest in terms of the overall problem. That is, express the previous equations in terms of $\bar{P}_i$, $\bar{T}_i^*$, $\bar{T}_j^*$, $\bar{a}_i^*$, $\bar{a}_j^*$, and $\bar{Q}_i$ only.

Then, for the right front($i = 1$; $j = 2$) or left front ($i = 5$; $j = 6$) hydraulic suspension system:

$$\bar{P}_i = \bar{T}_i^*/D_M \tag{50}$$

$$\bar{Q}_i = + D_M s(a_i^* + a_j^*) - \frac{L}{D_M} (\bar{T}_i^* + \bar{T}_j^*) - \frac{C_i}{D_M} sT_i^* - \frac{C_j}{D_M} sT_j^* \tag{51}$$

$$\frac{L_j/D_M}{1 + L_j \kappa_j s} (\bar{T}_j^* - \bar{T}_i^*) = D_M s a_j^* - \frac{L}{D_M} \bar{T}_j^* - \frac{C_j}{D_M} s T_j^* \qquad (52)$$

The above equations for i = 4 and j = 3, and for i = 8 and j = 7 also form part of the description of the rear suspension system. However, additional equations are required to describe the interconnecting line between actuators 4 and 8. The characteristics of this line are given by the following equations. The sum of the control and interconnect line compressibility flows must equal the sum of the flows out of actuators 4 and 8 (Q_4 and Q_8). Subscript, E, denotes quantities associated with the side-to-side interconnect piping in rear suspension.

$$\bar{Q}_E + \bar{Q}_{C_E} = \bar{Q}_4 + \bar{Q}_8 \qquad (53)$$

The interconnect line leakage flows are:

$$\bar{Q}_4 = \frac{L_E}{1 + L_E \kappa_E s} (\bar{P}_4 - \bar{P}_E) \qquad (54)$$

$$\bar{Q}_8 = \frac{L_E}{1 + L_E \kappa_E s} (\bar{P}_8 - \bar{P}_E) \qquad (55)$$

The interconnect line compressibility flow is:

$$\bar{Q}_{C_E} = C_E s P_E \qquad (56)$$

Again eliminating the variables of little interest, the result is:

$$\bar{Q}_E = \frac{-2L_E}{1 + L_E \kappa_E s} \bar{P}_E - C_E s P_E + \frac{L_E/D_M}{1 + L_E \kappa_E s} (\bar{T}_4^* + \bar{T}_8^*) \qquad (57)$$

$$\frac{L_j/D_M}{1 + L_j \kappa_j s} (\bar{T}_j^* - \bar{T}_i^*) = D_M s a_j^* - \frac{L}{D_M} \bar{T}_j^* - \frac{C_j}{D_M} s T_j^* \qquad (58,59)$$

for i = 4 and j = 3, and for i = 8 and j = 7

$$\frac{L_E/D_M}{1 + L_E K_E s}\,\bar{T}_1^* - \frac{L_E}{1 + L_E K_E s}\,\bar{P}_E = D_M s(a_i^* + a_j^*) - \frac{L}{D_M}(\bar{T}_i^* + \bar{T}_j^*) - \frac{C_i}{D_M} s\, T_i^* - \frac{C_j}{D_M} s\, T_j^*$$

for $i = 4$ and $j = 3$, and for $i = 8$ and $j = 7$ (60,61)

A simpler representation of the hydraulic system is adequate for systems analysis. This would include only actuator displacement and actuator leakage effects.

For the right front ($i = 1$; $j = 2$) or left front ($i = 5$; $j = 6$) suspension system:

$$\bar{P}_i = \bar{T}_i^*/D_M \tag{62}$$

$$\bar{Q}_i = D_M s(a_i^* + a_j^*) - \frac{L}{D_M}(\bar{T}_i^* + \bar{T}_j^*) \tag{63}$$

$$\bar{T}_i^* = \bar{T}_j^* \tag{64}$$

In actual fact, the rear suspension incorporates a self-leveling feature which was not included in the previous equations. This leveling device functions such that ideally $(a_4^* + a_8^*) = (a_{4_o} + a_{8_o})$. Assuming ideal behavior of the leveling system, the rear suspension equations become:

$$\bar{T}_4^* = \bar{T}_3^* = \bar{T}_7^* = \bar{T}_8^* = \bar{T} \tag{65}$$

$$\bar{P}_E = \bar{T}/D_M \tag{66}$$

$$Q_E = D_M s(a_3^* + a_4^*) - \frac{4L}{D_M}\bar{T} \tag{67}$$

Only Eq 65 is essential for the systems analysis.

B. ACTUATOR FORCE-TORQUE EQUATIONS

The torque on the vaneshaft of each actuator is determined solely by the support force on the associated roadwheel axle since the roadarm-

roadwheel-track segment systems are assumed to be massless. The situation is pictured in the sketch below. Notice that the longitudinal slope of the working surface at the contact patch is assumed to be zero.

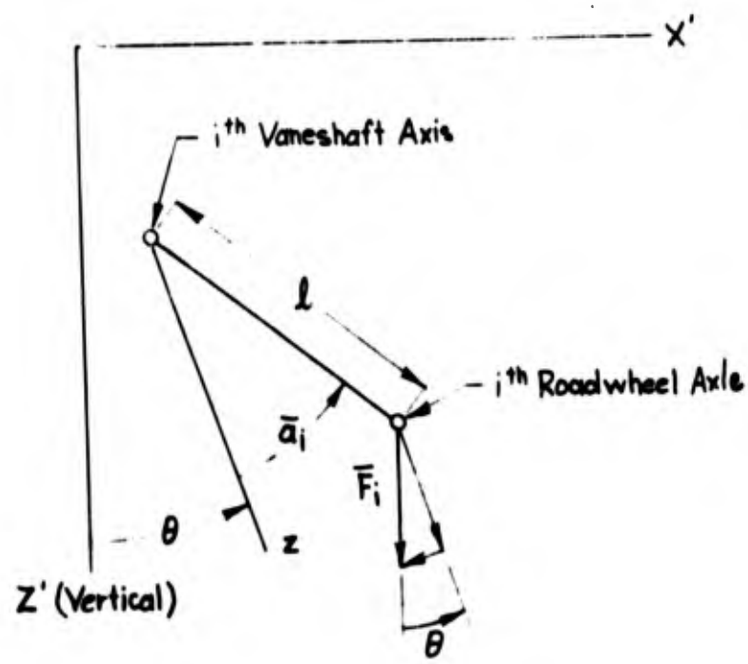

The support force on the ith roadwheel axle is $\bar{F}_i$. ($\bar{F}_i$ is always a negative number.) The force and torque on the ith vaneshaft are $\bar{F}_i$ and $\bar{T}_i$ respectively. On vaneshafts 4 and 8 there is an additional torque component, T_{P_i}, which arises from the track tension and change in track angle at the 4th and 8th roadwheels. $\bar{T}_{P_i}$ will be developed later.

$$\bar{T}_i = -F_i \, l \sin(\theta + \bar{a}_i) + \bar{T}_{P_i} \tag{68}$$

The linearized perturbation actuator force-torque equations are:

$$T_i = -F_{i_o} \, l \cos a_{i_o}(\theta + a_i) - l \sin a_{i_o} F_i + T_{P_i} \tag{69}$$

C. SUPPORT FORCE AND MOMENT EQUATIONS

The support forces and moments acting on the hull are given in hull-fixed coordinates below.

$$\bar{X}_s = -\sum_i \bar{F}_i \theta \tag{70}$$

Linearized perturbation equation is:

$$X_s = -\sum_i F_i \theta \tag{71}$$

The side force which must be developed at the track-soil interface and transmitted to the hull is determined by the no-net-track-sideslip constraint (Eq 23) and Eq 14. These are already available as linearized perturbation equations. Combining them to eliminate the v variable results in:

$$\sum Y = m(U_o r - g\varphi + z_B s \varphi) \tag{72}$$

$$\bar{Z}_s = \sum_i \bar{F}_i + \sum Y \sin \beta \tag{73}$$

Linearized perturbation equation is:

$$Z_s = \sum_i F_i \tag{74}$$

The rolling moment arising from the support forces has two components. One arises from the side force developed at the track-soil interface and the second arises from the $\bar{F}_i$ forces.

$$\bar{L}_s = -z_B \cos \beta \sum Y + \sum_i y_{i_o} \bar{F}_i \tag{75}$$

Linearized perturbation equation is:

$$L_s = -z_B \sum Y + \sum_i y_{i_o} F_i \tag{76}$$

The pitching moment arising from the support forces is:

$$\bar{M}_s = \sum_i (\bar{T}_i - \bar{T}_{P_i} - \bar{F}_i x_{i_o} \cos\theta - \bar{F}_i z_{i_o} \sin\theta) \tag{77}$$

Notice that the propulsion induced torque component, $\bar{T}_{P_i}$, is removed from $\bar{T}_i$ so that only support force effects are included. The linearized perturbation equation is:

$$\begin{aligned} M_s = -\sum_i (&F_{i_o} | z_{i_o} + l \cos a_{i_o} | \theta - F_{i_o} l \sin a_{i_o} a_i \\ &- | x_{i_o} + l \sin a_{i_o} | F_i) \end{aligned} \tag{78}$$

The yawing moment arising from support forces is assumed to manifest itself as a coulomb friction-like effect. This will be approximated here by a moment proportional to yaw rate. The numerical value of the coefficient expressing this N_{s_r}, will be chosen such that the yaw rate decays in approximately 0.1 sec in accordance with subjective observation of tractor operation. The linearized perturbation equation is:

$$N_s = N_{s_r} r \tag{79}$$

VI. PROPULSIVE FORCES AND MOMENTS

A. THROTTLE-GOVERNOR-ENGINE-TORQUE CONVERTER-TRANSMISSION CHARACTERISTICS

Two cases are of interest for this subsystem. The first assumes that there is no longitudinal slip at the track-soil interface. The second assumes that the tracks are always slipping. An extensive set of symbols is required in this section so they are defined below at the outset.

1. Symbols

ω_g	control setting of governor for engine speed (RPS)
ω_e	engine speed (RPS)
I_e	effective rotary inertia of engine (slug ft^2)
m_f	torque produced from fuel (ft lb)
m_l	torque of converter on engine (ft lb)
m_s	torque output at sprocket (ft lb)
ω_s	output speed at sprocket (RPS)
δ_t	engine throttle setting (arb.)
$( )_o$	operating point value
$\overline{( )}$	total value
$( )$	perturbation value
(STR)	stall torque ratio of converter
(GR)	gear ratio $\lvert(GR) > U_1\rvert$ for reduction between engine and sprocket with torque converter locked out
d	torque constant for converter-transmission combination

2. Complete Subsystem Description

a. Diesel engine is characterized by torque-speed or horsepower-speed curves with throttle setting as a parameter. (See Ref. 5, pp.18-2 through 18-7.)

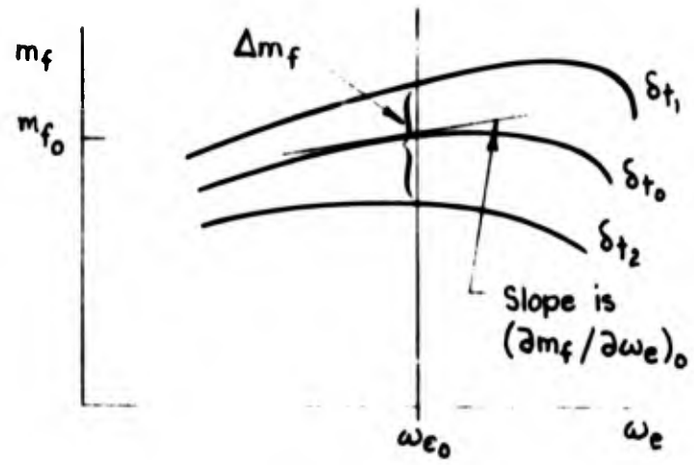

$$(\partial m_f/\partial \delta_t)_0 \doteq \frac{\Delta m_f}{(\delta_{t_1} - \delta_{t_2})}$$

$$\bar{m}_f = \bar{m}_f(\omega_e, \delta_t) = m_{f_o} + \left(\frac{\partial m_f}{\partial \omega_e}\right)_0 \omega_e + \left(\frac{\partial m_f}{\partial \delta_t}\right)_0 \frac{15}{s+15}\,\delta_t \tag{80}$$

b. Governor is characterized as a proportional plus integral controller. Also, assume a 1/15 sec time lag between δ_t and m_f.

$$\bar{\delta}_t = \left[k_1 + \frac{k_2 k_1}{s}\right](\bar{\omega}_g - \bar{\omega}_e) \tag{81}$$

The perturbation equations corresponding to Eq 75 and 76 are:

$$\delta_t = k_1 \frac{s + k_2}{s}(\omega_g - \omega_e) \tag{82}$$

$$m_f = \left(\frac{\partial m_f}{\partial \omega_e}\right)_0 \omega_e + \left(\frac{\partial m_f}{\partial \delta_t}\right)_0 \frac{15}{s+15}\,\delta_t \tag{83}$$

c. Engine acceleration characteristics are given by:

$$s\,\omega_e = \frac{1}{I_e}(m_f - m_e) \tag{84}$$

d. Torque converters are characterized by the following curves which include lockout effects. (See Ref. 26.)

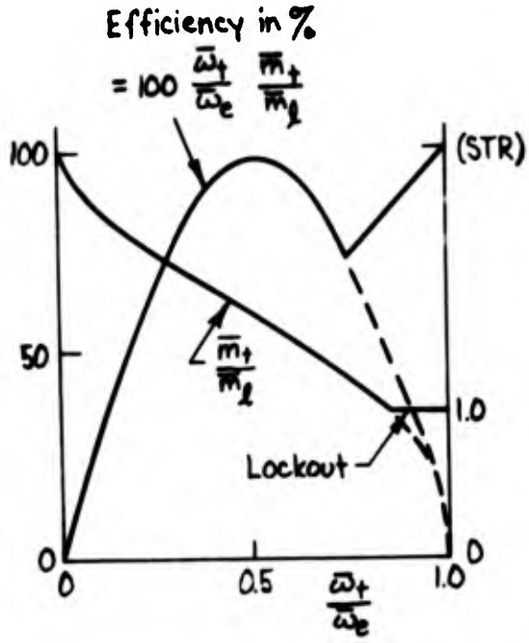

The t subscript indicates torque converter output quantities. Torque converter is characterized by the following equation which approximately describes the above torque ratio-speed ratio curve

$$\frac{\bar{m}_t}{\bar{m}_1} = \left[(\text{STR}) - 1\right]\left[1 - \frac{\bar{\omega}_t}{\bar{\omega}_e}\right] + 1 = (\text{STR})\left[1 - \frac{\bar{\omega}_t}{\bar{\omega}_e}\right] + \frac{\bar{\omega}_t}{\bar{\omega}_e} \qquad (85)$$

Consider the following model for the torque converter plus transmission

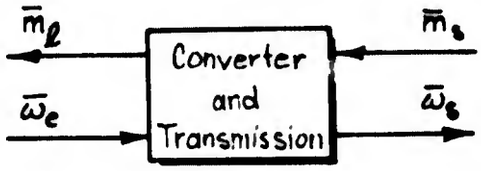

where $\bar{\omega}_s = \frac{1}{(GR)} \bar{\omega}_t$ and $\bar{m}_s = (GR)\bar{m}_t$. Then

$$\bar{m}_e = \frac{\bar{m}_s}{(GR)\left\{(STR)\left[1 - \frac{(GR)\bar{\omega}_s}{\bar{\omega}_e}\right] + \frac{(GR)\bar{\omega}_s}{\omega_e}\right\}} \tag{86}$$

3. No Track-Slip Case

a. Operating point equations

$$U_o = \omega_{s_o} b_s 2\pi \tag{87}$$

b_s is sprocket effective radius in feet.

$$m_{s_o} = (GR)\left\{(STR)\left[1 - \frac{(GR)\omega_{s_o}}{\omega_{e_o}}\right] + 1\right\} m_{l_o} \tag{88}$$

$$m_{l_o} = m_{f_o} \quad \text{(engine is not accelerating)} \tag{89}$$

$$m_{s_o} = -X_{B_o} b_s \tag{90}$$

X_{B_o} is steady state blade force.

At the operating point a given ω_{g_o} setting gives $\omega_{g_o} = \omega_{e_o}$ if $k_2 > 0$. Also ω_{e_o} gives $m_{l_o} = m_{f_o}$ from engine curves. Then Eq 88 and 89 contain only two unknowns, m_{s_o} and ω_{s_o}. These can be solved for the operating point values.

b. Perturbation equations

Next, obtain the perturbation equations for the torque converter-transmission combination by Taylor series explansion of the expression for $\bar{m}_l$ at the operating point

$$m_l = \left(\frac{\partial m_l}{\partial m_s}\right)_0 m_s + \left(\frac{\partial m_l}{\partial \omega_s}\right)_0 \omega_s + \left(\frac{\partial m_l}{\partial \omega_e}\right)_0 \omega_e \tag{91}$$

where

$$\left(\frac{\partial m_1}{\partial m_s}\right)_0 = \left(\frac{m_{1_o}}{m_{s_o}}\right) \tag{92}$$

$$\left(\frac{\partial m_1}{\partial \omega_s}\right)_0 = \left(\frac{m_{1_o}}{m_{s_o}}\right)\left(\frac{m_{1_o}}{\omega_{e_o}}\right)(GR)^2\left|(STR) - 1\right| \tag{93}$$

$$\left(\frac{\partial m_1}{\partial \omega_e}\right)_0 = -\left(\frac{m_{1_o}}{m_{s_o}}\right)\left(\frac{m_{1_o}}{\omega_{e_o}}\right)\left(\frac{\omega_{s_o}}{\omega_{e_o}}\right)(GR)^2\left|(STR) - 1\right| \tag{94}$$

Assume the output torque of the converter is proportional to the difference in speed between input and output members.

$$\bar{m}_t = \text{const.}\ (\bar{\omega}_e - \bar{\omega}_t) \tag{95}$$

$$\bar{m}_s = \text{const.}\ (\bar{\omega}_e - (GR)\bar{\omega}_s)(GR) \tag{96}$$

Then, use the torque, m_{s_o}, at the operating point, ω_{e_o}, ω_{s_o}, to find the constant.

$$(GR)\text{const.} = \frac{m_{s_o}}{\omega_{e_o} - \omega_{s_o}(GR)} = d \tag{97}$$

The perturbation equation is:

$$m_s = d\left(\omega_e - \omega_s(GR)\right) \tag{98}$$

Equations 82, 83, 84, 91, and 98 are shown in block diagram form in the following figure (Fig. B-6).

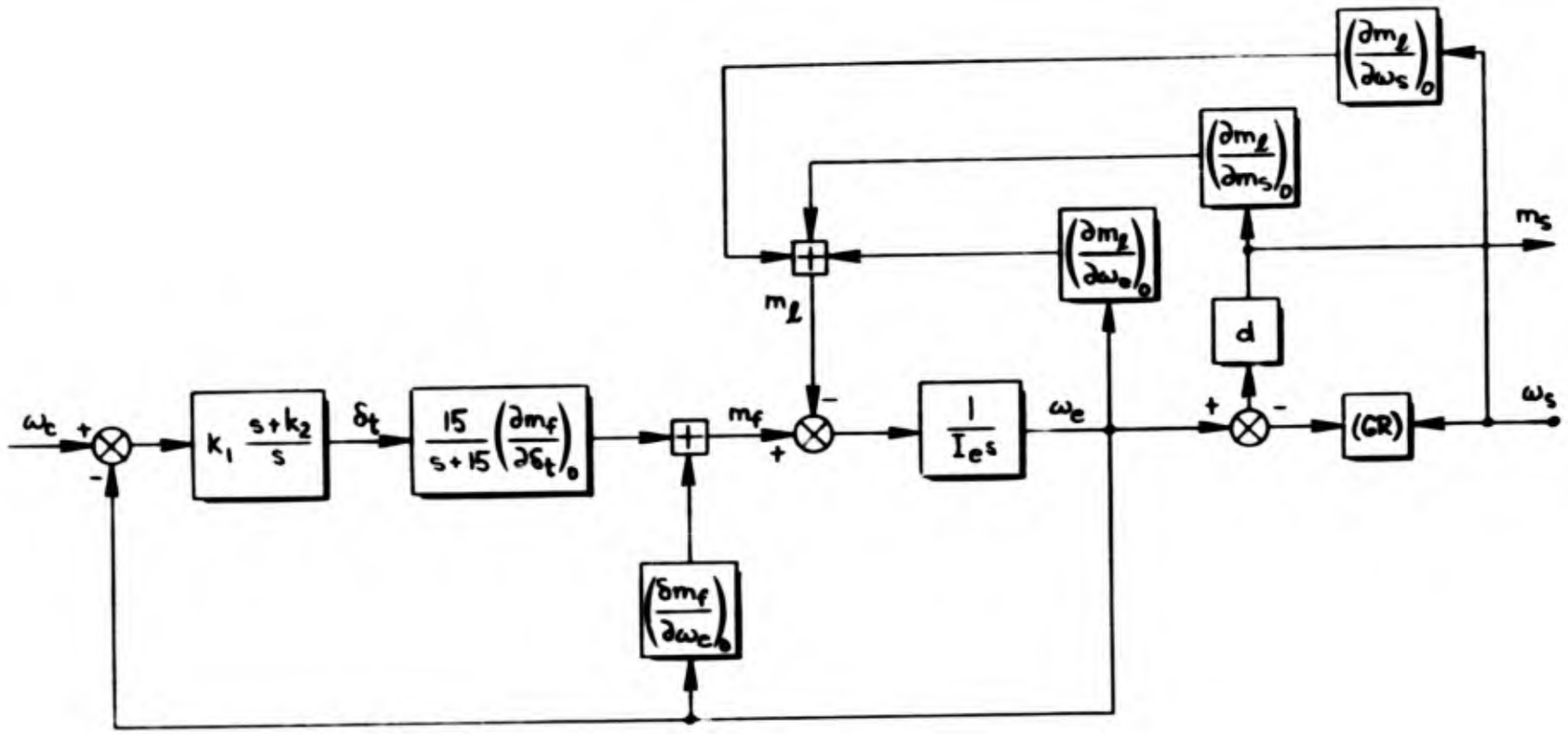

Figure B-6. Block Diagram of Throttle-Governor-Engine-Torque Converter Transmission Subsystem

The perturbation equation in terms of key perturbation variables is given below for this subsystem. It is obtained by substituting for those variables which are of little interest in the systems analysis.

$$\left[s(s+15)\left\{I_e s + \left(\frac{\partial m_1}{\partial \omega_e}\right)_0 + d\left(\frac{\partial m_1}{\partial m_s}\right)_0 - \left(\frac{\partial m_f}{\partial \omega_e}\right)_0\right\} + 15\, k_1 \left(\frac{\partial m_f}{\partial \delta_t}\right)_0 (s+k_2)\right] m_s =$$

$$- \frac{d(GR)}{2\pi\, b_s}\left[s(s+15)\left\{I_e\, s + \left(\frac{\partial m_1}{\partial \omega_e}\right)_0 - \left(\frac{\partial m_f}{\partial \omega_e}\right)_0 + \frac{1}{(GR)}\left(\frac{\partial m_1}{\partial \omega_s}\right)_0\right\}\right.$$

$$\left. + 15\, k_1 \left(\frac{\partial m_f}{\partial \delta_t}\right)_0 (s+k_2)\right] u + 15\, k_1\, d\left(\frac{\partial m_f}{\partial \delta_t}\right)_0 (s+k_2)\omega_g \qquad (99)$$

4. Continuous Track-Slip Case

a. In the slipping track case, the propulsive force is developed by way of the soil cohesion force acting at the slip surface between the soil volume entrained by the track grousers and the at-rest soil volume. The following sketch illustrates this situation.

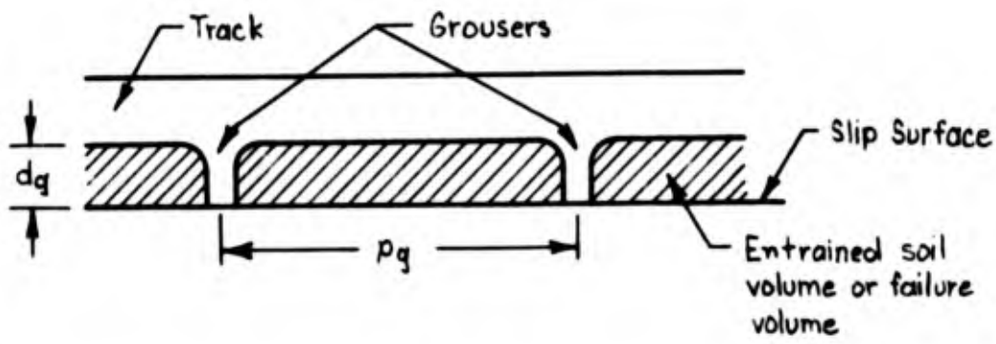

The grouser depth, pitch and projected width are d_g, p_g, and l_g,

respectively. The propulsive force developed per grouser by way of the soil cohesion force is

$$c\ p_g(l_g + 2\ d_g) \tag{100}$$

where c is the soil cohesion coefficient. The total propulsive force, $\bar{X}_p$, that can be developed is

$$\bar{X}P_{slip} = n\ c\ p_g(l_g + 2\ d_g) = XPo_{slip} \tag{101}$$

where n is the total number of grousers (on both tracks) submerged in the soil.

Notice that the slipping track propulsive force is invariant as indicated by $\bar{X}P_{slip} = XPo_{slip}$ in Eq 101. It is even independent of footprint pressure. Because the propulsive force is constant, the propulsive torque, $m_{s_{o_{slip}}} = XPo_{slip} b_s$ is constant, and the throttle-governor-engine torque converter-transmission subsystem perturbation equations are decoupled from those describing the dozer motion.

b. Operating point equations

The operating point values for the engine speed, sprocket speed, etc. are determined using Eq 88 and 89. m_{s_o} is determined from the propulsive force under tread-slip conditions. ω_{e_o} is equal to the governor setting, ω_{g_o}, if $k_2 > 0$. m_{f_o}, which equals m_{l_o}, can be determined from the engine curves. Equation 88 is then solved for ω_{s_o}. The average tread slip ratio is $2\pi\ b_s\ \omega_{s_o}/U_o$.

The operating point value for the forward speed, U_o, is found by equating X_{P_o} and $(-X_{B_o})$. X_{B_o} is a function of U_o^2. Solving the resulting equation for U_o.

5. Comment

It can be shown that the UET-E3 and 4 develop maximum propulsive

force with the tracks slipping when there are 12,960 lb in the bowl and the soil cohesion coefficient is 216 lb/ft^2. This would not necessarily be the case as the ballast weight in the bowl is increased and the soil cohesion coefficient decreased (c could easily be as small as 144 lb/ft^2 under certain soil conditions). If maximum propulsive force is developed with no track slip, care must be taken to operate at that condition if the dozing task is to be accomplished with maximum efficiency. The determination of whether a slipping or non-slipping condition should be used is made by comparing the slipping propulsive force derived above with the propulsive force developed at track breakaway. When the slipping propulsive force is largest, operate with the tracks slipping, and vice versa. The propulsive force at track breakaway, $X_{P_{O_{ba}}}$, is developed below.

$$\text{Cohesion force/grouser} = 2c \tan(45^\circ - \varphi_r/2) l_g \, \phi_g \qquad (102)$$

$$\text{Surload pressure force/grouser} = \tan^2(45^\circ - \varphi_r/2) l_g \, d_g \, \mathbf{P} \qquad (103)$$

$\mathbf{P}$ is the footprint pressure for the ballasted dozer.

$$X_{P_{O_{ba}}} = n \, l_g \, d_g \left[2c \tan(45^\circ - \varphi_r/2) + \mathbf{P} \tan^2(45^\circ - \varphi_r/2)\right] \qquad (104)$$

B. PROPULSION FORCES AND MOMENTS

The propulsion forces and moments acting on the hull are given in hull-fixed coordinates below.

$$\bar{X}_P = \begin{cases} \dfrac{m_{s_O} + m_R + m_L}{b_s} \text{ (slipping tracks)} \\ \dfrac{\bar{m}_s + m_R + m_L}{b_s} \text{ (non-slipping tracks)} \end{cases} \qquad (105)$$

The perturbation equation is:

$$X_p = \begin{cases} \dfrac{m_R + m_L}{b_s} \text{ (slipping tracks)} \\ \dfrac{r_s + m_R + m_L}{b_s} \text{ (non-slipping tracks)} \end{cases} \qquad (106)$$

m_R and m_L are sprocket torque perturbations on the right and left hand sides, respectively, arising from deflection of the steering wheel. There are no y or z components of propulsive force. There is no rolling moment arising from propulsive forces.

The propulsive pitching moments on the hull and the propulsion induced torque component on actuators 4 and 8 can be determined with the aid of the following sketch of the right hand sprocket, rear roadwheel and tread segment.

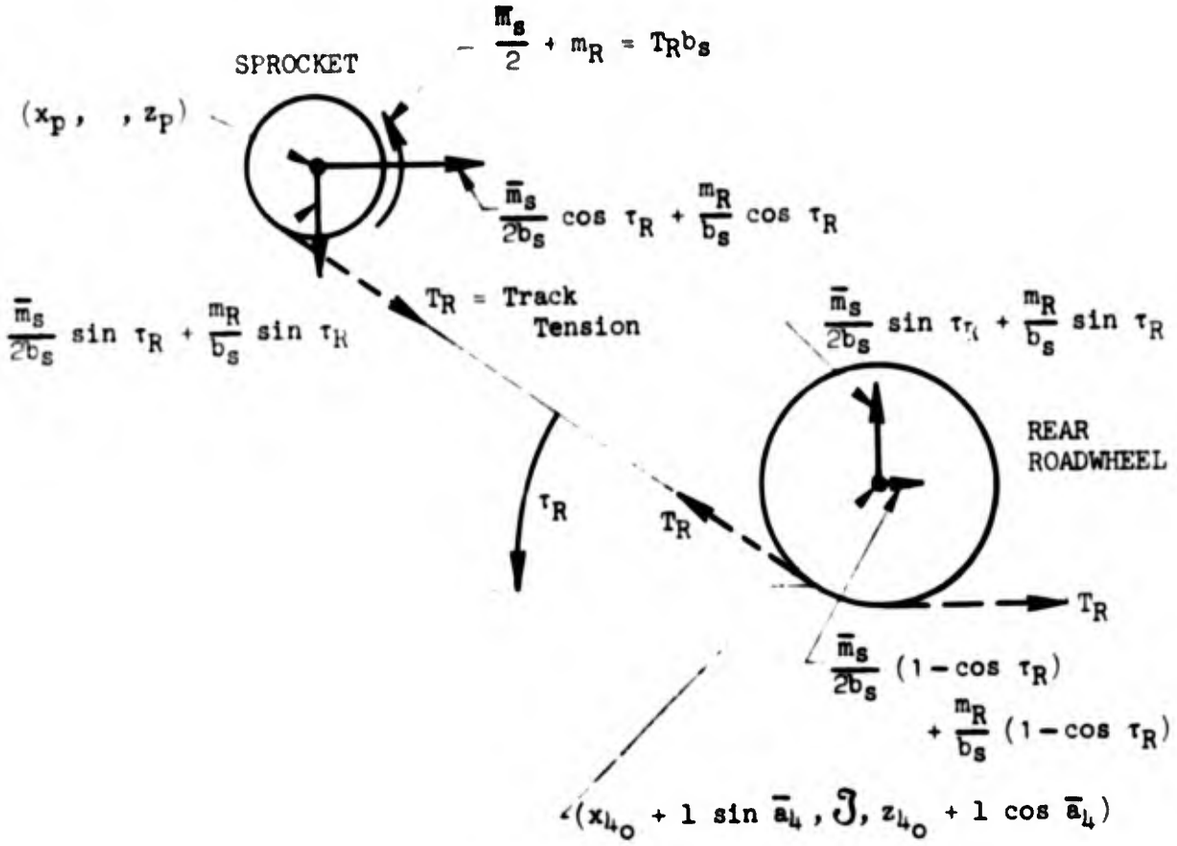

$$\bar{M}_P = \frac{\bar{m}_s + m_R + m_L}{b_s}\left\{1 - x_P \sin\tau_R + z_P \cos\tau_R\right\}$$
$$+ \frac{\bar{m}_s/2 + m_R}{b_s}\left\{(x4_o + l\sin\bar{a}_4)\sin\tau_R + (z4_o + l\cos\bar{a}_4)(1 - \cos\tau_R)\right\}$$
$$+ \frac{\bar{m}_s/2 + m_L}{b_s}\left\{(x8_o + l\sin\bar{a}_8)\sin\tau_L + (z8_o + l\cos\bar{a}_8)(1 - \cos\tau_L\right\} \quad (107)$$

For simplicity assume that the track angle τ_R is constant, and that $\tau_R = \tau_L = \tau$.

Then, the operating point equation is

$$Mp_o = \frac{m_{s_o}}{b_s}\left\{1 - x_P \sin\tau + z_P \cos\tau + (x4_o + l\sin a4_o)\sin\tau + (z4_o + l\cos a4_o)(1 - \cos\tau)\right\} \quad (108)$$

and the perturbation equation is:

$$Mp = \frac{1}{b_s}\left\{1 - x_P \sin\tau + z_P \cos\tau + (x4_o + l\sin a4_o)\sin\tau + (z4_o + l\cos a4_o)(1 - \cos\tau)\right\}(m_s + m_R + m_L)$$
$$+ \frac{m_{s_o} l}{2b_s}\left\{\cos a4_o \sin\tau - \sin a4_o(1 - \cos\tau)\right\}(a_4 + a_8) \quad (109)$$

The propulsion induced torque component on the right rear actuator vaneshaft is:

$$\bar{T}_{P4} = l\,\frac{\bar{m}_s/2 + m_R}{b_s}\left\{\sin\tau_R \sin\bar{a}_4 + (1 - \cos\tau_R)\cos\bar{a}_4\right\} \quad (110)$$

The equation for the left rear is similar. Again make the assumption that $\tau_R = \tau_L = \tau$ and that τ is constant. Then the operating point equations are

$$T_{P4_o} = \frac{m_{s_o} l}{2b_s}\left\{\sin\tau \sin a4_o + (1 - \cos\tau)\cos a4_o\right\} \quad (111)$$

$$T_{P8_o} = T_{P4_o} \quad (112)$$

and the perturbation equations are:

$$T_{P4} = \frac{1}{b_s}\left\{\sin\tau \sin a4_o + (1 - \cos\tau)\cos a4_o\right\}\left(\frac{m_s}{2} + m_R\right) + \frac{m_{s_o} l}{2b_s}\left\{\sin\tau \cos a4_o - (1 - \cos\tau)\sin a4_o\right\}a4 \quad (113)$$

$$T_{P8} = \frac{1}{b_s}\left\{\sin\tau \sin a4_o + (1 - \cos\tau)\cos a4_o\right\}\left(\frac{m_s}{2} + m_L\right) + \frac{m_{s_o} l}{2b_s}\left\{\sin\tau \cos a4_o - (1 - \cos\tau)\sin a4_o\right\}a8 \quad (114)$$

There are no propulsion induced torques on the other actuators. The yawing moment arising from propulsive forces is:

$$N_P = \frac{J}{b_s}(m_L - m_R) \quad (115)$$

C. STEERING CHARACTERISTICS

Clutch-brake steering is used at the speeds employed when dozing. The braking torque applied to one sprocket is assumed to be linear with steering wheel deflection, δ_s, for braking torque less than the track stall level.

Sprocket torque perturbations per unit steering wheel deflection given by:

$$m_L = \frac{k}{2}(\delta_s - |\delta_s|) \quad (116)$$

$$m_R = -\frac{k}{2}(\delta_s + |\delta_s|) \quad (117)$$

The above equations are non-linear. If linear equations are desired approximate Eq 116 and 117 by:

$$m_L = \frac{k}{2} \delta_s \tag{118}$$

$$m_R = -\frac{k}{2} \delta_s \tag{119}$$

VII. DOZING FORCES, MOMENTS AND KINEMATICS

A. KINEMATICS OF THE SURLOAD

The surload is assumed to have a semi-conical shape regardless of virgin terrain features or dozer blade tilt with respect to the terrain. The base angle of the cone is the soil repose angle, φ_r, where $\varphi_r = 30^\circ$ is a good number.

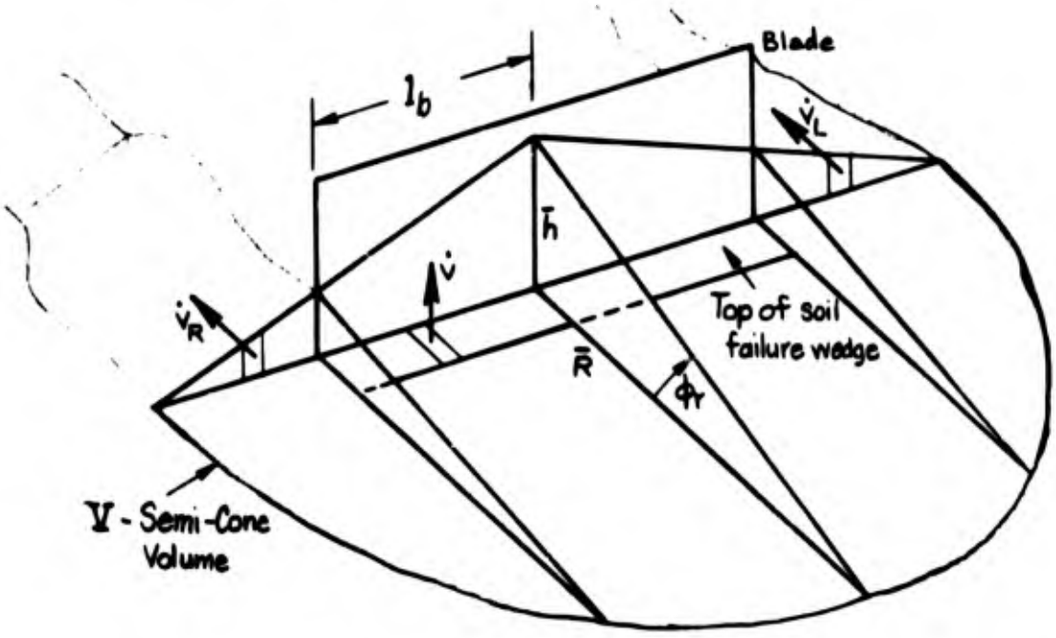

Assume that the surload always covers or extends beyond the end of the blade lip. That is, that $\bar{R} \geq l_b$. The volume of the surload semi-cone, V, is

$$V = \frac{\pi}{6} \bar{h} \bar{R}^2 = \frac{\pi}{6} \frac{\bar{h}^3}{\tan^2 \varphi_r} \tag{120}$$

The volume production per unit width of the blade, $\dot{v}$, is:

$$\dot{v} = \eta_s \left\{ Z - Z_a + y \left[\varphi - Z_{a_y} \right] \right\} (U_b + u - r\, y) \tag{121}$$

η_s is the loosened soil expansion factor, $\eta_s \geq 1$. A good number for $\eta_s = 1.25$. $\dot{v}$ is the rate at which the volume of the semi-cone increases because of the virgin soil dug up by the blade per unit width. Z_{a_y} is the slope of the virgin soil surface at the blade. When the surload base radius, $\bar{R}$, exceeds the half-width of the blade, l_b, soil volume is lost from the semi-cone at the rate, $\dot{v}_R$, from the right side and $\dot{v}_L$ from the left side per unit width.

$$\dot{v}_R = +(h - y \tan \varphi_r)(U_o + u - ry) \tag{122}$$

$$\dot{v}_L = +(h + y \tan \varphi_r)(U_o + u - ry) \tag{123}$$

The rate of change of the surload volume then is:

$$\dot{V} = \int_{-l_b}^{l_b} \dot{v}\, dy - \int_{l_b}^{\bar{h}/\tan \varphi_r} \dot{v}_R dy - \int_{-h/\tan \varphi_r}^{l_b} \dot{v}_L dy = \frac{\pi \bar{h}^2 \dot{\bar{h}}}{2 \tan^2 \varphi_r} \tag{124}$$

At the operating point $\dot{V} \equiv 0$. The above equation then leads to an expression for the operating point surload height, h_o, upon evaluating the integrals.*

$$h_o = l_b \tan \varphi_r + \sqrt{2 \eta_s (-Z_{a_o}) l_b \tan \varphi_r} \tag{125}$$

It is clear that the surload height, and hence volume, is increased with increasing operating point (trim) depth of cut, $(-Z_{a_o})$. This equation also yields the linearized perturbation equation for surload altitude, h.

$$\dot{h} = \frac{4 \eta_s U_o l_b \tan^2 \varphi_r}{\pi h_o^2} \left(Z - Z_a\right) - \frac{4 U_o \tan^2 \varphi_r}{\pi h_o^2} \left[\frac{h_o}{\tan \varphi_r} - l_b\right] h \tag{126}$$

*Altitude of the surload, $\bar{h}$, is positive in the direction of negative z. This exception to the sign convention used throughout the report is made because $\bar{h}$ is always positive.

B. FORCES AND MOMENTS ARISING FROM VIRGIN SOIL COHESION

In this subsection and in the following subsections, it is assumed that no friction forces act between the soil and the blade.

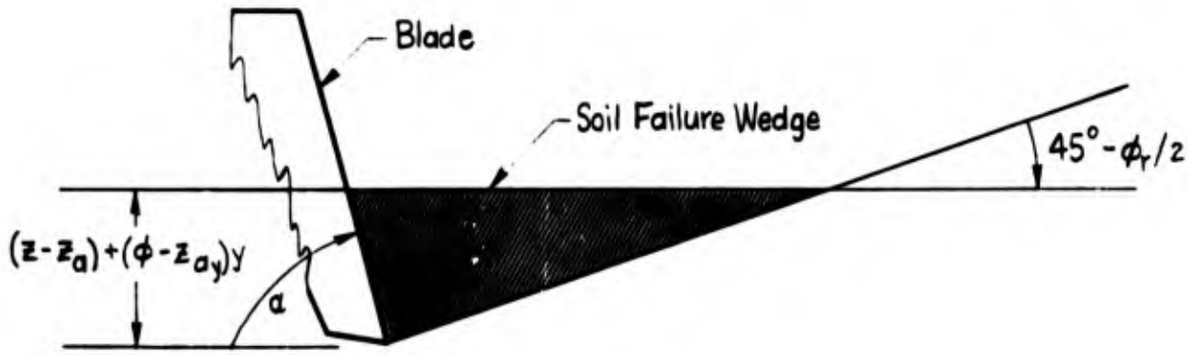

The dozer blade angle, α, is

$$\alpha = \alpha_o - \theta \tag{127}$$

where α_o is determined from the dozer blade geometry in the operating point condition. Assume the slope of the virgin surface is negligible. The cohesion force, $\bar{C}$, acting normal to the blade is given by:

$$\bar{C} = \frac{2c \tan(45^\circ - \varphi_r/2)}{\sin \alpha} \int_{-l_b}^{l_b} \left(z - \bar{z}_a + y\left|\varphi - z_{a_y}\right|\right) dy \tag{128}$$

See Ref. 27, pp. 152-156. The components of $\bar{C}$ in the directions of the hull-fixed axes are:

$$\bar{C}_x = - \frac{4c\, l_b \tan(45^\circ - \varphi_r/2)}{\sin(\alpha_o - \theta)} \sin \alpha_o \left(z - z_a\right) \tag{129}$$

$$\bar{C}_z = - \bar{C}_x / \tan \alpha_o \tag{130}$$

The pitching moment arising from this force is:

$$\overline{M}^c = \overline{C}_x\left(z_B - 1/2\left|Z - Z_a\right|\right) - \overline{C}_z\, x_B \tag{131}$$

The yawing moment is:

$$\overline{N}^c = \frac{2c\,\tan(45^\circ - \varphi_r/2)}{\sin(\alpha_o - \theta)}\,\sin\alpha_o \int_{-l_b}^{l_b} y\left\{Z - Z_a + y(\varphi - Z_{a_y})\right\}dy \tag{132}$$

$$\overline{N}^c = \frac{4l_b{}^3 c\,\tan(45^\circ - \varphi_r/2)}{3\sin(\alpha_o - \theta)}\,\sin\alpha_o(\varphi - Z_{a_y}) \tag{133}$$

The rolling moment is:

$$\overline{L}^c = \overline{N}^c/\tan\alpha_o \tag{134}$$

The operating point equations are obtained by replacing $\overline{(\ )}$ quantities with $(\ )_o$ quantities and setting the perturbation quantities to zero in the above equations.

The perturbation equations assume that $\sin(\alpha_o - \theta) = \sin\alpha_o$ for simplicity. The key linearized perturbation equations are:

$$C_x = -4cl_b\,\tan(45^\circ - \varphi_r/2)(Z - Z_a) \tag{135}$$

$$\begin{aligned} M^c = {} & -4cl_b\left[z_B + Z_{a_o} + \frac{x_B}{\tan\alpha_o}\right]\tan(45^\circ - \varphi_r/2)Z \\ & + 4cl_b\left[z_B + Z_{a_o} + \frac{x_B}{\tan\alpha_o}\right]\tan(45^\circ - \varphi_r/2)Z_a \end{aligned} \tag{136}$$

$$N^c = \frac{4cl_b{}^3\,\tan(45^\circ - \varphi_r/2)}{3}\,(\varphi - Z_{a_y}) \tag{137}$$

C. SURLOAD PRESSURE FORCE

This is the pressure force of the failure wedge on the blade arising from pressure force of the surload on the failure wedge. This force, $\bar{S}$, acts normal to the blade. Assume the surload height at the blade determines the static head. Then:

$$\bar{S} = \frac{\gamma \tan(45^\circ - \varphi_r/2)}{\eta_s \sin(\alpha_o - \theta)} \int_{-l_b}^{l_b} \int_0^{(Z-\bar{Z}_a+y\left|\varphi-Z_{a_y}\right|)} (\bar{h} - |y \tan \varphi_r|)dz\, dy \tag{138}$$

γ is the bank (virgin) soil density.

The components of $\bar{S}$ in the directions of the hull-fixed axes are:

$$\bar{S}_x = - \frac{\gamma\, l_b \tan^2(45^\circ - \varphi_r/2)}{\eta_s \sin(\alpha_o - \theta)} (2\bar{h} - l_b \tan \varphi_r)\sin \alpha_o (Z - \bar{Z}_a) \tag{139}$$

$$\bar{S}_z = - \bar{S}_x/\tan \alpha_o \tag{140}$$

The pitching moment arising from this force is:

$$\bar{M}^S = \bar{S}_x\left(z_B - 1/2\left|Z - Z_a\right|\right) - \bar{S}_z\, x_B \tag{141}$$

The yawing moment is:

$$\bar{N}^S = \frac{\gamma \tan^2(45^\circ - \varphi_r/2)}{\eta_s \sin(\alpha_o - \theta)} \sin \alpha_o \int_{-l_b}^{l_b} y(\bar{h} - |y \tan \varphi_r|) \times \left(Z - \bar{Z}_a + y\left|\varphi - Z_{a_y}\right| dy\right) \tag{142}$$

$$\bar{N}^S = \frac{\gamma \tan^2(45^\circ - \varphi_r/2)}{\eta_s \sin(\alpha_o - \theta)} \left(\frac{2 l_b^3 \bar{h}}{3} - \frac{l_b^4 \tan \varphi_r}{2}\right) \sin \alpha_o \left(\varphi - Z_{a_y}\right) \tag{143}$$

Rolling moment is:

$$\overline{L^s} = \overline{N^s}/\tan \alpha_o \tag{144}$$

The operating point equations are obtained in the usual way from the above equations.

The key linearized perturbation equations are (neglecting θ)

$$S_x = -\frac{\gamma l_b}{\eta_s}\left(2h_o - l_b \tan \varphi_r\right)\tan^2(45^\circ - \varphi_r/2)(Z - Z_a) + \frac{2\gamma l_b Z_{a_o}}{\eta_s}\tan^2(45^\circ - \varphi_r/2)h \tag{145}$$

$$M^s = -\frac{\gamma l_b}{\eta_s}\left(2h_o - l_b \tan \varphi_r\right)\left(z_B + Z_{a_o} + \frac{x_B}{\tan \alpha_o}\right)\tan^2(45^\circ - \varphi_r/2)Z + \frac{\gamma l_b}{\eta_s}\left[\left(2h_o - l_b \tan \varphi_r\right)\left(z_B + \frac{x_B}{\tan \alpha_o}\right) + Z_{a_o}h_o\right]\tan^2(45^\circ - \varphi_r/2)Z_a + \frac{2\gamma l_b Z_{a_o}}{\eta_s}\left(z_B + \frac{Z_{a_o}}{2} + \frac{x_B}{\tan \alpha_o}\right)\tan^2(45^\circ - \varphi_r/2)h \tag{146}$$

$$N^s = \frac{\gamma}{\eta_s}\left[\frac{2l_b^3 h_o}{3} - \frac{l_b^4 \tan \varphi_r}{2}\right]\tan^2(45^\circ - \varphi_r/2)\,(\varphi - Z_{a_y}) \tag{147}$$

D. HYDROSTATIC PRESSURE FORCE, $\overline{H}$.

This force arises from the hydrostatic head of the soil failure wedge. It acts normal to the blade.

$$\overline{H} = \frac{\gamma \tan^2(45^\circ - \varphi_r/2)}{\sin(\alpha_o - \theta)}\int_{-l_b}^{l_b}\int_0^{(Z-\overline{Z}_a+y\left|\varphi-Z_{a_y}\right|)} z\, dz\, dy \tag{148}$$

The components of this force in the hull-fixed axis directions are:

$$\bar{H}_x = -\frac{\gamma\, l_b \tan^2(45^\circ - \varphi_r/2)}{\sin(\alpha_o - \theta)} \left[\left(Z - \bar{Z}_a\right)^2 + \frac{l_b^2}{3} \left(\varphi - Z_{a_y}\right)^2 \right] \qquad (149)$$

$$\bar{H}_z = -\bar{H}_x/\tan\alpha_o \qquad (150)$$

The pitching arising from this force is:

$$\bar{M}^H = \bar{H}_x \left(z_B - 1/3 \left| Z - \bar{Z}_a \right| \right) - \bar{H}_z\, x_B \qquad (151)$$

The yawing moment is:

$$\bar{N}^H = \frac{\gamma \tan^2(45^\circ - \varphi_r/2)}{2\sin(\alpha_o - \theta)} \sin\alpha_o \int_{-l_b}^{l_b} y \left\{ Z - \bar{Z}_a + y\left(\varphi - Z_{a_y}\right) \right\}^2 dy \qquad (152)$$

$$\bar{N}^H = \frac{2\gamma\, l_b^3 \tan^2(45^\circ - \varphi_r/2)}{3\sin(\alpha_o - \theta)} \sin\alpha_o \left(Z - \bar{Z}_a\right)\left(\varphi - Z_{a_y}\right) \qquad (153)$$

The rolling moment is:

$$\bar{L}^H = \bar{N}^H/\tan\alpha_o \qquad (154)$$

Operating point equations are obtained in the usual way. The key linearized perturbation equations are (neglecting θ)

$$H_x = 2\gamma\, l_b\, Z_{a_o} \tan^2(45^\circ - \varphi_r/2)(Z - Z_a) \qquad (155)$$

$$M^H = 2\gamma\, l_b\, Z_{a_o} \left(z_B + \frac{Z_{a_o}}{2} + \frac{x_B}{\tan\alpha_o} \right) \tan(45^\circ - \varphi_r/2)(Z - Z_a) \qquad (156)$$

$$N^H = -\frac{2\gamma\, l_b^3 Z_{a_o} \tan(45^\circ - \varphi_r/2)}{3} \left(\varphi - Z_{a_y}\right) \qquad (157)$$

E. HYDROSTATIC PRESSURE FORCE, $\bar{H}_v$

This force arises from the surload pressure on the blade. It acts normal to the blade.

$$\bar{H}_v = \frac{\gamma \tan^2(45^\circ - \varphi_r/2)}{2\,\eta_s \sin(\alpha_o - \theta)} \int_{-l_b}^{l_b} \left(\bar{h} - |y \tan \varphi_r|\right)^2 dy \qquad (158)$$

The components of $\bar{H}_v$ in the directions of the hull-fixed axes are:

$$\bar{H}_{v_x} = - \frac{\gamma\, l_b \tan^2(45^\circ - \varphi_r/2)\tan^2\varphi_r \sin \alpha_o}{\eta_s \sin(\alpha_o - \theta)} \left[\frac{\bar{h}^2}{\tan^2\varphi_r} - \frac{l_b \bar{h}}{\tan \varphi_r} + \frac{l_b^2}{3}\right] \qquad (159)$$

$$\bar{H}_{v_z} = - \bar{H}_{v_x}/\tan \alpha_o \qquad (160)$$

The pitching moment arising from this force is:

$$\overline{M^{H_v}} = \bar{H}_{v_x}\left(z_B - \left|Z - \bar{Z}_a\right| - 1/3\left|\bar{h} - 1/2\, l_b \tan \varphi_r\right|\right) - \bar{H}_{v_z}\, x_B \qquad (161)$$

There are no yawing or rolling moments produced by this force.

The operating point equations are obtained in the usual way from the above equations. The key linearized perturbation equations are (neglecting θ)

$$H_{v_x} = - \frac{\gamma l_b}{\eta_s}\left(2h_o - l_b \tan \varphi_r\right)\tan^2(45^\circ - \varphi_r/2)h \qquad (162)$$

$$\begin{aligned} M^{H_v} = & - \frac{\gamma l_b}{\eta_s}\left\{\left(z_B + Z_{a_o} - \frac{h_o}{3} + \frac{l_b \tan \varphi_r}{6} + \frac{x_B}{\tan \alpha_o}\right)\left(2h_o - l_b \tan \varphi_r\right)\right. \\ & \left. - 1/3\left(h_o^2 - h_o l_b \tan \varphi_r + \frac{l_b^2 \tan \varphi_r}{3}\right)\right\}\tan^2(45^\circ - \varphi_r/2)h \\ & + \frac{\gamma l_b}{\eta_s}\left(h_o^2 - h_o l_b \tan \varphi_r + \frac{l_b^2 \tan^2 \varphi_r}{3}\right)\tan^2(45^\circ - \varphi_r/2)(Z - Z_a) \end{aligned} \qquad (163)$$

F. INERTIAL REACTION FORCES AND MOMENTS

These forces and moments arise from acceleration of the surload semi-cone and the soil failure wedge. Assumptions made so far concerning the surload limit its degrees of freedom to u and r. Similar assumptions will be applied for the soil failure wedge for the purpose of computing these forces and moments.

The force in the x direction is (neglecting θ):

$$\begin{aligned}\bar{A}_x &= \frac{-\gamma}{\eta_s g}\left[\frac{\pi h^3}{6\tan^2\varphi_r} + \frac{l_b(Z - Z_a)^2\eta_s}{\tan(45^\circ - \varphi_r/2)}\right]\dot{u} \\ &= -\left(m_{\text{surload}} + m_{\text{failure wedge}}\right)\dot{u}\end{aligned} \tag{164}$$

and in the z direction is:

$$\bar{A}_z = -\bar{A}_x/\tan\alpha_o \tag{165}$$

The pitching moment arising from these forces is complicated by the fact that the forces upon m_{surload} and $m_{\text{failure wedge}}$ act at different points on the blade.

$$\begin{aligned}\overline{M^A} = -\Big\{&\left(z_B - 2/3\left|Z - \bar{Z}_a\right|\right) m_{\text{failure wedge}} \\ &+ \left(z_B - \left|Z - \bar{Z}_a\right| - 1/3\left|\bar{h} - 1/2\, l_b \tan\varphi_r\right|\right) m_{\text{surload}}\Big\}\dot{u} - x_B\,\bar{A}_z\end{aligned} \tag{166}$$

The yawing moment is:

$$\begin{aligned}\overline{N^A} &= -\frac{\gamma}{\eta_s g}\left[\frac{\pi \bar{h}^5}{20\tan^4\varphi_r} + \eta_s\,\frac{2l_b^3(Z - \bar{Z}_a)^2 + l_b(Z - \bar{Z}_a)^4}{6\tan(45^\circ - \varphi_r/2)}\right]\dot{r} \\ &= -\left(I_{\text{surload}} + I_{\text{failure wedge}}\right)\dot{r}\end{aligned} \tag{167}$$

No operating point contribution results from this effect.

The key linearized perturbation equations are (neglecting θ):

$$A_x = -\frac{\gamma}{\eta_s g}\left[\frac{\pi h_o^3}{6\tan^2\varphi_r} + \frac{\eta_s l_b Z_{a_o}^2}{\tan(45^\circ - \varphi_r/2)}\right]\dot{u} \tag{168}$$

$$M^A = -\frac{\gamma}{\eta_s g}\left\{\left(z_B + Z_{a_o} - 1/3\left[h_o - 1/2\, l_b \tan\varphi_r\right] + \frac{x_B}{\tan\alpha_o}\right)\frac{\pi h_o^3}{6\tan^2\varphi_r} + \left(z_B + 2/3\, Z_{a_o} + \frac{x_B}{\tan\alpha_o}\right)\frac{\eta_s l_b Z_{a_o}^2}{\tan(45^\circ - \varphi_r/2)}\right\}\dot{u} \tag{169}$$

$$N^A = -\frac{\gamma}{\eta_s g}\left[\frac{\pi h_o^5}{20\tan^4\varphi_r} + \frac{2 l_b^3 Z_{a_o}^2 + l_b Z_{a_o}^4}{6\tan(45^\circ - \varphi_r/2)}\right]\dot{r} \tag{170}$$

G. FORCES AND MOMENTS ARISING FROM MOMENTUM EXCHANGE BETWEEN SOIL AND BLADE

The soil below the surload approaches the blade at an appreciable velocity in the axial direction. The soil impinging on the submerged portion of the blade must be brought to zero axial velocity with respect to the blade. This produces the soil momentum force, $\bar{M}$, normal to the blade.

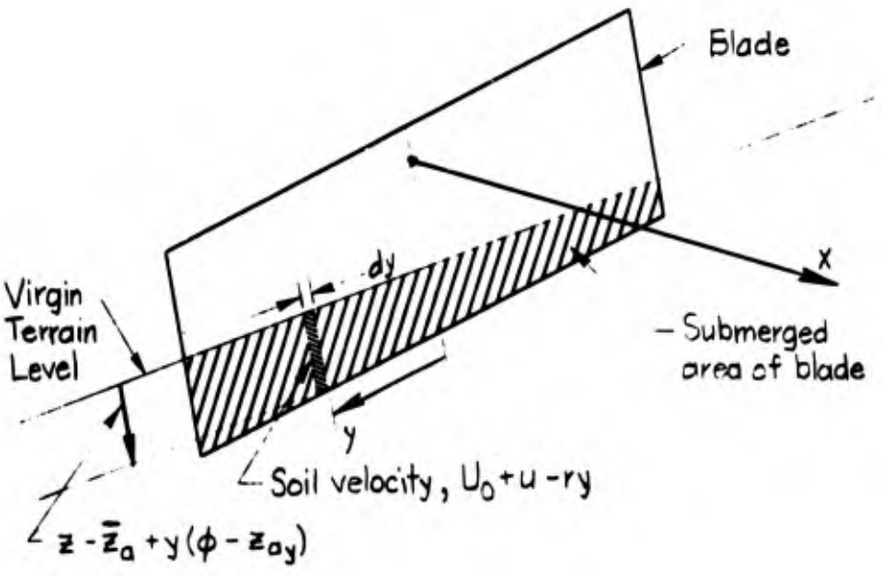

$$\bar{M}_x = -\frac{\gamma}{g}\int_{-l_b}^{l_b}\left(Z - \bar{Z}_a + y\left|\varphi - Z_{a_y}\right|\right)\left(U_o + u - ry\right)^2 dy \qquad (171)$$

$$\bar{M}_x = -\frac{2\gamma l_b}{g}\left\{\left(Z - \bar{Z}_a\right)\left(U_o + u\right)^2 + \frac{l_b^2}{3}\left(Z - Z_a\right)r^2 - \frac{2l_b^2}{3}\left(\varphi - Z_{a_y}\right)\left(U_o + u\right)r\right\} \qquad (172)$$

$$\bar{M}_z = -\bar{M}_x/\tan\alpha_o \qquad (173)$$

The pitching moment is:

$$\overline{M^m} = \bar{M}_x\left(z_B - 1/2\left|Z - \bar{Z}_a\right|\right) - \bar{M}_z\, x_B \qquad (174)$$

The yawing moment is:

$$\overline{N^m} = \frac{\gamma}{g}\int_{-l_b}^{l_b}\left(Z - \bar{Z}_a + y\left|\varphi - Z_{a_y}\right|\right)\left(U_o + u - yr\right)^2 y\, dy \qquad (175)$$

$$\overline{N^m} = \frac{2\gamma l_b^3}{g}\left\{\frac{1}{3}\left(\varphi - Z_{a_y}\right)\left(U_o + u\right)^2 - \frac{2}{3}\left(Z - \bar{Z}_a\right)\left(U_o + u\right)r + \frac{l_b^2}{5}\left(\varphi - Z_{a_y}\right)r^2\right\} \qquad (176)$$

The rolling moment is:

$$\overline{L^m} = \overline{M^m}/\tan\alpha_o \qquad (177)$$

The operating point equations are obtained in the usual way from the above equations.

The key linearized perturbation equations are:

$$M_x = -\frac{2\gamma l_b}{g}\left\{U_o^2\left(Z - Z_a\right) - 2Z_{a_o} U_o\, u\right\} \tag{178}$$

$$M^m = -\frac{2\gamma l_b}{g}\left\{\left(z_B + Z_{a_o} + \frac{x_B}{\tan\alpha_o}\right) U_o^2\left(Z - Z_a\right) - 2\left(z_B + \frac{Z_{a_o}}{2} + \frac{x_B}{\tan\alpha_o}\right) Z_{a_o} U_o u\right\} \tag{179}$$

$$N^m = \frac{2\gamma l_b^3}{3g}\left\{U_o^2\left(\varphi - Z_{a_y}\right) + 2U_o Z_{a_o} r\right\} \tag{180}$$

VIII. SUMMARY OF UET-E 3/4 OPERATING POINT AND LINEARIZED PERTURBATION EQUATIONS OF MOTION

A. UET-E 3/4 TRIM CONDITIONS AND EQUATIONS AND THEIR SOLUTION

1. Trim Conditions

$$U_o = \text{const.}, \quad Z_{a_o} = \text{const.}$$

Also in what follows, the virgin terrain transverse slope has been taken as zero for simplicity as explained below.

2. Trim Force and Moment Equations

$$\sum X_o = 0 = X_{P_o} + X_{B_o} \qquad \text{(See subheading 5)}$$

$$\sum Y_o = 0$$

$$\sum Z_o = -mg = Z_{S_o} + Z_{B_o} \qquad \text{(See subheading 6)}$$

$$\sum L_o = 0$$

$$\sum M_o = 0 = M_{S_o} + M_{P_o} + M_{B_o} \qquad \text{(See subheading 7)}$$

$$\sum N_o = 0$$

3. Trim Surload Height, h_o (fully developed surload)

$$h_o = l_b \tan \varphi_r + \sqrt{2\, \eta_s(-Z_{a_o}) l_b \tan \varphi_r}$$

trim depth of cut is $(-Z_{a_o})$, a positive number for "cut" in distinction to "fill."

4. Trim Blade Volume (for calculating production)

$$V_o = \frac{\pi}{6} \frac{h_o^3}{\tan^2 \varphi_r}$$

5. Trim X-Force Equation Components

$$\sum X_o = 0 = X_{P_o} + C_{x_o} + S_{x_o} + H_{x_o} + H_{v_{x_o}} + \cancel{A_{x_o}}^{\,0} + M_{x_o}$$

Trim propulsive force X_{P_o}

$$X_{P_o} = m_{s_o}/b_s$$

Trim cohesive force

$$C_{x_o} = 4c\, l_b\, Z_{a_o} \tan(45^\circ - \varphi_r/2)$$

Trim unload pressure force

$$S_{x_o} = \frac{\gamma l_b Z_{a_o}}{\eta_s} \left(2h_o - l_b \tan \varphi_r\right) \tan^2(45^\circ - \varphi_r/2)$$

Trim hydrostatic force of failure wedge

$$H_{x_o} = -\gamma l_b\, Z_{a_o}{}^2 \tan^2(45^\circ - \varphi_r/2)$$

Trim hydrostatic force of surload

$$H_{v_{x_o}} = -\frac{\gamma l_b}{\eta_s} \left[h_o{}^2 - h_o l_b \tan \varphi_r + \frac{l_b{}^2 \tan^2 \varphi_r}{3}\right] \tan^2(45^\circ - \varphi_r/2)$$

Trim momentum effect

$$M_{x_o} = 2\,\frac{\gamma l_b Z_{a_o} U_o{}^2}{g}$$

6. Trim Z-Force Equation Components

$$\sum{}' Z_o = \sum_1 F_{i_o} + \cancel{Z_{P_o}}^{\,0} + C_{z_o} + S_{z_o} + H_{z_o} + H_{v_{z_o}} + \cancel{A_{z_o}}^{\,0} + M_{z_o} = -mg$$

Trim F_{i_o} equations

$$T_{i_o} = - F_{i_o} l \sin a_{i_o} + T_{P_{i_o}} \qquad i = 1, \ldots, 8$$

Trim actuator moment arising from tread tension and angle

$$T_{P_{i_o}} = 0 \qquad i = 1, 2, 3, 5, 6, 7$$

$$T_{P_{i_o}} = \left(\frac{m_{s_o}}{2b_s} \sin \tau\right) l \sin a_{i_o} + \left(\frac{m_{s_o}}{2b_s} \left|1 - \cos \tau\right|\right) l \cos a_{i_o} \qquad i = 4, 8$$

Trim T_{i_o} equations are obtained from the hydraulics

$$T_{j_o} = \frac{1}{1 + L/L_j} T_{i_o} \qquad \begin{cases} i = 1, 4, 5, 8 \\ j = 2, 3, 6, 7 \end{cases}$$

$$Q_{i_o} = - \frac{L}{D_M} \frac{2 + L/L_j}{1 + L/L_j} T_{i_o}^* \qquad \begin{cases} i = 1, 5, 4, 8 \\ j = 2, 3, 6, 7 \end{cases}$$

$$P_{i_o} = T_{i_o}^*/D_M \qquad i = 1, 5$$

$$Q_{E_o} = Q_{4_o} + Q_{8_o}$$

$$P_{E_o} = \frac{1}{2}\left(\frac{T4_o^* + T8_o}{D_M} - \frac{Q_{E_o}}{L_E}\right)$$

Trim cohesion

$$C_{z_o} = - 4c\, l_b\, Z_{a_o} \frac{\tan(45^o - \varphi_r/2)}{\tan \alpha_o}$$

Trim surload pressure

$$S_{z_o} = - \frac{\gamma\, l_b\, Z_{a_o}}{\eta_s} \left(2h_o - l_b \tan \varphi_r\right) \frac{\tan^2(45^\circ - \varphi_r/2)}{\tan \alpha_o}$$

Trim hydrostatic head of failure wedge (assume $Z_{a_{s_{y_o}}} \equiv 0$)

$$H_{z_o} = \gamma\, l_b\, Z_{a_o}{}^2 \frac{\tan(45^\circ - \varphi_r/2)}{\tan \alpha_o}$$

Trim hydrostatic head of surload

$$H_{vz_o} = \frac{\gamma l_b}{\eta_s} \left(h_o^2 - h_o l_b \tan \varphi_r + \frac{l_b{}^2 \tan^2 \varphi_r}{3}\right) \frac{\tan^2(45^\circ - \varphi_r/2)}{\tan \alpha_o}$$

Trim momentum effect

$$M_{z_o} = - \frac{2\, \gamma\, l_b\, Z_{a_o}\, U_o{}^2}{g \tan \alpha_o}$$

7. Trim Pitching Moment Equation

$$\sum M_o = 0 = \sum_1 - F_{i_o}\left(x_{i_o} + l \sin a_{i_o}\right) + M_{P_o} + M_o^c + M_o^s + M_o^H + M_o^{Hv} + M_o^{A^o} + M_o^m$$

Trim propulsion pitching moment

$$M_o^P = m_{s_o} \left\{ \sin \tau \frac{x_{4_o} + l \sin a_{4_o} - x_P}{b_s} + 1 + \frac{z_P \cos \tau}{b_s} + \frac{z_{4_o} + l \cos a_{4_o}}{b_s} \left(1 - \cos \tau\right) \right\}$$

m_{s_o} is the torque output at the sprocket (trim)

Trim cohesion pitching moment

$$M_o^C = 4c\, l_b\, Z_{a_o} \tan(45^\circ - \varphi_r/2)\left[z_B + \frac{Z_{a_o}}{2} + \frac{x_B}{\tan \alpha_o}\right]$$

Trim surload pressure pitching moment

$$M_o^s = \frac{\gamma\, l_b Z_{a_o}}{\eta_s}\left(2h_o - l_b \tan \varphi_r\right)\left(z_B + \frac{Z_{a_o}}{2} + \frac{x_B}{\tan \alpha_o}\right)\tan^2(45^\circ - \varphi_r/2)$$

Trim pitching moment from hydrostatic head of failure wedge

$$M_o^H = -\gamma l_b\, Z_{a_o}{}^2\left[z_B + \frac{Z_{a_o}}{3} + \frac{x_B}{\tan \alpha_o}\right]\tan^2(45^\circ - \varphi_r/2)$$

Trim pitching moment from hydrostatic head of the surload

$$M_o^{H_v} = -\frac{\gamma l_b}{\eta_s}\left(h_o{}^2 - h_o l_b \tan \varphi_r + \frac{l_b{}^2 \tan^2 \varphi_r}{3}\right) \times \left\{Z_{a_o} - 1/3\left[h_o - 1/2\, l_b \tan \varphi_r\right] + \frac{x_B}{\tan \alpha_o}\right\}$$

Trim pitching moment from momentum effect

$$M_o^m = 2\,\frac{\gamma l_b U_o{}^2 Z_{a_o}}{g}\left[z_B + \frac{Z_{a_o}}{2} + \frac{x_B}{\tan \alpha_o}\right]$$

8. Solution of the Trim Equations

Determine $a_E = a_{4_o} = a_{8_o}$ set-point for leveling loop controlling the rear roadwheels.

From a scale elevation of the tractor, determine what the angles $a_{1_o} = a_{5_o}$, $a_{2_o} = a_{6_o}$, $a_{3_o} = a_{7_o}$ must be in order that all roadwheel surface contacts and the dozer blade lip are co-planar.

For forward facing roadarm units (1, 2, 5, 6)

$$( )_i^* = ( )_i \ , \quad i = 1, 2, 5, 6$$

For rearward facing roadarm units (3, 4, 7, 8)

$$( )_i^* = -( )_i, \quad i = 3, 4, 7, 8$$

(The star notation is merely a product of a device used to simplify sign conventions in the derivation of the hydraulic equations.)

Determine the surload height given the depth of cut.

$$h_o = l_b \tan \varphi_r + \sqrt{2 \eta_s(-Z_{a_o}) l_b \tan \varphi_r}$$

Obtain the blade force, X_{B_o}.

$$X_{B_o} = C_{x_c} + S_{x_o} + H_{x_o} + H_{v_{x_o}} + M_{x_o} = X_{B_o}(Z_{a_o}, h_o, U_o)$$

Using X_{B_o}, determine the transmission output torque required, m_{s_o}, for slipping tracks or non-slipping tracks as is appropriate (see Section VI).

Propulsive moments on hull are:

$$M_{P_o} = m_{s_o}\left\{\sin \tau \frac{x_{4_o} + l \sin a_{4_o} - x_p}{b_s} + \frac{z_p \cos \tau}{b_s} + 1 + \frac{z_{4_o} + l \cos a_{4_o}}{b_s}(1 - \cos \tau)\right\}$$

Soil moments on blade portion of the hull are:

$$M_{B_o} = M_o^C + M_o^S + M_o^H + M_o^{H_v} + M_o^m = M_{B_o}(Z_{a_o}, h_o, U_o)$$

Propulsive torque component on rear actuators is:

$$T_{P_{4_o}} = \left(\frac{m_{s_o}}{2b_s} \sin \tau\right) l \sin a_{4_o} + \left(\frac{m_{s_o}}{2b_s} \left|1 - \cos \tau\right|\right) l \cos a_{4_o} = T_{P_{8_o}}$$

Determine the soil Z forces on the blade.

$$Z_{B_o} = C_{z_o} + S_{z_o} + H_{z_o} + H_{v_{z_o}} + M_{z_o} = Z_{B_o}\left(Z_{a_o}, h_o, U_o\right)$$

Then plug in the numbers obtained above in the suspension system equations shown on p. 59.

Solve suspension system trim conditions set for:

$$T_{1_o}/T_{P_{4_o}},\ T_{4_o}/T_{P_{4_o}},\ T_{1_o}/M_{P_o},\ \text{and}\ T_{4_o}/M_{P_o}$$

Trim hydraulic system pressures and flows at trim are then given by

$$Q_{1_o} = -\frac{L}{D_M}\frac{2 + L/L_2}{1 + L/L_2} T_{1_o} = Q_{5_o}$$

$$P_{1_o} = T_{1_o}/D_M = P_{5_o}$$

$$Q_{E_o} = 2\frac{L}{D_M}\frac{2 + L/L_3}{1 + L/L_3} T_{4_o}$$

$$P_{E_o} = -\frac{T_{4_o}}{D_M} - \frac{Q_{E_o}}{2L_E}$$

B. UET-E 3/4 LINEARIZED PERTURBATION EQUATIONS AND THEIR SOLUTION

1. General Comments

The linearized* perturbation equations considered in their entirety

*One exception to linearity is retained in the steering equation to retain power loss effect with steering.

T_{1_o}	T_{2_o}	T_{3_o}	T_{4_o}	F_{1_o}	F_{2_o}	F_{3_o}	F_{4_o}			
$\frac{-1}{1+L/L_2}$	1	0	0	0	0	0	0	}	Prime Slave Actuator Relations	T_{1_o}
0	0	1	$\frac{-1}{1+L/L_3}$	0	0	0	0	}		T_{2_o}
1	0	0	0	$l \sin a_{1_o}$	0	0	0	}	Actuator Force-Torque Relations	T_{3_o}
0	1	0	0	0	$l \sin a_{2_o}$	0	0	}		T_{4_o}
0	0	1	0	0	0	$l \sin a_{3_o}$	0	}		F_{1_o}
0	0	0	1	0	0	0	$l \sin a_{4_o}$			F_{2_o}
0	0	0	0	-1	-1	-1	-1		ΣZ_o	F_{3_o}
0	0	0	0	$x_{1_o}+l \sin a_{1_o}$	$x_{2_o}+l \sin a_{2_o}$	$x_{3_o}+l \sin a_{3_o}$	$x_{4_o}+l \sin a_{4_o}$		ΣM_o	F_{4_o}

$$=$$

0
0
0
0
0
$T_{P_{4_o}}$
$m_g + M_{B_o}$
$M_{P_o}+M_{Z_o}$

Suspension System Trim Condition Equations

are fearsome things indeed, involving some 60 dependent variables. For this reason, these equations are summarized here in 16 sets. Each set comprising a subsystem of physical significance. Table B-III summarizes the number of equations in each set and indicates the interfacing input and output variables for each set. An intuitive feel for the manner in which the subsystems "fit together" can be obtained by consulting this table.

The following subsections summarize the equations for each subsystem.

TABLE B-III

SUMMARY OF MAIN SUBSYSTEMS OF PERTURBATION EQUATIONS AND THEIR INPUT AND OUTPUT VARIABLES

SUBSYSTEM	NO. OF EQUATIONS	OUTPUT VARIABLES		INPUT VARIABLES		FORCING
		COUPLED	TERMINAL	COUPLED	COMMAND	
Hydraulics	11	δT_i	P_1 P_5 P_E	δa_i	Q_1 Q_5 Q_E	
Propulsion Induced Actuator Torque	2	T_{P_L} T_{P_R}		a_L a_R ω_R ω_L ω_s		
Actuator Torque Equation	8	δF_i		δT_i δa_i T_{P_L} T_{P_R} θ		
Blade Lip Elevation	3	Z_R Z_L Z		Z'_{cm} θ φ		
Kinematic Delay	8	δZ_i		Z_R Z_L		
Hull-Roadarm-Surface Kinematics	8	δa_i		δZ_i Z'_{cm} θ φ		
Newton's Second Law for Hull Referred to Body-Axes	8	u w p q r φ θ Z Y		ZX ZZ ZY ZM ZN		
Tractor Center of Mass Trajectory	3	Z'_{cm}	X'_{cm} Y'_{cm}	u w r q φ		
Surload Height	1	h		Z u		Z_a
Steering	2	$\omega_R\omega_L$			δ_s	
Throttle	1	ω_s		u	δ_t	
X Force*	1	ZX		θ ω_R ω_L ω_s Z h φ u		Z_a
Z Force*	1	ZZ		δF_i Z h φ u		Z_a
L Moment†	1	YL		φ ZY δF_i h r		Z_{a_y}
M Moment	1	ZM		δF_i δa_i θ $\omega_T\omega_L\omega_s$ Z h u		Z_a
N Moment†	1	ZN		r $\omega_R\omega_L$ φ h		Z_{a_y}

*Can form auxiliary variable $X_B = X_B$ (Z Z_a h φ u) for X-Force Equation which is also useful in Z-Force Equation.

†Can form auxiliary variable $N_B = N_B$(φ Z_{a_y} h r) for N Moment Equation which is also useful in L Moment Equation

2. Hydraulics

Right Hand Corner System:

$$\begin{bmatrix} \left|L/D_M + C_1/D_M\, s\right| & \left|-D_M s\right| & \left|L/D_M + (C_2/D_M)s\right| & -D_M s & 1 & 0 \\ \left[\frac{-L_2/D_M}{1 + L_2K_2s}\right] & 0 & \left[\frac{L_2D_M}{1 + L_2K_2s} + (C_2/D_M)s\right] & -D_M s & 0 & 0 \\ \left|-1/D_M\right| & 0 & 0 & 0 & 0 & 1 \end{bmatrix} \begin{Bmatrix} T_1 \\ a_1 \\ T_2 \\ a_2 \\ Q_1 \\ P_1 \end{Bmatrix} = \begin{Bmatrix} 0 \\ 0 \\ 0 \end{Bmatrix}$$

Left Hand Corner Systems:

$$\begin{bmatrix} \left|L/D_M + (C_5/D_M)s\right| & \left|-D_M s\right| & \left|L/D_M + (C_6/D_M)s\right| & D_M s & 1 & 0 \\ \left[\frac{-L_6/D}{1 + L_6K_6s}\right] & 0 & \left[\frac{L_6D_M}{1 + L_6K_6s} + (C_6/D_M)s\right] & -D_M s & 0 & 0 \\ \left|-1/D_M\right| & 0 & 0 & 0 & 0 & 1 \end{bmatrix} \begin{Bmatrix} T_5 \\ a_5 \\ T_6 \\ a_6 \\ Q_5 \\ P_5 \end{Bmatrix} = \begin{Bmatrix} 0 \\ 0 \\ 0 \end{Bmatrix}$$

$$K_2 \equiv K_6 \equiv K_3 \equiv K_7$$

$$C_2 \equiv C_6 \equiv C_3 \equiv C_7$$

$$L_2 \equiv L_6 \equiv L_3 \equiv L_7$$

Rear System Equations (in matrix form)

$$
\begin{bmatrix}
\left[\frac{L_E/D_M}{1+L_E\kappa_E s}+\frac{L}{D_M}-\frac{C_4}{D_M}s\right] & -D_M s & \left[\frac{L}{D_M}-\frac{C_3}{D_M}s\right] & -D_M s & 0 & 0 & 0 \\
\left[\frac{L_3/D_M}{1+L_3\kappa_3 s}\right] & 0 & \left[\frac{L_3/D_M}{1+L_3\kappa_3 s}+\frac{L}{D_M}-\frac{C_3}{D_M}s\right] & D_M s & 0 & 0 & 0 \\
0 & 0 & 0 & 0 & \left[\frac{L_E/D_M}{1+L_E\kappa_E s}+\frac{L}{D_M}-\frac{C_8}{D_M}s\right] & -D_M s & \left[\frac{L}{D_M}-\frac{C_7}{D_M}s\right] \\
0 & 0 & 0 & 0 & \left[\frac{L_7/D_M}{1+L_7\kappa_7 s}\right] & 0 & \left[\frac{L_7/D_M}{1+L_7\kappa_7 s}+\frac{L}{D_M}-\frac{C_7}{D_M}s\right] \\
\left[\frac{L_E/D_M}{1+L_E\kappa_E s}\right] & 0 & 0 & 0 & \left[\frac{L_E/D_M}{1+L_E\kappa_E s}\right] & 0 & 0
\end{bmatrix}
$$

$$
\begin{bmatrix}
0 & 0 & \left[\frac{L_E}{1+L_E\kappa_E s}\right] \\
0 & 0 & 0 \\
-D_M s & 0 & \left[\frac{L_E}{1+L_E\kappa_E s}\right] \\
D_M s & 0 & 0 \\
0 & 1 & \left[\frac{2L_E}{1+L_E\kappa_E s}+C_E s\right]
\end{bmatrix}
\begin{Bmatrix} T_4 \\ a_4 \\ T_3 \\ a_3 \\ T_8 \\ a_8 \\ T_7 \\ a_7 \\ Q_E \\ P_E \end{Bmatrix}
=
\begin{Bmatrix} 0 \\ 0 \\ 0 \\ 0 \\ 0 \end{Bmatrix}
$$

3. **Propulsion Induced Actuator Torque**

$$T_{P_4} = \frac{m_{s_o} l}{2b_s}\left\{\sin\tau\cos a_{4_o} - (1-\cos\tau)\sin a_{4_o}\right\}a_4 + \frac{l}{b_s}\left\{\sin\tau\sin a_{4_o} + (1-\cos\tau)\cos a_{4_o}\right\}m_R + \frac{l}{2b_s}\left\{\sin\tau\sin a_{4_o} + (1-\cos\tau)\cos a_{4_o}\right\}m_s$$

$$T_{P_8} = \frac{m_{s_o} l}{2b_s}\left\{\sin\tau\cos a_{4_o} - (1-\cos\tau)\sin a_{4_o}\right\}a_8 + \frac{l}{b_s}\left\{\sin\tau\sin a_{4_o} + (1-\cos\tau)\cos a_{4_o}\right\}m_L + \frac{l}{2b_s}\left\{\sin\tau\sin a_{4_o} + (1-\cos\tau)\cos a_{4_o}\right\}m_s$$

4. **Actuator Torque Equations**

$$0 = -T_i - F_{i_o} l\cos a_{i_o}\,\theta - F_{i_o} l\cos a_{i_o}\,a_i - l\sin a_{i_o} F_i \qquad i = 1, 2, 3, 5, 6, 7$$

$$0 = -T_i - F_{i_o} l\cos a_{i_o}\,\theta - F_{i_o} l\cos a_{i_o}\,a_i - l\sin a_{i_o} F_i + T_{P_i} \qquad i = 4, 8$$

5. **Blade Lip Elevation Equations**

$$z = z'_{cm} - x_B\theta$$

$$z_R = z + \mathfrak{Z}\varphi$$

$$z_L = z - \mathfrak{Z}\varphi$$

6. Kinematic Delay Equations

$$z_1(t) = z_R(t - l_1/U_o)$$

$$z_2(t) = z_R(t - l_2/U_o)$$

$$z_3(t) = z_R(t - l_3/U_o)$$

$$z_4(t) = z_R(t - l_4/U_o)$$

$$z_5(t) = z_L(t - l_1/U_o)$$

$$z_6(t) = z_L(t - l_2/U_o)$$

$$z_7(t) = z_L(t - l_3/U_o)$$

$$z_8(t) = z_L(t - l_4/U_o)$$

7. Hull-Roadarm-Surface Kinematic Equations

$$z'_{cm} - z_i - \left|x_{i_o} + l \sin a_{i_o}\right|\theta + y_{i_o}\varphi - l \sin a_{i_o}\, a_i = 0$$

$$i = 1 - 8$$

8. Newton's Second Law for Hull Referred to Body Axes

$$su = \frac{\Sigma X}{m} - g\,\theta$$

$$\Sigma Y = mU_o r - mg\,\varphi + m\,Z_B\,\dot{\Phi}$$

$$sw = \frac{\Sigma Z}{m} + U_o\, q$$

$$s^2\varphi = sp = \frac{\Sigma L}{I_x} + \frac{I_{xz}}{I_x}\, sr$$

$$s^2\theta = sq = \frac{\Sigma M}{I_y}$$

$$sr = \frac{\Sigma N}{I_z} + \frac{I_{xz}}{I_z}\, sp$$

9. **Tractor Center of Mass Trajectory Equations**

$$s\ X'_{cm} = u$$

$$s^2\ Y'_{cm} = U_o r + z_D \Phi$$

$$s\ Z'_{cm} = \omega - U_o \theta$$

10. **Surload Height Equation**

$$\left\{ s + \frac{4U_o \tan^2\varphi_r}{\pi\ h_o^2} \left[\frac{h_o}{\tan\varphi_r} - l_b \right] \right\} h + \frac{4\eta_s U_o l_b \tan^2\varphi_r}{\pi\ h_o^2} Z_a - \frac{4\eta_s U_o l_b \tan^2\varphi_r}{\pi\ h_o^2} Z = 0$$

11. **Steering Equations**

$$m_L = \frac{k}{2} \left(\delta_s - |\delta_s| \right)$$

$$m_R = -\frac{k}{2} \left(\delta_s - |\delta_s| \right)$$

Linear steering relations might be used in place of the above nonlinear equations. Appropriate linear equations are:

$$m_L = \frac{k}{2}\ \delta_s$$

$$m_R = -\frac{k}{2}\ \delta_s$$

12. **Throttle Equation**

$$\left\{ s(s+15)\left(s + \frac{\left(\frac{\partial m_1}{\partial \omega_e}\right)_o + d\left(\frac{\partial m_1}{\partial m_s}\right)_o - \left(\frac{\partial m_f}{\partial \omega_e}\right)_o}{I_e}\right) + \frac{15k_1}{I_e}\left(\frac{\partial m_f}{\partial \delta_t}\right)_o (s+k_2)\right\} m_s$$

$$= \frac{15k_1 d}{I_e}\left(\frac{\partial m_f}{\partial \delta_t}\right)_o (s+k_2)\,\omega_c$$

$$- \frac{d(GR)}{2\pi b_s}\left\{ s(s+15)\left(s + \frac{\left(\frac{\partial m_1}{\partial \omega_e}\right)_o + \frac{1}{(GR)}\left(\frac{\partial m_1}{\partial \omega_s}\right)_o - \left(\frac{\partial m_f}{\partial \omega_e}\right)_o}{I_e}\right) + \frac{15k_1}{I_e}\left(\frac{\partial m_f}{\partial \delta_t}\right)_o (s+k_2)\right\} \omega_s$$

13. **X Force Equation**

$$\Sigma X = X_s + X_p + X_B$$

where

$$X_s = \sum_1 - F_{1_o}\,\theta$$

$$X_p = 1/b_s(m_R + m_L + m_s)$$

$$X_B = C_x + S_x + H_x + H_{v_x} + A_x + M_x$$

$$= X_B(Z,\ Z_a,\ h,\ u)$$

The coefficients of the variables in X_B are reasonably complex. For that reason, they are presented in Table B-IV.

TABLE B-IV

COEFFICIENTS FOR X_B

VARIABLE	COEFFICIENT OF VARIABLE
$(Z - Z_a)$	$-4c\ l_b \tan(45^\circ - \varphi_r/2) - \frac{\gamma l_b}{\eta_s}\left[\tan^2(45^\circ - \varphi_r/2)\right](2h_o - l_b \tan\varphi_r) + 2\ Z_{a_o}\gamma l_b \tan^2(45^\circ - \varphi_r/2) - \frac{2\gamma l_b U_o^2}{g}$
h	$+\frac{2\gamma l_b}{\eta_s}\left[\tan^2(45^\circ - \varphi_r/2)\right]Z_{a_o} - \frac{\gamma l_b}{\eta_s}\left[\tan^2(45^\circ - \varphi_r/2)\right](2h_o - l_b \tan\varphi_r)$
u	$\frac{\gamma}{\eta_s g}\left[\frac{\pi}{6}\frac{h_o^3}{\tan^2\varphi_r} + \eta_s \frac{l_b Z_{a_o}^2}{\tan(45^\circ - \varphi_r/2)}\right]s + \frac{4\gamma l_b U_o Z_{a_o}}{g}$

14. **Z Force Equation**

$$\sum Z = Z_S + Z_B$$

where

$$Z_S = \sum_i F_i$$

$$Z_B = -X_B/\tan \alpha_o$$

15. **L Moment Equation**

$$\sum L = L_S + L_B$$

where

$$L_S = \sum_i y_{i_o} F_i - z_B \sum Y$$

$$L_B = N_B/\tan \alpha_o \quad \text{(see subheading 17)}$$

16. **M Moment Equation**

$$\sum M = M_S + M_P + M_B$$

where

$$M_S = -\sum_i F_{i_o} \left[z_{i_o} + l \cos a_{i_o} \right] \theta - \sum_i F_{i_o} l \cos a_{i_o} a_i - \sum_i \left[x_{i_o} + l \sin a_{i_o} \right] F_i$$

$$M_P = \left\{ 1 - \frac{x_P \sin \tau}{b_s} + \frac{z_P \cos \tau}{b_s} + \frac{x4_o + l \sin a4_o}{b_s} \sin \tau + \frac{z4_o + l \cos a4_o}{b_s} (1 - \cos \tau) \right\} (m_R + m_L + m_s) + \frac{m_{s_o} l}{2b_s} \left\{ \cos a4_o \sin \tau - \sin a4_o (1 - \cos \tau) \right\} (a_4 + a_8)$$

$$M_B = M^C + M^S + M^H + M^{Hv} + M^A + M^m = M_B(Z, Z_a, h, u)$$

TABLE B-V

COEFFICIENTS FOR M_B

VARIABLE	COEFFICIENT OF VARIABLE
$(Z - Z_a)$	$- 4cl_b\left[z_B + Z_{a_o} + \frac{x_B}{\tan \alpha_o}\right]\tan(45^\circ - \varphi_r/2) - \frac{\gamma l_b}{\eta_s}\left[\tan^2(45^\circ - \varphi_r/2)\right]\left(2h_o - l_b\tan \varphi_r\right)\left(z_B + Z_{a_o} + \frac{x_B}{\tan \alpha_o}\right)$ $+ 2 Z_{a_o}\gamma\, l_b\left[\tan^2(45^\circ - \varphi_r/2)\right]\left(z_B + \frac{Z_{a_o}}{2} + \frac{x_B}{\tan \alpha_o}\right)$ $+ \frac{\gamma l_b}{\eta_s}\left[\tan^2(45^\circ - \varphi_r/2)\right]\left(h_o^2 - h_o l_b\tan \varphi_r + \frac{l_b^2\tan^2\varphi_r}{3}\right) - \frac{2\gamma l_b}{g}\left(z_B + Z_{a_o} + \frac{x_B}{\tan \alpha_o}\right)U_o^2$
h	$+ 2\gamma l_b\left[\tan^2(45^\circ - \varphi_r/2)\right]Z_{a_o}\left(z_B + \frac{Z_{a_o}}{2} + \frac{x_B}{\tan \alpha_o}\right)$ $- \frac{\gamma l_b}{\eta_s}\left[\tan^2(45^\circ - \varphi_r/2)\right]\left[\left(z_B + Z_{a_o} - \frac{h_o}{3} + \frac{l_b\tan \varphi_r}{6} + \frac{x_B}{\tan \alpha_o}\right)\left(2h_o - l_b\tan \varphi_r\right)\right.$ $\left. - 1/3\left(h_o^2 - h_o l_b\tan \varphi_r + \frac{l_b^2\tan^2\varphi_r}{3}\right)\right]$
u	$- \left[\left(z_B + \frac{2 Z_{a_o}}{3} + \frac{x_B}{\tan \alpha_o}\right)\frac{\gamma\, l_b\, Z_{a_o}^2}{g\tan(45^\circ - \varphi_r/2)}\right.$ $\left. + \left(z_B + Z_{a_o} - 1/6\left[2h_o - l_b\tan \varphi_r\right] + \frac{x_B}{\tan \alpha_o}\right)\frac{\pi\,\gamma\, h_o^3}{\eta_s\, 6\, g\tan^2\varphi_r}\right] s$ $+ \frac{4\gamma l_b U_o Z_{a_o}}{g}\left(z_B + \frac{Z_{a_o}}{2} + \frac{x_B}{\tan \alpha_o}\right)$

The coefficients of the variables in M_B are reasonably complex. For that reason, they are presented in Table B-V.

17. N Moment Equation

$$\sum N = N_S + N_P + N_B$$

where $$N_S = N_{S_r} r$$

(No literal expression for N_{S_r} has been derived. The effect represented is yaw damping arising from friction effects between tracks and soil.)

$$N_P = \frac{\mathcal{J}}{b_s} (m_L - m_R)$$

$$N_B = N^C + N^S + N^H + N^{H_V} + N^A + N^m$$
$$= N_B (\varphi, Z_{a_y}, r)$$

The coefficients of the variables in N_B are reasonably complex. For that reason, they are presented in Table B-VI.

TABLE B-VI

COEFFICIENTS FOR N_B

VARIABLE	COEFFICIENT OF VARIABLE
$(\varphi - Z_{a_y})$	$+ \frac{4cl_b^3}{3} \tan(45^\circ - \varphi_r/2) + \frac{\gamma}{\eta_s}\left[\tan^2(45^\circ - \varphi_r/2)\right]\left(\frac{2l_b^3 h_o}{3} - \frac{l_b^4}{2}\tan\varphi_r\right) - \frac{2l_b^3\gamma Z_{a_o}}{3}\tan^2(45^\circ - \varphi_r/2) + \frac{2\gamma l_b^3 U_o^2}{3g}$
r	$-\frac{\gamma}{\eta_s g}\left[\frac{\pi h_o^5}{20\tan^4\rho_r} + \frac{l_b^3 Z_{a_o}\eta_s}{3\tan(45^\circ - \varphi_r/2)} + \frac{Z_{a_o}^4 l_b\,\eta_s}{6\tan(45^\circ - \varphi_r/2)}\right]s + \frac{4\gamma l_b^3 U_o Z_{a_o}}{3g}$

IX. SIMPLIFIED MODEL FOR THE UET

A. ASSUMPTIONS AND SIMPLIFICATIONS

Suspension and Configuration: The tractor is assumed to have only 3 road wheels instead of the actual 8. Two wheels are in front, 1 on each side, replacing wheels 1, 2, 5, and 6, respectively. All 4 rear wheels are replaced by 1 wheel on the centerline, at the midpoint of the rear wheels in a fore and aft direction. The geometry is shown in Fig. B-7. Each of the 2 front wheels of the model are located midway between the 2 front road wheels on the actual tractor (between 1 and 2, and between 5 and 6). The height of these wheels with respect to the hull is controlled by an ideal (no leakage) rotary actuator of twice the displacement of the actual actuators.

The assumption of a single equivalent rear wheel affects only the roll dynamics of the model and is based on the nature of the rear suspension self-leveling system used in the actual tractor. This system incorporates a line running from the 2 rear road wheels on the left to the 2 on the right. Fluid is valved into the system only when both rear wheel actuators are deflected in the same direction from the trim position. Thus terrain height differences between left and right can introduce roll moments only by means of restriction in the flow between the two sides. Thus the approximation of a single rear wheel assumes negligible flow restriction in this line in the frequency range of interest, and means that terrain slant or tilt at the rear wheels produces no roll moment on the UET.

Degrees of Freedom: Only pitch angle, roll angle, and vertical translation (height) motions with respect to an inertial reference frame are considered. The tractor is assumed to be moving forward at a constant speed, U_o, with load dynamics having no effect on vehicle motion. Only perturbational motion is considered.

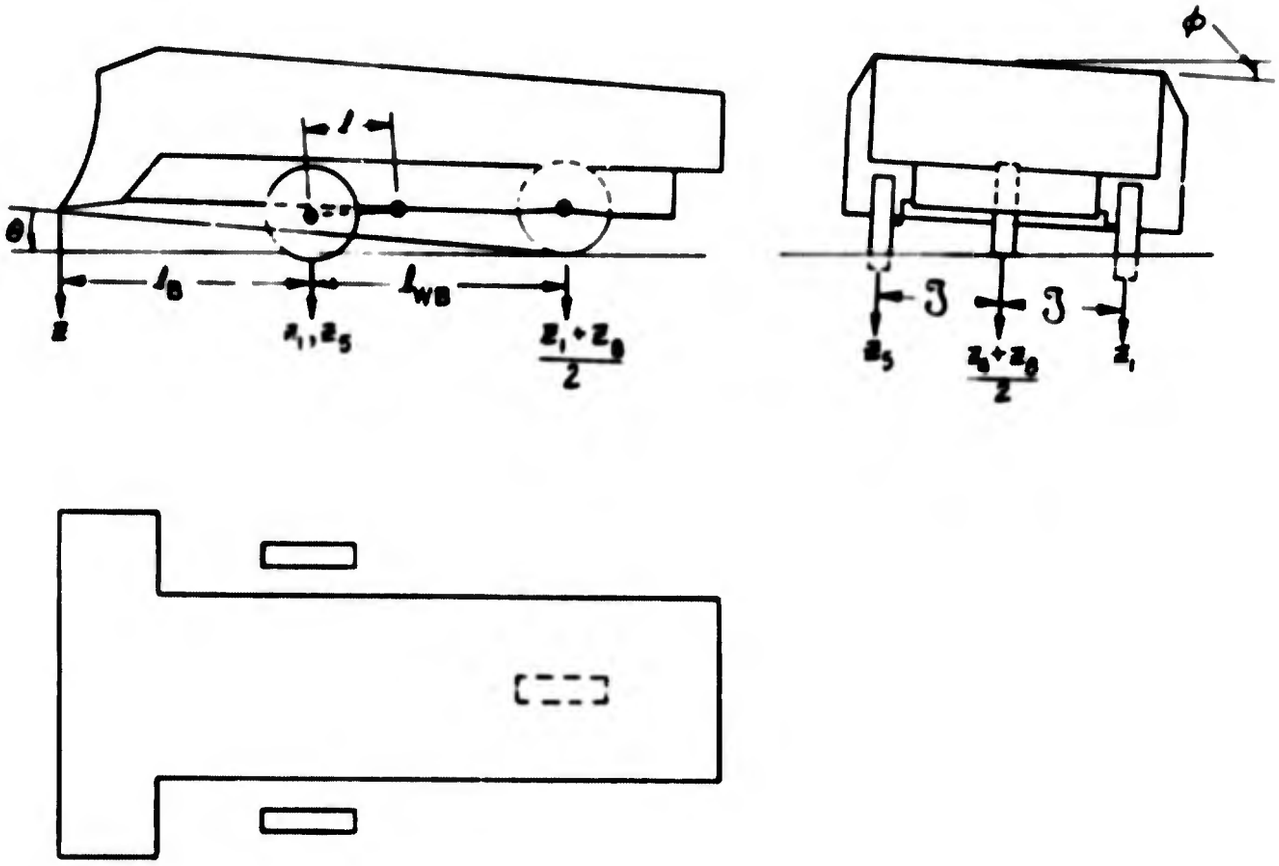

Figure B-7. Motion Quantities and Dimensions for Simplified Tractor Model

Terrain Contour: The path followed by the blade edge in space defines the path followed by the tractor's suspension. Thus the blade is assumed to be either cutting into the ambient (before blade passage) terrain, or spilling load under the blade. The weight of the tractor does not cause the wheels to sink into the soil more than the steady-state amount.

B. DEFINITIONS AND SYMBOLS

Figure B-7 illustrates the motion quantities of interest for the simplified model. The symbology is given in Table B-VII.

C. EQUATIONS OF MOTION

Because of the assumptions made, the lateral motion (roll) can be decoupled from the longitudinal motions (pitch and height), by considering the system inputs to be sums and differences of the valve flows. The simplified equations of motion are presented below in Laplace transform notation.

1. Longitudinal Equations:

a. Road arm angle

$$s\left(\frac{a_1 + a_5}{2}\right) = \frac{1}{D_M}\left(\frac{Q_1 + Q_5}{2}\right)$$

b. Pitch angle

$$\theta = \frac{1}{\ell_{WB}}\left[\frac{z_4 + z_8}{2} - \frac{z_1 + z_5}{2}\right] - \frac{\ell}{\ell_{WB}}\left(\frac{a_1 + a_5}{2}\right)$$

c. Blade height

$$z = \left(\frac{z_4 + z_8}{2}\right) - (\ell_{WB} + \ell_B)\theta$$

TABLE B-VII

SYMBOLOGY FOR SIMPLIFIED MODEL

SYMBOL	UNITS	DEFINITION
a_1, a_5	rad	Angular deflection of the right and left equivalent road arms
D_M	$in.^3/rad$	Equivalent actuator displacement
e	—	Base of natural logarithms
ℓ	ft	Road arm length
ℓ_B	ft	Distance from blade to equivalent road wheels 1 and 5
ℓ_{WB}		Equivalent wheel base
Q_1, Q_5	$in.^3/sec$	Actuator (or valve) flows
s	sec^{-1}	Laplace transform variable
$\mathfrak{I}$	ft	Distance from tractor centerline to road wheel centerline
$\tau_1 \tau_4$	sec	Time delays from blade to equivalent road wheels 1 and 5, or 4 and 8, respectively
U_o	ft/sec	Forward velocity
z	ft	Blade height (or depth)
z_1, z_5	ft	Depth of road wheels 1 (right) and 5 (left)
$\frac{z_4 + z_8}{2}$	ft	Depth of rear equivalent road wheel
φ	rad	Tractor roll attitude
θ	rad	Tractor pitch attitude

d. Kinematic delays

$$\frac{z_1 + z_2}{2} = ze^{-(\ell_B/U_o)s} = ze^{-\tau_1 s}$$

$$\frac{z_4 + z_8}{2} = ze^{-[(\ell_B + \ell_{WB})/U_o]s} = ze^{-\tau_4 s}$$

2. Lateral Equations:

a. Road arm angle

$$s\left(\frac{a_1 - a_2}{2}\right) = \frac{1}{D_M}\left(\frac{Q_1 + Q_2}{2}\right)$$

b. Roll angle

$$\gamma = \frac{\ell}{\mathfrak{J}}(a_1 - a_5) + \frac{1}{\mathfrak{J}}\left(\frac{z_1 - z_5}{2}\right)$$

c. Kinematic delay

$$\frac{z_1 - z_5}{2} = \mathfrak{J}_{ze}e^{-(\ell_B/U_o)s} = \mathfrak{J}_{ze}e^{-\tau_1 s}$$

D. TRANSFER FUNCTIONS

The preceding equations of motion may be combined to yield transfer functions relating valve flow to the various tractor motion quantities. These transfer functions are given below in terms of pure time delays.

1. Longitudinal Transfer Functions

a. Road arm angle

$$\frac{a_1 + a_5}{Q_1 + Q_5} = \frac{1}{D_M s}$$

b. Blade height

$$\frac{z}{Q_1 + Q_5} = \frac{\frac{\ell}{2D_M}}{s\left[\frac{\ell_{WB}}{\ell_{WB} + \ell_B}\left(1 - e^{-\tau_4 s}\right) - \left(e^{-\tau_1 s} - e^{-\tau_4 s}\right)\right]}$$

c. Pitch angle

$$\frac{\theta}{Q_1 + Q_5} = -\frac{\frac{\ell}{2D_M(\ell_{WB} + \ell_B)}\left(1 - e^{-\tau_4 s}\right)}{s\left[\frac{\ell_{WB}}{\ell_{WB} + \ell_B}\left(1 - e^{-\tau_4 s}\right) - \left(e^{-\tau_1 s} - e^{-\tau_4 s}\right)\right]}$$

2. **Lateral Transfer Functions**

a. Road arm angle

$$\frac{a_1 - a_5}{Q_1 - Q_5} = \frac{1}{D_M s}$$

b. Roll angle

$$\frac{p}{Q_1 - Q_5} = \frac{\frac{\ell}{2\mathcal{J} D_M}}{s(1 - e^{-\tau_1 s})}$$

E. APPROXIMATIONS FOR TIME DELAYS

Pure time delays occur in the tractor equations of motion between the blade and successive road arms. The transfer function for a pure time delay of duration τ is $e^{-\tau s}$. It presents difficulties for the analyst because of its transcendental character. The usual practice is to replace the exact expression, $e^{-\tau s}$, with a ratio of polynomials in s which approximates $e^{-\tau s}$ over a limited frequency range; the higher the order of the polynomials, the wider the frequency range of validity. For the simplified model, the following Pade approximation was used:

$$e^{-\tau s} \doteq \frac{\left(-\frac{2}{\tau}s + \frac{6}{\tau^2}\right)}{\left(s^2 + \frac{4}{\tau}s + \frac{6}{\tau^2}\right)}$$

This form gives a reasonably accurate approximation out to frequencies in the vicinity of the second-order pole, i.e., for $\omega > /6/\tau$. Using this approximation, the transfer functions relating blade height, pitch angle, and roll angle to the valve flows may be written as follows:

a. Blade height

$$\frac{z}{Q_1 + Q_5} \doteq \frac{\ell(\ell_{WB} + \ell_B)}{2D_M \ell_{WB}} \frac{\left[s^2 + \frac{4U_o}{\ell_B}s + \frac{6U_o^2}{\ell_B^2}\right]\left[s^2 + \frac{4U_o}{\ell_B + \ell_{WB}}s + \frac{6U_o^2}{(\ell_B + \ell_{WB})^2}\right]}{s^3\left[s^2 + 6U_o\left(\frac{1}{\ell_B} + \frac{1}{\ell_{WB}}\right)s + 18U_o^2\frac{1}{\ell_B(\ell_{WB} + \ell_B)}\right]}$$

b. Pitch angle

$$\frac{\theta}{Q_1 + Q_5} \doteq \frac{\ell}{2D_M \ell_{WB}} \frac{\left[s^2 + \frac{4U_o}{\ell_B}s + \frac{6U_o^2}{\ell_B^2}\right]\left(s + \frac{6U_o}{\ell_B + \ell_{WB}}\right)}{s^2\left[s^2 + 6U_o\left(\frac{1}{\ell_B} + \frac{1}{\ell_B + \ell_{WB}}\right)s + 18U_o^2\frac{1}{\ell_B(\ell_B + \ell_{WB})}\right]}$$

c. Roll angle

$$\frac{\gamma}{Q_1 + Q_5} \doteq \frac{\ell}{2D_M \ell_3} \frac{\left[s^2 + \frac{4U_o}{\ell_B}s + \frac{6U_o^2}{\ell_B^2}\right]}{s^2\left(s + \frac{6U_o}{\ell_B}\right)}$$

The tractor speed, U_o, has been left in literal form to show its effect on the dynamics. The quadratic numerators in these expressions are characterized by damping ratios of $\zeta = 2/\sqrt{6} = .816$. The quadratic denominator in the Z and θ equations has two real poles at

$$s = -3U_o\left[\frac{1}{\ell_B} + \frac{1}{\ell_B + \ell_{WB}} \pm \sqrt{\frac{1}{\ell_B^2} + \frac{1}{(\ell_B + \ell_{WB})^2}}\right]$$

X. EFFECT OF ACTUATOR LEAKAGE AND BLADE LOAD DYNAMICS

Three different mathematical models have been used to describe the dynamics of the controlled element consisting of tractor-plus-road arm actuation system:

- An eight-wheeled model which includes soil loads on the blade and actuator leakage
- A three-wheeled model which includes soil loads and actuator leakage, but a simpler geometric description
- A simplified (version of the three-wheeled) model which does not include soil loads and actuator leakage

The first is most accurate while the last provides good insight to basic effects. The second provides a good compromise between completeness and simplicity. This section compares the three-wheeled model and the simplified model; illustrating the effect of including soil load and actuator leakage. The longitudinal transfer function between blade height, z, and valve flow, $Q_1 + Q_5$, provides the example.

The essential difference between these two models lies in the equation describing the motions of the two equivalent front road arms. The more complicated model considers the effects of induced road arm torques due to soil forces, changes in the tractor attitude, and accelerations of the tractor mass. These torques produce road arm motion in the three-wheeled model because of leakage past the vane seals. The simplified model (Section IX) assumes no leakage, hence no road arm motion occurs due to these effects. In both instances, the compressibility of the hydraulic fluid is neglected, as the associated frequencies are outside the frequency range of interest.

The equation describing road arm motion with road arm torques is given in Laplace transform notation by:

$$(a_1 + a_5) = \frac{1}{D_M s}\left[Q_1 + Q_5 + \frac{12L}{D_M}(T_1 + T_5)\right]$$

The induced actuator torques, $(T_1 + T_5)$, are seen to produce road arm motions by virtue of the leakage coefficient, L.

The transfer function relating blade height to road arm motion is given by:

$$\frac{z}{a_1 + a_5} = \frac{\ell(\ell_{WB} + \ell_B)}{2\ell_{WB}} \cdot \frac{\left[s^2 + \frac{4}{\tau_1}s + \frac{6}{\tau_1^2}\right]\left[s^2 + \frac{4}{\tau_4}s + \frac{6}{\tau_4^2}\right]}{s^2\left[s^2 + \left(\frac{6}{\tau_1} + \frac{6}{\tau_4}\right)s + \frac{18}{\tau_1\tau_4}\right]}$$

Pure time delays occur between the time the blade contours the soil and the time the road wheel runs over it. In the above these pure time delays have been replaced by the second order Padé approximation

$$e^{-\tau s} \doteq \frac{-\frac{2}{\tau}s + \frac{6}{\tau^2}}{s^2 + \frac{4}{\tau}s + \frac{6}{\tau^2}}$$

The time constants τ_1 and τ_4 are equal to the time lags between the dozer blade and the first and last road wheels. The transfer function for z is identical to that of the simplified model.

The expression for the induced road arm torques, $(T_1 + T_5)$, is exceedingly complex in literal form. At a forward speed, U_o, of 2 ft/sec it is given by

$$(T_1 + T_5) = \frac{\ell}{\ell_{WB}}\left\{ - \frac{m\ell_4^2 + I_y}{\ell_B + \ell_{WB}} \frac{(s + .31)(s + 2.16)s^2}{\left[s^2 + 2(.82)(.34)s + (.34)^2\right]} z \right.$$

$$\left. + \frac{15600(s - .052)(s + .52)\left[s^2 + 2(.90)(.20)s + (.20)^2\right]}{(s + .057)(s + .14)\left[s^2 + 2(.82)(.34)s + (.34)^2\right]} z \right.$$

The first term inside the braces on the right hand side is due to inertial accelerations of the vehicle mass, while the second is primarily due to soil forces and moments acting on the blade. The

fore-and-aft weight distribution change due to change in the tractor's pitch attitude is also included in the second term. The first term consists mainly of high frequency effects, while the second is lower frequency. The block diagram of the effective controlled element with these factors broken out is given in Fig. B-8.

The effect of leakage on the controlled element can be analyzed by successively closing the two feedback loops in Fig. B-8. The characteristic equation of the system obtained when considering the inertial acceleration loop only, is given by:

$$1 + \frac{6L\ell^2(m\ell_4^2 + I_y)}{D_M^2 \ell_{WB}^2} \frac{\left[s^2 + 2(.82)(.68)s + (.68)^2\right](s + .31)(s + 2.16)}{s(s + .32)(s + 2.20)} = 0$$

The gain shown is a very small number with the result that the open-loop poles move very little due to inertial accelerations of the vehicle. The main result is that another high frequency pole is added to the forward loop transfer function which can be closely approximated by:

$$\frac{z}{a_1 + a_5} = \frac{\ell(\ell_{WB} + \ell_B)}{2\ell_B} \frac{\left[s^2 + 2(.82)(.68)s + (.68)^2\right]\left[s^2 + 2(.82)(.34)s + (.34)^2\right]}{s^2(s + .32)(s + 2.20)(Ts + 1)}$$

where $T = \frac{6L\ell^2(m\ell_4^2 + I_y)}{D_M^2 \ell_{WB}^2} = \frac{1}{2140}$ sec.

Since this time constant, T, is outside the frequency range of interest by two orders of magnitude, it can be neglected. In effect, the contribution of the inertial acceleration of the vehicle mass tc the road arm angles via leakage is negligible, and the forward loop transfer function is essentially unchanged.

The remaining feedback loop in Fig. B-8 represents the effects of blade loads and weight shift on the vehicle dynamics. It gives a characteristic equation of the form, $1 - Q_L/Q = 0$, positive feedback, where the open-loop transfer function is given by:

$$-\frac{Q_L}{Q} = \frac{-4.15L\left[s^2+2(.82)(.68)s+(.68)^2\right]\left[s^2+2(.90)(.20)s+(.20)^2\right](s-.052)(s+.52)}{s^3(s+.057)(s+.14)(s+.32)(s+2.20)}$$

The variable gain term, L, is the actuator leakage which has a nominal value of 4×10^{-4} in.^{5}/lb-sec.

The effect of leakage, L, on the characteristic (closed loop) poles of the tractor can be seen with the system survey of Fig. B-9. A root locus plot is on the left, and it shows how the poles move (from the X's to the O's) as leakage increases from zero. Frequency response plots are shown on the right; both conventional $j\omega$-Bode plots and less common σ-Bode plots [$G(+\sigma)$ and $G(-\sigma)$] which show how the real poles move with a change in leakage. The zero dB line (for given leakage) intersects the σ-Bode plots at points which correspond to closed-loop poles. The zero dB line moves down as leakage increases, and up as it decreases. The $G(+\sigma)$ curves* are loci of right half plane real poles, which $G(-\sigma)$ curves are left half plane (stable) poles. For very low leakage three poles are at the origin. As leakage increases, two of these form an unstable quadratic pair while the third moves to the left along the real axis. For sufficiently high leakage (−92 dB) the real axis poles break off and go toward the quadratic zeros at 0.2 rad/sec. As leakage is further increased to −48 dB, the unstable quadratic pair goes back into the real axis and becomes two divergent real poles.

The zero dB crossover line for nominal leakage, $L = 4\times10^{-4}$, is shown on Fig. B-9. This gives the $z \rightarrow Q$ transfer function poles for 2 ft/sec, i.e.,

$$\frac{z}{q_1+q_5} = \frac{\overbrace{.0126(.057)(.14)}^{\text{Load Dynamics}}\overbrace{[.82,.68][.82,.34]}^{\text{Kinematic Delay}}}{\underbrace{[-.77,.04][.79,.07](.14)}_{\text{Load Dynamics and Leakage}}\underbrace{(.32)(2.20)}_{\text{Kinematic Delay}}}$$

*The $G(+\sigma)$ plots are shown dashed while $G(-\sigma)$ plots are solid. The amplitude curves only exist where the "phase angle" of the transfer function for $s=\sigma$ is zero degrees.

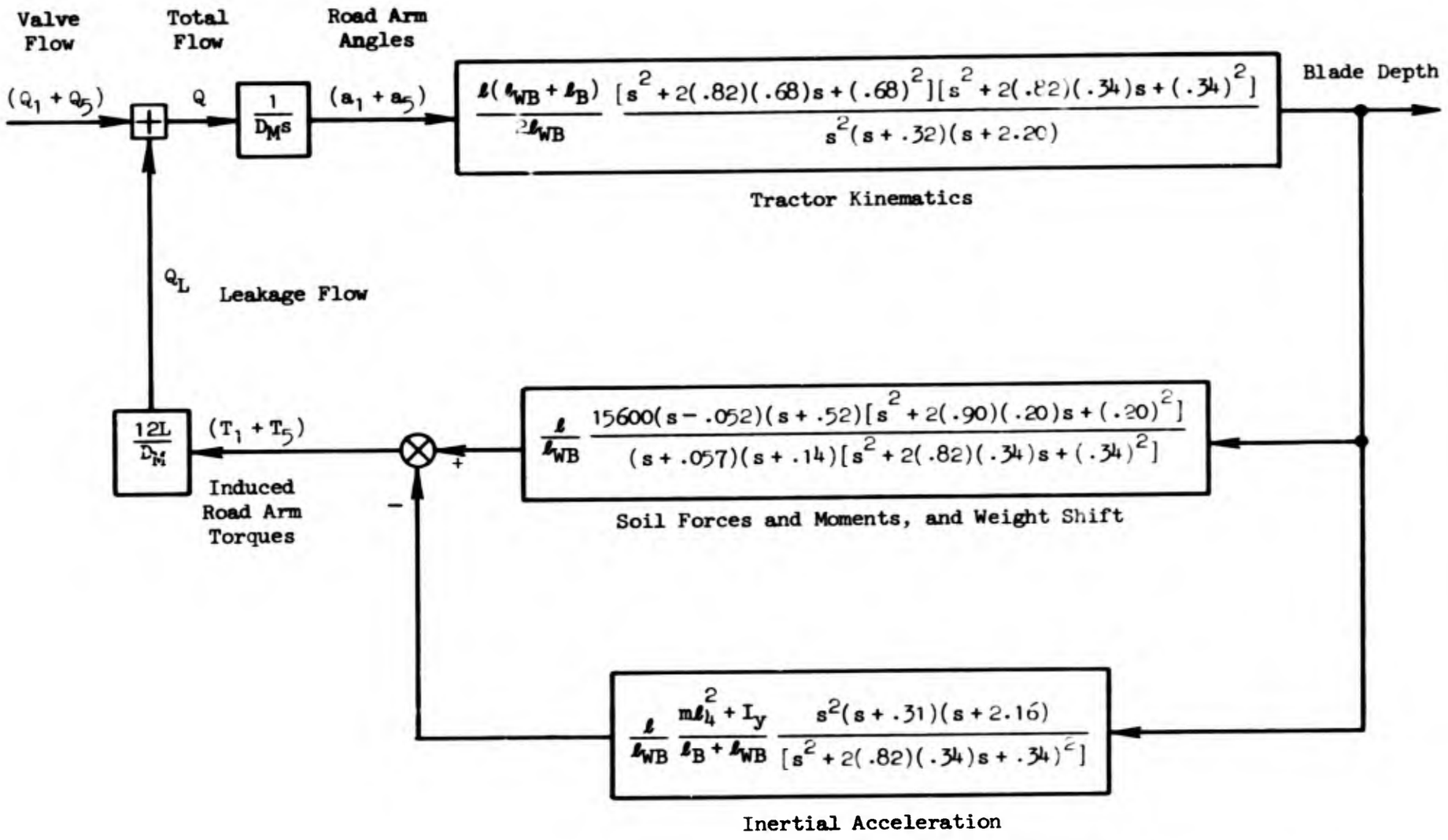

Figure B-8. Block Diagram Showing Effects of Leakage on Controlled Element, U_o = 2 fps

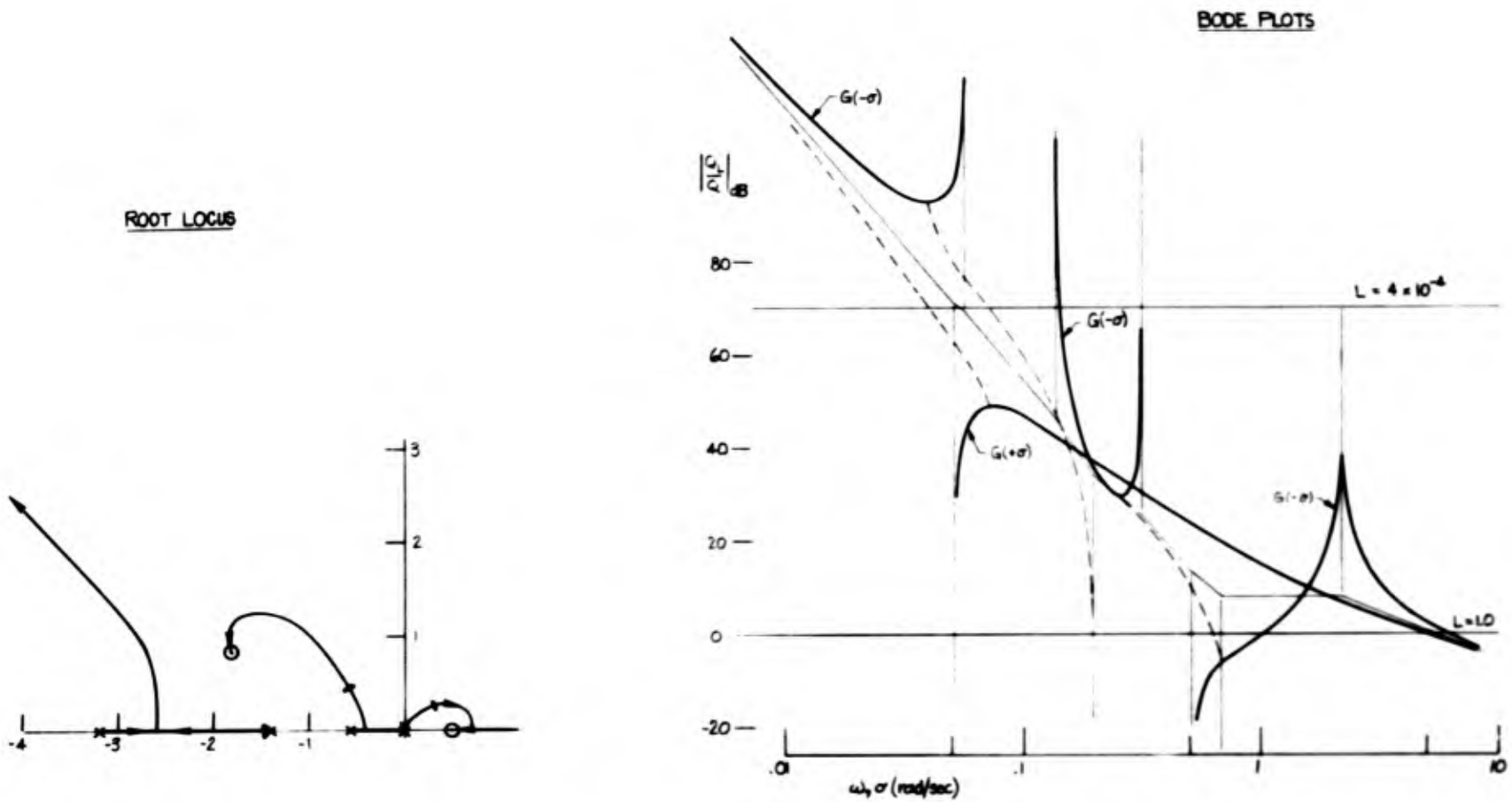

Figure B-9. Effect of Leakage on Open-Loop Poles of Blade Height Transfer Function

The dominant source of the various poles and zeros is shown. The high frequency pole ($1/T = 2140$) has been neglected.

The differences between the three-wheeled model (with leakage) and the simplified model is shown in the $j\omega$-Bode plot of Fig. B-10, which compares the frequency response of the two models. The effects of changes in leakage are also sketched in. At frequencies above $\omega \doteq .1$ rad/sec (for the nominal leakage and speed), both models are essentially identical, while below this point, leakage acts to reduce the controlled element gain. Physically, this means that the operator must maintain an average flow rate to overcome the effects of leakage, and low frequency control over blade position is more difficult.

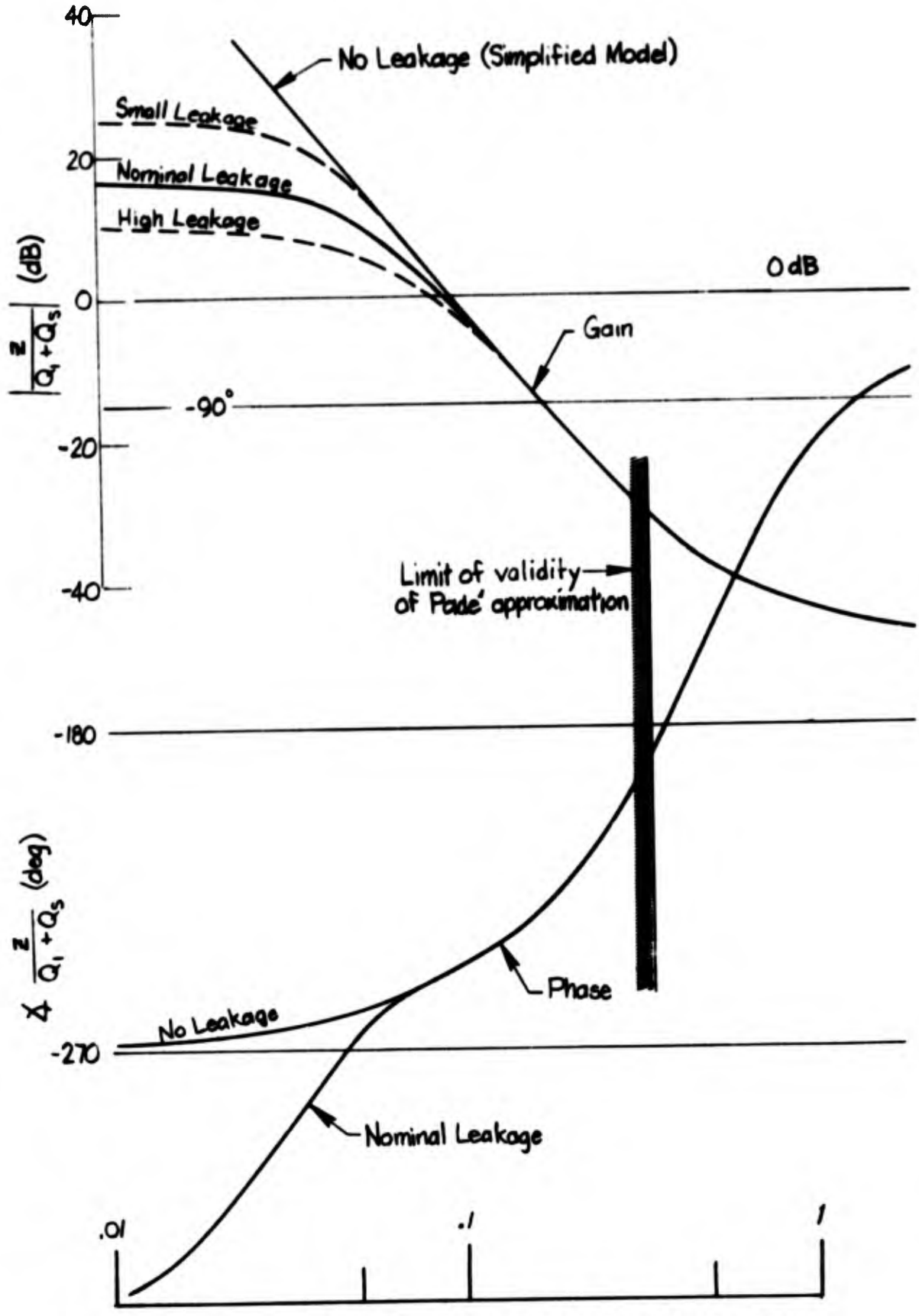

Figure B-10. Effect of Leakage on Blade Height Transfer Function

BLANK PAGE

APPENDIX C

DETAILS OF THE SINGLE-LOOP ANALYSES

Possible single-loop system structures for dozing and tilt dozing control are examined in this appendix, using the operator describing function of Section IV and the tractor (tool-plus-vehicle) dynamics of Table I. The motion cues considered* are:

z_{cm}, height of tractor center of mass

θ, tractor pitch angle

u, forward velocity

$\dot{u}$, forward acceleration

Δz or $z - z_a$, blade height, z, relative to average terrain height, z_a

h, surload height

a, road arm angle

$\dot{u} + g\theta$, output of a pendulous accelerometer

ϕ, tilt or roll angle

Most of the cues involve the visual modality, although some are primarily vestibular. Certain cues can be sensed better than others, as noted subsequently. Ability to sense is a secondary consideration here, where the main concern is how the cue permits the operator to control the tractor, assuming that it can be adequately sensed.

The analyses are presented as "system surveys" comprising a root locus plot, a $j\omega$-Bode or frequency response plot, and appropriate portions of the σ-Bode plot. Various approximations are used for plotting convenience.

---

*Vertical velocity at vehicle center of mass, w, has not been included in the surveys because the operator's ability to perceive it visually at small levels is virtually nil.

The operator's effective time delay is represented by a Padé approximation on the root locus, i.e.,

$$e^{-\tau_e s} \doteq \frac{-(s-2/\tau_e)}{(s+2/\tau_e)}$$

It is included exactly on the jω-Bode as $e^{-\tau_e j\omega}$. The $e^{-\tau_e s}$ is not included in the σ-Bode for simplicity. The $e^{-j(\alpha/\omega)}$ effect is shown only on the jα-Bode. Its deletion on the root locus results in a small difference near the origin. These approximations and simplifications do not reduce the accuracy of the ultimate answer, instead they merely delete less important parts of each plot. Conversely, the plots are complementary, and the portions shown provide the most useful information and insight.

Each system survey shows two sets of curves; the basic tractor dynamics, and this plus the operator indicating the predicted closed-loop system characteristics. The surveys are presented below and summarized in Table III of the main text.

HEIGHT OF TRACTOR CENTER OF MASS, z_{cm}

The system survey for the tractor, Y_c, is shown in Fig. C-1. The jω-Bode amplitude ratio looks approximately like K/s^3 in the potential crossover region from 0.1 to 0.5 rad/sec. This implies a need for low frequency second-order lead equalization from the operator. The corresponding effective time delay is very large at about 2/3 sec (Ref. 2). This plus the combination of high frequency controlled element lags and low frequency operator lags (due to the α-effect) should make it very difficult to achieve stable operation. Finally, it is difficult to sense the small differences in center of mass height (e.g., a couple of inches) over which control must be effected. For these reasons, it is an extremely unlikely single-loop candidate and the operator's describing function has not even been plotted on this system survey.

HEIGHT OF BLADE, Δz OR $z - z_a$

This motion is the height of the center of the blade relative to the average terrain height, where the terrain height is assumed to be a

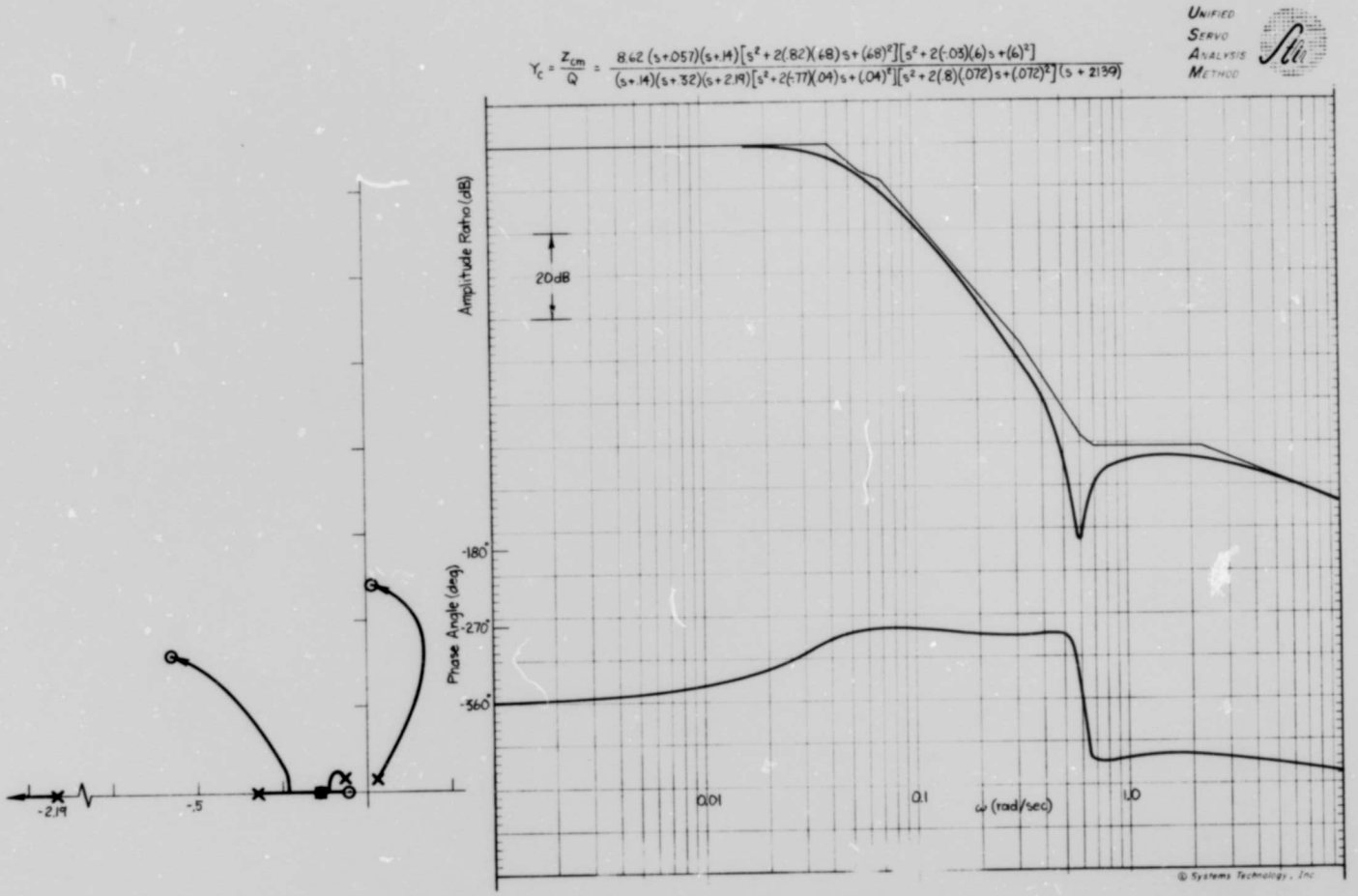

Figure C-1. Height of Center of Mass Survey

stationary random process. The system surveys for the tractor alone, Y_c, and tractor plus operator, Y_pY_c, are shown in Fig. C-2. Lag/lead equalization by the operator can create a K/s-like amplitude ratio in the region of 1 to 2 rad/sec. The resultant system dynamics, Y_pY_c, are analogous to a lead-equalized second-order critical task (Ref. 9), i.e.,

$$Y_pY_c \doteq \frac{K_pK_c(j\omega + 1/T_L)}{j\omega(j\omega - 1/T)} e^{-j(\tau_e\omega + \alpha/\omega)}$$

with $$\frac{1}{T} \doteq 0.1$$

$$\frac{1}{T_L} \doteq 0.68$$

For a low frequency forcing function, Figs. 3 and 4 (main text) give

$$\tau_e \doteq 0.36$$

$$\alpha \doteq 0.12/0.36 = 0.33$$

The operator can close the loop at about 1.8 rad/sec with the gain and phase margins shown in Table III. The closed-loop roots are shown on the root locus of Fig. C-2. Note that the plots for the low frequency phase angle and root loci for Y_pY_c are somewhat inconsistent because the α-effect is not included in the root locus.

VEHICLE PITCH ATTITUDE, θ

This motion is the pitch angle between the tractor and the average (flat) terrain slope. The system surveys for tractor alone, Y_c, and tractor plus operator, Y_pY_c, are given in Fig. C-3. In the region of crossover they look very similar to the blade height surveys in Fig. C-2, and lag/lead equalization gives the desired K/s-like amplitude ratio with phase properties analogous to the second-order critical task, as before. The describing function parameters are shown in Table III. The operator can close the loop at a 1.7 rad/sec crossover frequency with the stability margins in Table III. The closed-loop roots are shown in Fig. C-3. The

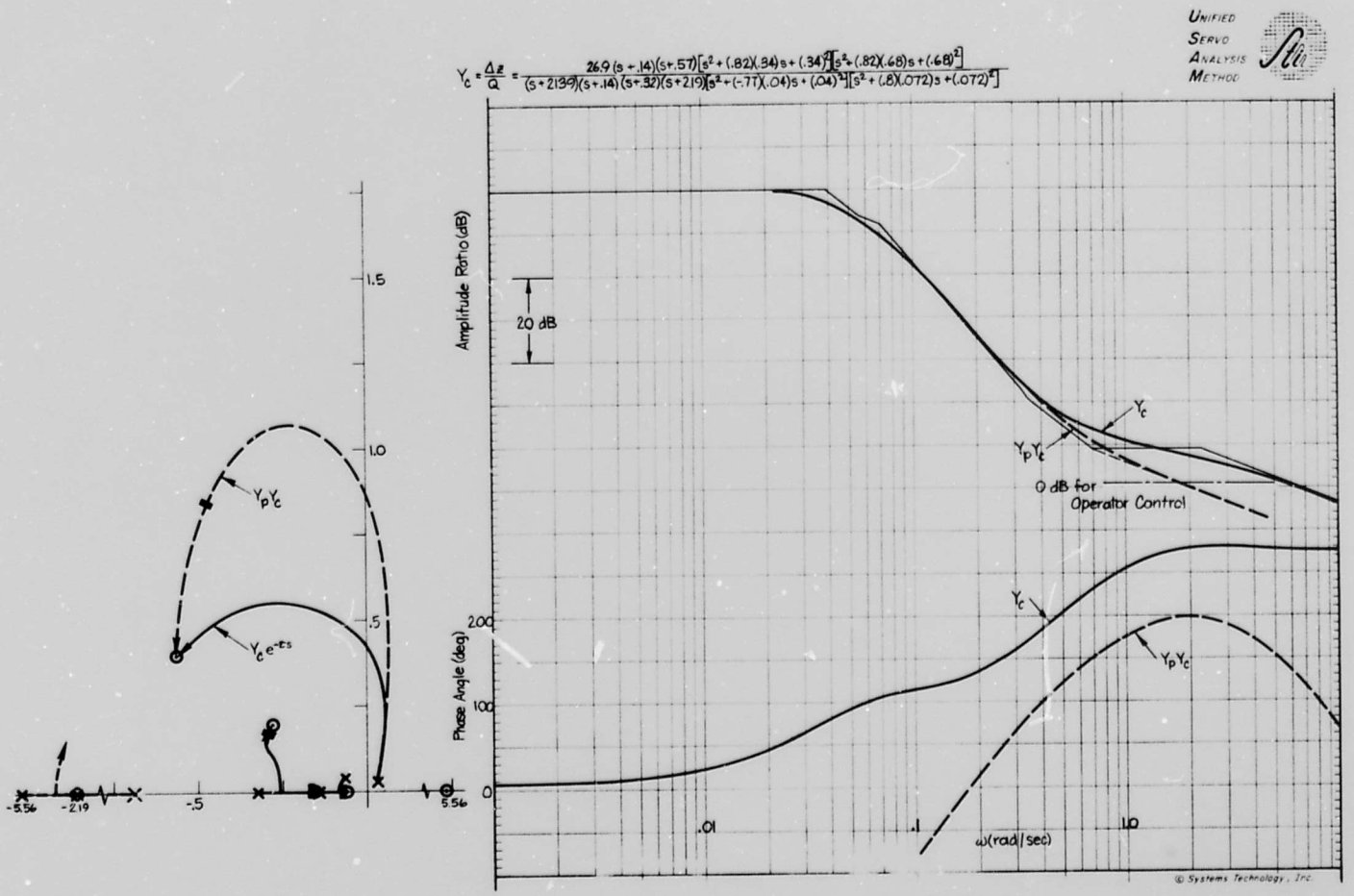

Figure C-2. Blade Height System Survey

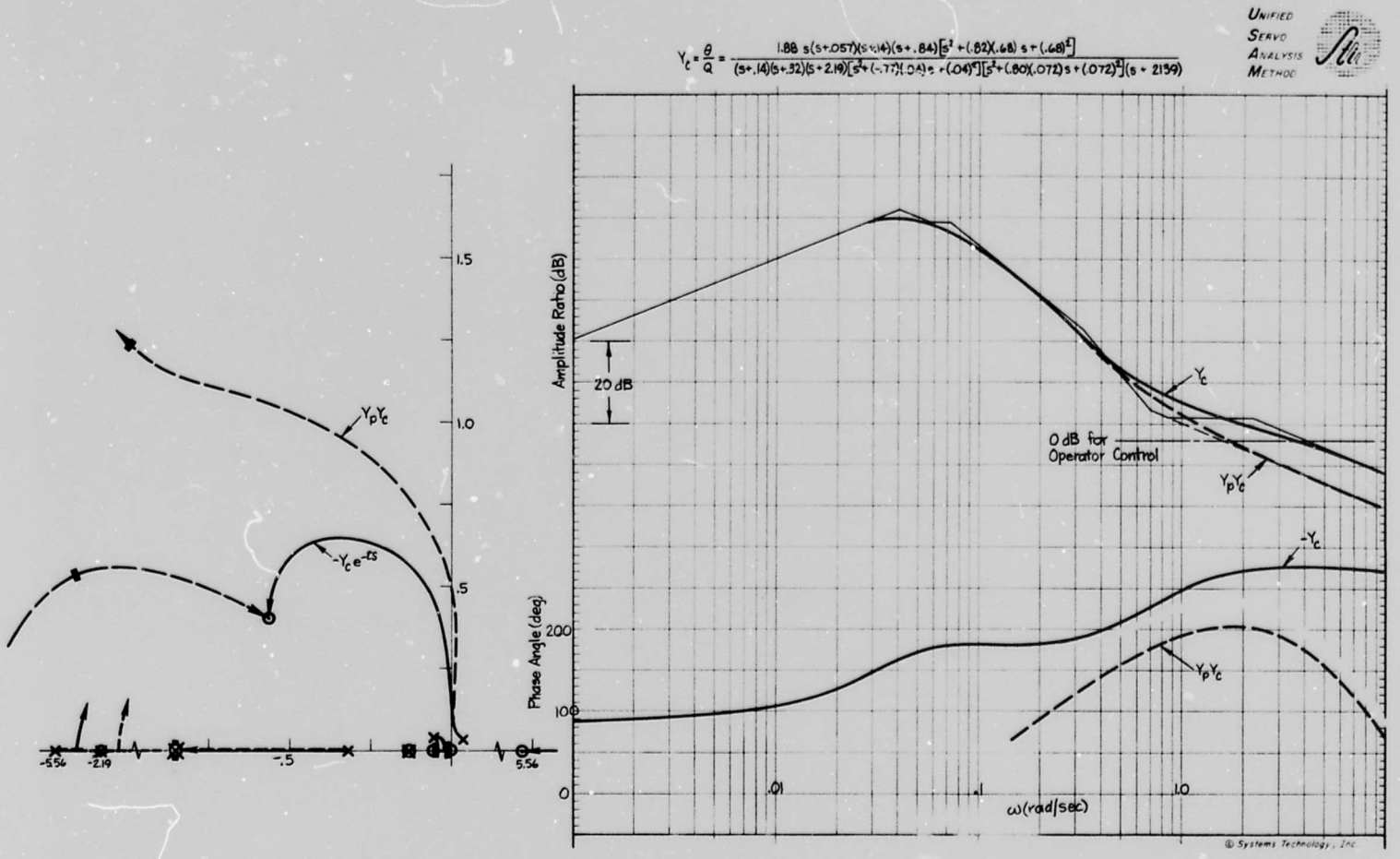

Figure C-3. Pitch Attitude System Survey

root locus for small s differs from the low frequency phase angle because the α-effect is not included in the locus.

FORWARD VELOCITY, u

The system survey for tractor alone, Y_c, and tractor plus operator, $Y_p Y_c$, are given in Fig. C-4. The tractor dynamics look like a lagged blade height motion. Hence, the appropriate operator equalization is simple lead at higher frequency (2.19 rad/sec) analogous to the blade height system survey of Fig. C-2. The resultant effective controlled element in the crossover region looks like the usual second-order critical task, so τ_e from Fig. 3 should be about 0.36 sec, and the $\alpha\tau_e$ values from Fig. 4 give $\alpha \doteq 0.33$. The operator can close the loop at 2.0 rad/sec with the gain and phase margins shown in Table III. The closed roots are shown on Fig. C-4. The low frequency root locus and Bode phase differ slightly because the α-effect is only included in the Bode phase angle plot. The operator can readily sense u visually, but is relatively hard to lead equalize, partly due to the sensing threshold. The operator might use a vestibular $\dot{u}$ cue as an "alerting aid" to lead equalization. The better way to achieve the needed lead is via an inner feedback loop as discussed in the multiloop analyses.

FORWARD ACCELERATION, $\dot{u}$

This motion would be sensed vestibularly by the operator rather than visually, hence appropriate lags for vestibular sensing must be included in the operator dynamics. This is well approximated by a first-order lag at 1.5 rad/sec. The system survey is shown in Fig. C-5. The tractor alone dynamics look like those for blade height except that the low frequency lead moves to the origin, eliminating the dc gain. The effective time delay is that for the vestibular system, giving $\tau = 0.3$ sec and $\alpha \doteq 0.4$. The operator should provide lead equalization, providing for a crossover at 1.9 rad/sec with the stability margins shown in Table III. The closed-loop roots are shown on the root locus, where the α-effect is not included, as usual. Sensing forward acceleration probably involves a relatively large threshold, and this will detract from its merit as a single-loop system candidate.

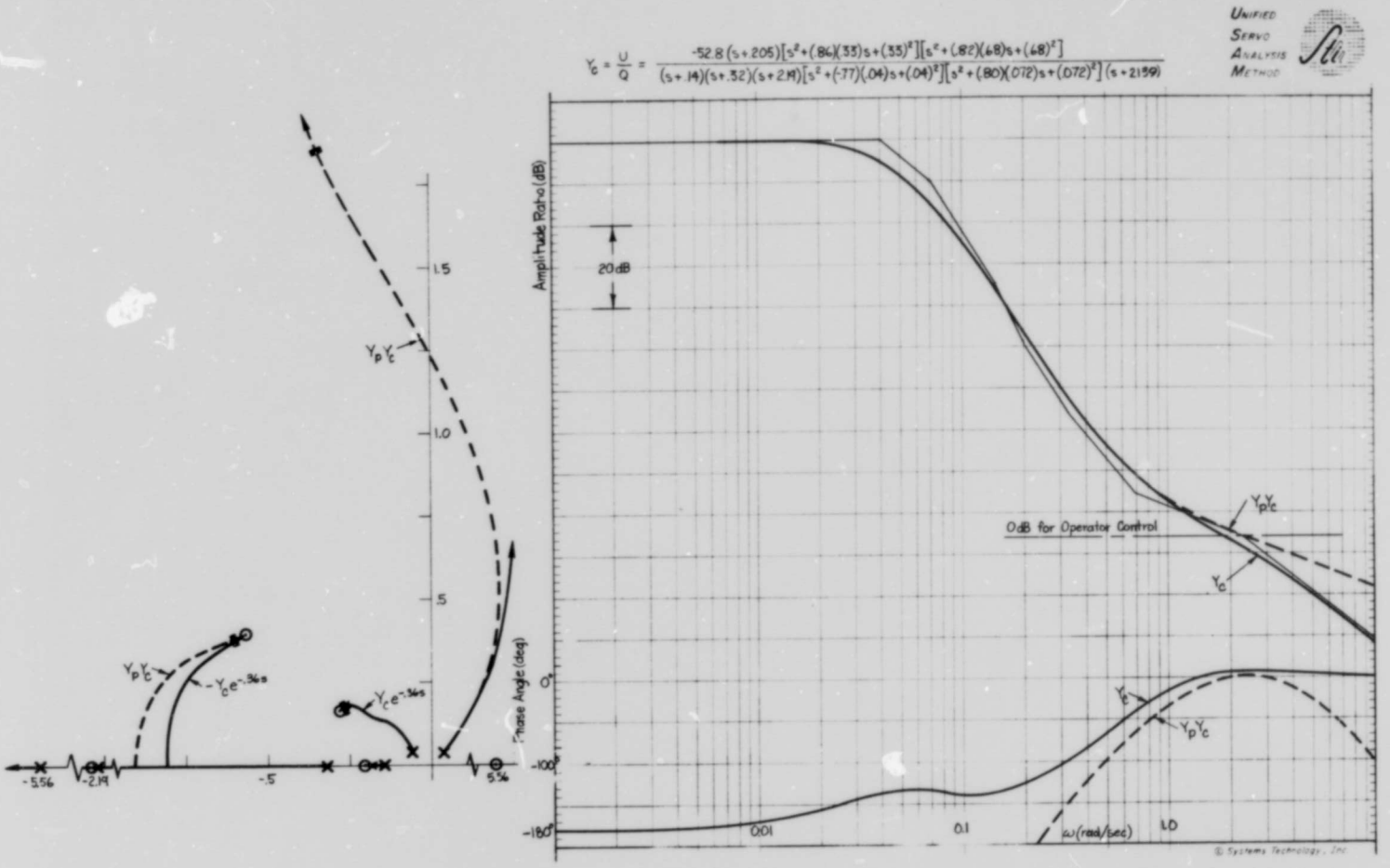

Figure C-4. Forward Velocity System Survey

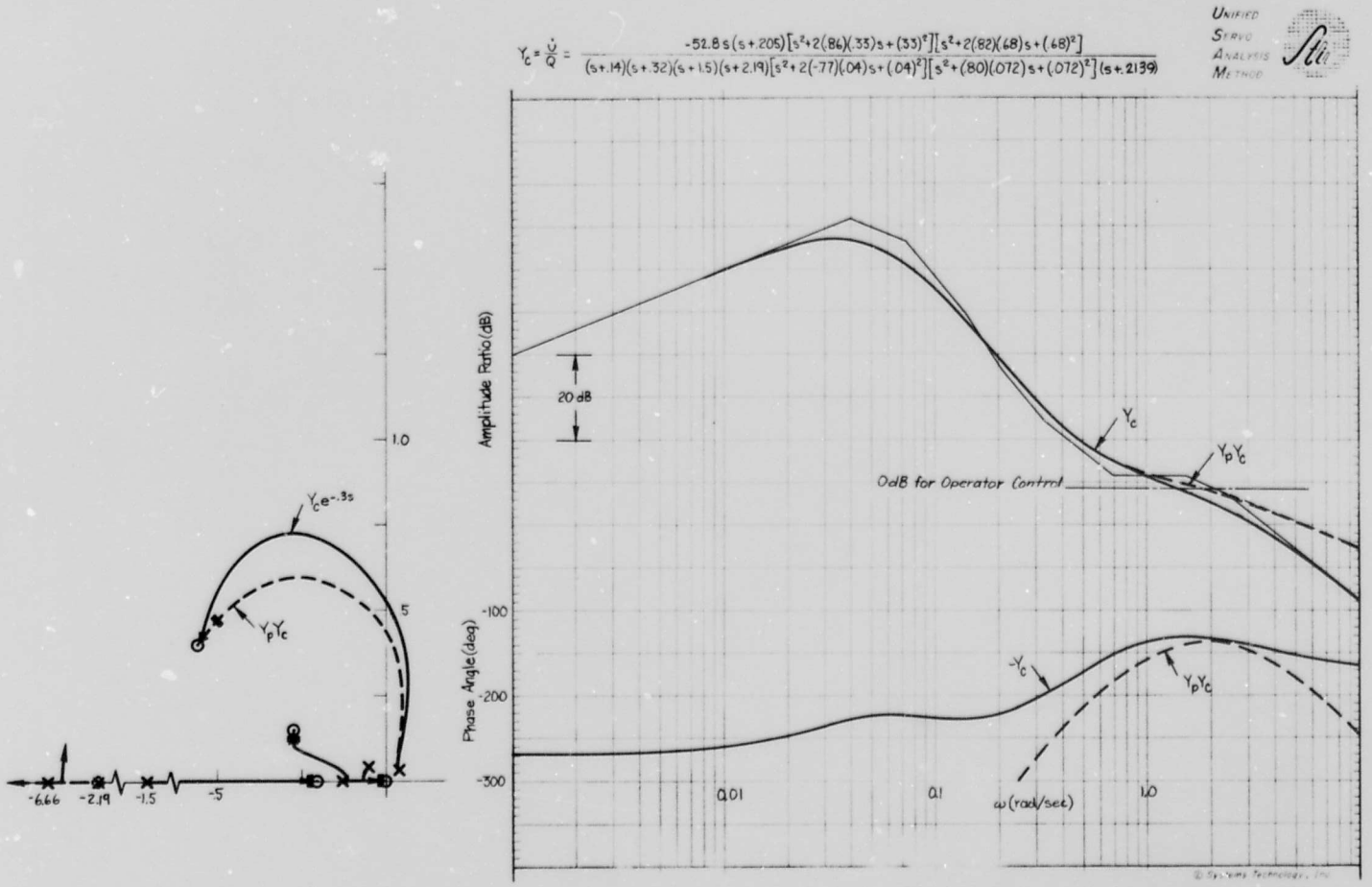

Figure C-5. Forward Acceleration System Survey

SURLOAD HEIGHT, h

The surload is the soil which piles up in front of the blade and above the ambient terrain level. Its height (if sensed) provides a possible motion cue. The system surveys for the tractor and tractor-plus-operator are given in Fig. C-6. The dynamics of the tractor alone look like a lagged blade height motion, much like forward velocity. The needed operator equalization is a simple lead at 2.19 rad/sec which will degrade his subjective opinion somewhat. The analogy of Y_pY_c with the second-order critical task implies $\tau_e \doteq 0.36$ and $\alpha \doteq 0.33$. The predicted crossover frequency is about 2 rad/sec with the stability margins shown in Table III. The closed-loop roots are shown on the root locus which differs by the α-effect from the low frequency phase plot. The basic problem is sensing surload height. Typically some soil curls above the blade, but it is intermittent, with a piece appearing every second or so and then breaking off and falling out of the operator's sight. Hence the operator samples h at a relatively low rate which implies a large additional increment in the effective time delay, τ_e. Table III shows that only a small increment can be tolerated and retain stable operation. The possibility of modifying the blade to improve the operator's perception of surload height immediately suggests itself.

ROAD ARM ANGLE, a

This is the angular motion of a single front road arm due to a single lever deflection. The system survey is shown in Fig. C-7 for the tractor alone and for the tractor-plus-operator. A good stretch of K/s is present and no operator equalization is needed to achieve stable operation. The effective time delay from Fig. 3 is about 0.3 sec. The Y_pY_c system is still analogous to the second-order critical task in its conditional stability, so $\alpha \doteq 0.4$. The closed-loop roots are shown on the root locus (where the α-effect is omitted, as usual) for a crossover at about 2 rad/sec. The stability margins are given in Table III. The basic problem with road arm angle is that it is difficult for the operator to see, although mechanical pointers might be used. A second problem is that the operator would have trouble relating the desired terrain height

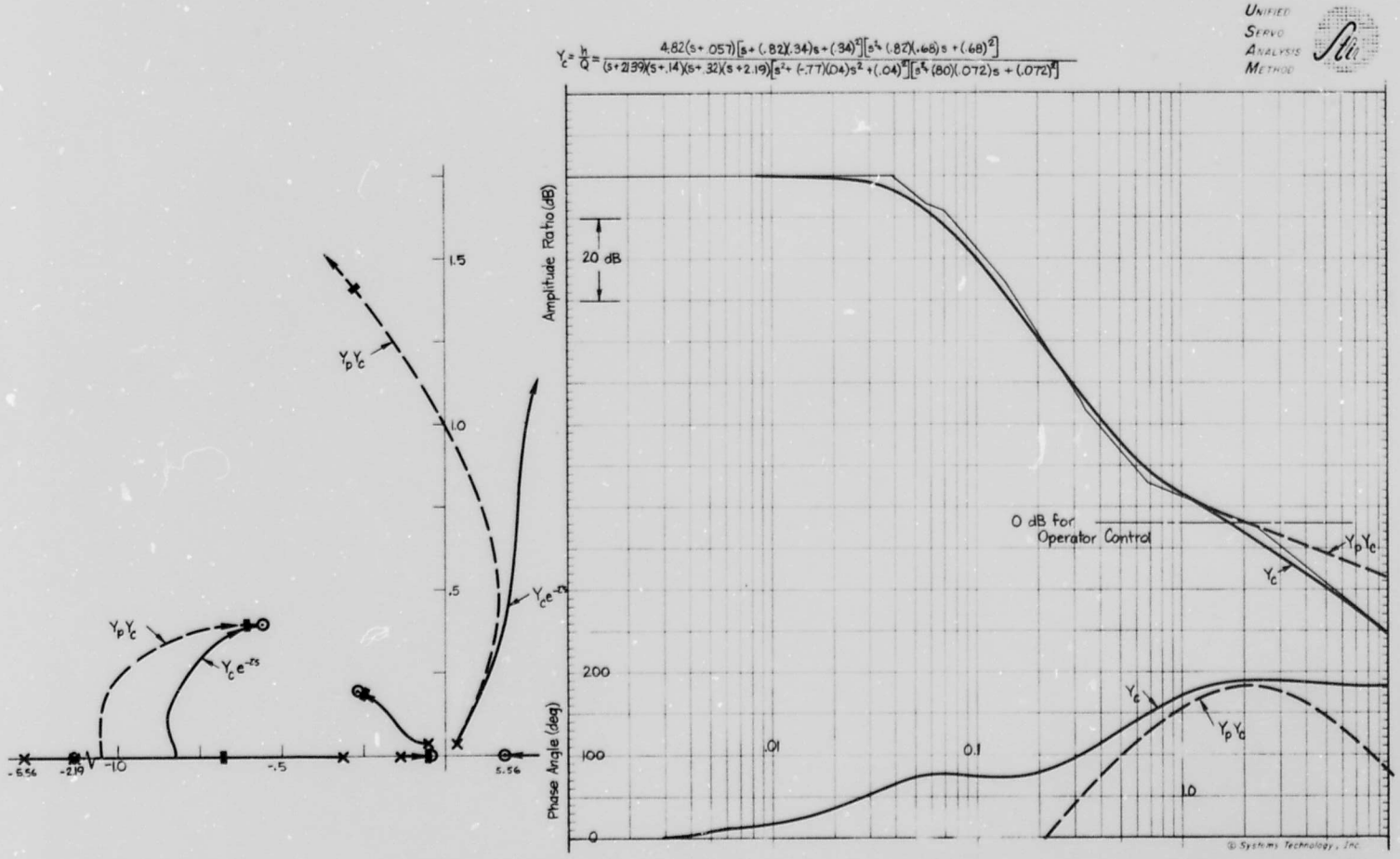

Figure C-6. Surload Height System Survey

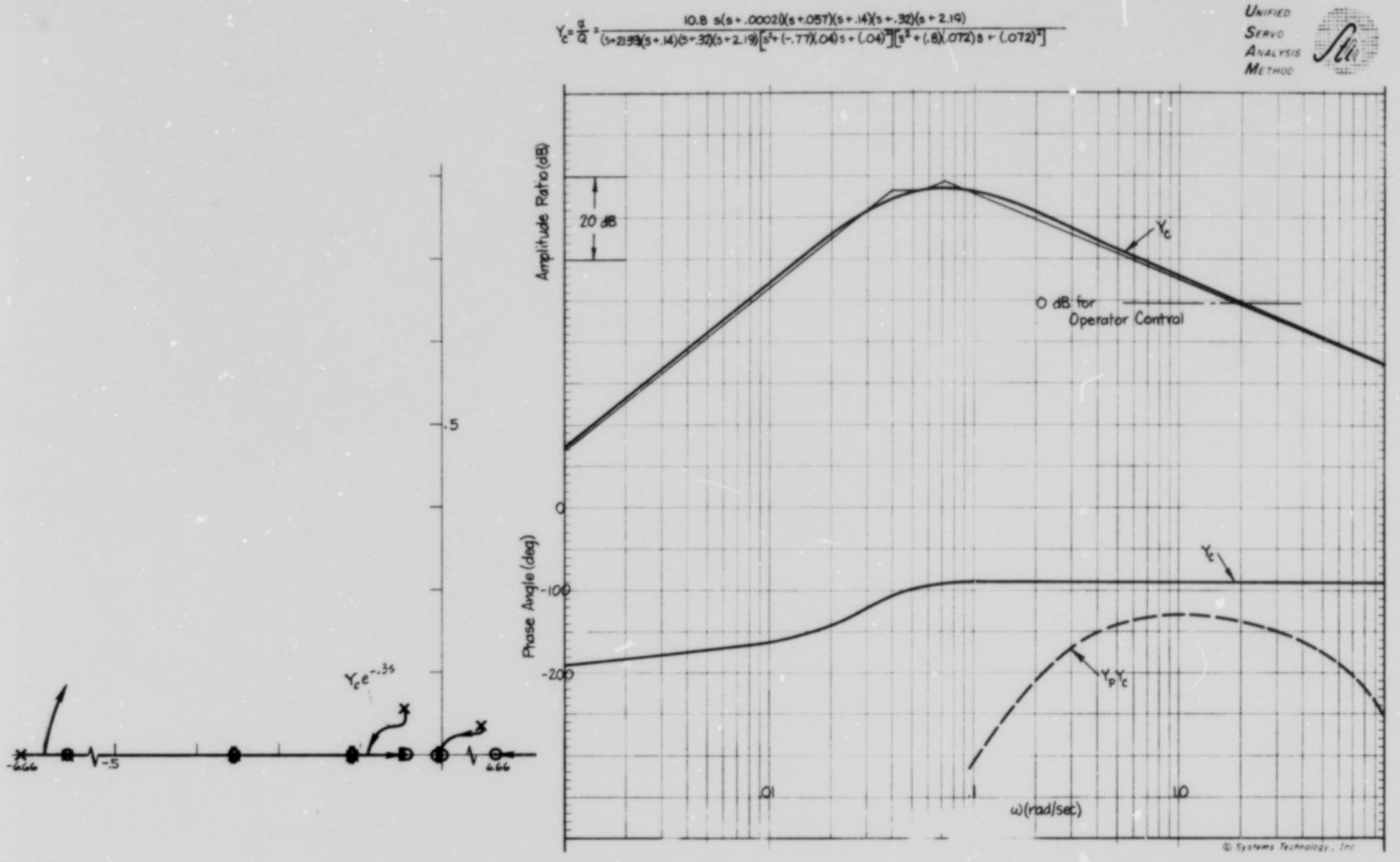

Figure C-7. Road Arm Angle System Survey

at the blade to an equivalent road arm reference position as a basis for closing the loop.

PENDULOUS ACCELEROMETER, $\dot{u} + g\theta$

This is the signal from a pendulous accelerometer. For example, if the operator's head were suitably aligned and rigidly attached to the tractor the otoliths would pick this up.* The system surveys are shown in Fig. C-8, and they are quite similar to $\dot{u}$ in Fig. C-5. The otoliths introduce a first-order lag at about 1.5 rad/sec. The appropriate τ_e is 0.3 sec (Ref. 10). The otolith lag plus operator lead equalization at about 2.19 rad/sec leads to a region of K/s-amplitude ratio and permits a crossover at about 1.8 rad/sec with the stability margins shown in Table III. The closed-loop roots are shown on the root locus, where the α-effect is deleted, as usual. The basic problem here, again, is the lack of a reference equivalent to the terrain input to the blade. The operator may have difficulty, also, with a threshold in sensing $\dot{u} + g\theta$. Lead equalizing the vestibular cue may be more difficult than for equivalent visual cue (but there are no hard data on this subject).

TILT OR ROLL ANGLE, φ

The basic lateral motion of the tractor is tilt or roll angle, controlled by differential (or separate) operation of the suspension levers. The dynamics are relatively good, based on approximate results, and complete transfer functions have not been computed. A good approximation is given in Table II. Noting that leakage causes the s^2 in the denominator to break up into a second-order pair gives

$$Y_c = \frac{\varphi}{Q} \doteq \frac{0.0016[s^2 + 2(0.82)(0.68)s + (0.68)^2]}{(s + 1.67)[s^2 + 2(-0.77)(0.04)s + (0.04)^2]}$$

The system survey is shown in Fig. C-9. Pure gain equalization gives the desired amplitude ratio properties and permits a crossover at 1.6 rad/sec with the stability margins shown in Table III. The closed-loop roots are shown on the root locus. The α-effect is not included in the root locus, as usual.

---

*It could also be obtained visually by a pendulum suitably affixed to the tractor.

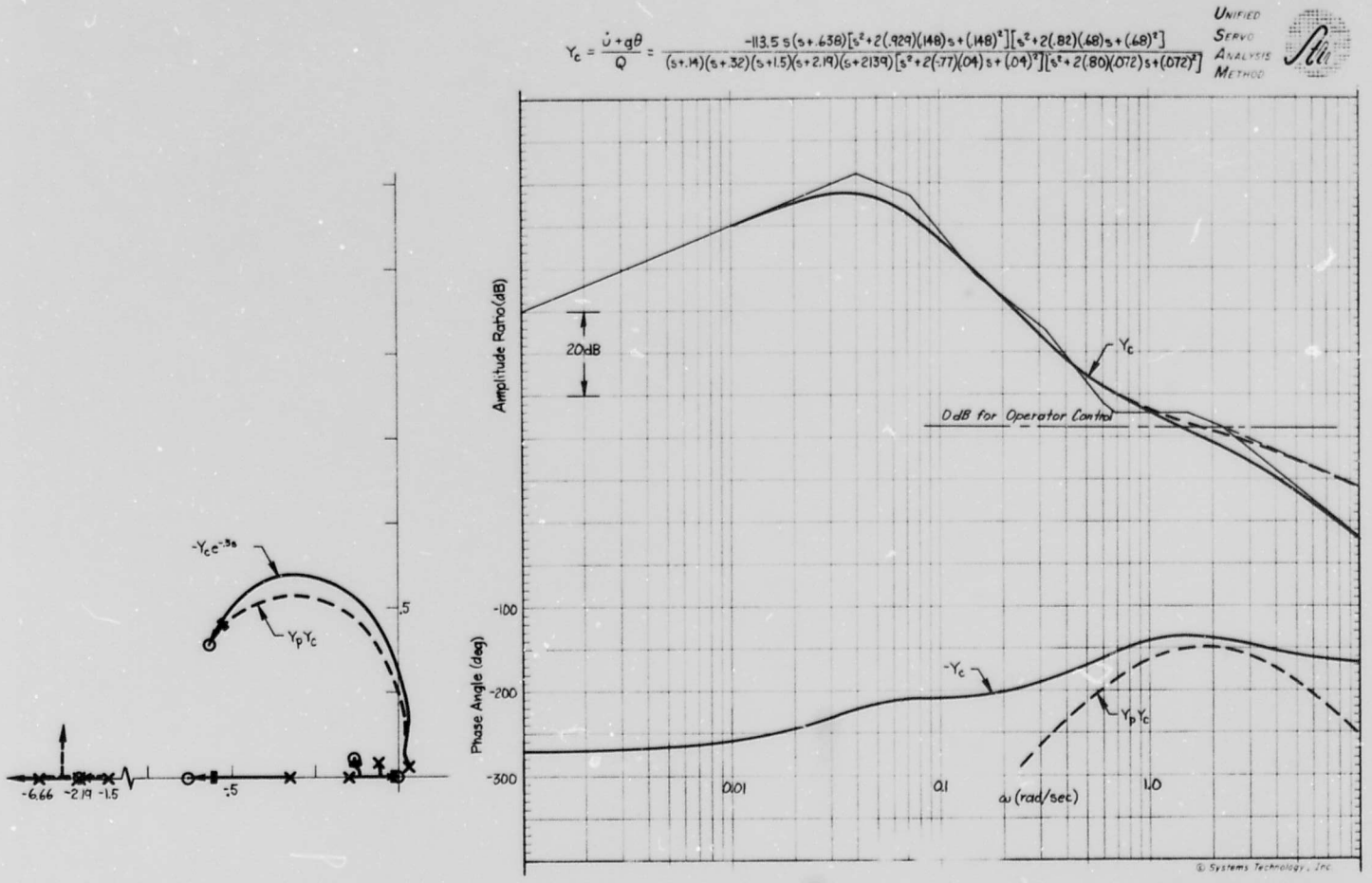

Figure C-8. Pendulous Accelerometer System Survey

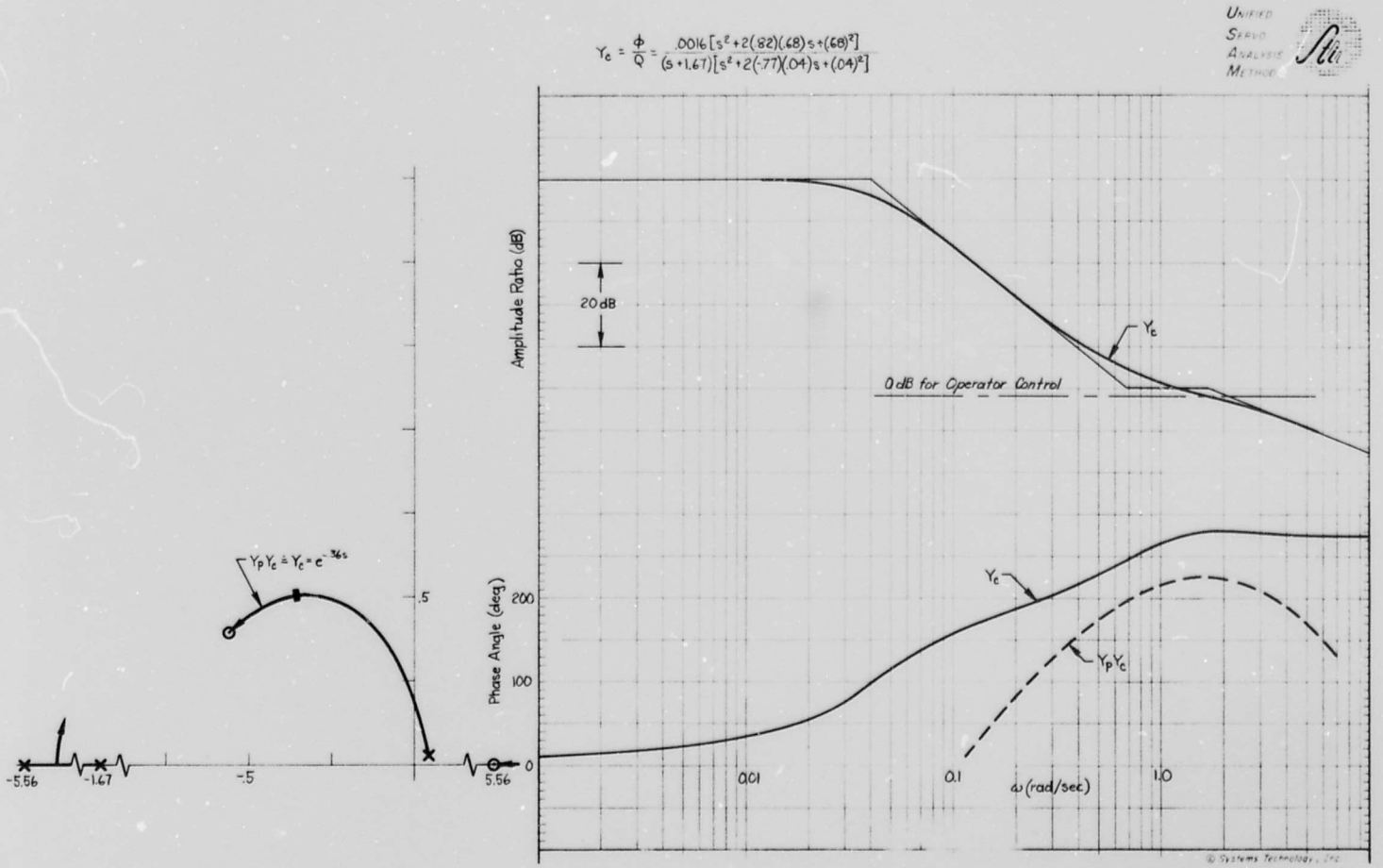

Figure C-9. Tilt Angle System Survey

APPENDIX D

DYNAMIC SIMULATION

The tractor mockup and simulation consists of three major portions: an analog computer simulation of the tractor dynamics, the mechanical and electrical mockup of manipulator feel and valve flow characteristics, and the operator's display. The latter two are physically located in a wooden mockup of the operator's control station. This appendix contains a description of the simulation used in the evaluation of various manipulators and augmentation schemes.

TRACTOR DYNAMICS

The tractor dynamics were simulated on two adjacent EAI 16-31R analog computer consoles. Table D-I lists the equations of motion simulated. Both actuator leakage and blade loading effects are included in the tractor's lateral and longitudinal dynamics. The kinematic delays between the blade and the first and last roadwheels of the three-wheeled model simulated were approximated by the expression shown in Table D-I (Ref. 11). This approximation, due to King and Rideout, gives the time response to a step input shown in Fig. D-1 where the output of the first delay is the input to the second.

Figure D-2 contains the simulation diagram for the equations of motion of Table D-I as well as the connections to the manipulator and display CRT. Not shown are certain auxiliary circuits used for scoring and for simulation checkout. The former consists of absolute value circuits followed by integrators — thus the integrated absolute value of the input signal may be read out at the conclusion of a run. The simulation checkout circuits are basically manual switching circuits for applying initial condition voltages to the various integrators.

Figure D-3 illustrates, in block diagram form, the manipulator connections to the simulation. The valve flows are simulated using diode function generators. For the isometric manipulators the signal, which consists of partially filtered rectified ac, is fed through a lag filter having

TABLE D-I

SIMULATION EQUATIONS OF MOTION

1. Actuator Flows (in^3/sec)

$$Q_1 = Q_{v_1} + (12L/D_M)(T_1 + T_{10})$$

$$Q_5 = Q_{v_5} + (12L/D_M)(T_5 + T_{50})$$

2. Road Arm Angles (deg)

$$\left.\begin{aligned} \dot{a}_1 &= (57.3/D_M)Q_1 \\ \dot{a}_5 &= (57.3/D_M)Q_5 \end{aligned}\right\} \quad a_1 \text{ and } a_5 \text{ limited to } \pm 36 \text{ deg}$$

3. Pitch Angle (deg)

$$\theta = (57.3/12\ell_{WB})\left[\left(\frac{z_4 + z_8}{2}\right) - \left(\frac{z_1 + z_5}{2}\right)\right] - (\ell/\ell_{WB})(a_1 + a_5)$$

4. Blade Depth (in.)

$$z = \left(\frac{z_4 + z_8}{2}\right) - (12/57.3)(\ell_B + \ell_{WB})\theta$$

5. Kinematic Delay to Roadwheels 1 and 5

$$\frac{z_4 + z_5}{2} = z[e^{-\tau s}]_{approx}$$

6. Kinematic Delay to Roadwheels 4 and 8

$$\frac{z_4 + z_8}{2} = \frac{z_1 + z_5}{2}[e^{-\tau s}]_{approx}$$

7. Time Delay Approximation

$$[e^{-\tau s}]_{approx} = \frac{476 - 160.5\tau s + 22.8\tau^2 s^2 - 1.48\tau^3 s^3}{476 + 309\tau s + 91.8\tau^2 s^2 + 12.1\tau^3 s^3 + \tau^4 s^4}$$

8. Surload Height (in.)

$$\dot{h} = -H_h h + H_z(z - z_a)$$

9. Blade Force (lb)

$$X_B = X_{\dot{u}}\dot{u} + X_u u + (X_h/12)h + (X_z/12)(z - z_u)$$

TABLE D-I (Concluded)

10. Blade Pitch Moment (ft-lb)

$$M_B = (M_z/12)(z - z_a) + (M_h/12)h + M_{\dot{u}}\dot{u} + M_u u$$

11. Forward Velocity (ft/sec)

$$\dot{u} = \frac{\sum_i (-F_{iO}) - mg}{57.3m}\theta + (1/m)X_B$$

12. Induced Road Arm Torques (ft-lb)

$$(T_1 + T_5) = -\frac{\ell}{\ell_{WB}}\left\{M_B + \sum_i \left[-\frac{F_{iO}}{57.3}(z_{iO} + \ell \cos a_{iO})\right]\theta + \ell_4 \frac{X_B}{\tan \alpha_o}\right\}$$

13. Roll Angle (deg)

$$\varphi = \frac{\ell}{\mathfrak{J}}\left(\frac{a_1 - a_5}{2}\right) + \varphi(t-\tau)$$

14. Kinematic Delay to Roadwheels 1 and 5

$$\varphi(t-\tau) = \varphi[e^{-\tau s}]_{approx}$$

15. Blade Roll Moment (ft-lb)

$$N_B = \frac{N_\varphi}{57.3}(\varphi - 57.3 z_{a_y}) + \frac{N_{\dot{r}}}{57.3}\dot{r} + \frac{N_r}{57.3}r$$

16. Yaw Rate (deg/sec)

$$\dot{r} = \frac{N_{sr}}{I_z}r + \frac{57.3}{I_z}N_B$$

17. Induced Road Arm Torques (ft-lb)

$$(T_1 - T_5) = \frac{\ell}{\mathfrak{J}}\left(\frac{N_B}{\tan \alpha_o} \quad \frac{mgz_B}{57.3}\varphi - \frac{mz_B U_o}{57.3}r\right)$$

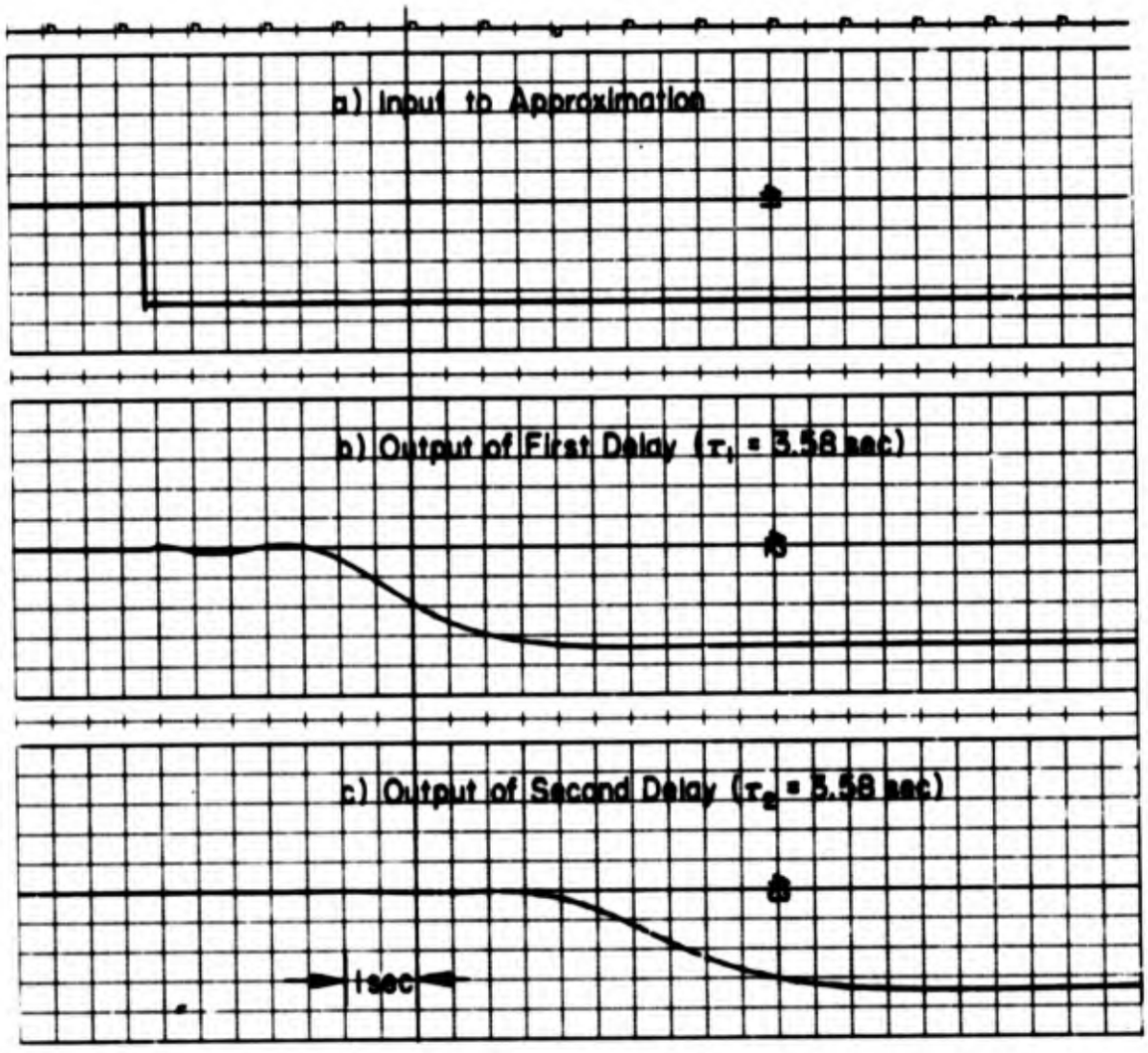

Figure D-1. Step Response of the King-Rideout Approximation to a Pure Time Delay

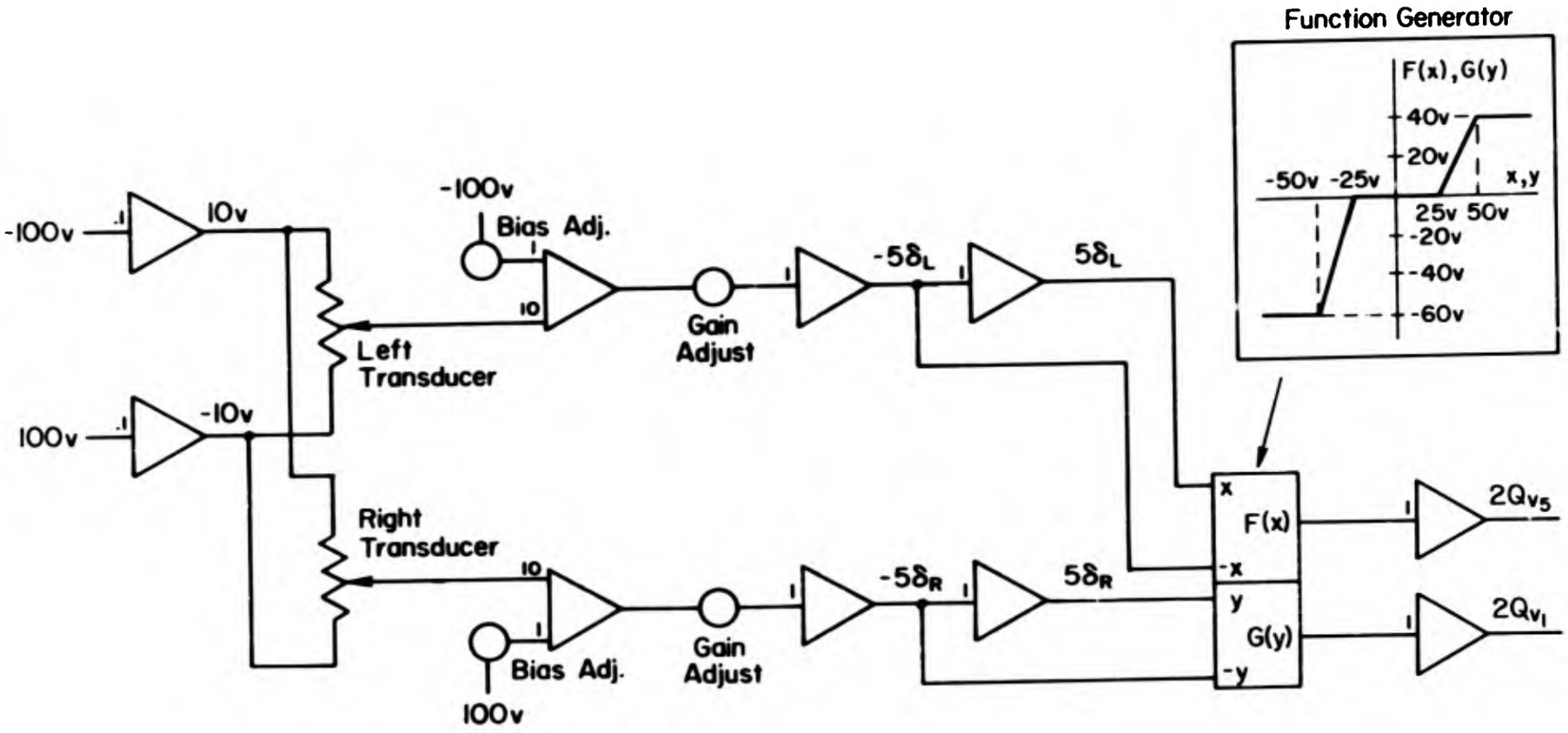

Figure D-2a. Simulation of Standard Manipulator and Valve Flows

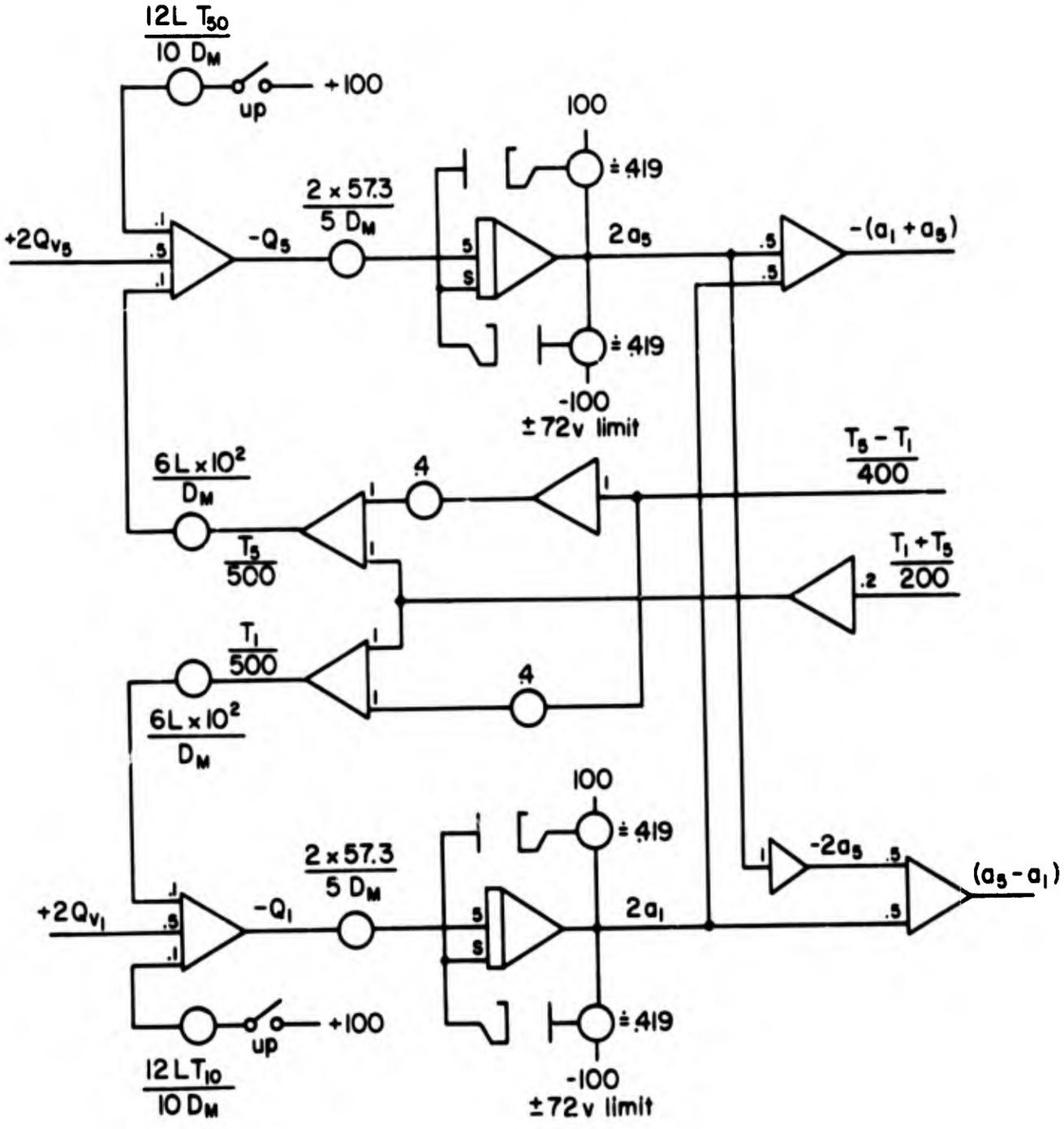

Figure D-2b. Simulation of Road Arm Angles

BLANK PAGE

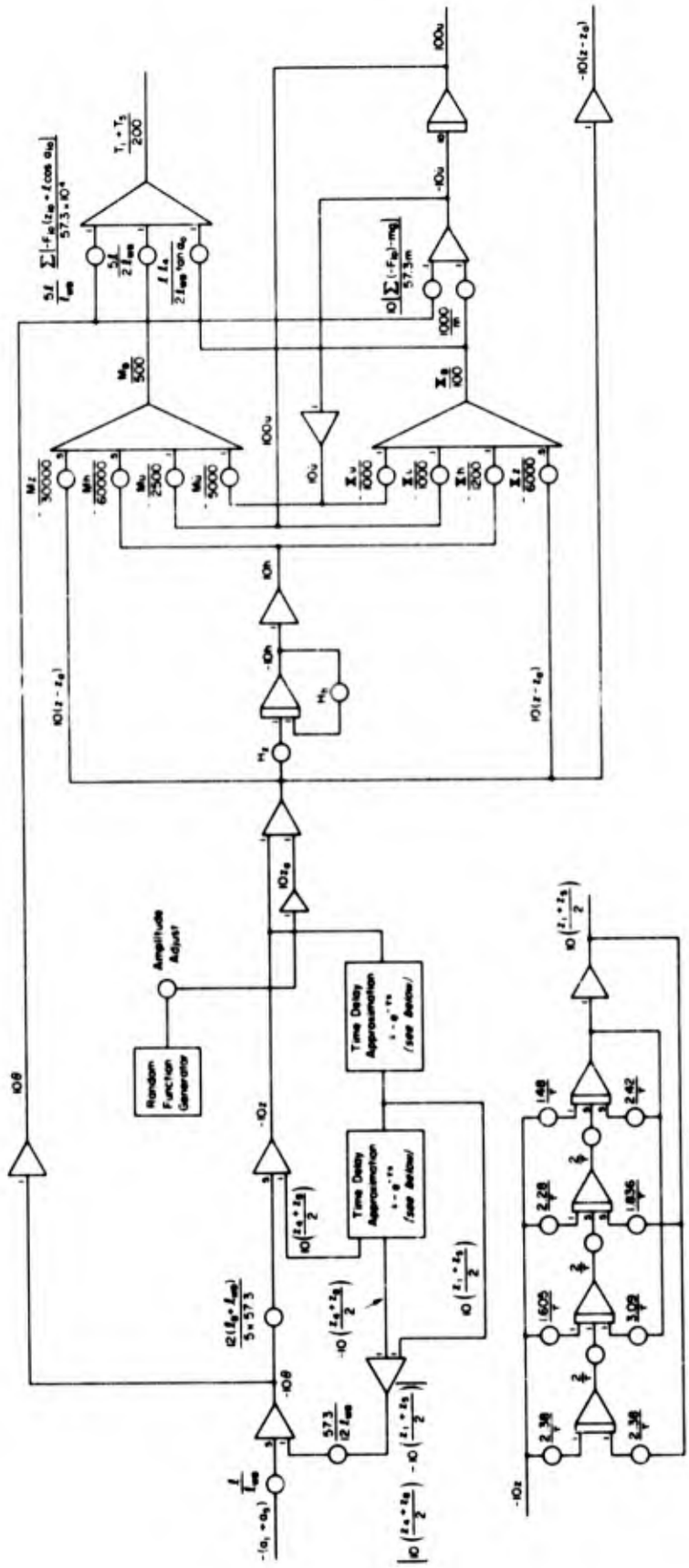

Figure D-2c. Simulation of Longitudinal Dynamics

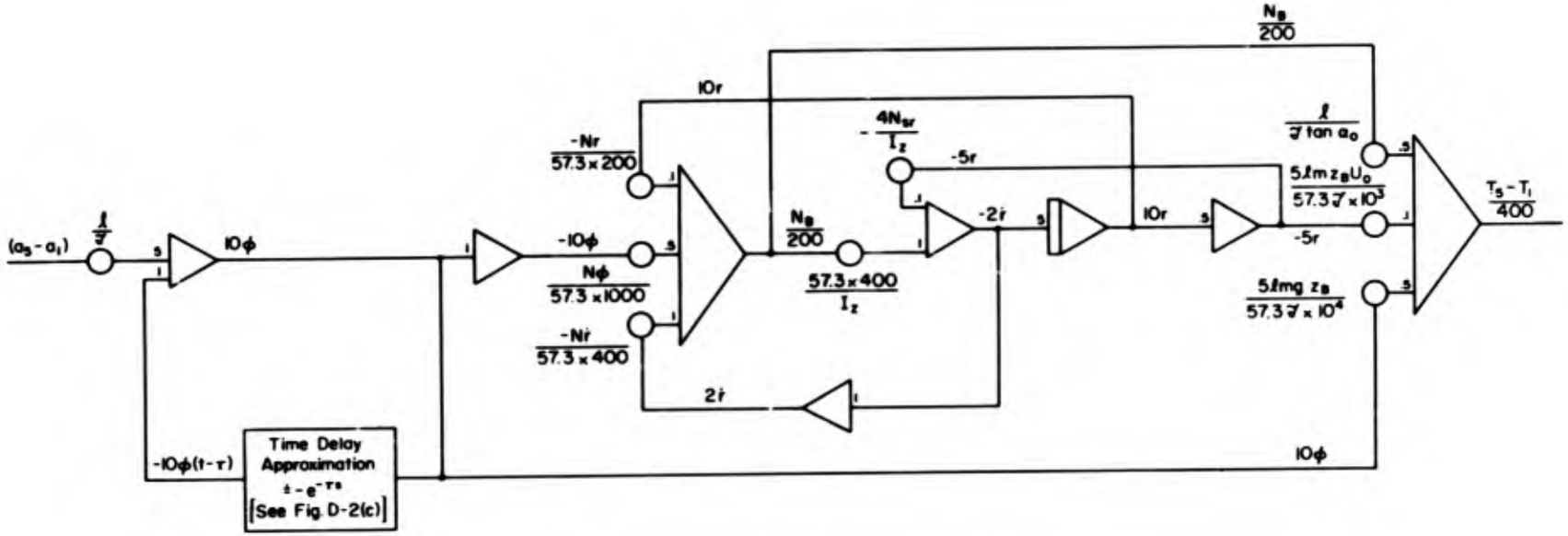

Figure D-2d. Simulation of Lateral Dynamics

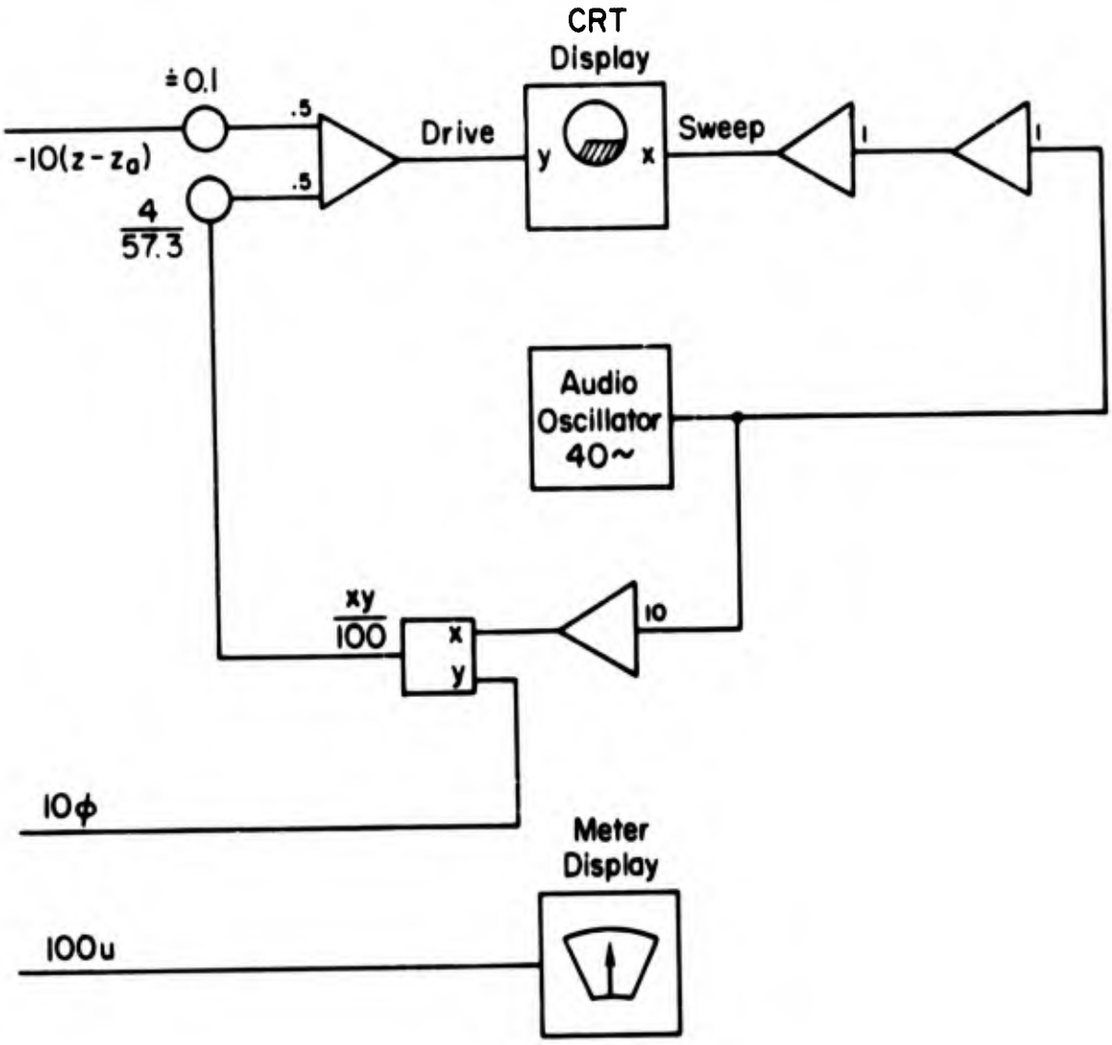

Figure D-7e. Simulation of Display

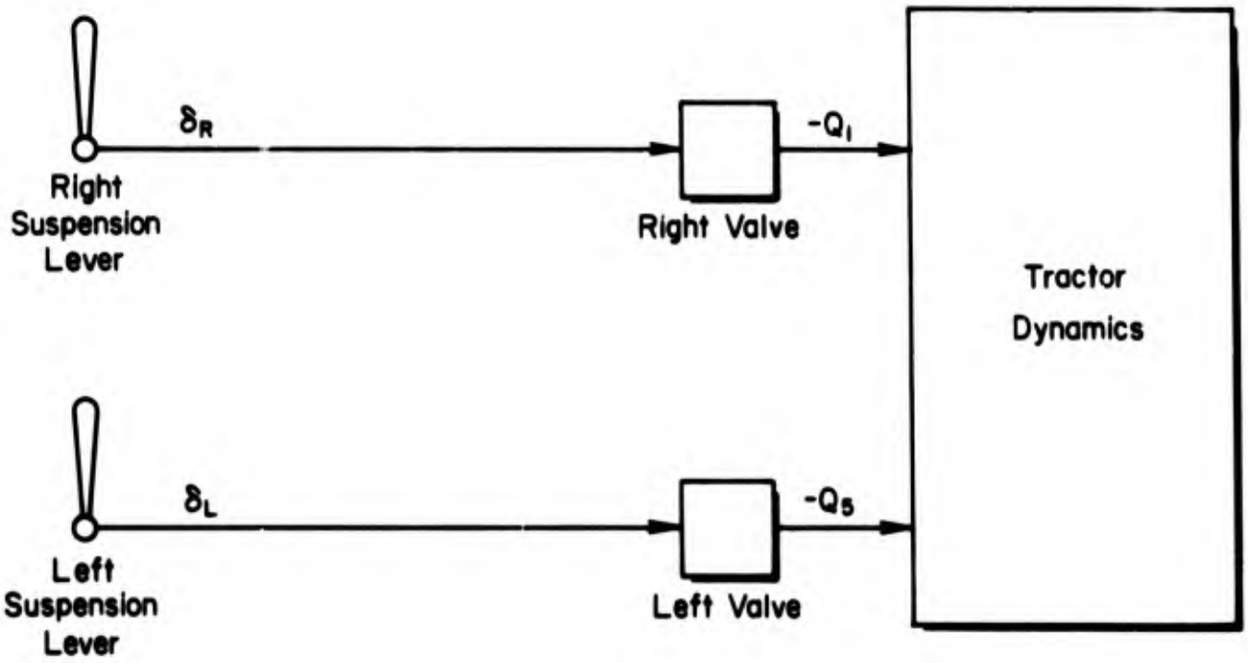

a) Standard or Linearized Manipulators

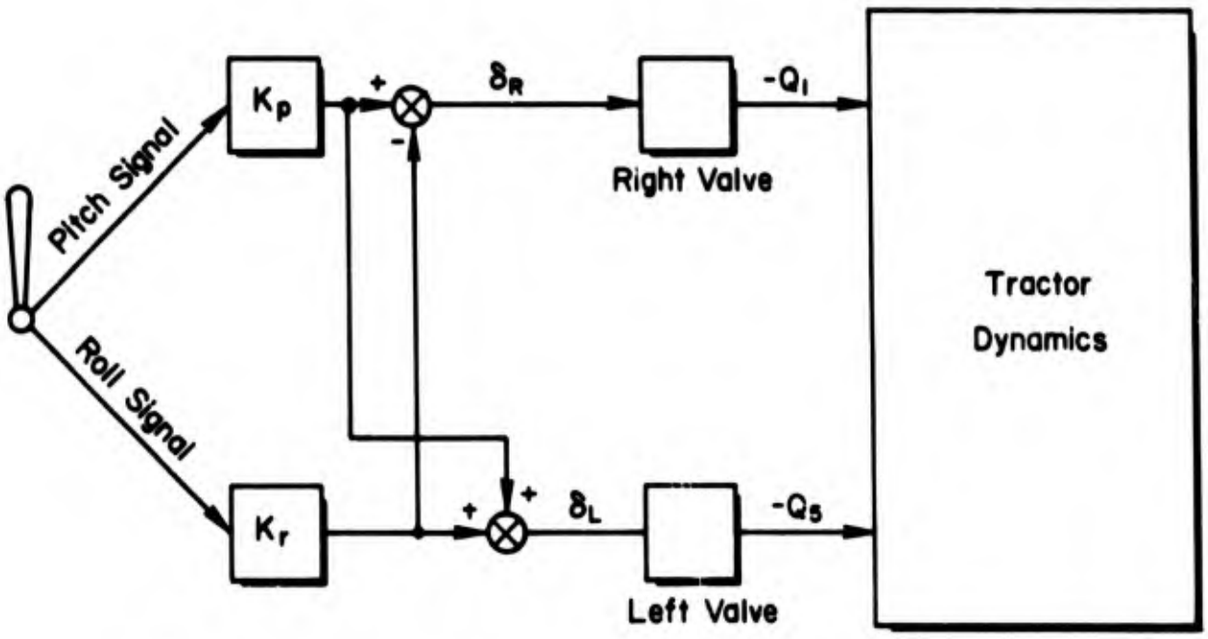

b) Isometric Control or Two Axis Stick

Isometric	Two-Axis
K_p = .989 deg/lb	K_p = 1.49 deg/deg
K_r = .643 deg/lb	K_r = .46 deg/deg

Figure D-3. Manipulator Connections

$1/\tau$ = 16 rad/sec. All other manipulators had a "clean" output requiring no filtering. Note that the variables δ_R and δ_r are retained in Fig. D-3(b) as a common reference between the manipulation schemes.

Figure D-4 illustrates the two augmentation schemes used. The gains shown result in effective crossovers for both closed-loop systems at 2 rad/sec.

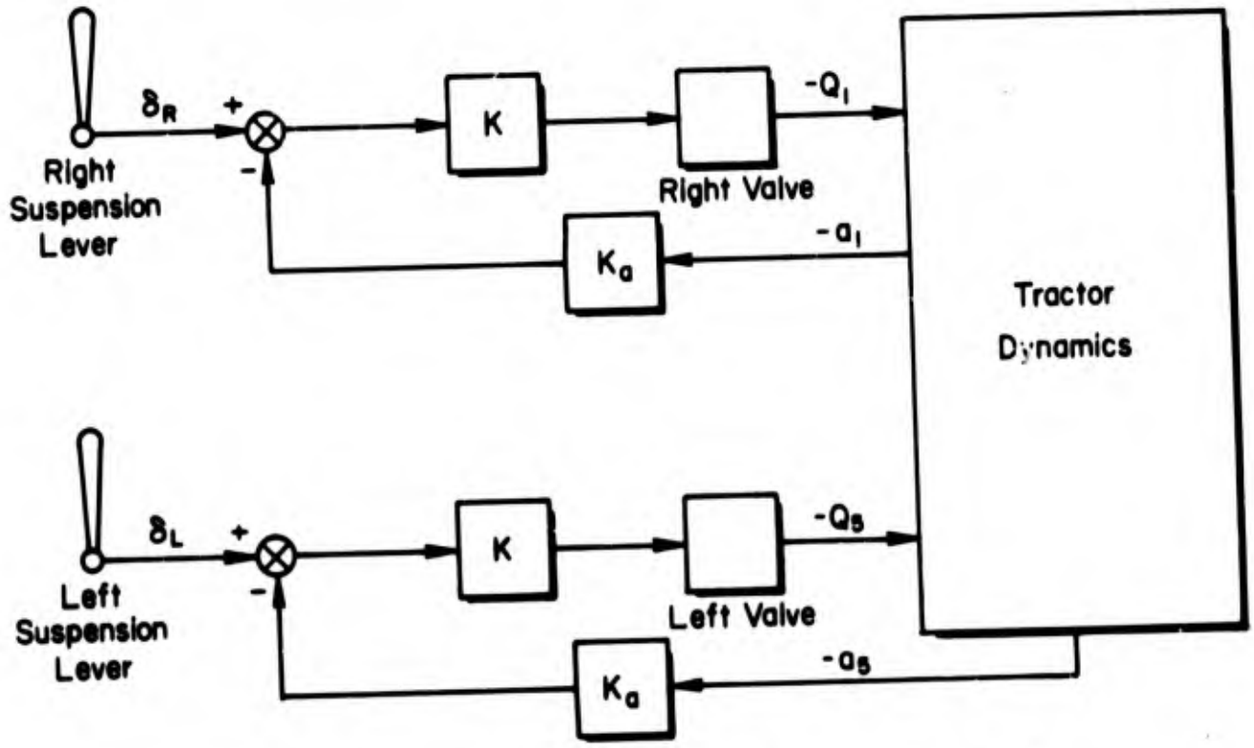

a) Roadarm Position Feedback ($K = 5$ deg/deg, $K_a = .25$ deg/deg)

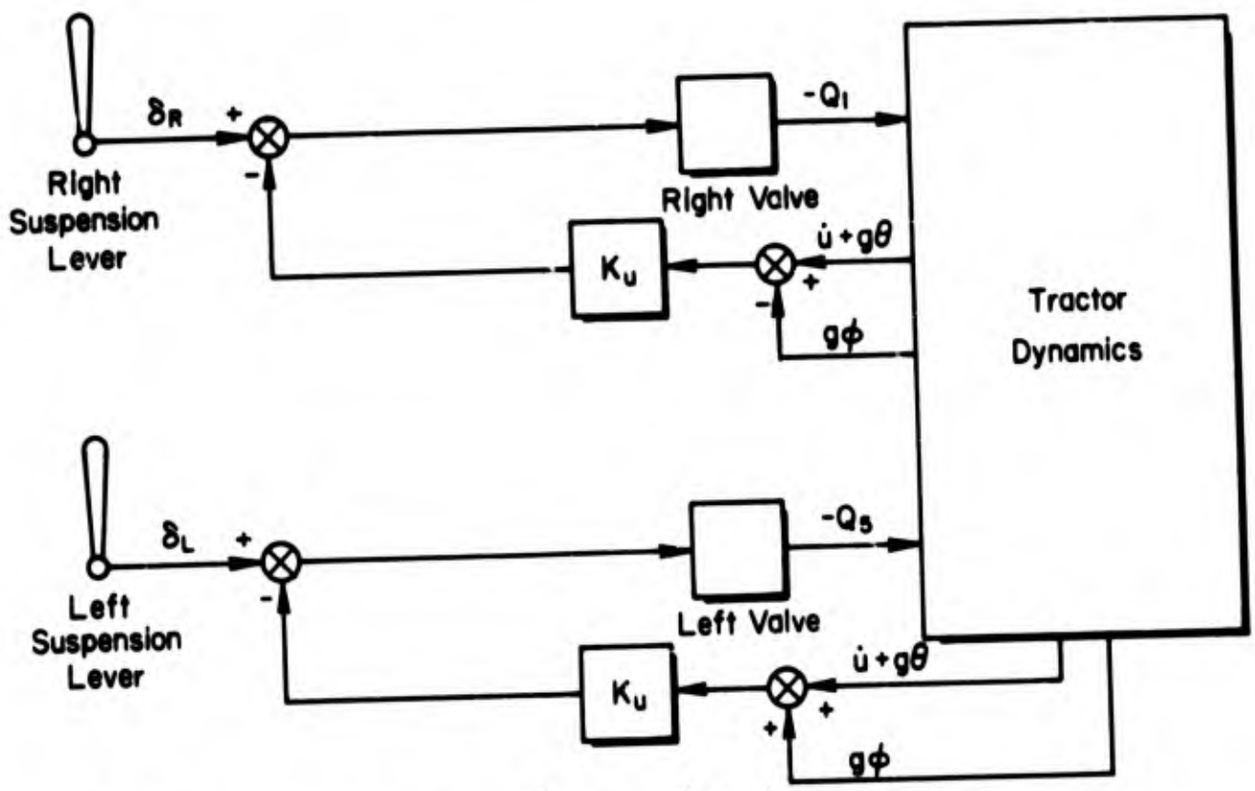

b) Acceleration Feedback $\left(K_u = 10 \frac{\text{deg}}{\text{ft/sec}^2}\right)$

Figure D-4. Augmentation Schemes

APPENDIX E

DESIGN SPECIFICATIONS

The following basic design constraints formed the foundation for the prototype controller system:

1. Must be rugged, simple, reliable; easily installed and maintained.
2. Maximum usage of off-the-shelf parts.
3. Sidestick and arm rest bolt to existing lever mount.
4. Operate on available UET-E4 power.
   - 4000 psi hydraulic system (peak to 5000 psi) with 3 micron filtration
   - 24 volt dc (unregulated generator-battery system)
5. Not exceed ±10 lb maximum stick forces (contractual item).

Satisfaction of the above constraints and the requirements and considerations of Section II are obviously well within the state of art. Therefore, design activities were only carried to the point of identifying off-shelf components, modifications (if any) to off-shelf components, and establishing requirements for specially fabricated components.

The electronics and sidestick are the least problem. The electronics will be a special fabrication, but employs off-shelf components and standard fabrication technology. An existing sidestick assembly was found in military surplus which, with minor modification, will satisfy all requirements plus offer additional flexibility for the prototype system.

The major stumbling block involved the 4000 psi working pressure for the electrohydraulic transfer valves and sizing the EHTV to match or exceed the flow capabilities of the existing manual valves. A 4000 psi working pressure has been employed in some missile applications and EHTV's have been designed for this application. However, these valves are

miniaturized, light weight, somewhat delicate and costly devices which only have to operate for a very short time and essentially on a one-shot basis. The need for a long life in a very rugged environment, plus the desire for low unit cost, dictated use of industrial type valves if at all possible. The nominal maximum working pressure for this class of valve is 3000 psi. After considerable search it was determined that the industrial version of the Moog, Inc., EHTV would meet the requirements for the prototype system if special (but off-shelf) O-rings were installed at the factory.

Determination of the equivalent valve size was hampered by not being able to obtain the precise valve pressure drop at which the present valves are rated. However, by making use of several crude dynamic measurements which were made during the early portions of this study plus known static characteristics of the vehicle and hydraulic system, an estimate of the necessary valve pressure drop rating for the existing valve was derived. This value was then employed to establish the equivalent EHTV flow requirement. Details of this analysis are presented along with the specification for the electrohydraulic valve.

It was intended that the prototype controller would be fabricated in the STI model shop where there would be ample interchange between the technicians and engineers. Hence all drawings, specifications, etc., presented in this section are considered to be working-level documents rather than design procurement documents.

CASE ASSEMBLY

1. General

    1.1 Dimensions. All dimensions are as shown in Fig. E-1.

    1.2 Materials

        1.2.1 Case. The case will be of 0.25 in. aluminum plate. All joints will be welded to seal out dust and moisture.

        1.2.2 Arm Rest/Cover. The cover will be of 0.125 in. aluminum with all joints welded to seal out dust and moisture.

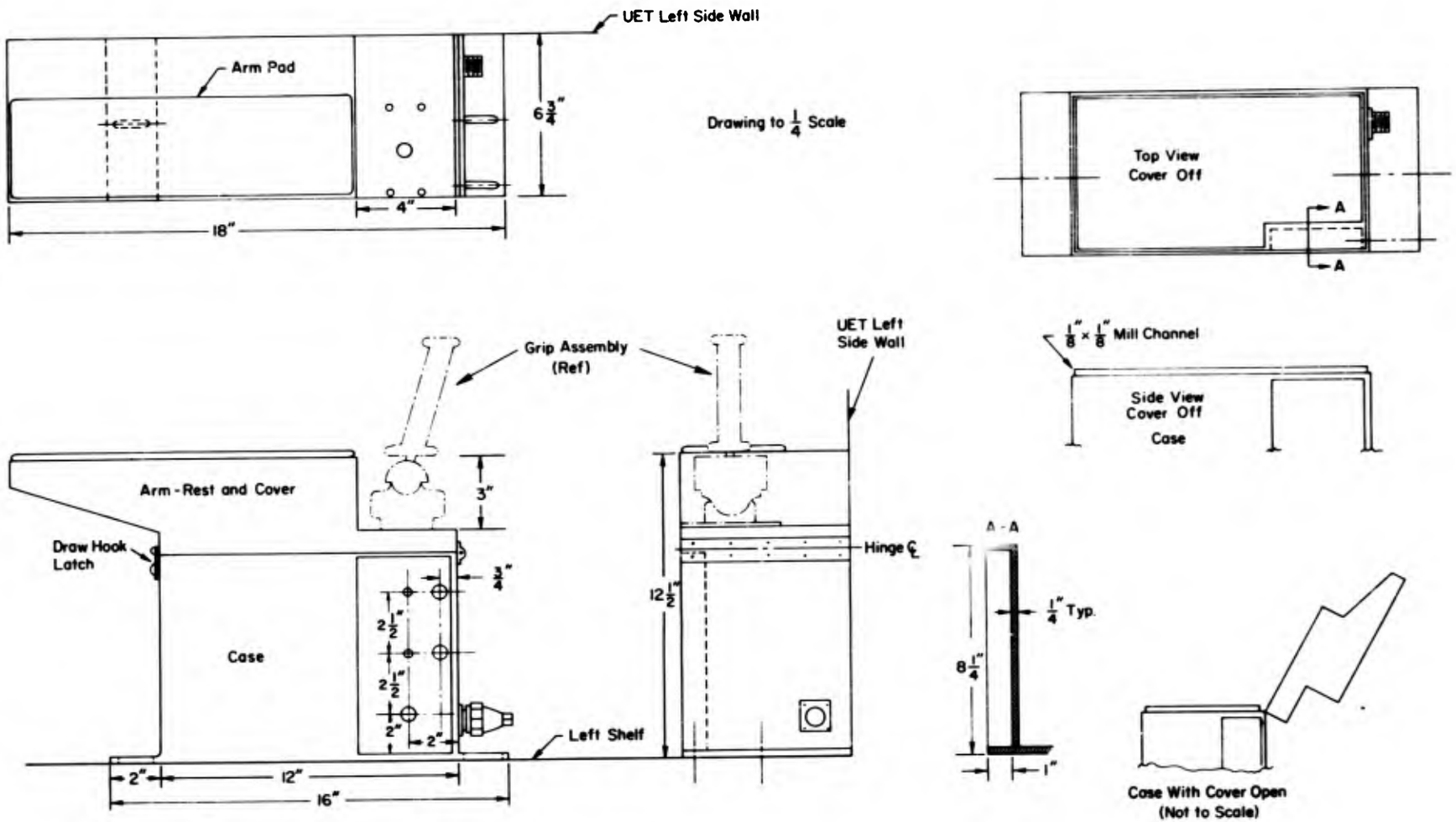

Figure E-1. Prototype Case Assembly

1.2.3 Arm Rest Pad. The pad will be covered with the same material as the tractor seat.

1.3 Mounting. See Fig. E-1. The front two mounting holes match the existing lever mounting bolts. One additional mounting bolt is included at the rear for rigidity and maintenance of proper alignment.

1.4 Finish. The case and arm rest/cover finish will be standard gray anodize.

2. Cover Lock. The single cover lock will be a standard draw-hook latch.

3. Control Console. The control console will be recessed 1 in. to protect the switches and trim adjust knobs from inadvertent operation from bumping.

4. Seals

4.1 Cover. A silicone rubber seal will be fitted to the milled channel of the top of the case so that an airtight seal is obtained when the cover is closed.

4.2 Toggle Switch. The toggle switch will be fitted with a HEX SEAL (or equivalent) silicone rubber toggle switch boot.

4.3 Trim Pot Shafts. The trim pot shafts will be fitted with a HEX SEAL (or equivalent) silicone rubber rotary shaft seal.

5. Electrical Connection. A standard 9-pin Cannon (or equivalent) connector shall be provided as shown in Fig. E-1.

MANIPULATOR ASSEMBLY

1. Two-Axis Pivot Assembly. The two-axis pivot assembly with its associated electrical pickoffs and force feel springs might be especially designed for a production application. However, for this prototype installation a surplus two-axis airborne radar controller (Hughes Aircraft Co. Part No. 435-19-3001) can be easily modified to meet requirements. This assembly is of rugged construction and has been fully qualified for military application including vibration, shock, salt spray, humidity, sand and dust, etc. Pictures of the assembled and partially disassembled unit are shown in Figs. E-2 and E-3.

The advantages of this unit (in addition to its ruggedness) are that it

- Requires little modification.
- Has the necessary 10 deg grip mounting offset.

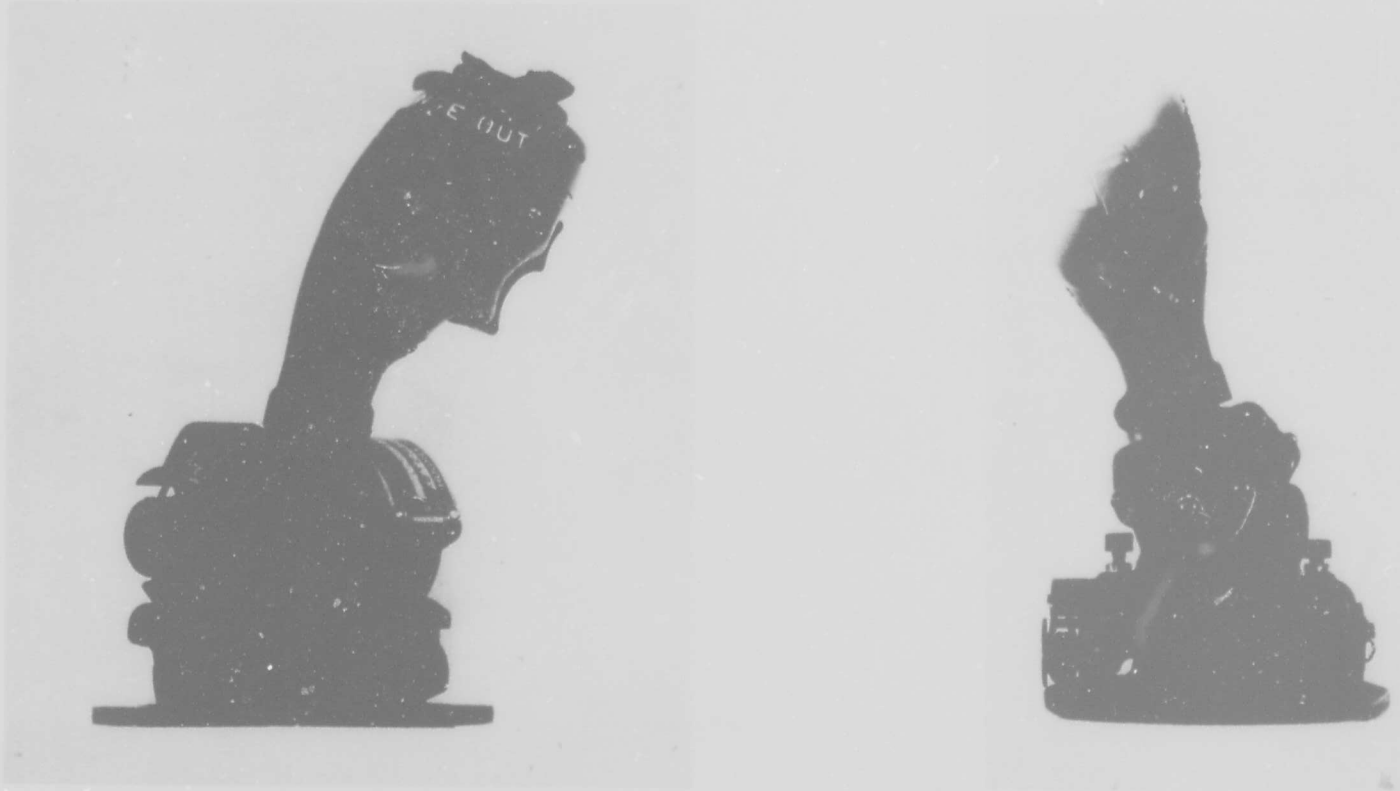

Figure E-2. Prototype Manipulator

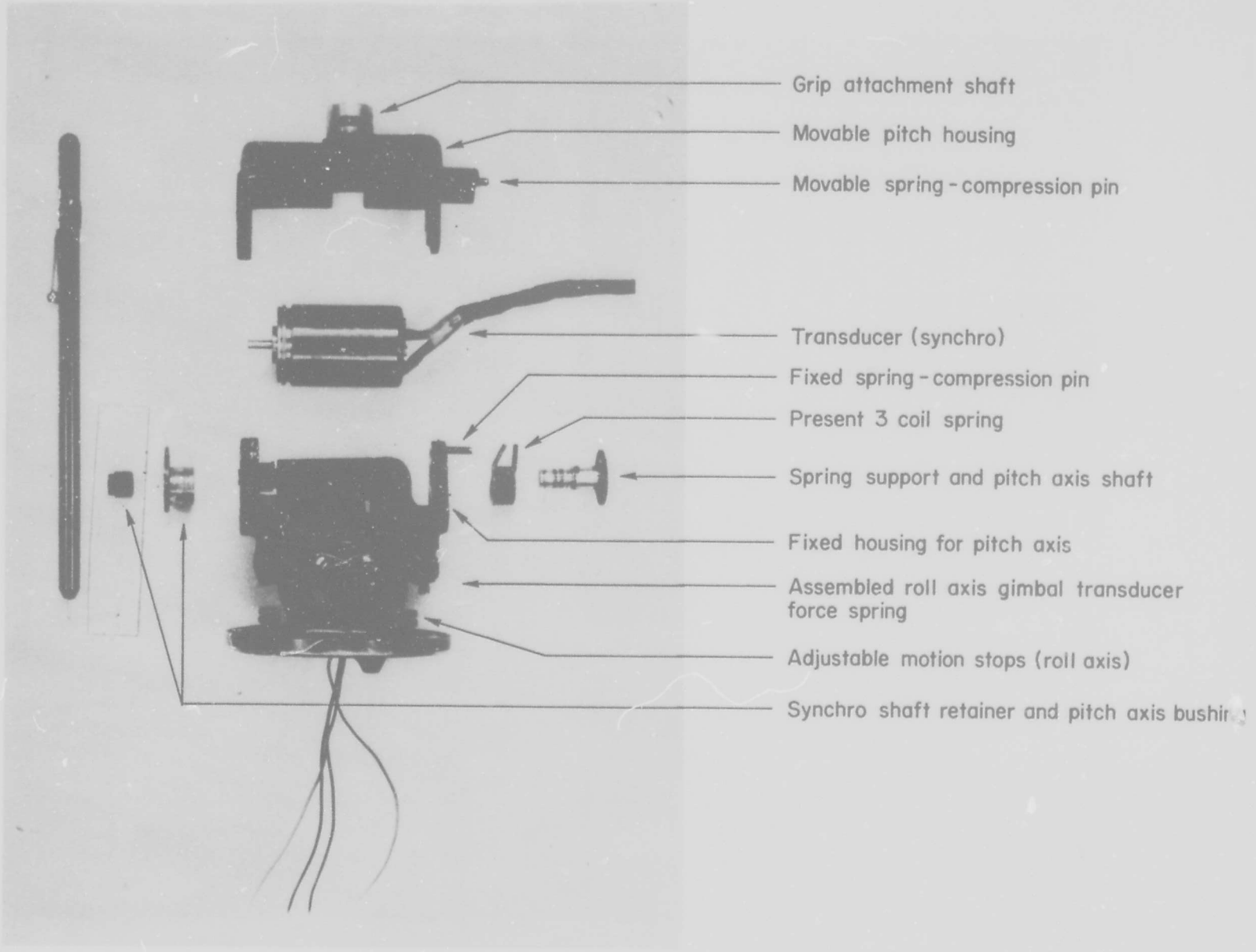

Figure E-3. Exploded View, Prototype Manipulator

- Has standard size 11 synchro pickoffs which can be used directly or can be readily changed for standard size 11 induction potentiometers.
- Has adjustable stops in both axes to limit stick grip travel.
- Is readily available.
- Is relatively inexpensive.

The only modifications required are to replace the hand grip and the centering and force springs with stiffer springs. Replacement of the existing synchros with induction pots is not necessary but may be desirable because the induction pots afford a higher transformation ratio between excitation voltage and output voltage and hence require less amplification of the manipulator output signal in the electronics unit. This is because the induction pots only operate over 90 deg full travel versus the 360 deg of synchros. Since we are only using ±10 deg, the induction pots offer adequate movement at a higher signal sensitivity. Typical characteristics for such an induction pot are shown in Table E-I.

TABLE E-I

INDUCTION POTENTIOMETER CHARACTERISTICS

(General Precision, Inc., R916-01 or equivalent)

Size		11
Input voltage (line to line)	(volts)	26
Frequency	(cps)	400
Input current	(ma)	39
Input power	(watt)	0.25
Input Z	(ohms)	855 ∠ 77.5 deg
Output Z	(ohms)	8520 ∠ 79.5 deg
dc Stator Resistance	(ohms)	800
Output voltage (open circuit)	(volts)	60
Linearity	(%)	0.25
Sensitivity	(mv/deg)	1000
Residual (null) voltage	(mv)	30
Transformation ratio		.308

2. Feel Springs. The specification for the two torsion springs is given in Table E-II. Figure E-4 shows the end alignment required. Figure E-5 shows that the resulting force-displacement characteristics lie within the desirable range from Fig. 26.

3. Hand Grip. The hand grip is to be machined from aluminum bar stock. Dimensions and details are shown in Fig. E-6.

TABLE E-II

SPECIFICATION — TORSION SPRINGS

Material: AS5 music wire (or equivalent)
Work Over: 0.3125 in. diameter shaft
Torque: 0.0 in. lb when α between ends is 3.5 deg (unloaded)
7.5 in. lb when α between ends is 0 deg
Length Space: 0.35 in.
Direction of Coil: Righthanded
Maximum Wound Position: 13.5 deg
Wire Diameter: Rectangular h = 0.08 in., b = 0.16 in.
Inside Diameter: 0.3525 in. (loaded 3.5 deg)
No. of Coils: 1
Calc. Torque/Turn: 835 in. lb
Maximum Allowable Load: 21.5 deg
Safety Factor: 61.5%
Free End Alignment: See Fig. E-4

Drawing Scale 1" = 0.1"

Preload = 3.5° = 0.0094 Turn

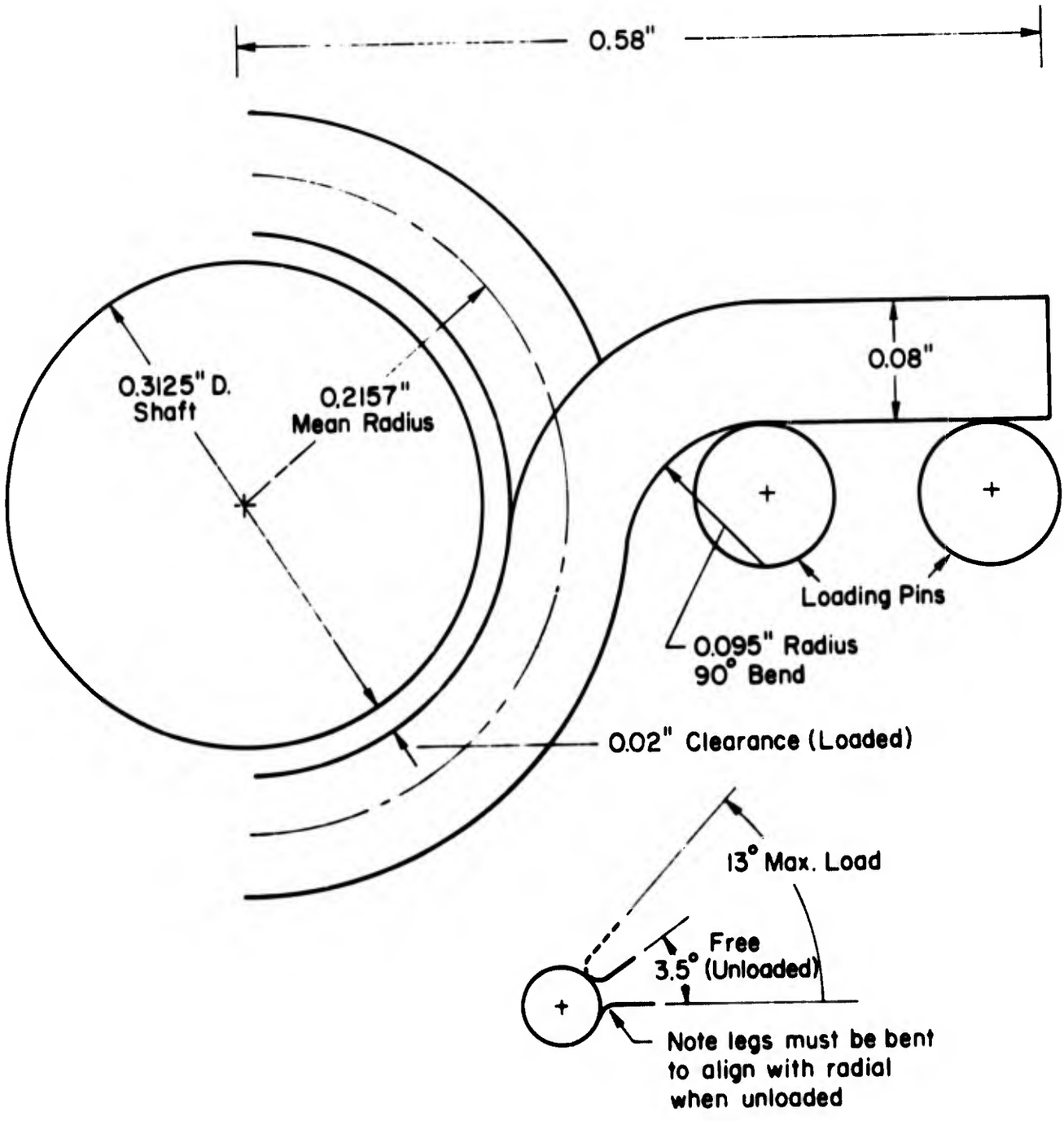

Figure F-4. Spring Free End Alignment

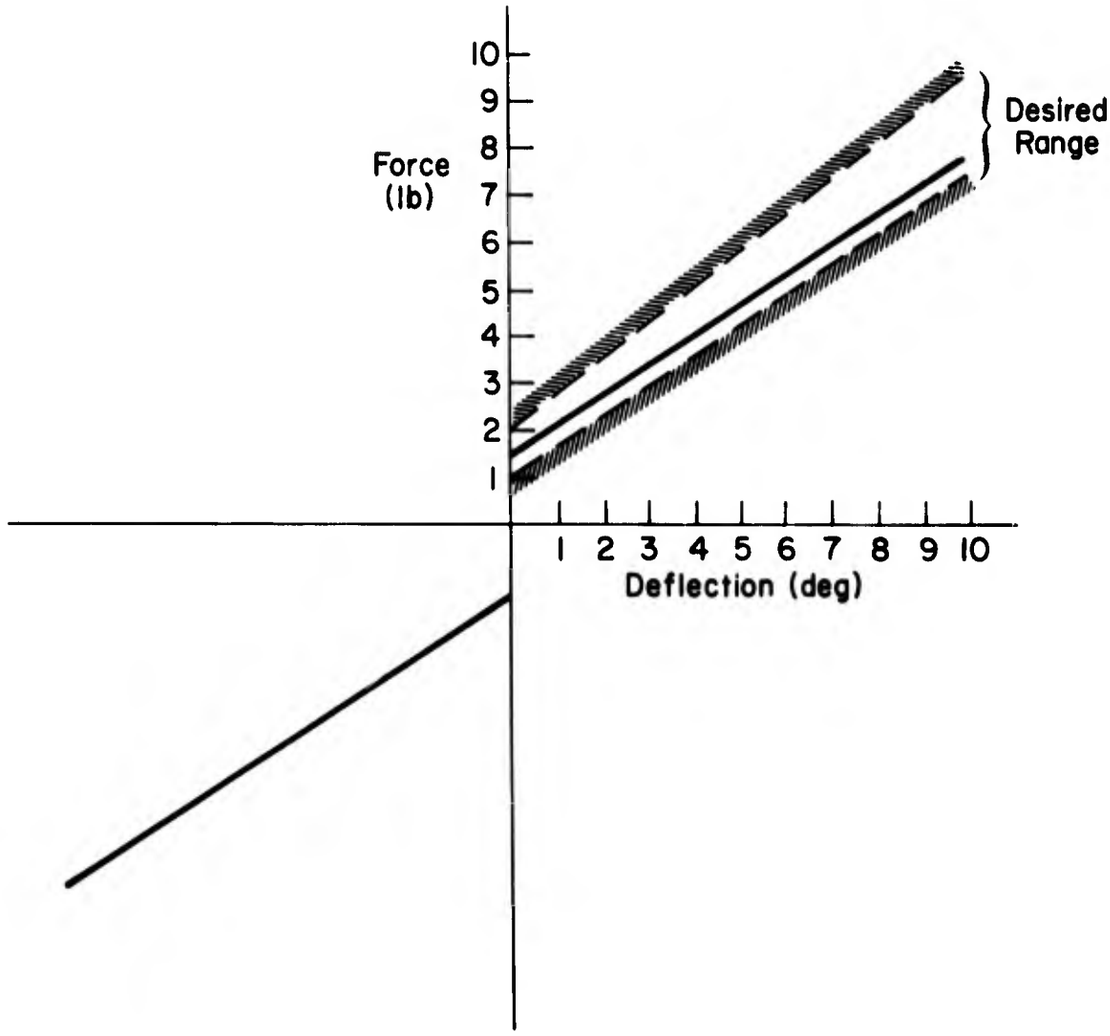

Figure E-5. Resulting Manipulator Force Characteristic

Drawing to Half Scale (Approx.)

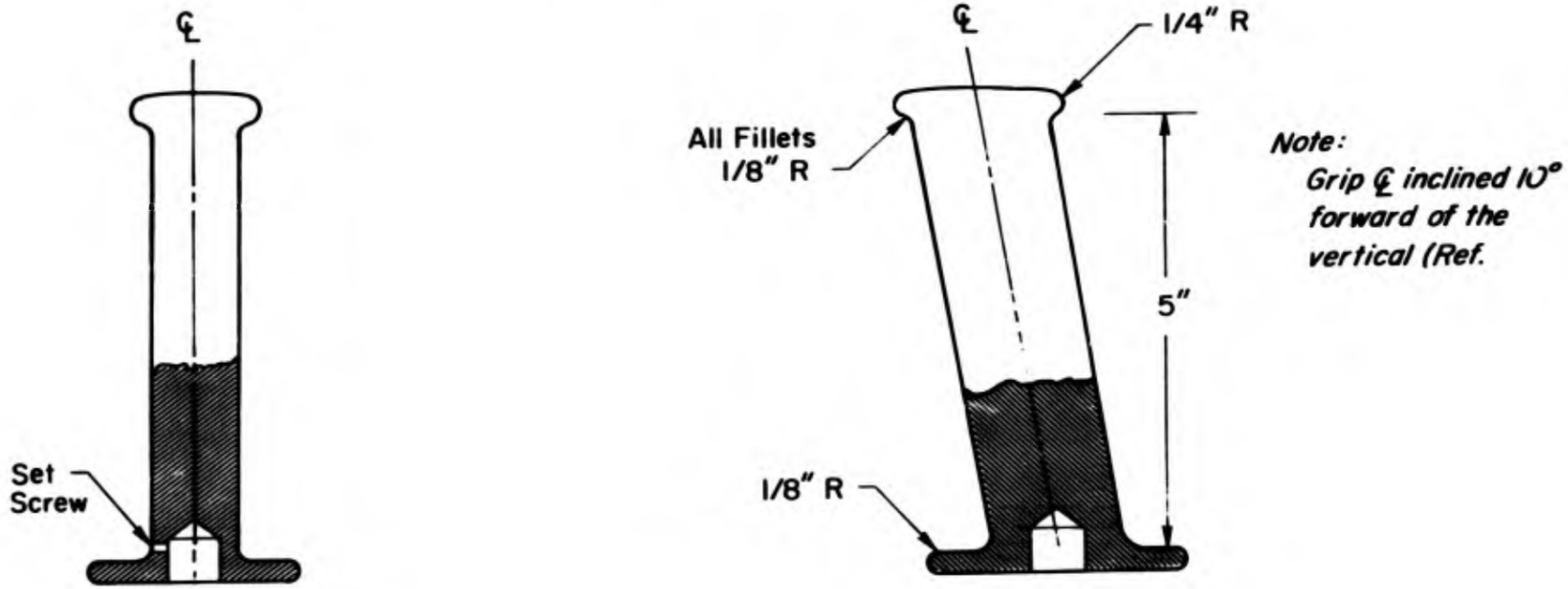

Material - Aluminum Bar Stock
Finish - Grey Anodize

Figure E-6. Hand Grip Details

ELECTRONICS

A functional schematic of the system electronics is shown in Fig. 17. The preliminary design specification is as follows:

1. Power Available: 24 V dc (unregulated battery).

2. Envelope Available: The maximum envelope available is shown in the sketch below. Every effort should be made to minimize the envelope required.

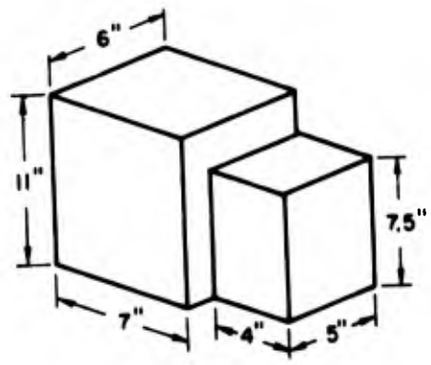

3. Accessibility

   3.1 Access will be via top for any adjustments, maintenance, etc.

   3.2 Electronics plug-in modules to be removable from the "hard box" for major test and repair.

   3.3 Mounting fasteners, locks, or bolts must be accessible from the top only.

4. Environment

   4.1 Temperature. The electronics must operate and meet its performance requirements over a nominal temperature range of $-40^{\circ}F$ to $+150^{\circ}F$.

   4.2 Rain, Dust, Dirt. The electronics unit will be encased in the "hard box" made up of 1/4 in. thick aluminum plate. The hard box will be as weather-tight as possible. However, due to the severe environment, the electronics unit shall be designed to be reasonably insensitive to these environmental factors.

4.3 Vibration and Shock. The vibration and shock environment will be extremely severe due to engine, track, terrain, etc., inputs. No numbers are available as design guides, but every precaution must be employed to rigidly support all components. Components sensitive to shock or vibration shall not be used. Every consideration shall be given to potting small inexpensive elements. Parts which cannot be potted shall be securely locked in place.

4.4 Heat Sink. The case of the manipulator assembly will serve as a heat sink. All heat-generating parts shall be mounted so that the heat will be dissipated into the case structure (and the shelf structure to which the case is attached).

5. Function

5.1 General. The electronics unit shall supply the excitation to, and accept signals from, the two electrical motion pickoffs of the manipulator. The electronic unit output shall drive two electrohydraulic transfer valves (see functional schematic). The unit shall incorporate:

5.1.1 Power Supply. Any necessary electrical dc voltage regulation necessary for the amplification, demodulation, etc., stages of the system and the necessary dc to 400 cycle power conversion for the motion pickoffs shall be incorporated within the unit.

5.1.2 Gain Variation. For independently varying the gain of the pitch and roll channels. The gain pots shall be screwdriver-adjust, friction-lock type.

5.1.3 Output Null Adjust. For independently nulling or biasing the output of the two amplifiers driving the transfer valves. This null (bias) adjust shall have a swing of 50% of full amplifier output. These pots shall be located on the interior of the hard case (control console).

5.1.4 Test Points. Test points shall be accessible via the top of the unit (accessible by opening the cover of the hard box) which will allow troubleshooting of the complete unit. These test points shall include, as a minimum,

- inputs from the pitch and roll pickoffs
- outputs of each gain, sign changing, driving amplifier
- supply voltages

5.1.5 On-Off Switch. The toggle switch shall be mounted on the interior of the hard box control console as shown in Fig. 16.

5.1.6 External Connections. All input and output wires (except the manipulator pickoff) shall terminate at the cannon type connector which will be securely fastened to the hard case.

5.1.7 Plug-In Cards. All plug-in cards shall be securely locked in place with suitable means to prevent movement or accidental unplugging.

5.2 Future Provisions. Allowance (i.e., space, power, spare boards, connector pins, etc.) shall be made for future incorporation of the following auxiliary functions.

- Voltage supply to and signal from an accelerometer.
- Two summing points, one each on the pitch and roll signal inputs.
- Additional amplifiers, preamplifiers, modulator-demodulators (one each).

6. Performance

6.1 Gain

6.1.1 Pitch Axis. The nominal gain from the pitch pickoff input to the transfer valve power amplifier output shall be 1.5 ma/deg. This gain shall be adjustable via the screwdriver-adjust pot from 0 to 3.0 ma/deg.

6.1.2 Roll Axis. The nominal gain from the roll pickoff input to the transfer valve power amplifier output shall be 1.5 ma/deg. This gain shall be adjustable via the screwdriver-adjust pot from 0 to 3.0 ma/deg.

6.2 Linearity. The output current to the electrohydraulic valves shall vary linearly with input voltage over an input range equivalent to ±10 deg of pitch and roll pickoff movement and employing the nominal gains indicated in 6.1, above.

6.3 Drift. Since this controller operates open-loop, drift in the output will be especially critical. Therefore, the electronic unit shall be designed to hold output drift due to any cause (temperature, supply voltage, warm-up, etc.) to an absolute minimum.

6.4 Noise. Noise shall be kept to a minimum consistent with meeting the requirements of 6.1, 6.2, and 6.3, above.

6.5 Switching Transients. Any transients in the output due to turning the electronic unit on or off shall not persist for more than 0.1 sec and shall not exceed 1.5 ma.

6.6 Warm-Up. Warmup time shall not be greater than 5 sec.

ELECTROHYDRAULIC VALVES

The Moog Model 73-103 electrohydraulic transfer valve meets the requirements for this system. Characteristics and specification for this valve are shown below as obtained from Moog catalog 720/730:

Flow	10 gpm
Operating supply pressure	4000 psi (with special O rings)
Proof pressures	
at pressure port	150% supply
at return port	100% supply
Burst pressure (return open)	7500 psi
Temperature range	-65°F to 275°F
External leakage	None
Fluid	Petroleum-base hydraulic fluid
System filtration	10 microns recommended
Weight	2.6 lb
Rated input signal (differential current)	15 milliamp
Coil resistance	200 ± 12% ohm
Mounting	See Fig. E-7
Manifold	4-line, No. 8 SAE straight thread (3/4 in. — 16 thread)

The basis for selection of this valve is:

1. Flow Required

The existing UET hydraulic system characteristics are:

Supply pressure: 4000 psi

Filtration level: 3 micron

Pressure to raise empty tractor: 2000 psi

Hydraulic line: 3/4 in.

Volume per actuator: 50 $in.^3$/rad

Actuator travel: 72 deg

Actuators supplied per valve: 2

Operating valve: 4 way sliding

Valve rating: 13 gal per min each (2 valves)

The valve pressure drop for the rated 13 gpm is unspecified, but is calculated as follows:

a. Volume of oil required for full travel =

$$2 \times \frac{50\ in.^3}{rad} \times 72\ deg \times \frac{1}{57.3}\ \frac{rad}{deg} = 125.5\ in.^3$$

$$= 0.544\ gal$$

b. Time from full-down to full-up travel for empty tractor = 3.5 sec (timed by STI personnel at Ft. Belvoir)

c. Flow to raise empty tractor =

$$\frac{0.544\ gal}{3.5\ sec} \times \frac{60\ sec}{min} = 9.33\ gal/min$$

d. Calculation of valve pressure drop for 13 gpm flow is based on the equation

$$Q_2 = Q_1\sqrt{\frac{\Delta P_2}{\Delta P_1}} \quad \text{or} \quad \Delta P_1 = \Delta P_2 \frac{Q_1^2}{Q_2^2}$$

where Q_1 = rated valve flow = 13 gpm

Q_2 = required flow for unloaded tractor = 9.33 gpm

ΔP_2 = pressure drop for unloaded tractor

$= P_S - P_L = 4000 - 2000 = 2000$ psi

ΔP_1 = pressure drop at rated 13 gpm flow

Valve phasing: Flow out C_2 will result when:

A. Series operation—"B&C" connected, "A+", "D-".

B. Push-Pull operation—"B&C"+, "A&D-".
current "C-D" > "B-A".

SERIES 73

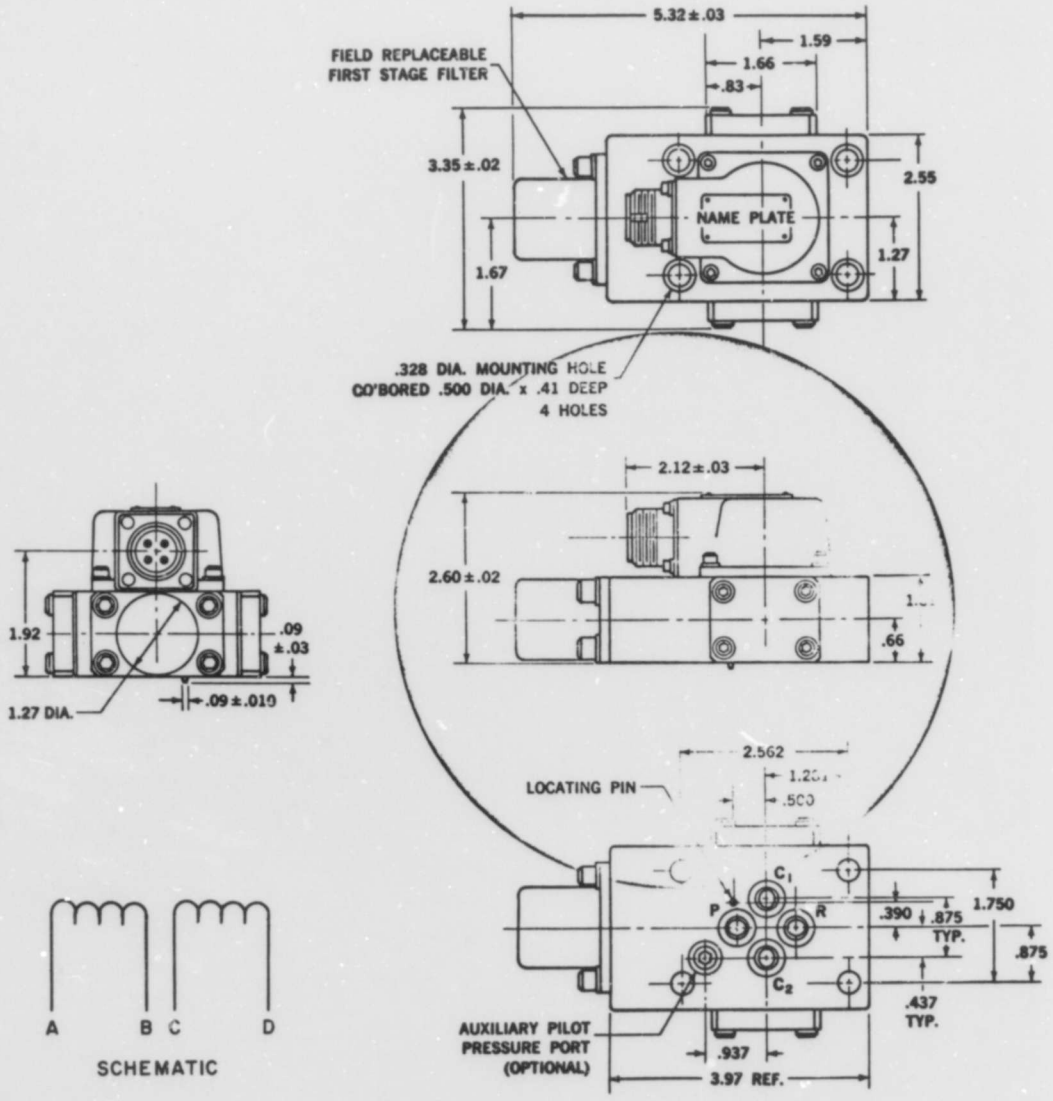

Figure E-7. Electrohydraulic Valve Configuration

$$\Delta P_1 = 2000 \frac{(13)^2}{(9.33)^2} = 2000(1.94)$$

$$= 3880 \text{ psi}$$

Since this closely approximates the hydraulic supply pressure, it is therefore assumed that the present valves were rated at 13 gpm for a 4000 psi valve pressure drop (i.e., no load).

The flow for most electrolydraulic valves is quoted on the basis of a 1000 psi valve pressure drop. Therefore, the electrohydraulic valve equivalent to the present 13 gpm valve would be rated at

$$Q_2 = Q_1\sqrt{\frac{\Delta P_2}{\Delta P_1}} = 13\sqrt{\frac{1000}{4000}}$$

$$= 6.5 \text{ gpm}$$

2. Selection of Valve

The closest off-the-shelf four-way sliding valve is a Moog Industrial Servovalve, Model 73-103, which is rated at 10 gpm for a 1000 psi valve pressure drop. The series 73 servovalves are "ruggedized" versions of their normal military valves. Although only advertised as a 3000 psi operating supply pressure unit, the manufacturer indicated that this same valve can be safely operated at 4000 psi when special (but off-the-shelf) O-rings are used.

The load flow versus load pressure drop for this valve at 100% rated current indicates 70% load flow at 50% of supply pressure load drop and 35% load flow at 90% of supply pressure load drop. At 4000 psi supply and zero load pressure drop the 100% flow is as follows:

$$Q_2 = Q_1\sqrt{\frac{\Delta P_2}{\Delta P_1}} = 10\sqrt{\frac{4000}{1000}} = 20 \text{ gpm}$$

Thus at 50% of supply pressure load drop

- Require for equivalence to present valves: 9.33 gpm
- Obtain 70% of 20 gpm: 14 gpm

At 90% of supply pressure load drop (equivalent to fully loaded vehicle)

- Require for equivalence to present valves

$$Q_c = 9.33\sqrt{\frac{0.4000 - 0.9(4000)}{2000}} = 9.33\sqrt{\frac{400}{2000}}$$

$$= 9.33(0.45) = 4.2 \text{ gpm}$$

- Obtain 30% of 20 gpm = 7.0 gpm

Thus the Moog servovalve model 73-103 meets or exceeds all requirements.

E. INSTALLATION SCHEMATICS

1. Hydraulic

A simplified schematic of the hydraulic installation for the left wheel control is shown in Fig. 19. The right wheel control would be the same except for replacing L for R on the line codes. The sprung-unsprung valves (manual control and wheel) are shown in the unsprung mode. The existing hydraulic connections are shown by the solid lines and the new lines for the EHTV are shown dashed. The installation requires four tees to be attached at the connections to the existing Hydreco or Husco valve banks. New lines from these tees are then run to the EHTV manifold. The existing valve bank need not be disturbed further since the manually operated levers that control the left and right front wheel valves will be disconnected and removed in the operator's cockpit.

Note that in the sprung mode the wheel valve moves so that line 3L is blocked while the sprung-unsprung valve opens 1/L to return (line 7 . Thus any inadvertent operation of the EHTV will not affect the rotary actuator and no additional va ves, switches, etc., are necessary for protective means.

2. Electrical

A simplified schematic of the electrical installation is shown in Fig. 20. The 24V electrical supply from the instrument panel should be obtained from the ignition switch such that electrical power is not available to the electronics unit unless the ignition switch is on.

Unclassified

Security Classification

DOCUMENT CONTROL DATA · R&D

(Security classification of title, body of abstract and indexing annotation must be entered when the overall report is classified)

1 ORIGINATING ACTIVITY (Corporate author)

Systems Technology, Inc.
13766 S. Hawthorne Blvd.
Hawthorne, California 90250

2a REPORT SECURITY CLASSIFICATION

Unclassified

2b GROUP

N/A

3 REPORT TITLE

Development of a Controller Element
for Compatible Operator Control of Earthmoving Machines

4 DESCRIPTIVE NOTES (Type of report and inclusive dates)

Final Report

5 AUTHOR(S) (Last name, first name, initial)

Johnston, D. E.; Weir, D. H.; Ringland, R. F.; Hofmann, L. G.

6 REPORT DATE	7a TOTAL NO OF PAGES	7b NO OF REFS
August 1969	209	27

8a CONTRACT OR GRANT NO	9a ORIGINATOR'S REPORT NUMBER(S)
DAAK02-68-C-0186	TR-178-4
b PROJECT NO	
c	9b OTHER REPORT NO(S) (Any other numbers that may be assigned this report)
d	

10 AVAILABILITY/LIMITATION NOTICES

This document has been approved for public release and sale; its distribution is unlimited.

11 SUPPLEMENTARY NOTES	12 SPONSORING MILITARY ACTIVITY
	Department of the Army U.S. Army Mobility Equipment R&D Center Fort Belvoir, Virginia 22060

13 ABSTRACT

Manual control of dozing with an earthmoving tractor is studied to determine ways to modify the manipulator and control system properties to improve performance and reduce operator workload. The Universal Engineer Tractor is used as a numerical example. Linearized equations are derived for longitudinal and lateral motions which include manipulator and suspension properties, vehicle hull and blade dynamics, and terrain loads on the blade. The resultant detailed dynamic model is reduced to a simplified equivalent for analysis and simulation. Transfer functions are computed and used to study the operator's blade control in response to various visual and motion cues. This indicates which feedbacks the operator should use, and how the controlled element dynamics can be improved through design modifications. A fixed-base mock-up and dynamic simulation are used to evaluate competing manipulator/controller configurations. As a result, a prototype manipulator is defined which has the potential of improving dozing performance, reducing training time, and easing the operator workload.

DD FORM 1 JAN 64 1473

Unclassified

Security Classification

Unclassified
Security Classification

14 KEY WORDS	LINK A		LINK B		LINK C	
	ROLE	WT	ROLE	WT	ROLE	WT
Universal Engineer Tractor						
Equations of motion						
Mathematical models						
Human operator						
Human factors						
Earthmoving						
Construction equipment						
Bulldozing						
Off-road mobility						
Manipulators						
Land locomotion						
Vehicle-terrain interaction						

INSTRUCTIONS

1. **ORIGINATING ACTIVITY**: Enter the name and address of the contractor, subcontractor, grantee, Department of Defense activity or other organization *(corporate author)* issuing the report.

2a. **REPORT SECURITY CLASSIFICATION**: Enter the overall security classification of the report. Indicate whether "Restricted Data" is included. Marking is to be in accordance with appropriate security regulations.

2b. **GROUP**: Automatic downgrading is specified in DoD Directive 5200.10 and Armed Forces Industrial Manual. Enter the group number. Also, when applicable, show that optional markings have been used for Group 3 and Group 4 as authorized.

3. **REPORT TITLE**: Enter the complete report title in all capital letters. Titles in all cases should be unclassified. If a meaningful title cannot be selected without classification, show title classification in all capitals in parenthesis immediately following the title.

4. **DESCRIPTIVE NOTES**: If appropriate, enter the type of report, e.g., interim, progress, summary, annual, or final. Give the inclusive dates when a specific reporting period is covered.

5. **AUTHOR(S)**: Enter the name(s) of author(s) as shown on or in the report. Enter last name, first name, middle initial. If military, show rank and branch of service. The name of the principal author is an absolute minimum requirement.

6. **REPORT DATE**: Enter the date of the report as day, month, year, or month, year. If more than one date appears on the report, use date of publication.

7a. **TOTAL NUMBER OF PAGES**: The total page count should follow normal pagination procedures, i.e., enter the number of pages containing information.

7b. **NUMBER OF REFERENCES**: Enter the total number of references cited in the report.

8a. **CONTRACT OR GRANT NUMBER**: If appropriate, enter the applicable number of the contract or grant under which the report was written.

8b, 8c, & 8d. **PROJECT NUMBER**: Enter the appropriate military department identification, such as project number, subproject number, system numbers, task number, etc.

9a. **ORIGINATOR'S REPORT NUMBER(S)**: Enter the official report number by which the document will be identified and controlled by the originating activity. This number must be unique to this report.

9b. **OTHER REPORT NUMBER(S)**: If the report has been assigned any other report numbers *(either by the originator or by the sponsor)*, also enter this number(s).

10. **AVAILABILITY/LIMITATION NOTICES**: Enter any limitations on further dissemination of the report, other than those imposed by security classification, using standard statements such as:

(1) "Qualified requesters may obtain copies of this report from DDC."

(2) "Foreign announcement and dissemination of this report by DDC is not authorized."

(3) "U. S. Government agencies may obtain copies of this report directly from DDC. Other qualified DDC users shall request through _____."

(4) "U. S. military agencies may obtain copies of this report directly from DDC. Other qualified users shall request through _____."

(5) "All distribution of this report is controlled. Qualified DDC users shall request through _____."

If the report has been furnished to the Office of Technical Services, Department of Commerce, for sale to the public, indicate this fact and enter the price, if known.

11. **SUPPLEMENTARY NOTES**: Use for additional explanatory notes.

12. **SPONSORING MILITARY ACTIVITY**: Enter the name of the departmental project office or laboratory sponsoring *(paying for)* the research and development. Include address.

13. **ABSTRACT**: Enter an abstract giving a brief and factual summary of the document indicative of the report, even though it may also appear elsewhere in the body of the technical report. If additional space is required, a continuation sheet shall be attached.

It is highly desirable that the abstract of classified reports be unclassified. Each paragraph of the abstract shall end with an indication of the military security classification of the information in the paragraph, represented as *(TS)*, *(S)*, *(C)*, or *(U)*.

There is no limitation on the length of the abstract. However, the suggested length is from 150 to 225 words.

14. **KEY WORDS**: Key words are technically meaningful terms or short phrases that characterize a report and may be used as index entries for cataloging the report. Key words must be selected so that no security classification is required. Identifiers, such as equipment model designation, trade name, military project code name, geographic location, may be used as key words but will be followed by an indication of technical context. The assignment of links, rules, and weights is optional.

Unclassified
Security Classification